REPORT NO. CG-D-05-98

LOW FIRE LOAD COMPARTMENT FLASHOVER TESTING

Michelle J. Peatross
Craig L. Beyler
Hughes Associates, Inc.
Baltimore, MD 21227-1652

C. Michael Sprague, PE
Worcester Polytechnic Institute
Worcester, MA 01609

Brian L. Dolph
U.S. Coast Guard
Research & Development Center
1082 Shennecossett Road
Groton, CT 06340-6096

Final Report
December 1997

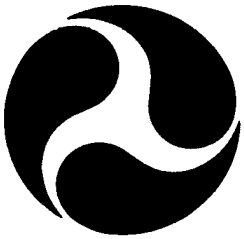

Prepared for:

U.S. Department of Transportation
United States Coast Guard
Marine Safety and Environmental Protection, (G-M)
Washington, DC 20593-0001

NOTICE

This document is disseminated under the sponsorship of the Department of Transportation in the interest of information exchange. The United States Government assumes no liability for its contents or use thereof.

The United States Government does not endorse products or manufacturers. Trade or manufacturers' names appear herein solely because they are considered essential to the object of this report.

The contents of this report reflect the views of the Coast Guard Research & Development Center. This report does not constitute a standard, specification, or regulation.

Marc B. Mandler
Technical Director
United States Coast Guard
Research & Development Center
1082 Shennecossett Road
Groton, CT 06340-6096

Technical Report Documentation Page

1. Report No.	2. Government Accession Number	3. Recipient's Catalog No.
CG-D-05-98		

4. Title and Subtitle	5. Report Date
Low Fire Load Compartment Flashover Testing	December 1997
	6. Performing Organization Code Project No. 3308.3

7. Author(s)	8. Performing Organization Report No.
Michelle J. Peatross, Craig L. Belyer, C. Michael Sprague, Brian L. Dolph	R&DC 26/97

9. Performing Organization Name and Address			10. Work Unit No. (TRAIS)
Hughes Associates, Inc. 3610 Commerce Dr, Suite 817 Baltimore, MD 21227-1652	Worcester Polytechnic Institute Worcester, MA 01609-2280	U.S. Coast Guard Research & Development Center 1082 Shennecossett Road Groton, CT 06340-6096	SHRD Report No. 118 11. Contract or Grant No. DTCG39-96-F-E00179

12. Sponsoring Organization Name and Address	13. Type of Report & Period Covered
U.S. Dept of Transportation United States Coast Guard Systems, (G-M) Washington, DC 20593-0001	Final Report, Apr 96 - Aug 97
	14. Sponsoring Agency Code Commandant (G-MSE-4) U.S. Coast Guard Headquarters Washington, DC 20593-0001

15. Supplementary Notes

The Coast Guard technical contact and COTR is Brian Dolph (860-441-2817) of the U.S. Coast Guard Research and Development Center. The project officer is LT Anthony DiSanto (G-MSE-4), Coast Guard Headquarters.

16. Abstract

The Low Fire Load Compartment Flashover Testing was conducted to evaluate the effects on fuel load density, material fire resistance, and fuel package distribution on the potential for flashover in commercial Type 5A spaces as defined in Policy File Memorandum on Structural Insulation Requirements for Low Fire Load Spaces on Certain Vessels (PFM 1-94). The testing was also conducted to evaluate the appropriateness of select fire growth models utilized in the Ship Applied Fire Engineering (SAFE) computer program.

The full-scale shipboard testing program was conducted onboard STATE OF MAINE at the Fire & Safety Test Detachment in Mobile, Alabama, in February 1997. The results indicate that the assumptions used to develop the requirements in PFM 1-94 were appropriate as applied and the Type 5A compliant compartment did not achieve flashover conditions. The results also indicate that SAFE's Fire Growth Model #16 (Very Low Density Storage) appropriately defined the fire conditions experimentally measured within the fire room.

17. Key Words	18. Distribution Statement
low fire load, fuel load density, fuel load distribution fire resistant materials, non-fire resistant materials, compartment fires, aluminum	This document is available to the U.S. public through the National Technical Information Service, Springfield, VA 22161

19. Security Class (This Report)	20. Security Class (This Page)	21. No of Pages	22. Price
UNCLASSIFIED	UNCLASSIFIED		

Form DOT F 1700.7 (8/72) Reproduction of form and completed page is authorized.

METRIC CONVERSION FACTORS

Approximate Conversions to Metric Measures

Symbol	When You Know	Multiply By	To Find	Symbol
		LENGTH		
in	inches	* 2.5	centimeters	cm
ft	feet	30	centimeters	cm
yd	yards	0.9	meters	m
mi	miles	1.6	kilometers	km
		AREA		
in^2	square inches	6.5	square centimeters	cm^2
ft^2	square feet	0.09	square meters	m^2
yd^2	square yards	0.8	square meters	m^2
mi^2	square miles	2.6	square kilometers	km^2
	acres	0.4	hectares	ha
		MASS (WEIGHT)		
oz	ounces	28	grams	g
lb	pounds	0.45	kilograms	kg
	short tons (2000 lb)	0.9	tonnes	t
		VOLUME		
tsp	teaspoons	5	milliliters	ml
tbsp	tablespoons	15	milliliters	ml
fl oz	fluid ounces	30	milliliters	ml
c	cups	0.24	liters	l
pt	pints	0.47	liters	l
qt	quarts	0.95	liters	l
gal	gallons	3.8	liters	l
ft^3	cubic feet	0.03	cubic meters	m^3
yd^3	cubic yards	0.76	cubic meters	m^3
		TEMPERATURE (EXACT)		
°F	Fahrenheit temperature	5/9 (after subtracting 32)	Celsius temperature	°C

*1 in = 2.54 (exactly).

Approximate Conversions from Metric Measures

Symbol	When You Know	Multiply By	To Find	Symbol
		LENGTH		
mm	millimeters	0.04	inches	in
cm	centimeters	0.4	inches	in
m	meters	3.3	feet	ft
m	meters	1.1	yards	yd
km	kilometers	0.6	miles	mi
		AREA		
cm^2	square centimeters	0.16	square inches	in^2
m^2	square meters	1.2	square yards	yd^2
km^2	square kilometers	0.4	square miles	mi^2
ha	hectares (10,000 m^2)	2.5	acres	
		MASS (WEIGHT)		
g	grams	0.035	ounces	oz
kg	kilograms	2.2	pounds	lb
t	tonnes (1000 kg)	1.1	short tons	
		VOLUME		
ml	milliliters	0.03	fluid ounces	fl oz
l	liters	0.125	cups	c
l	liters	2.1	pints	pt
l	liters	1.06	quarts	qt
l	liters	0.26	gallons	gal
m^3	cubic meters	35	cubic feet	ft^3
m^3	cubic meters	1.3	cubic yards	yd^3
		TEMPERATURE (EXACT)		
°C	Celsius temperature	9/5 (then add 32)	Fahrenheit temperature	°F

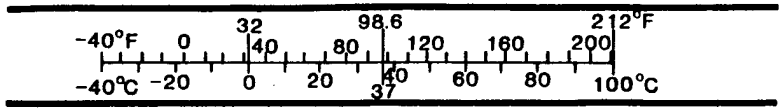

CONTENTS

CONTENTS (Concluded)

FIGURES

FIGURES (Concluded)

TABLES

Executive Summary

The purpose of this report is to present results of the full-scale experimental testing program. This program was designed to evaluate the flashover potential of certain fuel loading configurations in Type 5A spaces and to evaluate the appropriateness of select fire growth models utilized in the Ship Applied Fire Engineering (SAFE) computer program.

Policy File Memorandum on Structural Insulation Requirements For Low Fire Load Spaces On Certain Vessels (PFM 1-94), prepared by Chief, Marine Technical and Hazardous Materials Division (G-MTH-4), provides minimum insulation and bulkhead classifications for certain vessels containing low risk passenger accommodation spaces with not more than 5 kg/m^2 (1 lb/sqft) combustibles fire loading. The requirements set forth in this memorandum were largely established based on computer fire modeling with various qualifying assumptions. The subject testing program was designed to evaluate the appropriateness of the major assumptions and resulting requirements from this modeling. The three main variables which were considered included fire load density, flame-retardant material properties, and fuel package distribution.

The testing results indicate that fuel package distribution has a tremendous effect on the size of fire that could be produced within a space meeting the requirements of an overall low fire load density comprised of flame-retardant materials. However, flashover was not achieved in the test compartment utilizing the low fuel loading, even with an unrealistically high fuel package concentration (i.e. all seat cushions piled in the center of the compartment). It appears that the assumptions used in developing PFM 1-94 requirements are appropriate.

Various fire growth models (equations) are used in the SAFE computer program to describe the fire conditions within a compartment as part of a performance-based fire safety analysis using the Ship Fire Safety Engineering Method (SFSEM). The key parameters of fire growth rate and maximum heat release rate are based on various factors depending on fuel load characteristics within a compartment. By comparing the conditions within the fire room predicted by various fire growth models in SAFE to the conditions experimentally measured

during the full-scale testing, an indication can be made as to the appropriateness of the SAFE models for evaluating the fire room characteristics.

The test results indicate that the fire room characteristics as defined by SAFE's fire growth model #16 (Very Low Density Storage) were relatively good predictors of the conditions actually measured in the Type 5A compliant compartment. When the Type 5A space requirements were violated (i.e. localized fuel distribution), the experimentally measured conditions within the space were more severe than those estimated by fire growth model #16. This is to be expected and indicates that this fire growth model is appropriate for a Type 5A compliant space.

[BLANK]

1.0 INTRODUCTION

The use of aluminum for structural barriers on small passenger vessels is becoming more prevalent. It is advantageous because it reduces the cost of construction and it is considerably lighter than steel. Shipboard compartments with this aluminum construction are classified as Type 5A spaces. These spaces are required to have fuel loading of no greater than 5 kg/m^2, to contain only non-combustible veneers and trims, and to have fire resistant (FR) furnishings [1]. In addition, the combustible materials must be evenly distributed through the space [1].

In the event of a fire, aluminum presents a higher likelihood of thermal or structural failure than that presented by steel. This is due to its higher thermal conductivity and, more importantly, its lower melting point. The Ship Applied Fire Engineering (SAFE) computer program used to implement Ship Fire Safety Engineering Methodology (SFSEM) does not consider heat that is transferred to compartment bulkheads prior to the fire reaching flashover in the assessment of barrier failure [2]. This assumption is certainly not accurate in the case of aluminum bulkheads. However, it is uncertain whether this inaccuracy is significant in determining times to barrier failure. While these spaces have been designed so that flashover will not occur, this has not been verified. As a result, the fire conditions which result from typical fuel loadings and configurations need to be assessed. Furthermore, the integrity of these bulkheads under fire conditions needs to be evaluated.

2.0 OBJECTIVE

The primary objective of this test program was to perform experiments that characterize the fire conditions that are likely to result from typical fuel loading in Type 5A compartments. These tests investigated the effect of (1) fuel load density, (2) fuel load material properties, and (3) fuel load package distribution on the fire conditions. The purpose of these tests was to determine whether flashover would result from the different fuel configurations.

3.0 APPROACH

Fire tests were conducted in an instrumented mockup of a Type 5A space furnished with seats. As a baseline, the conditions that would result from a fire in a normal Type 5A compartment (i.e., 5 kg/m^2 evenly distributed fuel load, FR materials) were examined. The furnishings were varied from Type 5A specifications to determine the affect on the fire conditions. The effect of using non-FR versus FR materials was assessed by changing the type of seat cushions used in the space. The effect of a higher fuel load density was evaluated by testing with a density of 10 kg/m^2 versus 5 kg/m^2. The effect of having an undistributed fuel load was examined by decreasing the distance between the seat arrays. Since ignition took place near the bottom center of the compartment in these tests, the performance of the bulkheads and ceiling when exposed to direct flame impingement was addressed separately. Small-scale experiments were conducted to assess this scenario. These results were compared with one- and two-dimensional heat transfer models. The two-dimensional model was also used to estimate the fire size needed to achieve temperatures sufficient to melt the aluminum. In addition, experimentally measured temperatures and heat release rates were compared with those obtained using algorithms defined in SAFE.

4.0 EXPERIMENTAL SETUP

A typical passenger compartment was constructed onboard the United States Coast Guard test vessel, STATE OF MAINE, located in Mobile, AL. The test compartment had nominal dimensions of 4.6 m wide by 5.0 m deep by 2.5 m high (Figure 1). All bulkheads were constructed of steel. A drop ceiling composed of 6 mm aluminum panels was installed 0.1 m below the overhead. These aluminum panels were approximately 61 cm by 122 cm and were bolted to the framing for the drop ceiling. Two doors, 0.89 m wide by 2 m high, were located in the starboard bulkhead. The aft door was closed during tests and the forward door was used as the vent. Compartment instrumentation is shown in Figures 2 through 4 and is detailed below.

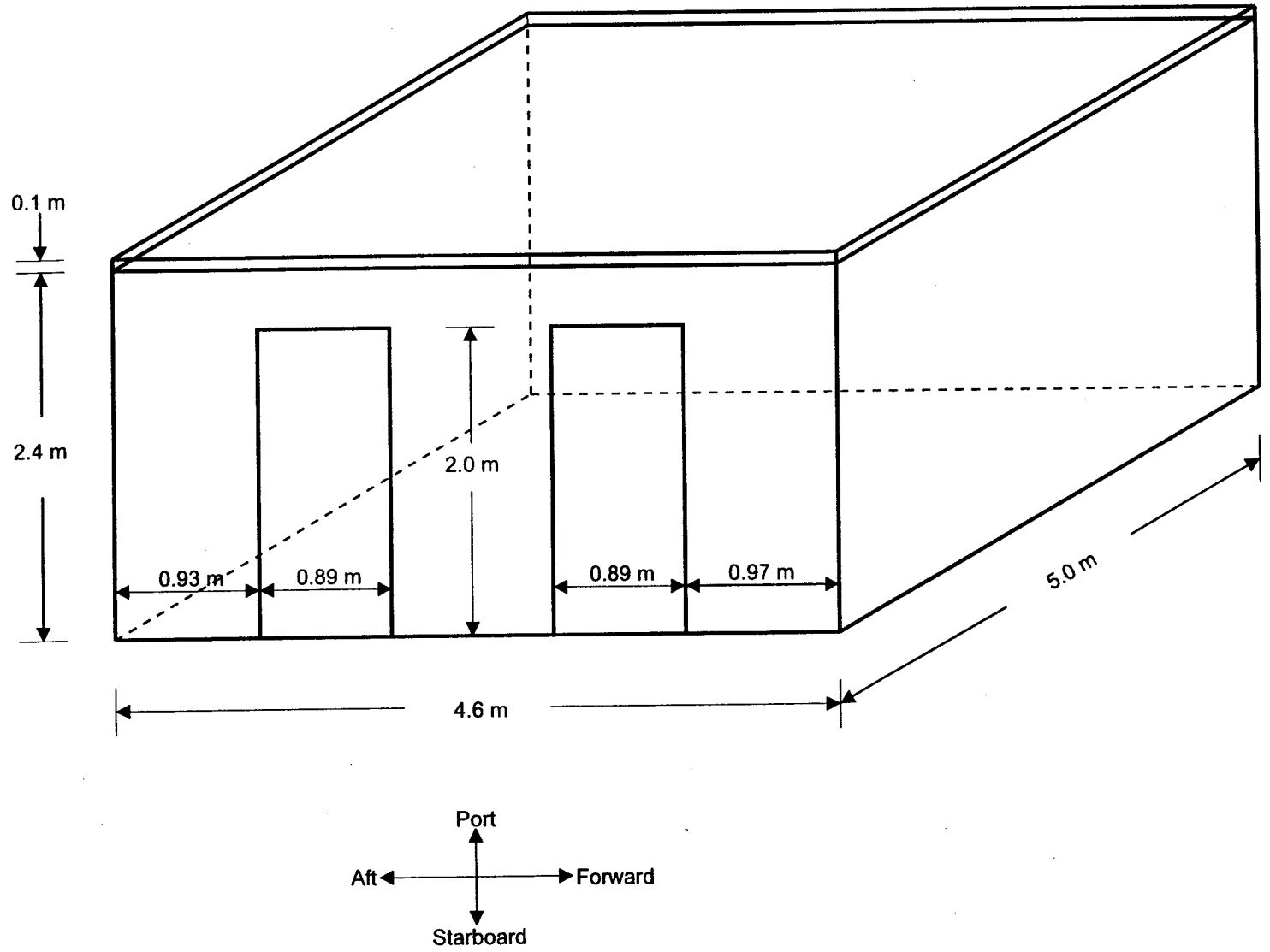

Figure 1. Isometric of test compartment

KEY

(HF) Heat flux transducers (Radiometer/calorimeter pair)

(TC) Thermocouple tree

(BP) Bi-directional probe

(GT) Gas species sampling tree

(ΔP) Differential pressure transducer (referenced to ambient)

(CP) Ceiling panel thermocouple (interior and exterior)

(C) Camera

Figure 2. Instrumentation key

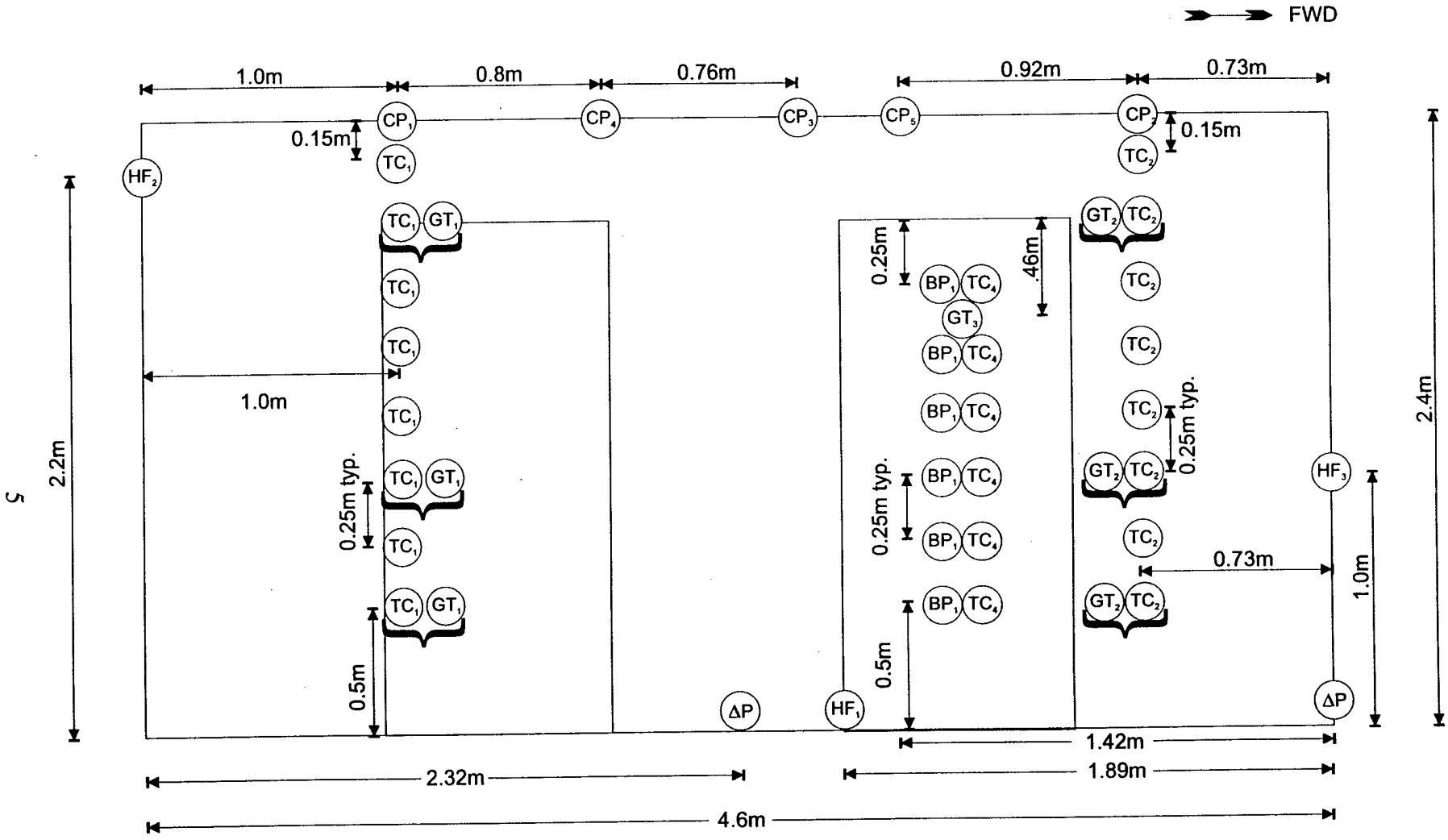

Figure 3. Profile view of compartment instrumentation

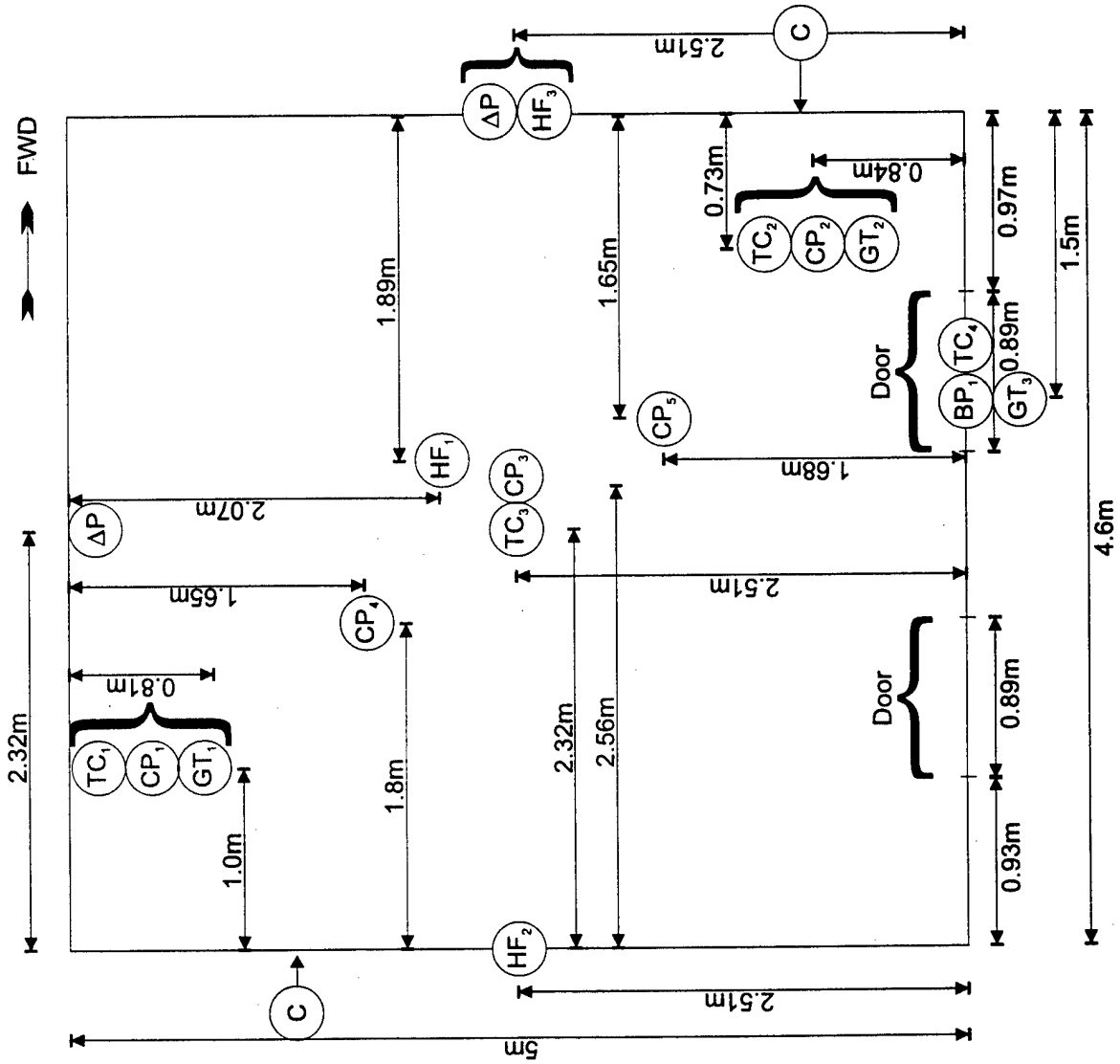

Figure 4. Plan view of compartment instrumentation

4.1 Compartment Instrumentation

4.1.1 Temperature Measurements

Ceiling and gas temperatures were measured using 3 mm Type K, inconel sheathed thermocouples. Three thermocouple trees were positioned as shown in Figures 3 and 4. Each tree consisted of eight thermocouples spaced 0.25 m apart beginning 0.5 m above the deck. Also, thermocouples were peened into the aluminum ceiling panels on both the interior and exterior side of the panel at five locations. In addition, 3 mm Type K thermocouples were located beside each bi-directional probe at the locations specified in Section 4.1.3.

4.1.2 Heat Flux Measurements

Radiometer and calorimeter pairs were positioned at three locations in the test compartment. These transducers were Schmidt-Boelter gages manufactured by Medtherm Corporation. The radiometers had sapphire windows. One pair was located in the horizontal center of the aft bulkhead 0.3 m below the overhead (Location 1). The second pair was located in the forward bulkhead, centered horizontally 1 m above the deck facing aft (Location 2). The third pair was approximately in the center of the test compartment at deck level facing the overhead (Location 3). All transducers were water-cooled and, with the exception of the radiometer at Location 2, had a range of 0 to 100 kW/m^2. The radiometer at Location 2 had a range of 0 to 50 kW/m^2.

4.1.3 Vent Flow Rate Measurements

The forward door was instrumented with bi-directional probes for the calculation of vent flow rates [3]. These probes were located at heights of 0.5, 0.75, 1.0, 1.25, 1.5, 1.75, and 2.0 m above the deck at the doorway centerline. The pressure transducers used to measure the pressure differential across the probe were manufactured by Setra Systems, Inc. and had a

range of ± 25 Pa with an accuracy of ± 0.25 Pa. As stated above in Section 4.1.1, 3 mm Type K inconel sheathed thermocouples were located next to each probe.

4.1.4 Gas Species Measurements

Carbon monoxide (CO), carbon dioxide (CO_2), and oxygen concentrations (O_2) were measured in the test compartment and in the forward doorway. The analyzer ranges were 0-5% for CO, 0-25% for CO_2, and 0-25% for O_2. There were three gas sampling trees which were located adjacent to the thermocouple trees. For Gas Trees 1 and 2 (noted as GT_1 and GT_2 in Figures 3 and 4), sampling points were located 0.5, 1.0, and 2.0 m above the deck. There was only one sampling point at a height of 2 m on Gas Tree 3 (GT_3). In order to measure exhaust gas concentrations for oxygen calorimetry calculations, there was also a sampling point located in the forward doorway 46 cm below the top of the door.

These analyzers were calibrated each morning prior to testing. The transit time from the test compartment was nominally 30 seconds. Water was removed from all gas samples by passing the samples through filters containing Drierite. As a result, all gas concentrations were recorded on a dry basis.

4.1.5 Pressure Measurements

The compartment pressure was measured at deck level in two locations (Setra Systems, Inc., ± 250 Pa range). One location was at the horizontal center of the port bulkhead, and the other location was at the horizontal center of the forward bulkhead. The pressure measurements were referenced to the compartment located directly below the test compartment.

4.2 Video Monitoring

Two video cameras were positioned outside of the test compartment as shown in Figure 4. One camera was positioned on the forward side of the test compartment viewing aft through

the room and the other camera was positioned on the aft side of the test compartment viewing forward through the room. Each test was recorded using video recorders.

4.3 Fixed CO_2 Extinguishing System

A remotely actuated, fixed CO_2 system was installed to extinguish fires at the end of each test. This system was used because it minimized the turn around time between tests.

5.0 DESCRIPTION OF FUELS

The normal fuel load density configuration of 5 kg/m^2 consisted of carpet and seat cushions. These materials are described in detail below in Sections 5.1 and 5.2. Wood cribs were used in addition to these fuels for the tests with a fuel load density of 10 kg/m^2 and are discussed in Section 5.3.

5.1 Carpet

The carpet was composed of broadloom tufted wool and weighed 2.8 kg/m^2 (Sisalcraft DN876, distributed by Lee's Commercial Carpet). This carpet met National Fire Protection Association (NFPA) Class 1 when tested under ASTM-E-648 (American Society for Testing and Materials). All damaged carpet was replaced prior to each test.

5.2 Seating

All seat backs were approximately 57 cm long by 43 cm wide by 6 cm thick. The seat bottom cushions were approximately 40 cm long by 43 cm wide by 6 cm thick. The combustible mass of the seat bottom was estimated as 0.6 kg, and the combustible mass of the seat back was estimated as 0.4 kg.

5.2.1 Fire Resistant (FR)

Fire resistant seat cushions consisted of FR upholstery and FR foam. As stated in PFM 1-94, seating furniture is considered fire resistant if it passes Underwriters Laboratories Standard 1056 which incorporates California Fire Code Technical Bulletin 133 [1]. According to the cushion distributor, the FR upholstery passed California Technical Bulletin 117 Class 1; United Furniture Action Council (UFAC) Class 1; DOC CS 191-53 Class 1 Business and Institutional Manufacturers (BIFMA); HSTMI E-84 Class-A; NFPA 260, "Standard Methods of Tests and Classification System for Cigarette Ignition Resistance of Components of Upholstered Furniture," B Class 1; and NFPA 701, "Standard Methods of Fire Tests for Flame-Resistant Textiles and Films." The FR foam passed California Technical Bulletin 117, Section A Part I; Motor Vehicle Safety Standard (MVSS) 302, SEC D Part II; and Federal Aviation Administration (FAA), Federal Aviation Regulation (FAR) 25.853 (B). The nominal foam density was 45 kg/m^3.

5.2.2 Non-fire Resistant (non-FR)

The non-FR foam was a urethane foam with no fire retardant. The non-FR upholstery passed California Bulletin 117-E and UFAC Class 1. The nominal foam density was 35 kg/m^3.

5.2.3 Cone Calorimeter Tests

Prior to shipboard experiments, cone calorimeter tests were conducted using both cushion types (Appendix A). The purpose of these tests was to examine the burning characteristics of the FR and the non-FR cushions. Experiments were conducted at incident heat fluxes of 15 kW/m^2 and 25 kW/m^2. At an incident heat flux of 15 kW/m^2, the FR sample ignited in 178 seconds whereas the non-FR sample did not even ignite after eight minutes (480 seconds). Both samples ignited when the incident heat flux was increased to 25 kW/m^2. The FR sample ignited after 21 seconds while the non-FR sample ignited after 68 seconds. Although the distributor reported that the FR cushions passed more stringent tests than the non-FR cushions, the cone calorimeter

the cone calorimeter results suggested that non-FR cushions were more fire resistant that the FR cushions. A more detailed discussion of these tests is included in Appendix A.

5.3 Wood Cribs

The higher fuel load density scenario of 10 kg/m^2 consisted of the 5 kg/m^2 materials described above in addition to 5 kg wood cribs. Each crib consisted of three layers of six 43 cm by 4 cm by 4 cm sticks spaced 4 cm apart. Twenty-four cribs were spaced throughout the compartment so that a nominal fuel load of 10 kg/m^2 was achieved.

6.0 TESTS CONDUCTED

The test matrix outlined in the test plan [4] described 8 tests. A shortage of reusable seat frame assemblies required several of these tests to be omitted from the final test matrix (Test 3-1 and Test 3-2). The tests actually conducted are described in Table 1. The standard configuration consisted of four rows of seats spaced evenly in the compartment as shown in Figure 5. Three of these rows consisted of three 3-seat frames. Due to the presence of an I-beam, it was not possible to fit nine seats in the remaining row. As a result, one row consisted of two 3-seat frames and one 2-seat frame. There were 35 seats in total, and each seat was covered with a seat bottom and back (see Figure 5).

For tests with a fuel load density of 10 kg/m^2 (Tests 2-1 and 2-2), twenty-four 5 kg wood cribs were placed on top of the seat bottoms to achieve the higher density. This arrangement is shown in Figure 6 where each crib is designated with a "C". There were two different configurations for tests with localized fuel load distributions. In the first test (Test 1-4), two rows of seats were placed back-to-back 0.1 m apart instead of 0.7 m as in the standard configuration (Figures 7 and 8). In the back-to-back configuration (Test 1-4), the back of the ignition row was 0.1 m away from the back of the adjacent row. In the normal configuration, the back of the ignition row was 0.7 m away from the front seat edge of the adjacent row.

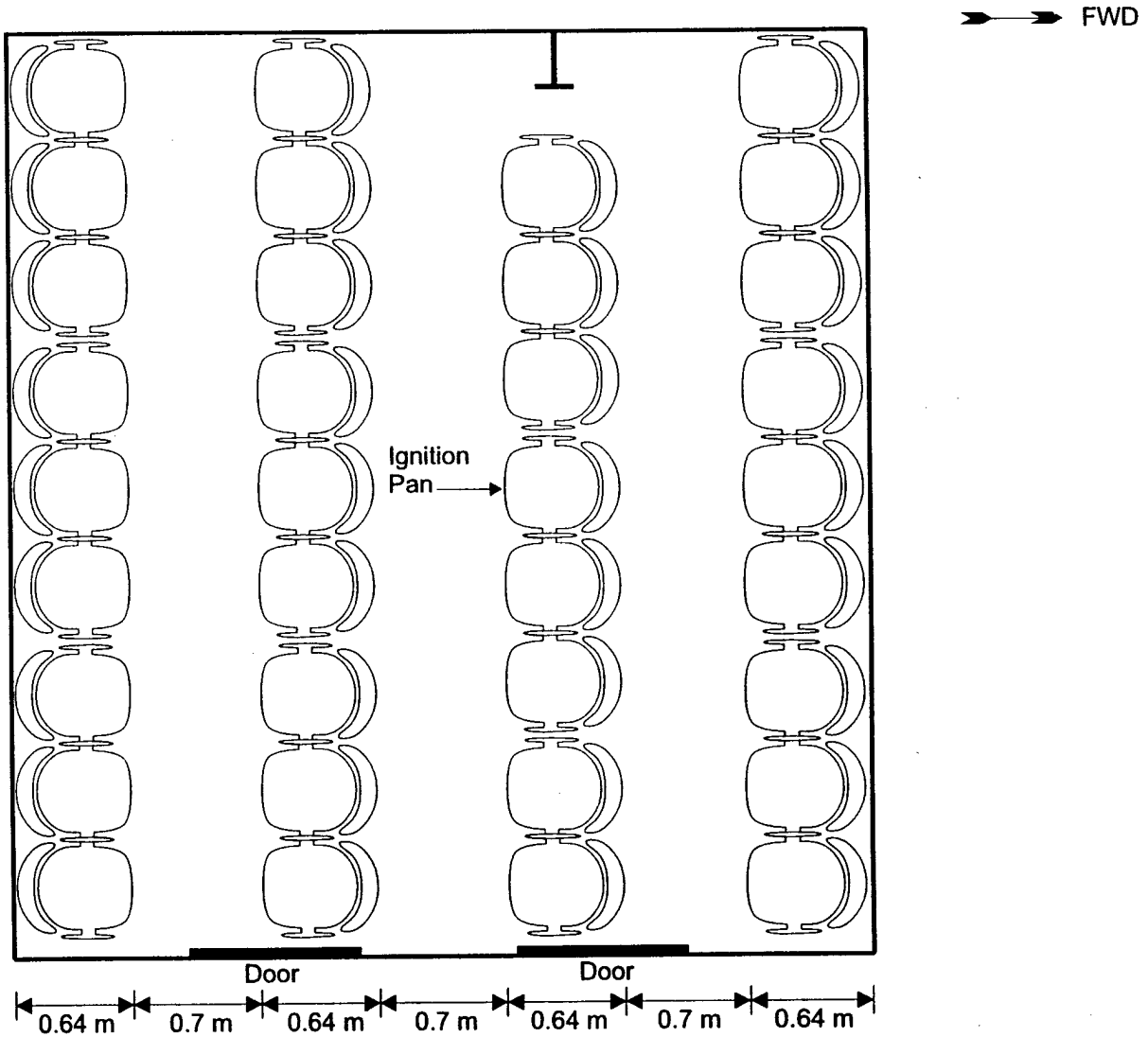

Figure 5. Plan view of normal compartment configuration

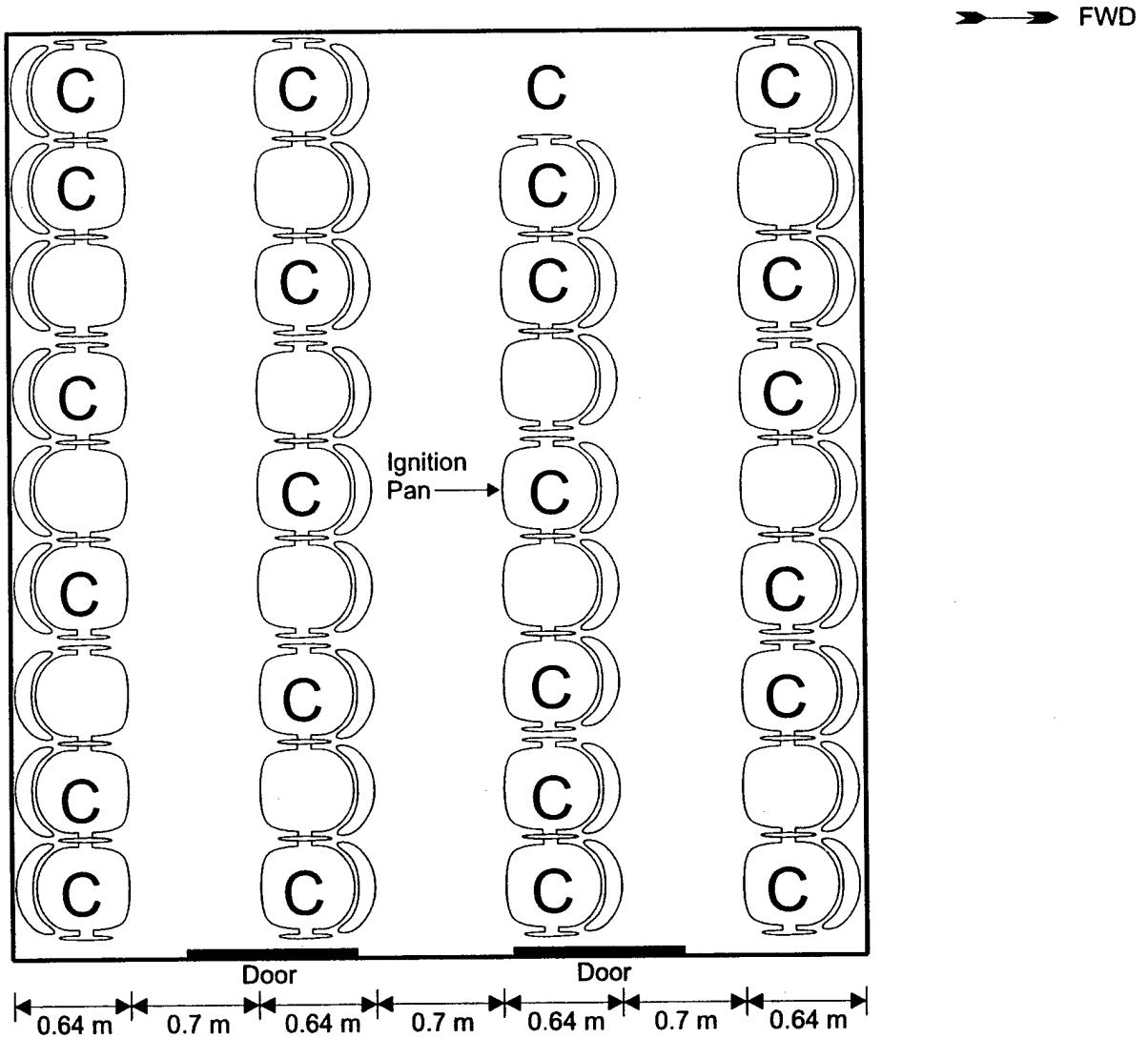

Figure 6. Compartment configuration for tests with 10 kW/m^2 fuel load density

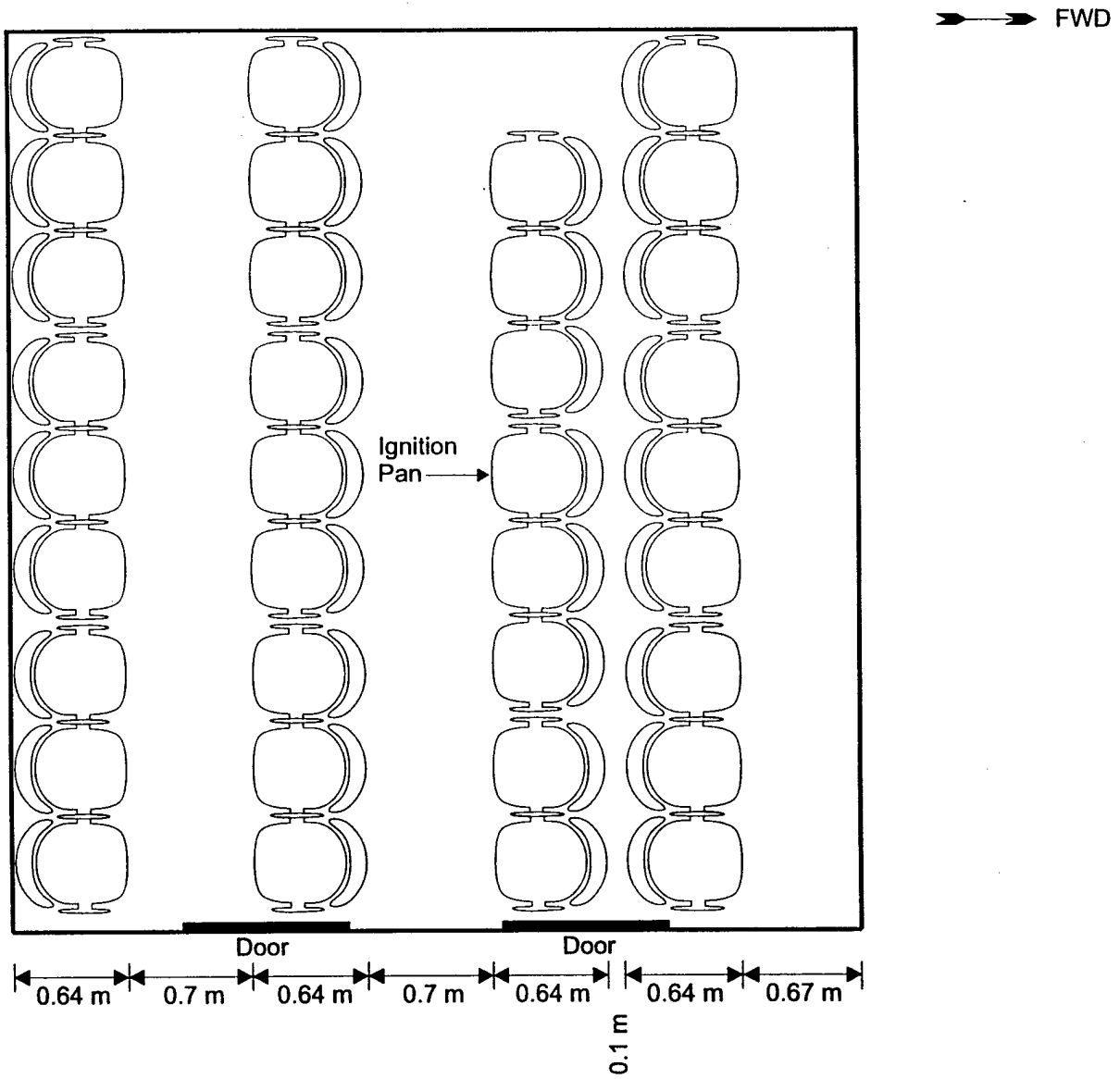

Figure 7. Compartment configuration for Test 1-4

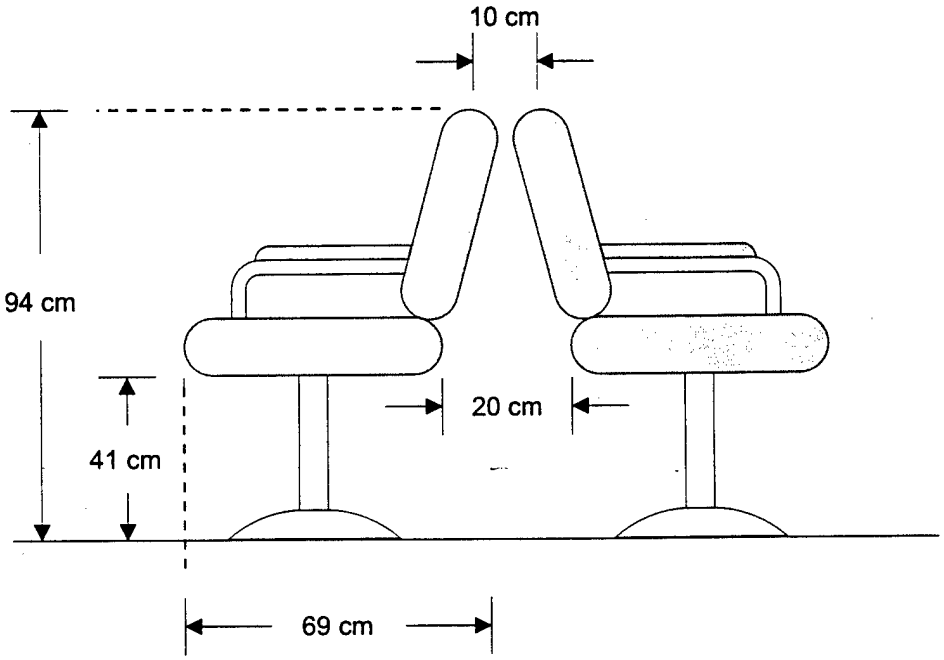

Figure 8. Seat spacing for Test 1-4

For the second test (Test 4-1), all cushions were stacked in the center of the room to present the concentrated scenario with the normal fuel load density (see Figures 9 and 10).

Table 1. Description of Tests Conducted

Test Number	Fuel Load Density	Material Type	Description
1-1	5 kg/m^2	FR	35 individual fixed seats spaced evenly with FR cushions, 10 cm pan used for ignition
1-2	5 kg/m^2	non-FR	35 individual fixed seats spaced evenly with non-FR cushions, 10 cm pan used for ignition
1-2a	5 kg/m^2	non-FR	35 individual fixed seats spaced evenly with non-FR cushions, 15 cm pan used for ignition
1-4	5 kg/m^2 - localized distribution	non-FR	35 individual fixed seats with 2 rows closely spaced and non-FR cushions, 15 cm pan used for ignition
2-1	10 kg/m^2	FR	35 individual fixed seats spaced evenly with FR cushions, additional 5 kg wood cribs placed in individual chairs within each square meter, 10 cm pan used for ignition
2-2	10 kg/m^2	non-FR	35 individual fixed seats spaced evenly with non-FR cushions, additional 5 kg wood cribs placed in individual chairs within each square meter, 15 cm pan used for ignition
4-1	5 kg/m^2 - concentrated distribution	FR and non-FR	6 individual fixed seats placed in the center of the compartment with cushions from the 29 remaining seats located on or around the seats, 10 cm and 15 cm pans used for ignition

7.0 TEST PROCEDURES

When the fuel loading was arranged and proper instrument operation was verified, all personnel were staged in their appropriate locations. Ignition was achieved with either a 10 cm diameter or a 15 cm diameter pan filled to a depth of approximately 3 cm with heptane (free-burn was approximately 10 minutes). As discussed below in Section 9.0, the 10 cm diameter pan was

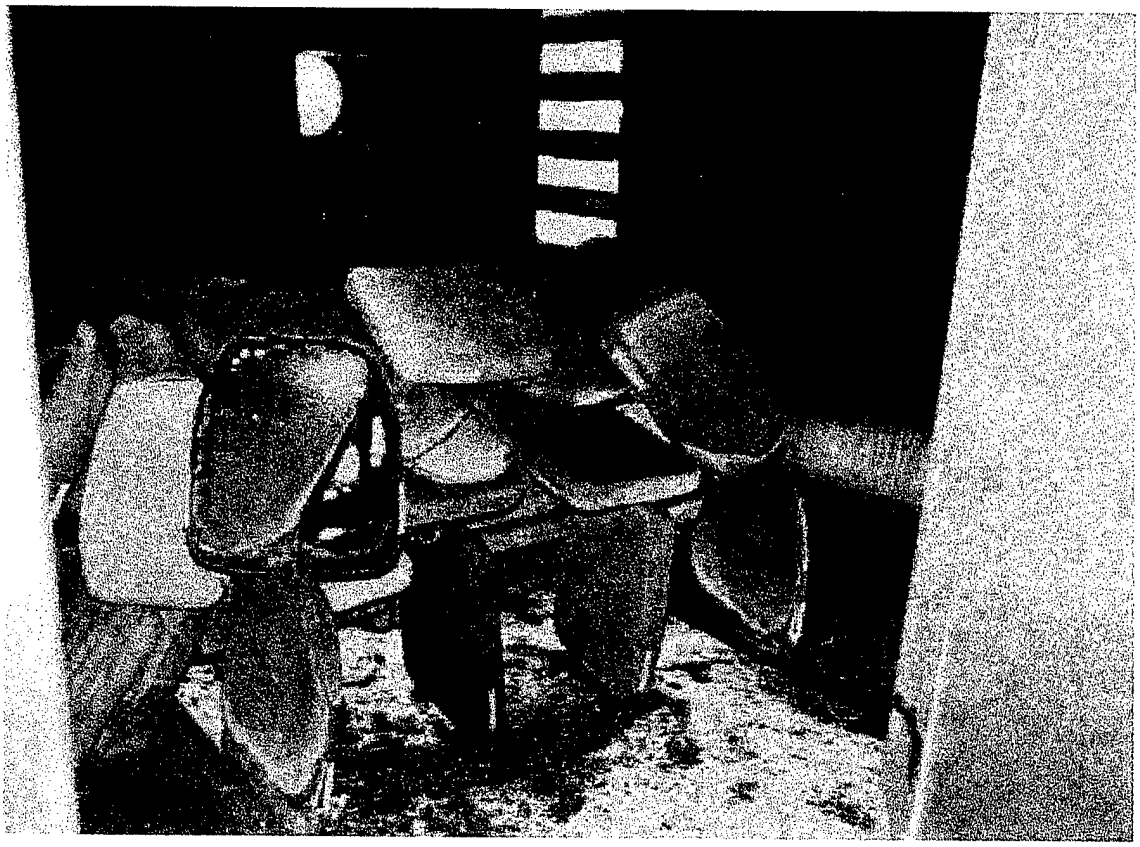

Figure 9. Compartment configuration for Test 4-1

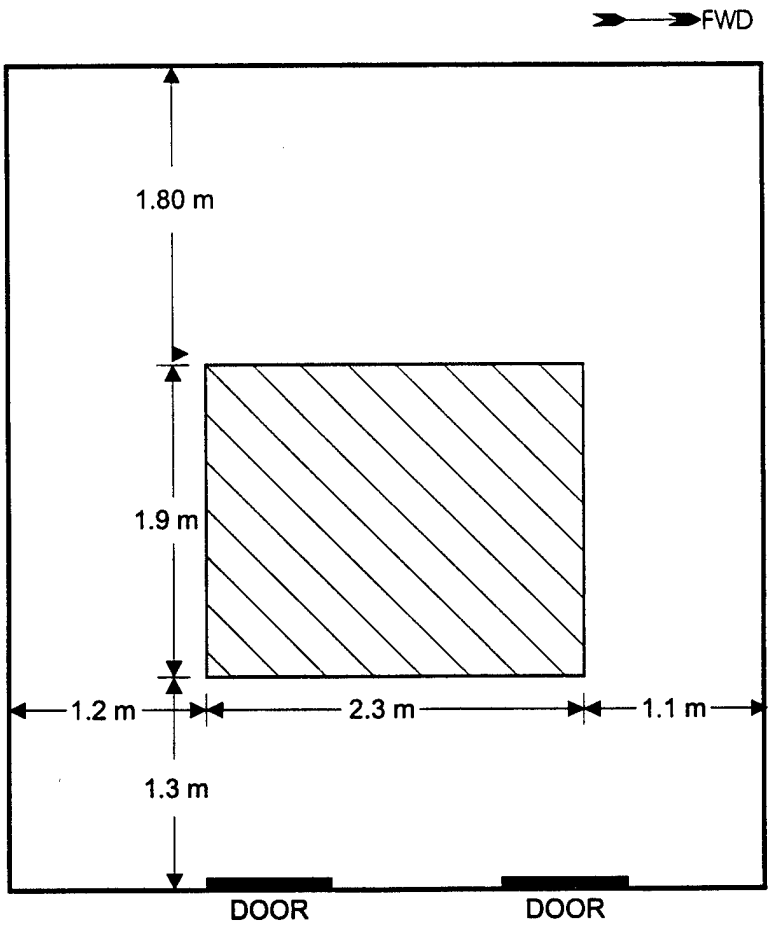

Figure 10. Fuel distribution for Test 4-1

used in tests with FR materials, and the 15 cm diameter pan was used in tests with non-FR materials. The appropriate pan was located on the deck beneath the seat identified in Figure 5. Once the heptane was ignited, the flame impinged under and in front of the seat cushion until the cushion ignited. The fire was allowed to continue until it self-extinguished or until 45 minutes had elapsed, whichever occurred sooner. In tests where there was substantial burning at 45 minutes, the fixed CO_2 system was activated to extinguish the flames.

8.0 DATA ANALYSIS

Heat release rates were calculated using the principle of oxygen consumption calorimetry [5]. These calculations used gas species concentrations (CO, CO_2, and O_2) measured in the doorway and experimentally measured air mass flow rates. The gas species concentrations at the sample point in the doorway were assumed to be representative of the exhaust gas concentrations. These concentrations were measured on a dry basis and were corrected for the transit time. Air mass flow rates were calculated from bi-directional probe and thermocouple data [3]. In order to calculate the flow rate into and out of the compartment, the neutral plane was first identified. The neutral plane is the height where the pressure differential across the door is zero. Above this height, the air is flowing out of the compartment, and below this height, the air is entering the compartment. Therefore, it could be identified by determining where the pressure differentials changed signs. Then, the measured velocities were integrated over the area which extended to the midpoint of the distance to the adjacent probe. This included cases where probes were missing. Due to erratic measurements, some bi-directional probe data were not used in the analysis. While this adjustment helped to conserve mass, mass conservation was not observed in most tests. As a result of this discrepancy, heat release rates calculated using the mass flow rate of air into and out of the compartment were substantially different. In order to resolve this difference, heat release rates using both mass flow rates were integrated to determine the total energy released during the test. These values were compared with those estimated using the mass of cushions and cribs lost and their respective heats of combustion to determine which mass flow rate measurement (in or out of the compartment) should be used. The cushion heat of

combustion to determine which mass flow rate measurement (in or out of the compartment) should be used. The cushion heat of combustion was estimated as 21000 kJ/kg based on cone calorimeter tests (Appendix A), and each cushion pair weighed approximately 1 kg. Wood cribs weighed approximately 5 kg each, and the heat of combustion was estimated as 13000 kJ/kg [6]. The carpeting was not included in this calculation since it did not burn enough to contribute a significant amount of energy. Agreement between the cumulative energy release calculated using the most suitable mass flow rate measurement and that estimated based on mass lost was better than 12%. Further details concerning this analysis are included in Appendix B.

In most cases, there was no clear layer interface in the compartment as indicated by thermocouple measurements or visual observation. The lowest thermocouple was located 0.5 m above the deck. The neutral plane was between 0.75 and 1.0 m in each test. Since the layer interface must be below the neutral plane, it is probable that the layer interface was below the lowest thermocouple. As a result, it was assumed that all thermocouples were located in the upper layer. The upper layer temperature was calculated by averaging over the entire tree height. This value will be referred to henceforth as the average compartment temperature.

9.0 RESULTS

Time-history plots for heat release rate, gas temperatures, gas species concentrations, heat flux, and ceiling panel temperatures are included in Appendix C for each test. Summaries of the results are included in Tables 2 and 3. Table 2 shows the peak compartment temperature, minimum O_2 concentration measured at 2 m above the deck, peak CO and CO_2 concentration measured at 2 m above the deck, and peak heat release rate for each test. The peak compartment temperature represents the highest average temperature (i.e., averaged over the height of the compartment) based on the three thermocouple trees (Trees 1-3). Due to the unsteady nature of the burning, peak values are reported rather than average, steady-state values.

Table 2. Summary of Test Results

Test Name	Peak Compartment Temperature (°C)	Min. O_2 Conc. at 2 m (% vol.)	Peak CO_2 Conc. at 2 m (% vol.)	Peak CO Conc. at 2 m (% vol.)	Peak Heat Release Rate (kW)
1-1	129	17.8	1.4	0.1	240
1-2a	64	19.7	0.8	0.0	90
1-4	271	11.8	4.7	0.2	740
2-1	279	14.9	n/a	0.2	560
2-2	177	16.8	2.7	0.1	370
4-1	430	1.9	10.7	1.6	2200

Table 3. Peak Ceiling Panel Temperatures (°C)

Test Name	Location 1 (Interior / Exterior)	Location 2 (Interior / Exterior	Location 3 (Interior / Exterior)	Location 4 (Interior / Exterior)	Location 5 (Interior / Exterior)
1-1	92 / 56	77 / 66	102 / 80	116 / 75	113 / 76
1-2a	36 / 25	38 / 32	108 / 47	81 / 30	64 / 45
1-4	169 / 138	247 / 233	420 / 182	387 / 163	266 / 228
2-1	273 / 232	204 / 187	331 / 225	385 / 247	273 / 227
2-2	147 / 121	153 / 143	261 / 163	231 / 146	207 / 174
4-1	524 / 365	421 / 346	657 / 500	649 / 467	619 / 436

Table 3 lists the peak ceiling panel temperature measured on both sides at each location. It should be noted that the temperature differential between the interior and exterior side of the panel was sometimes in excess of 200 °C. This result was suspicious since the thermal conductivity of aluminum is so high. In some tests, the thermocouples detached from the ceiling panels. This may account for some of the inconsistencies, particularly if the thermocouple was located near the fire plume.

The results of each test are described below.

9.1 Test 1-1

This test was the baseline with FR cushions and a distributed fuel load density of 5 kg/m^2. A photograph of the compartment prior to the test is shown in Figure 11. Five seat cushion sets (bottom and back), contained within one row, were consumed (Figure 12). This area of damage is highlighted in gray in Figure 13. A peak heat release rate of 240 kW and a peak compartment temperature of 129 °C were achieved during this fire. The peak interior ceiling panel temperature was 116 °C (Location 4), and the peak exterior ceiling panel temperature was 80 °C (Location 3).

9.2 Test 1-2

This test was identical to Test 1-1 except that non-FR cushions were used. Ignition did not take place using the ignition pan from Test 1-1 (10 cm diameter). Upon post-test examination, there was a round section on the underside of the cushion where the upholstery had pulled away to expose the foam. The foam was slightly charred but did not appear to have been close to igniting.

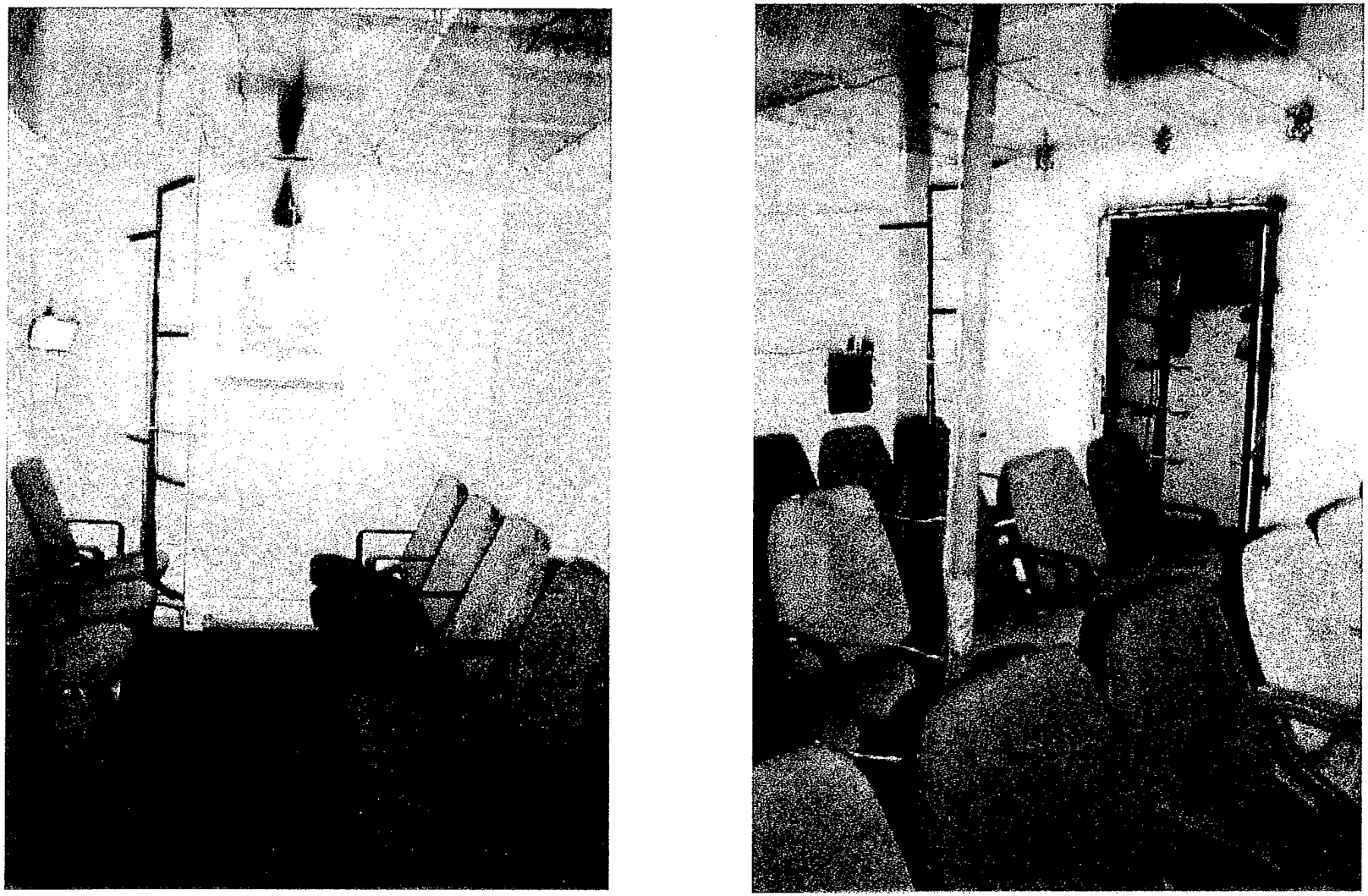

Figure 11. Compartment configuration for Test 1-1

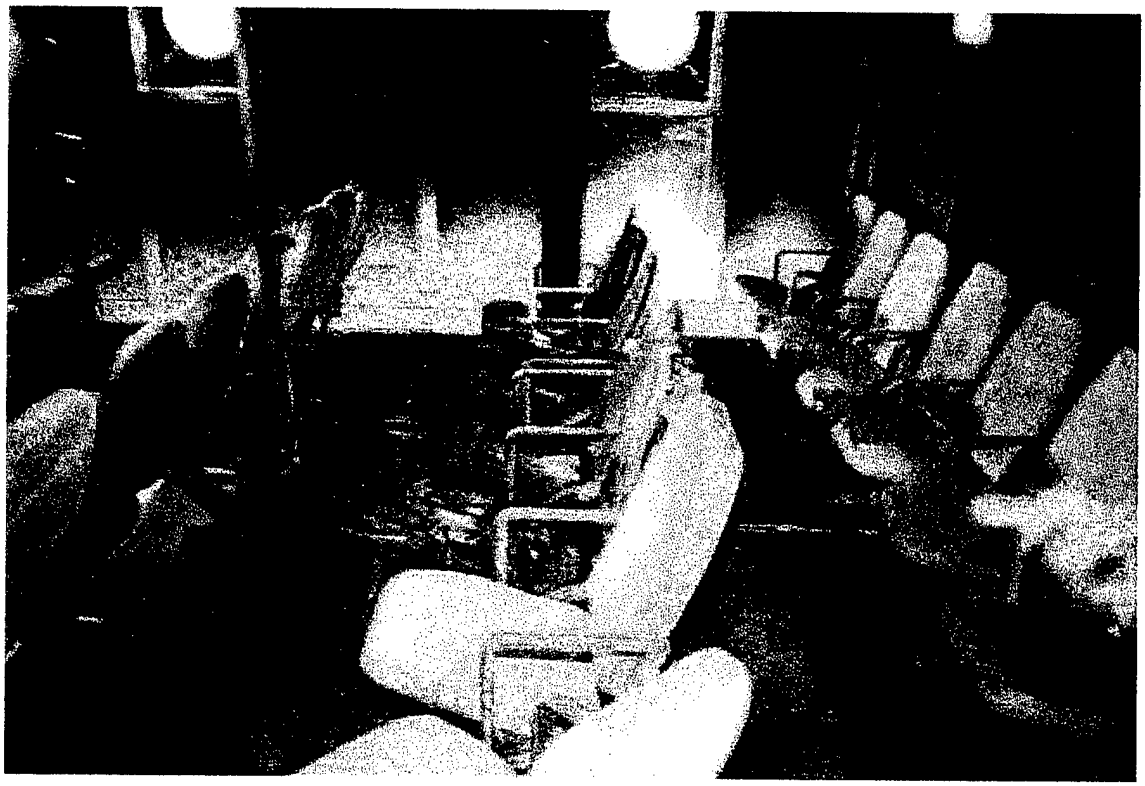

Figure 12. Test compartment after Test 1-1

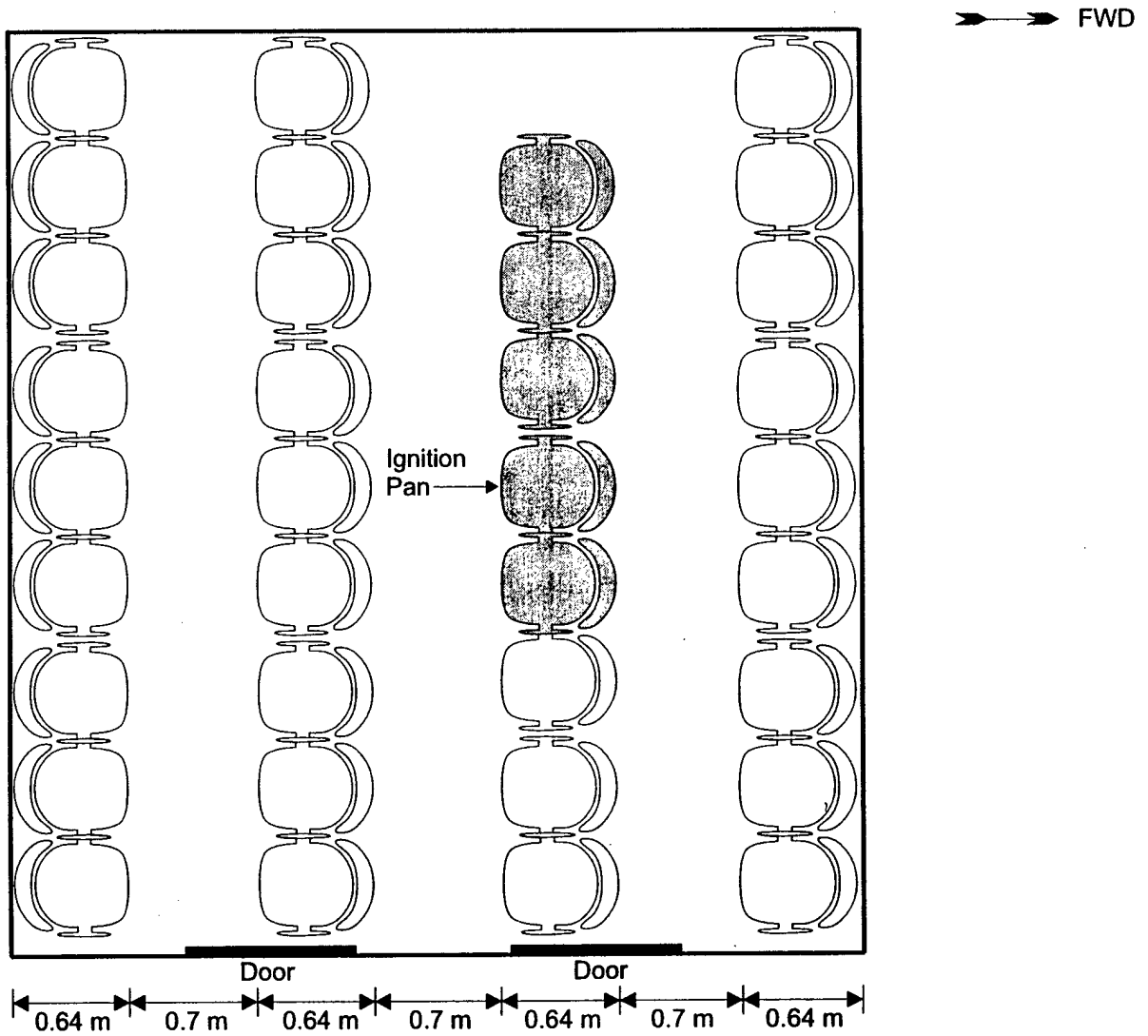

Figure 13. Test 1-1 material damage (indicated by area in gray)

9.3 Test 1-2a

This test was a repeat of Test 1-2a using a 15 cm diameter ignition pan. Cushion ignition occurred easily with this pan as compared to the smaller diameter pan. As a result, the 15 cm diameter pan was used during the remaining non-FR material tests. The 10 cm diameter pan was used in the remaining FR test. Damage was limited to the seat that the ignition pan was placed under (Figures 14 and 15). Therefore, the peak heat release rate was substantially lower than that measured in Test 1-1 (90 versus 240 kW), and the peak compartment temperature was 64 °C. The highest interior and exterior temperatures measured on the ceiling panels were 108 °C and 47 °C (Location 3), respectively.

9.4 Test 1-4

This test was identical to Test 1-2a (non-FR materials, 5 kg/m^2 fuel load density) with the exception of the fuel load distribution. A localized distribution was investigated by placing two rows of seats back-to-back about 10 cm apart (Figures 7 and 16). As seen in Figures 17 and 18, both rows of seats were consumed (17 cushion sets). However, the row aft of these seats did not sustain notable damage. This fire caused the most severe damage with the exception of Test 4-1. In addition, the peak heat release rate of 740 kW and peak compartment temperature of 271°C were the highest measured in any test with the exception of Test 4-1. Ceiling panel Locations 3 and 4 peaked at 420 and 387 °C, respectively. However, the exterior thermocouple measurements were 182 and 163 °C, respectively. This indicates that the interior thermocouples may have fallen off of the panels during the test.

9.5 Test 2-1

This test was similar to Test 1-1 (FR materials, uniform fuel load distribution) except that the fuel load density was 10 kg/m^2 rather than 5 kg/m^2. The additional fuel load was created by placing twenty-four wood cribs (approximately 5 kg each) on top of the bottom seat cushion throughout the compartment as shown in Figure 19. Nine cushion sets and 5 cribs were

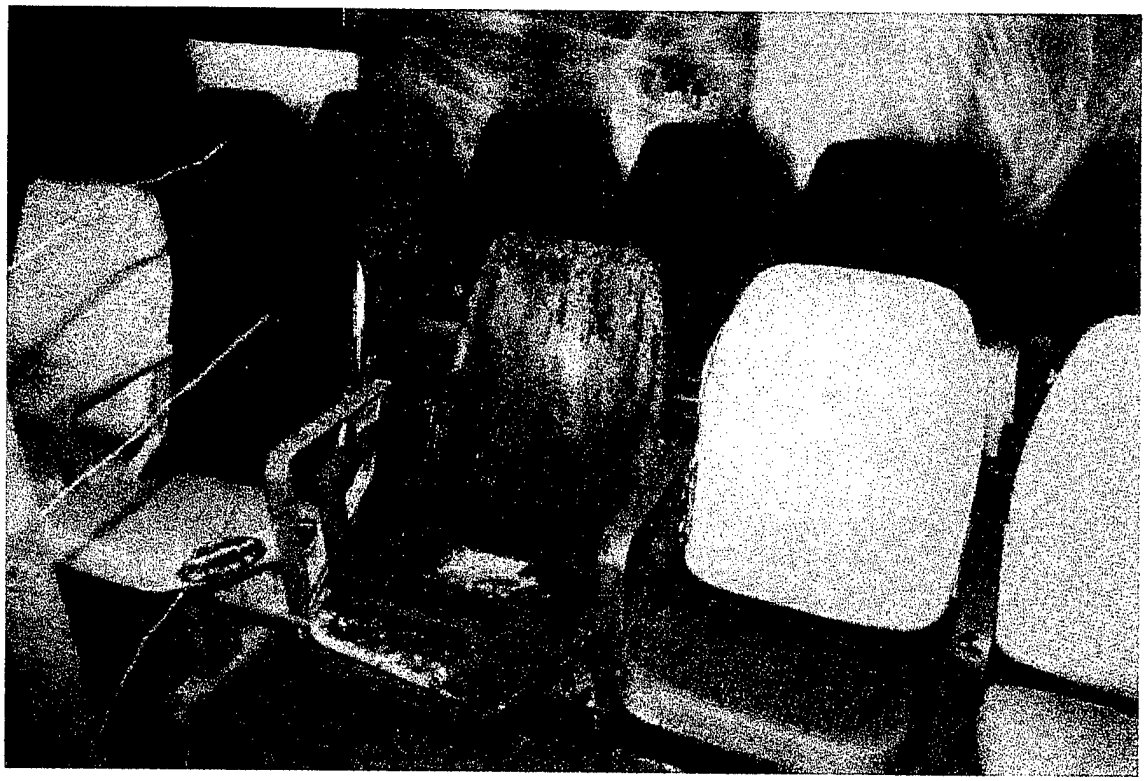

Figure 14. Test compartment after Test 1-2a

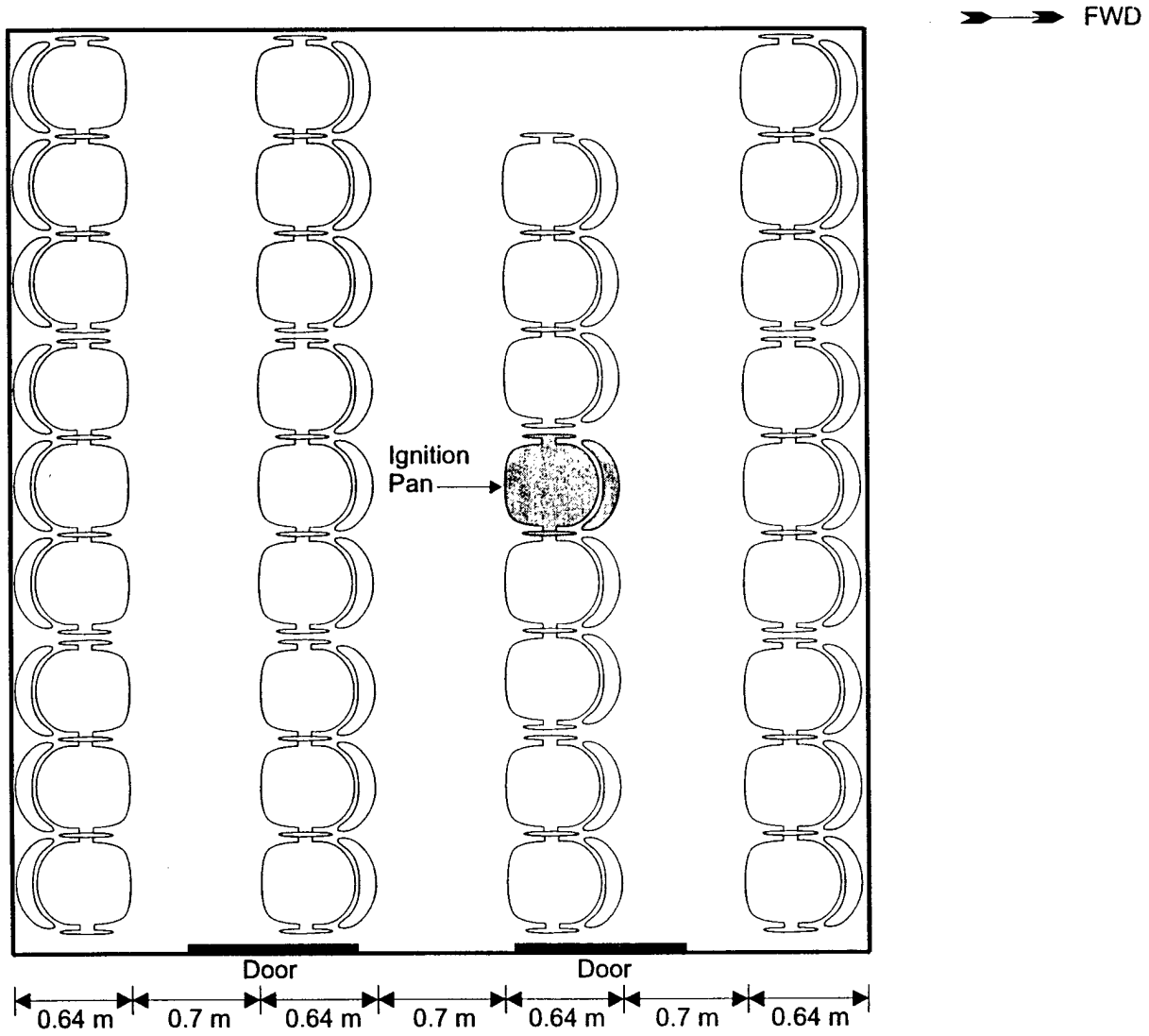

Figure 15. Test 1-2a material damage (indicated by area in gray)

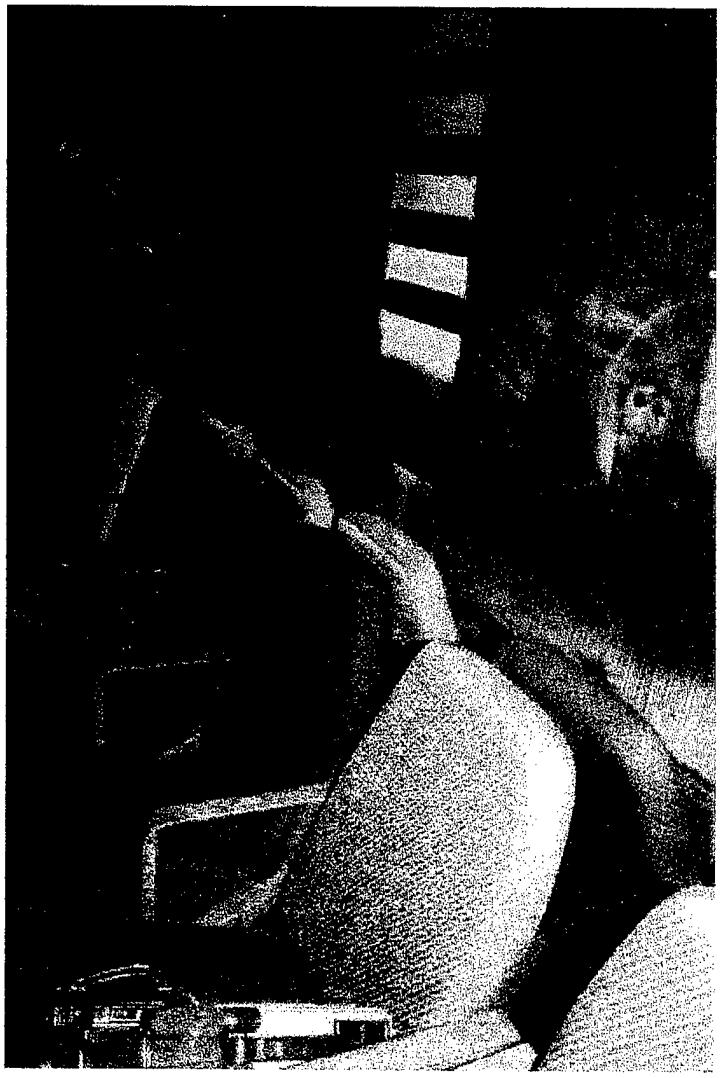

Figure 16. Test 1-4 configuration

Figure 17. Test compartment after Test 1-4

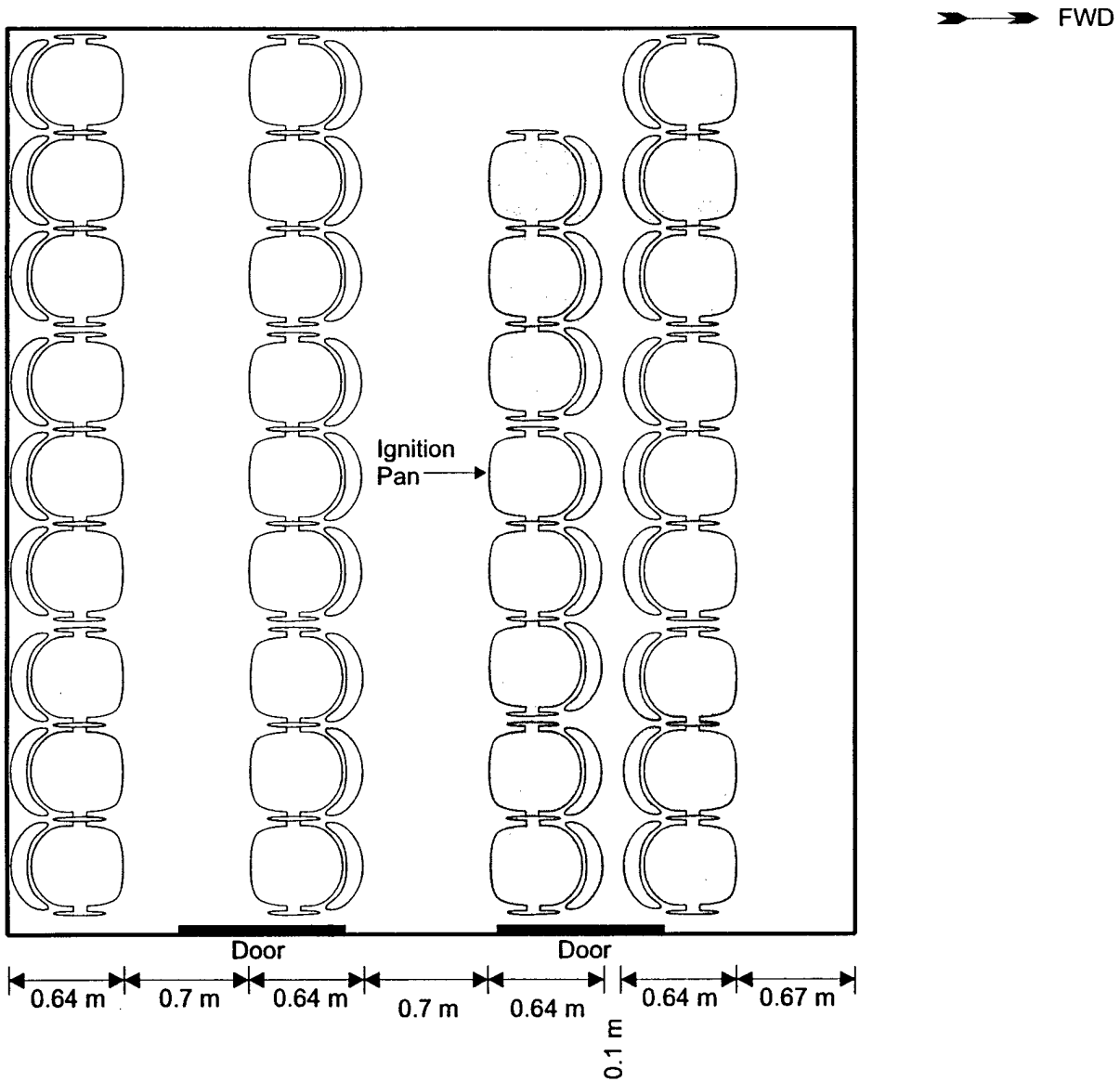

Figure 18. Test 1-4 material damage (indicated by area in gray)

Looking outboard through aft door

Looking outboard through fwd door

Figure 19. Compartment configuration for Test 2-1

consumed (Figures 20 and 21). The fire spread from the row of origin to the row aft of it. The peak heat release rate was 560 kW and the peak compartment temperature was 279 °C. The highest interior and exterior ceiling panel temperatures of 385 °C and 247 °C, respectively, were measured at Location 4.

9.6 Test 2-2

This test was identical to Test 2-1 (uniform fuel load distribution, 10 kg/m^2) with the exception that the seat cushions were composed of non-FR materials instead of FR materials. The damage was less extensive than that incurred in Test 2-1. Six cushions and four cribs, all contained in one row, were consumed (Figures 22 and 23). The peak heat release rate was 370 kW, and the peak compartment temperature was 177 °C. The peak interior ceiling panel temperature was 261 °C (Location 3), and the peak exterior ceiling panel temperature was 174 °C (Location 5).

9.7 Test 4-1

The purpose of this test was to evaluate the fire severity for a very localized fuel load and examine how the results differed from the normal configuration. Two of the three-seat frames were placed back-to-back in the center of the fire compartment. Thirty-five cushion sets, approximately 31 non-FR and 4 FR, were then arranged on top of these frames (Figure 9). Both pans were used for ignition, each located underneath a middle seat on opposite sides of the pile. Ignition was almost immediate, and all cushions burned completely (Figure 24). The peak heat release rate was 2200 kW, and the peak compartment temperature was 430 °C. This fire had the highest peak heat release rate and average compartment temperature; however, the configuration was not realistic. Temperatures as high at 657 °C were measured on the ceiling panels (Location 2). However, large temperature differentials were noted between the interior and exterior side of the panels. As a result, it is uncertain whether the thermocouples remained attached throughout the test.

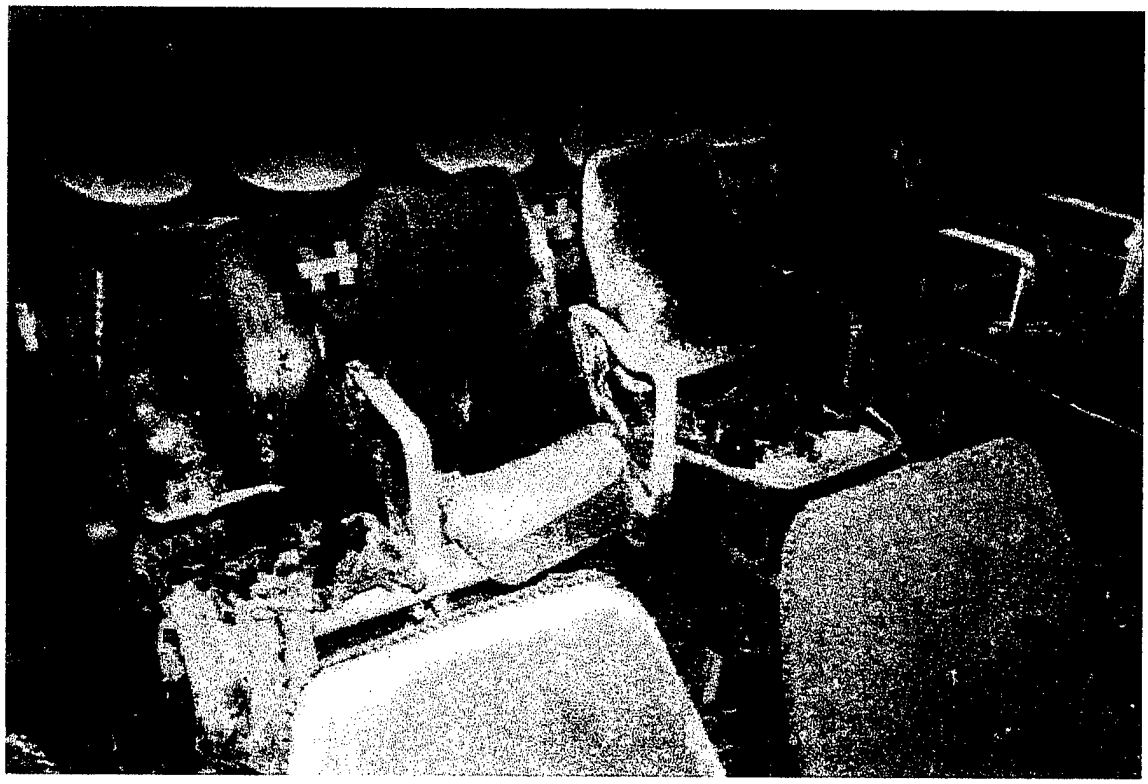

Figure 20. Test compartment after Test 2-1

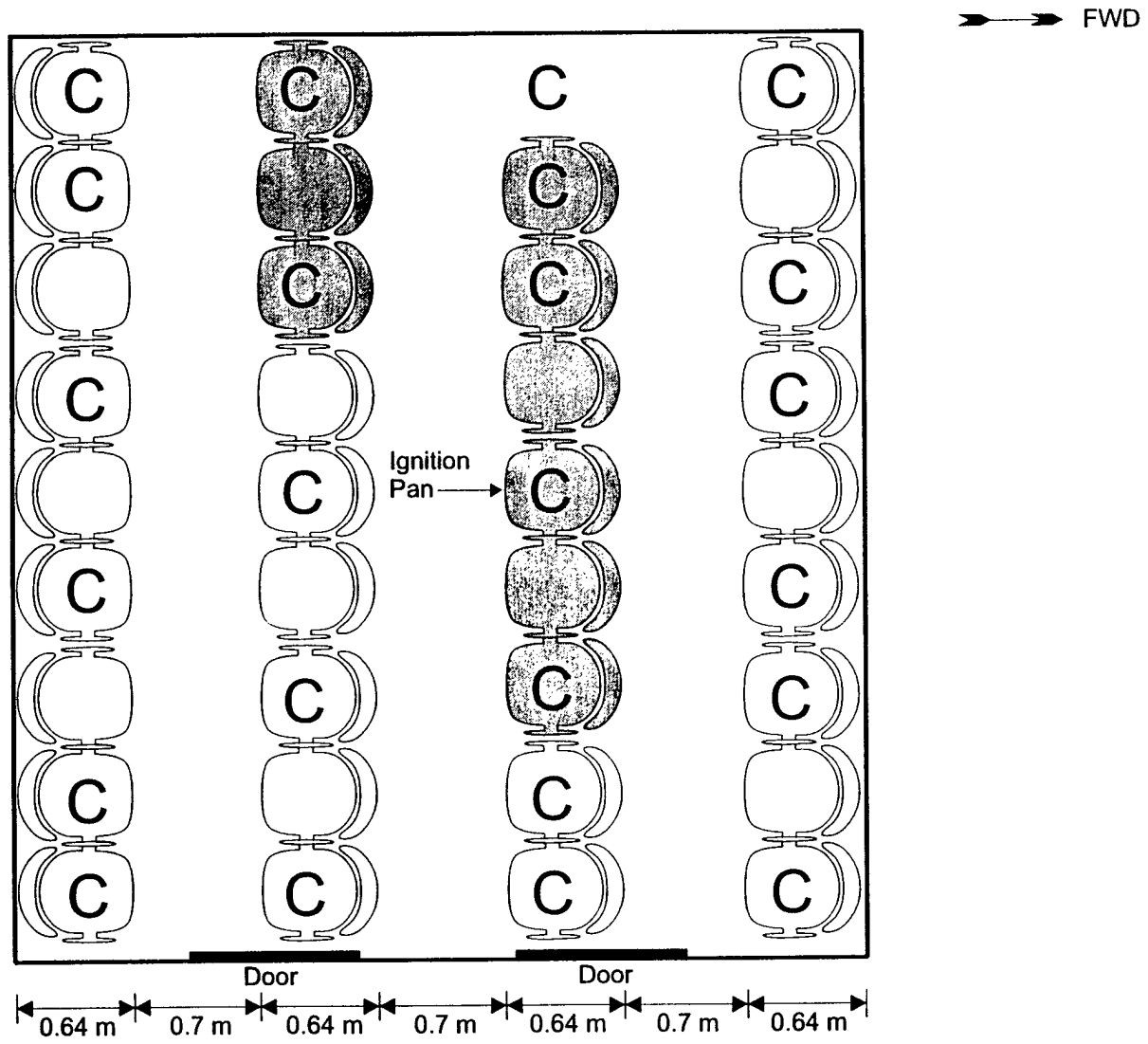

Figure 21. Test 2-1 material damage (indicated by area in gray)

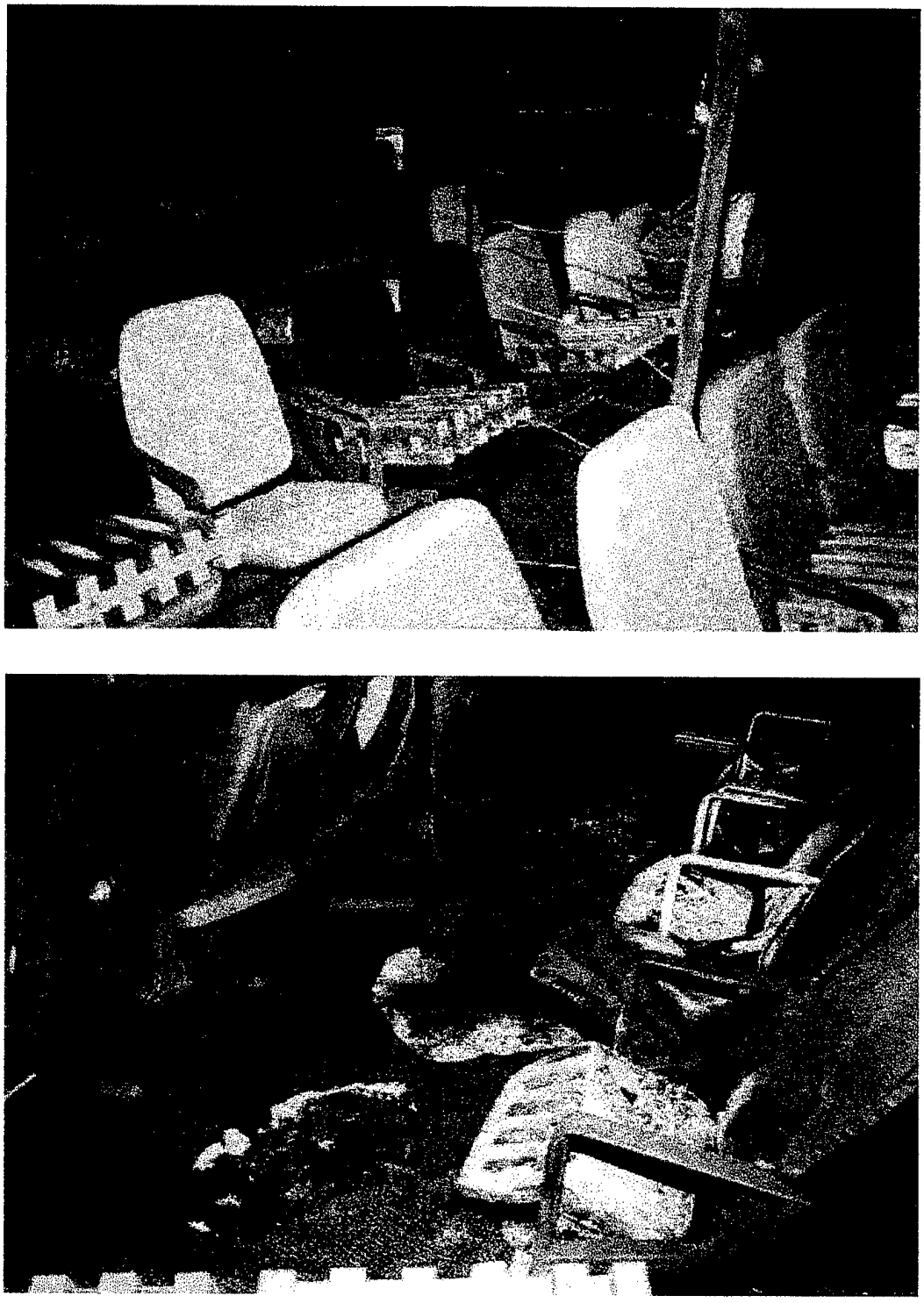

Figure 22. Test 2-2 configuration and material damage

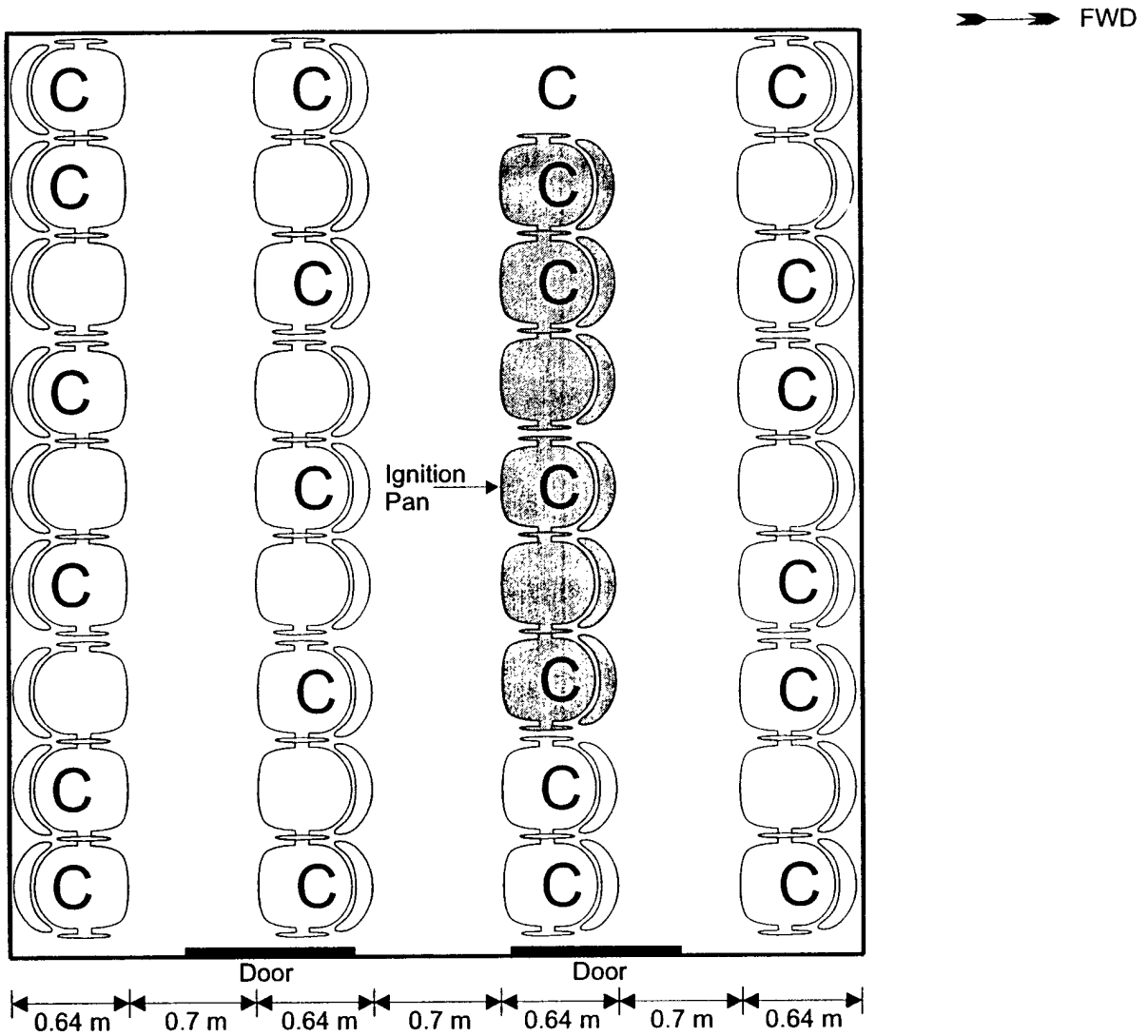

Figure 23. Test 2-2 material damage (indicated by area in gray)

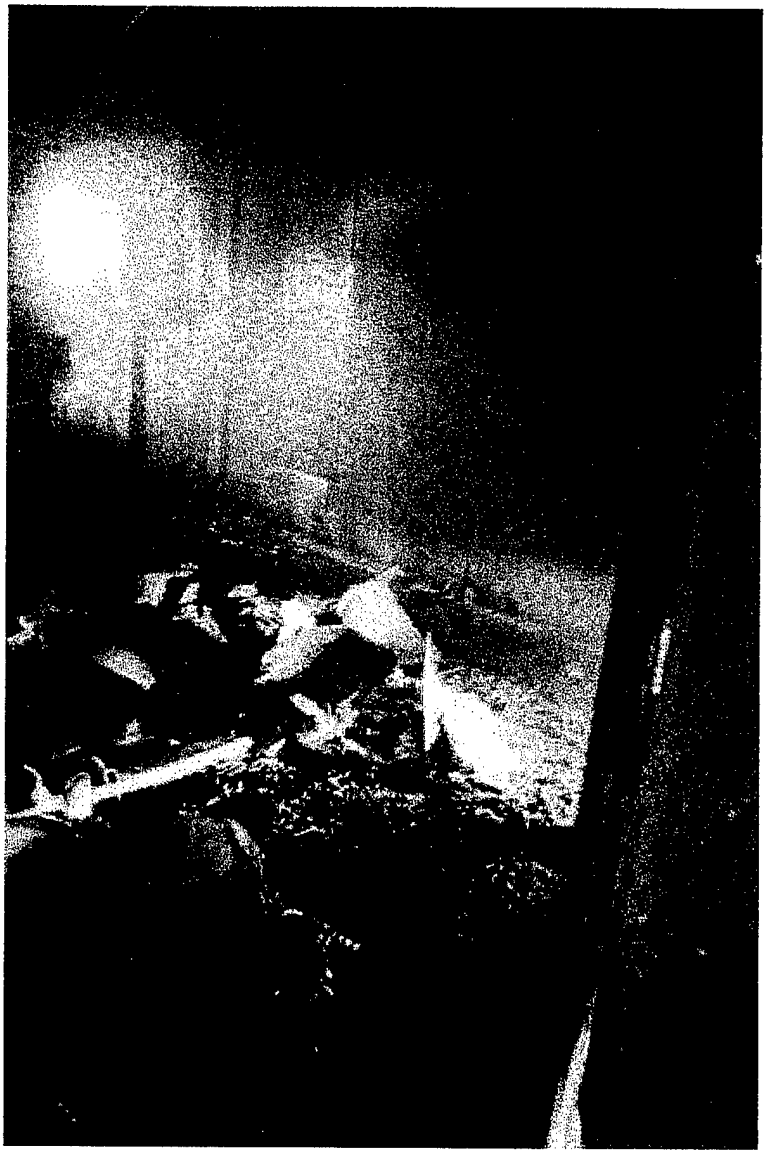

Figure 24. Test compartment after Test 4-1

A summary of the material damage is shown in Table 4. This table includes the estimated time to cushion ignition and the test duration. The final two columns list the material lost during the test (i.e., number of cushion sets and wood cribs). A cushion set consisted of a seat bottom and seat back. Cushion sets and cribs that were consumed by at least 50 percent are included in this tabulation as consumed. It is important to note that more damage occurred with FR cushions than with non-FR cushions. No fire spread was noted across the carpet except where driven by material that had dripped off of the cushions.

Table 4. Summary of Material Damage

Test number	Estimated time to ignition (seconds)	Test duration (minutes)	Number of cushion sets burned (35 total)	Number of wood cribs burned (24 total)
1-1	435	45	5	n/a
1-2	n/a	Cushion did not ignite prior to heptane burnout at 567 sec.	0	n/a
1-2a	48	15	1	n/a
1-4	94	45	17	n/a
2-1	412	45	9	5
2-2	76	45	6	4
4-1	<120	45	35	n/a

Both video camera views became obscured within 10 minutes after cushion ignition. As a result, it was not possible to determine how quickly the fire spread from cushion to cushion or how each cushion burned. In addition, it was not possible to characterize the flame spread pattern.

10.0 DISCUSSION

The use of aluminum versus steel for ship construction is beneficial because it is lighter. The tradeoff that occurs with the use of this lighter material as compared to steel is that it fails structurally at lower temperatures and it has a lower melting temperature [7]. Half of the material strength will be lost when the material reaches 232 °C, and most will be lost when it reaches 370 °C [7]. Depending on the alloy, aluminum will then melt between 593 and 649 °C [7]. During some fires aboard ships with aluminum hulls, the ship was lost because the hull was not insulated well enough to prevent melting [7]. Therefore, there is generally a requirement for aluminum bulkheads and hulls to be insulated. Studies have been performed to evaluate the performance of these passive fire protection materials [7-10]. Type 5A spaces are unique in this respect since there is a reduced requirement for the aluminum ceilings and bulkheads to be insulated [1]. This is due to the requirement for low fuel load density and for the use of non-combustible or fire resistant materials in these spaces [1]. As a result, there are little data available concerning the structural performance of aluminum when exposed to fire. One documented study evaluated the integrity of aluminum hatch covers when exposed to a pool fire [11]. Since the fire obscured the view of the hatch during much of the test, the investigator was unable to determine the exact time of failure. However, in each of three tests, failure had occurred within the first 17 minutes of the fire. In two of these tests, the hatch temperature was at least 800 °C at the time of failure and in the other test, the temperature was at least 600 °C.

In the current experiments, aluminum ceiling panel temperatures as high as 657 °C were measured. However, this was not achieved with a realistic fuel load distribution. Also, it was not possible to determine when thermocouples detached from the panels. In some tests, the temperature difference between the interior and exterior surface of the ceiling was in excess of 200 °C. In order to determine whether this temperature differential was realistic, several experiments were conducted. For these experiments, a 10 cm by 10 cm section of the aluminum ceiling panel was heated using a radiant heater. A small hole was drilled on either side of this sample, and 3 mm Type K, inconel sheathed thermocouples were inserted. These thermocouples were the same type as those used in the shipboard tests. Temperatures on the exposed side

reached values as high as 175 °C. The maximum difference between the temperature on the exposed and unexposed side was 40 °C. This result indicates that in tests where large temperature differentials were measured, the thermocouples may have detached from the ceiling panels, and gas temperatures were recorded.

None of the ceiling panels burned through during these tests. In some cases, the panels warped and became unbolted at several points. The aluminum panels were bolted in a minimum number of locations so that panel replacement would be more efficient. As a result, it is not probable that parts of the aluminum ceiling would fall down as easily in an actual Type 5A space.

The results presented in Section 9.0 show that a greater amount of damage resulted when the fuel load density was increased. This is evident when comparing Test 2-1 (9 cushion sets and 5 cribs lost) with Test 1-1 (5 cushion sets lost) and Test 2-2 (6 cushion sets and 4 cribs lost) with Test 1-2a (1 cushion set lost). Tests 2-1 and 2-2 both used a fuel load density of 10 kg/m^2 while Tests 1-1 and 1-2a both used 5 kg/m^2. The material damage was more than twice as high when the fuel load was doubled. In addition, the FR cushions performed worse than the non-FR materials as shown by comparing Test 1-2 (1 cushion set lost) with Test 1-1 (5 cushion sets lost) and Test 2-2 (6 cushion sets and 4 cribs lost) with Test 2-1 (9 cushion sets and 5 cribs lost). This result is surprising; however, material identification was confirmed by the distributor. Furthermore, it was also observed in cone calorimeter tests that the non-FR material was more difficult to ignite than the FR material. The fire load distribution also had a significant impact on the test results. The damage incurred during Test 1-4 (17 cushion sets lost) was more severe than that in Test 1-2a (1 cushion set lost). Test 1-4 used a back-to-back seat configuration while 1-2a used the normal seat configuration. This result suggests that it is important to maintain the maximum amount of space possible between the seat rows and to avoid placing seats back-to-back. In all tests, increased material damage corresponded to higher peak heat release rates and peak compartment temperatures.

10.1 Aluminum Heat Transfer Analysis

Since ignition was near the bottom center of the compartment during these tests, all types of bulkhead and/or ceiling exposure were not examined. Another important scenario would occur when a fire starts near a bulkhead and the flames impinges on the aluminum bulkhead or if flames directly impinge on the aluminum ceiling. Since visibility via the video cameras was lost during the tests, it is uncertain if there was ceiling flame impingement. In order to examine this type of exposure, a series of tests that simulated a fire against an aluminum bulkhead was conducted. Aluminum surface temperatures were measured and compared with those predicted using one- and two-dimensional finite element modeling. Upon good agreement with experimental and predicted results, the model was used to estimate the fire size necessary to achieve aluminum temperatures in the range of the melting temperature (i.e., 600 °C).

Experiments were conducted by vertically orienting a small section of the aluminum ceiling panel adjacent to a propane sand burner. The panel section was 61 cm by 61 cm and was instrumented with Type K, 22 gauge, thermocouples. Eight thermocouples were welded along the centerline of each side of the panel using a thermocouple welder (Hot Spot Thermocouple Welder manufactured by DCC Corporation). These thermocouples were spaced 6 cm apart beginning 9 cm from each edge. The panel was arranged so that the line of thermocouples was vertical. The 28 cm by 28 cm propane sand burner was positioned such that the edge of the burner was 6 cm from the aluminum plate. The propane flow rate was regulated using Dywer rotameters. One of these rotameters had a range of 0-100 standard cubic feet per hour (SCFH) (part no. RMC-102-SSV) while the other rotameter had a range of 0-200 SCFH (part no. RMC-103-SSV). The range of the rotameter used was dependent on the desired fuel flow rate. Both rotameters were calibrated using a dry gas meter (American Meter Company, part no. DTM200A) to account for the density difference between air and propane. For most tests, a 1.52 m wide by 1.09 m high piece of gypsum board was placed behind the aluminum plate. The purpose of the board was to insulate the back side of the plate (to generate higher plate temperatures) and to help minimize edge effects.

Ten tests were conducted. The results from these tests are shown below in Table 5. Three of the tests have been omitted since there were problems with the flame leaning due to the air currents in the room. The peak temperature and the corresponding height above the burner have been included. In Tests 1, 2, and 4, a range of heights is given since there was no discernable difference between the temperatures measured at these locations. Unless stated otherwise in the comments, the burner was centered with respect to the thermocouples and the gypsum board was in place.

It is noted that in Test 1, the burner was not centered with respect to the center of the plate as it was in the other tests. The purpose of this test was to assess the importance of lateral conduction through the plate. The similarity of the results from Tests 1 and 2 show that lateral conduction effects may be significant. Since the plate was small in comparison to the burner, it was not possible to determine this conclusively. As a result, both one-dimensional and two-dimensional modeling was performed to further examine lateral conduction effects and will be discussed below.

It is also noted in many tests that the temperature did not reach steady state. This occurred for two reasons. When the gypsum board was used, it was heated at the same time as the aluminum. This increased the thermal mass dramatically which resulted in a much larger system time constant. In some tests, the temperature was still rising after the fire had been burning for 30 minutes. Also, due to the test compartment limitations, the burner could not operate with heat release rates of 84 kW and higher for a time period which allowed the plate to reach steady-state conditions. The fact that many of these results do not represent steady-state conditions is important since the steady-state temperatures may be significantly higher than those shown in Table 5.

Table 5. Summary of Aluminum Panel Tests

Test Number	Burner Heat Release Rate (kW)	Peak Temperature (°C)	Height of Peak Temperature Above Top of Burner (cm)	Comments
1	14	57	17-41	burner center 27 cm from plate center, temperature not steady state
2	14	62	10-17	temperature not steady state
3	25	300	17	temperature not steady state
4	60	400	27-39	temperature steady state
7	100	440	32	temperature nearly steady state
8	84	340	32	gypsum board removed, temperature not steady state
9	60	370	32	gypsum board removed, temperature steady state

The highest aluminum temperature of 440 °C was achieved with a burner heat release rate of 100 kW and with the plate insulated. This is at least 150 °C lower than the melting temperature. Since larger fires could not be tested, finite element methods were used to estimate the fire size necessary to heat the aluminum to its melting temperature. The software used was STAR*CD which is a general purpose 3-dimensional computational fluid dynamics code (CFD) [12]. For this application, the package solved the energy equation using a finite volume based method.

The model was developed for an uninsulated plate and accounted for two-dimensional heat transfer incorporating the mechanisms shown in Figure 25 where:

$\dot{q}''_{incid}$ = incident radiative heat flux, (kW/m^2),

$\dot{q}''_{conv(h)}$ = convective heat flux on exposed side, (kW/m^2),

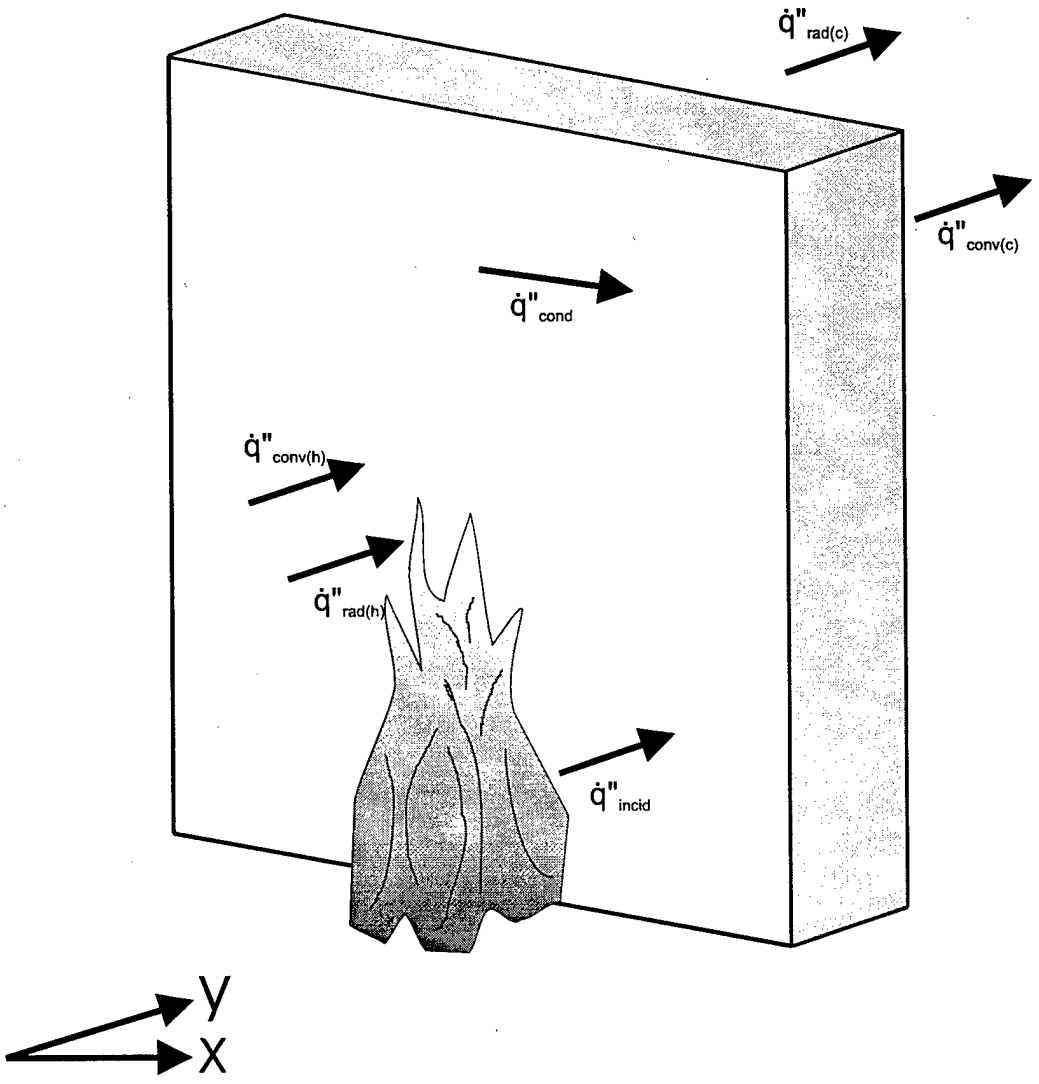

Figure 25. Schematic of heat transfer mechanisms

$\dot{q}''_{rad(h)}$ = surface re-radiation on exposed side, (kW/m^2),

$\dot{q}''_{cond}$ = lateral conduction through slab, (kW/m^2),

$\dot{q}''_{conv(c)}$ = convective heat flux on unexposed side, (kW/m^2), and

$\dot{q}''_{rad(c)}$ = surface radiation on unexposed side, (kW/m^2).

The model was initially evaluated using incident heat flux values that were measured during several tests. The predicted steady-state temperature was compared with those measured during experiments. An emissivity of 0.9 was assumed since the front surface quickly turned black and the back surface was tarnished. This emissivity would also be suitable for Type 5A bulkheads and ceilings since they would be painted. The value used for the thermal conductivity was 180 kW/m*K. Since the convective heat transfer coefficient is difficult to calculate accurately, it was varied within the range of reasonable coefficients until the predicted and measured temperatures agreed well. The value which was used for all values presented in this report was 20 kW/m^2*K. Using these parameters, agreement between the measured and predicted temperatures was within 30 °C.

The transient solution was also evaluated to determine how long it takes for the temperature to level off in the 61 cm by 61 cm plate. Results showed that the peak temperature of the uninsulated plate will begin to level off after 10 minutes. As shown in Figure 26, this result agrees well with the data obtained experimentally.

By eliminating the contribution from lateral conduction and using the same system parameters, predictions were made using a one-dimensional heat transfer model. A comparison of the one- and two-dimensional results is shown in Figure 27. In all cases, the one-dimensional results are higher than the two-dimensional results. However, the difference between the two values decreases as the heat flux increases. Even at low heat fluxes, this difference is not considered significant although the two-dimensional results are more accurate.

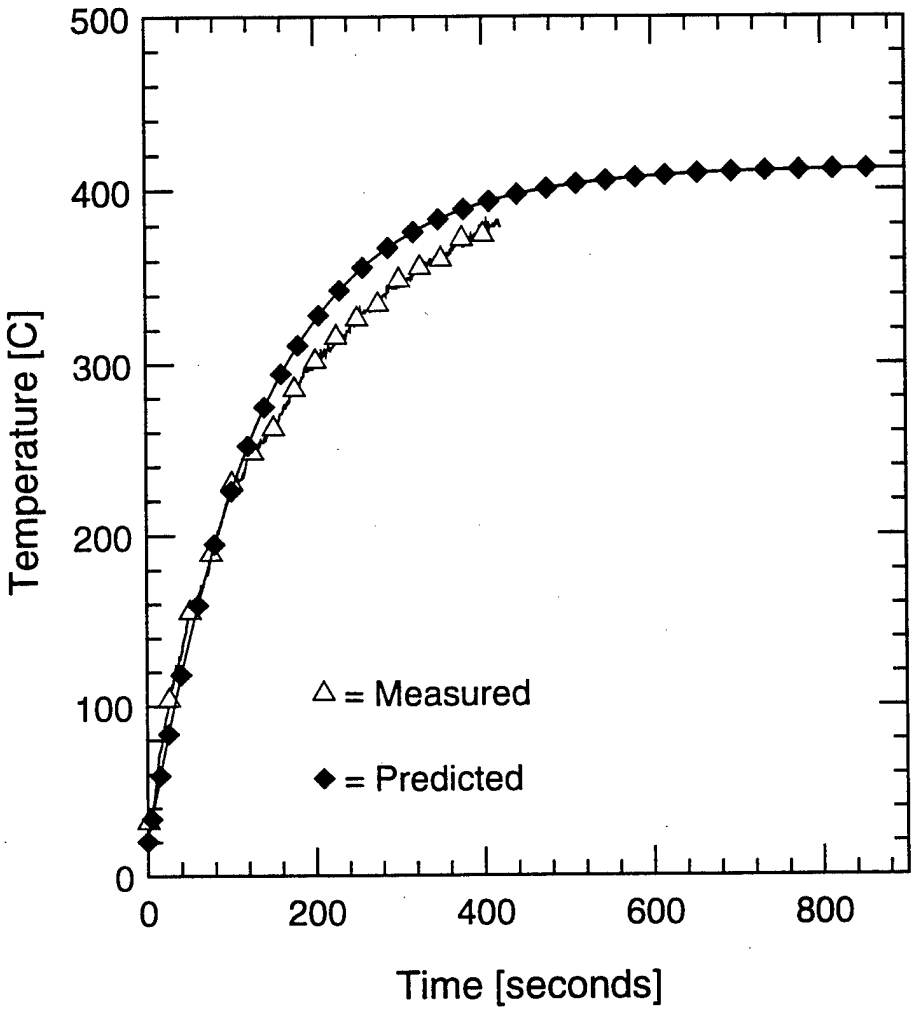

Figure 26. Predicted and measured plate temperature time histories

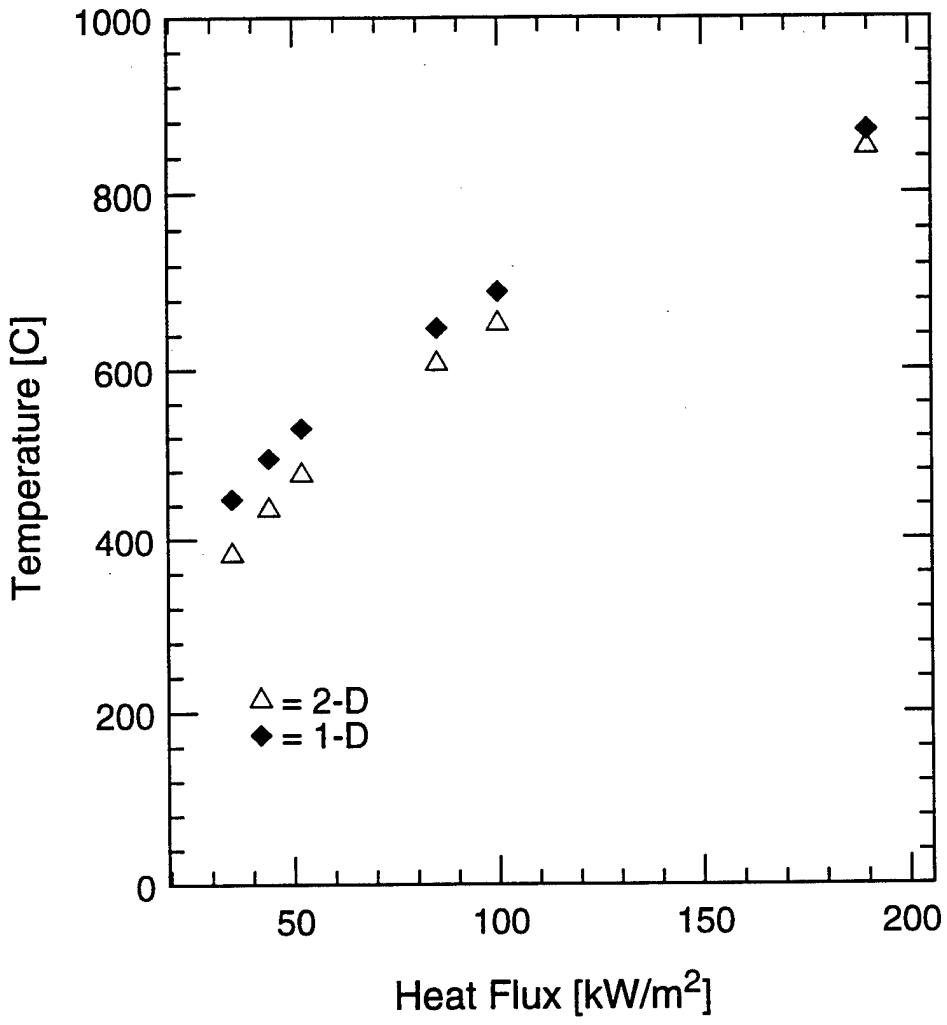

Figure 27. Comparison of one- and two-dimensional temperature prediction models

From the two-dimensional data presented in Figure 27, it is evident that the panel will approach its melting temperature when the applied flux is approximately 80 kW/m^2. In order to relate this flux to a fire size, an experimental correlation was used. This correlation was developed by Back et. al. [13] and is applicable for fires against a wall. It was validated for fire sizes in the range of 50 to 500 kW. Using this correlation, an estimated fire size of 180 kW corresponds to a flux of 80 kW/m^2.

It should be noted that several heat flux values were measured in the current experiments. In all tests, the measured fluxes were lower than those predicted by the correlation. In some cases, the difference was as much as 25 percent. One explanation is that the burner separation in these experiments was larger than that in Back's experiments. It is well known that the heat flux will decrease when the burner separation distance is increased. As a result, it should be recognized that this approach only serves as an estimation of the fire size necessary to achieve melting temperatures for fires adjacent to a bulkhead. Furthermore, the length of exposure must also be considered when identifying hazardous fire exposures. As stated above, the temperature will begin to level off after 10 minutes of steady exposure.

10.2 Comparison of Test Results to SAFE Algorithms

Experimentally measured heat release rates and temperatures may be compared with those predicted using algorithms outlined in SFSEM. SFSEM incorporates fire growth and temperature rise models to predict whether a compartment will reach flashover in the event of a fire. A proportionality constant, alpha (kW/sec^2), must first be defined to dictate the modeled fire growth rate. The fire growth rate model selected is dependent on the type of fuel and how it is distributed within the compartment. The maximum heat release rate, Q_{max}, must also be specified. The predicted heat release rate will then be defined as:

$$\dot{Q} = minimum\ (\alpha t^2,\ \dot{Q}_{max})$$

While fire growth rates and maximum heat release rates may be determined by the user, Table C-1 in the Theoretical Basis of the SFSEM lists some values that can be used as guidelines [2]. These values were determined primarily based on experiments. For the purpose of this discussion, several of these models will be used for comparison with the current experimental results. These models, their associated growth rates and $\dot{Q}_{max}$ equations are listed in Table 6.

Table 6. Fire Growth Rates and Maximum Heat Release Rates for Several Fire Growth Models Defined in SFSEM [2]

Number	Fire Growth Model	Alpha (kW/sec^2)	Q_{max} (kW)
8	Office spaces	0.7 for F>6 0.3 for F<6 0.1 for vent limited	7.5*A for F>6 5*A for 6≥ F>3 3*A for F≤6
9	Lounge spaces	0.3 for F>4 0.2 for F<4 0.01 for vent limited	5*A for F>4 2.2.5*A for F≤4 1.2*A for vent limited
10	Berthing areas	0.1 for F>4 0.01 for F<4 0.01 for vent limited	3.75*A for F>4 2.9*A for F<4 1.2*A for vent limited
15	Passageways	0.01	2*A*F
16	Very low density storage	0.001	0.5*A*F

where F=Fuel load density (lbs/ft^2)
A=Area of deck occupied by fuel (ft^2)

Once the heat release rate is known or modeled, the temperature rise may be calculated using the Peatross/Beyler FRI Time correlation [14,15]. This correlation is applicable to compartments with conductive barriers and is defined as

$$\Delta T = \frac{\dot{Q}}{\dot{m}_o * c_p + h_k * A_T}$$

where ΔT = compartment temperature rise (°C),
Q = heat release rate (W),
$\dot{m}_o$ = mass flow rate of air leaving the compartment (kg/sec),
c_p = specific heat of air (1040 J/kg*K),

A_T = surface area of the compartment (89 m^2), and

h_k = overall heat transfer coefficient for thermally thin (steel) boundaries, defined with the following equation:

$$h_k = 30 - 18\left(1 - \exp\frac{-136*t}{\rho*\delta*c_p}\right)$$

where ρ = barrier density (7860 kg/m^3),

δ = barrier thickness (0.006 m), and

c_p = specific heat of the barrier (560 J/kg*K).

SAFE makes a simplification and defines $\dot{m}_o$ as the stoichiometric burning rate. This is calculated by dividing the heat release rate (Q) by the heat of reaction of air (3 MJ/kg).

Using the maximum heat release rates (Q_{max}) predicted using each fire growth model, a maximum temperature rise may be calculated. Values are shown in Figure 28 for a 5 kg/m^2 fuel load density and in Figure 29 for a 10 kg/m^2 fuel load density. The bars which correspond to the current test results are labeled with the test number, and the bars which correspond to the predicted results are labeled with the number of the fire growth model from Table 6. From Figure 28, it is noted that the maximum heat release rate and temperature rise measured in Tests 1-1 and 1-2a is most closely predicted by Fire Growth Model (FGM) 16 (very low density storage). However, the maximum heat release rate measured in Test 1-4 is more closely predicted by FGMs 8 and 10 (office spaces and berthing areas, respectively). Fire Growth Model 16 very nearly predicts the temperature rise measured in Test 1-1 and slightly overpredicts that in Test 1-2a. This model is not as suitable for predicting the temperature rise in Test 1-4 however. The temperature rise for Test 1-4 falls between that predicted using FGMs 8 or 10 and FGM 16.

From Figure 29, it is observed that the maximum heat release rate measured in Test 2-1 is best predicted by FGM 9 while the maximum heat release rate measured in Test 2-2 is best predicted by FGM 16. However, FGM 16 most closely predicts the temperature rise measured in both of these tests. FGM 16 underpredicts the temperature rise in Test 2-1 and slightly

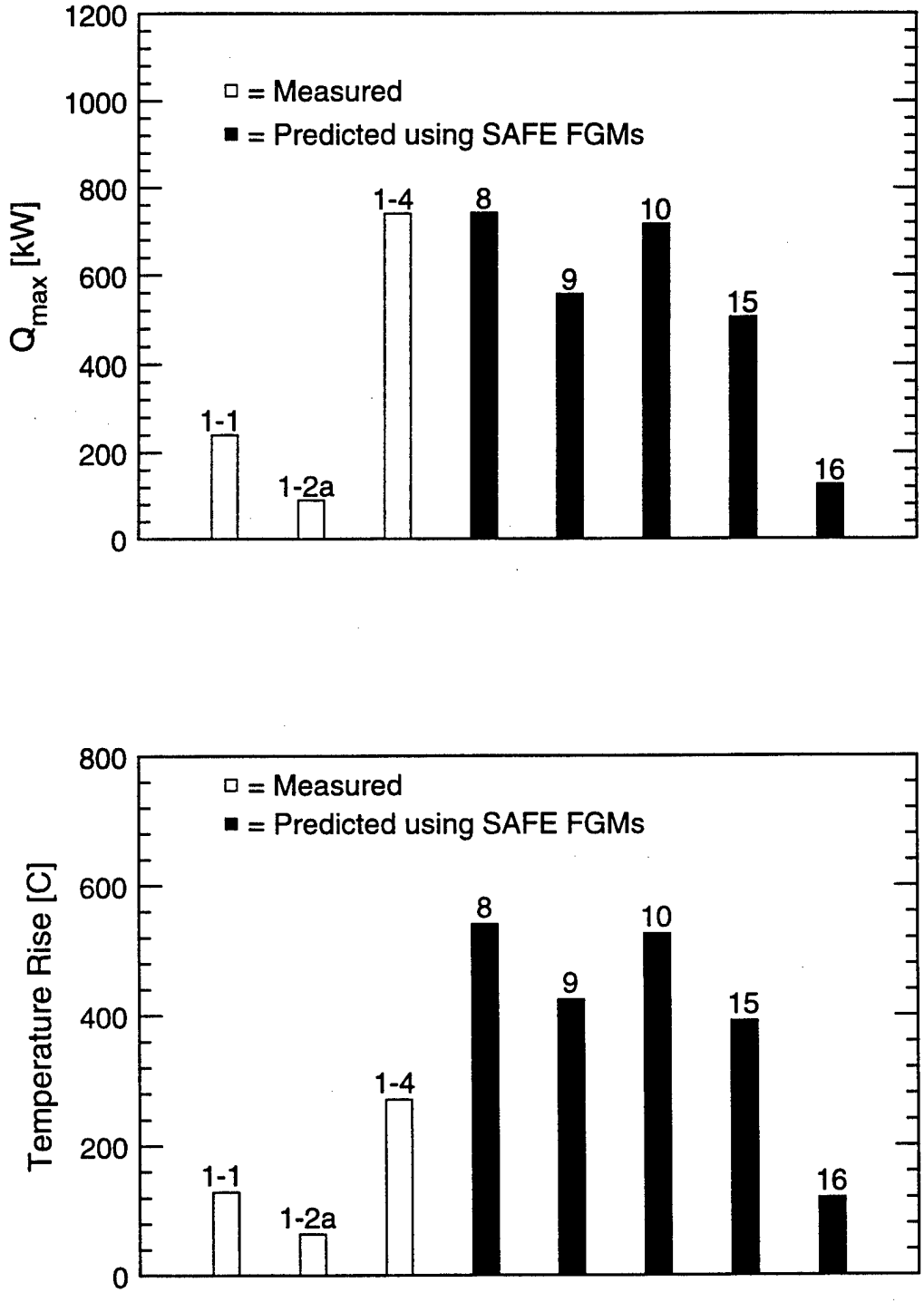

Figure 28. Comparison of experimentally measured and predicted peak heat release rates and temperature rises for a fuel load density of 5 kg/m^2

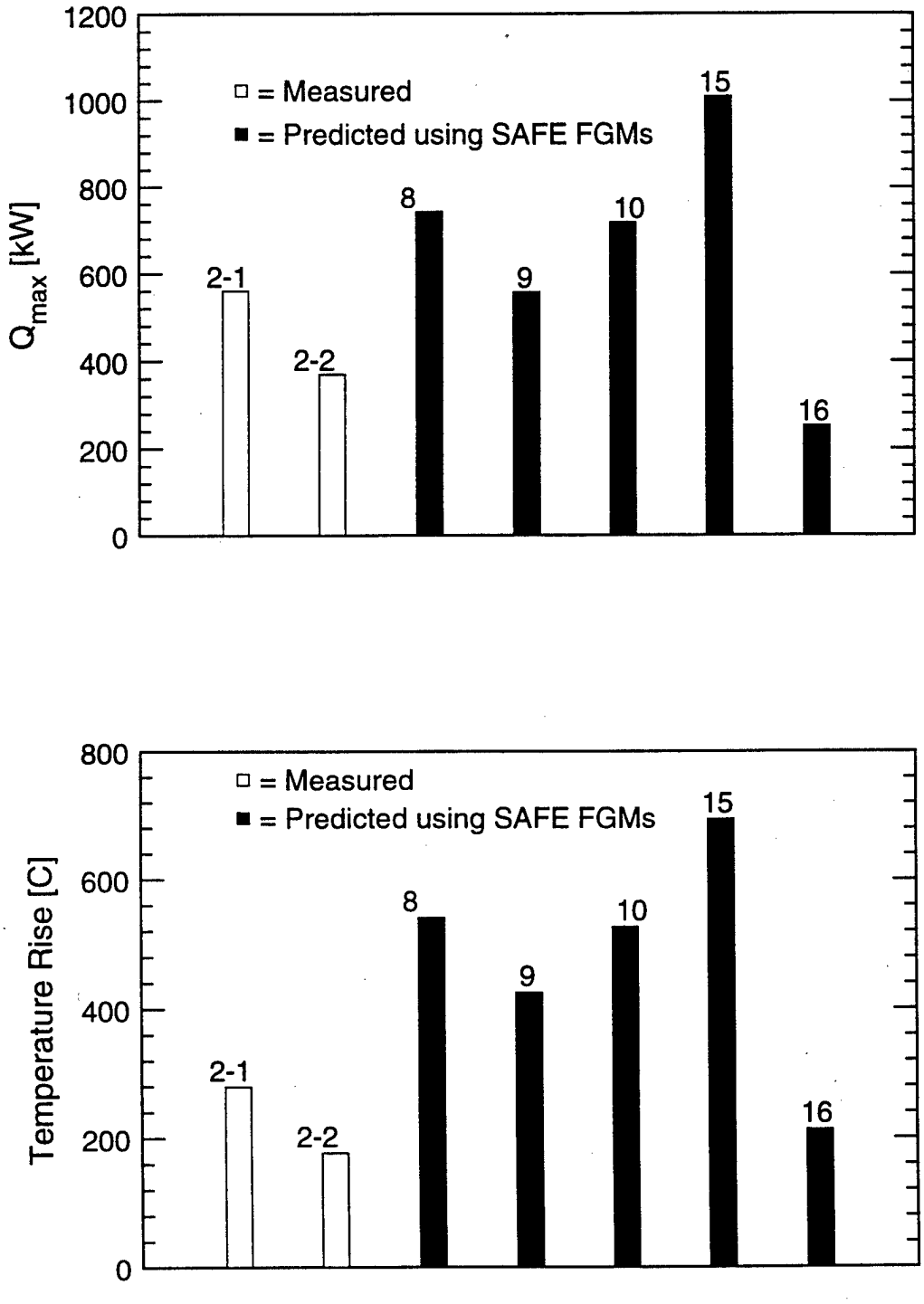

Figure 29. Comparison of experimentally measured and predicted peak heat release rates and temperature rises for a fuel load density of 10 kg/m^2

overpredicts that in Test 2-2. The results shown in Figures 28 and 29 demonstrate the difficulty that can arise when assigning fire growth rates and maximum heat release rates. Certainly, the fuel load distribution and fuel properties impact the accuracy of the predictions.

Fire growth rates were calculated using the current experimental data in order to compare them with that defined in FGM 16. With the exception of Test 4-1, the growth rates (alphas) were in the range of 0.001 to 0.002 kW/s^2. Test 4-1 was not considered since it represented a specialized scenario which would be unlikely to occur. As a result, the fire growth rate is comparable to that used in FGM 16.

Figures 30, 31, and 32 show temperature rise-time histories for all tests. Three sets of data are shown for each test with the exception of Test 4-1 which shows two sets of data. The first set of data was measured during the test. These values were calculated by subtracting the initial compartment temperature from the average compartment temperature. The second set of data was predicted using the FRI Time correlation with experimentally measured heat release rates and compartment exhaust rates. The third set of data was also predicted using the FRI Time correlation. In contrast to the second set, however, the heat release rates (and compartment exhaust rate) were determined using Fire Growth Model 16. A horizontal dotted line is shown when the maximum heat release rate has been achieved. These data were not included for Test 4-1 since FGM 16 was inappropriate for this scenario.

In general, the predictions using experimentally measured heat release rates and compartment exhaust rates are within 50 °C of the actual values. However, there are two discrepancies. The first discrepancy is shown in Figure 32 for Test 1-4 where the predictions exceed the actual measurements during the initial peak by nearly 200 °C. The other discrepancy is seen in Figure 32 for Test 4-1. During most of the test, the predicted results are at least 300 °C higher than the actual results. No explanation may be offered for this overprediction.

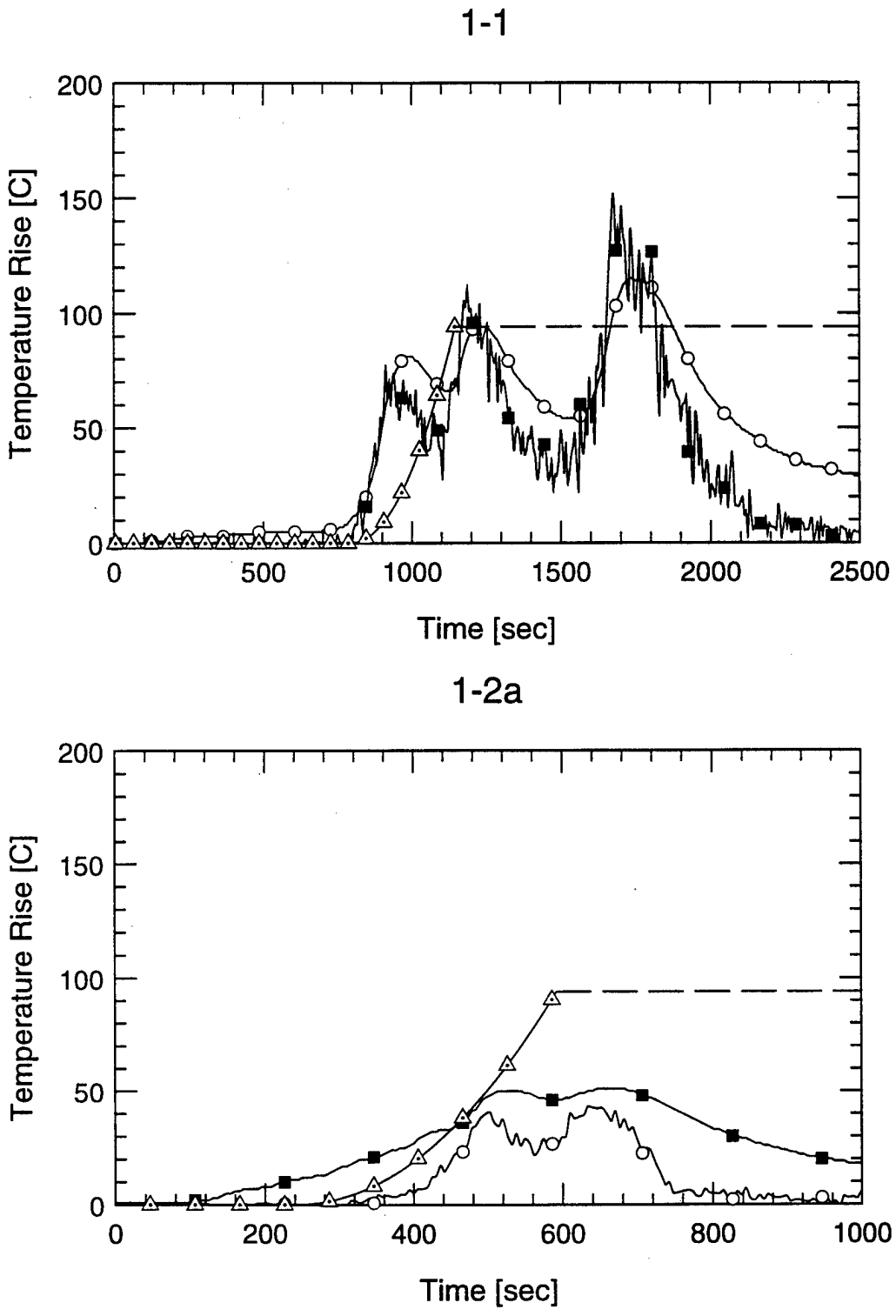

Figure 30. Comparison of measured and predicted compartment temperature rises for Test 1-1 and Test 1-2a

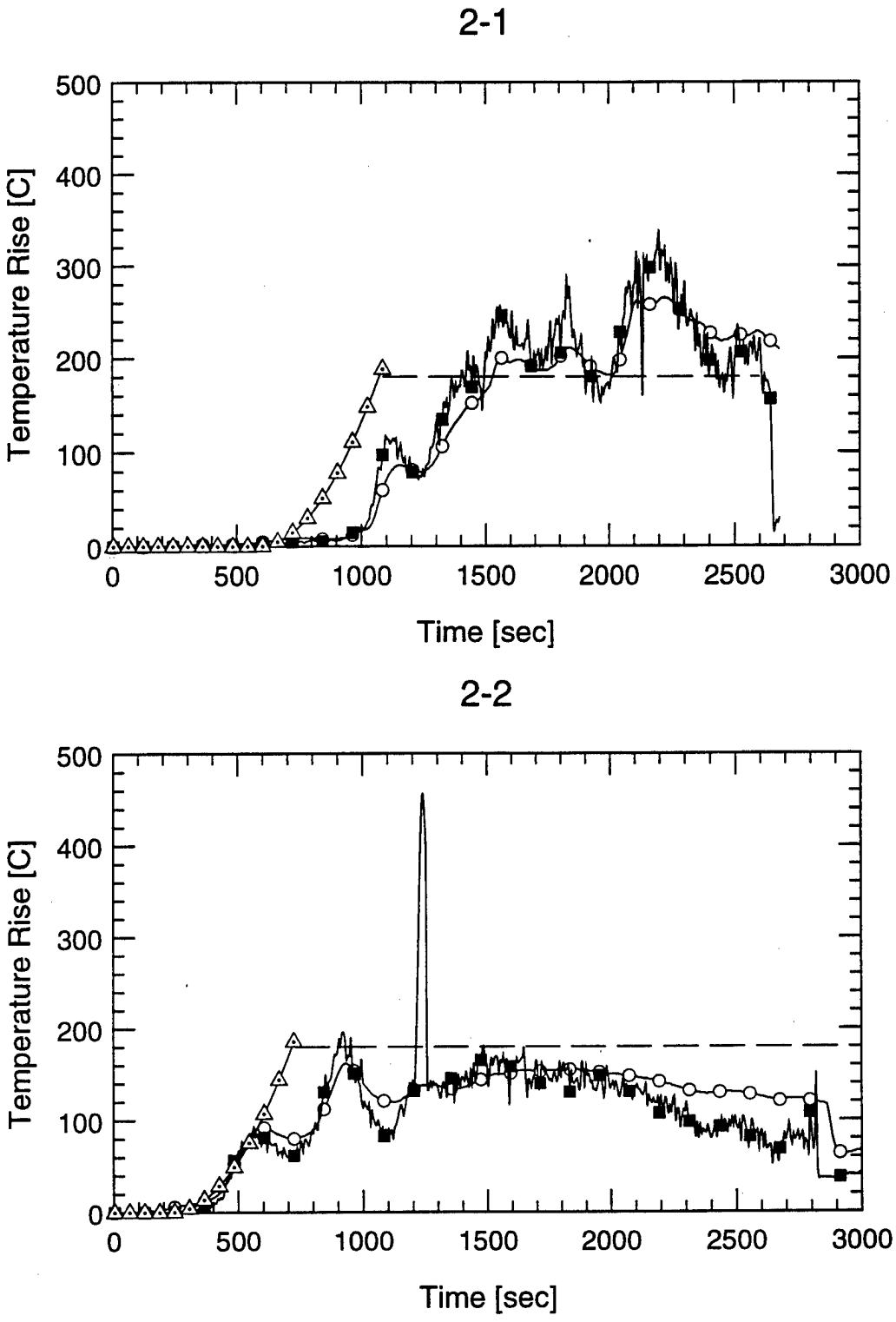

Figure 31. Comparison of measured and predicted compartment temperature rises for Test 2-1 and Test 2-2

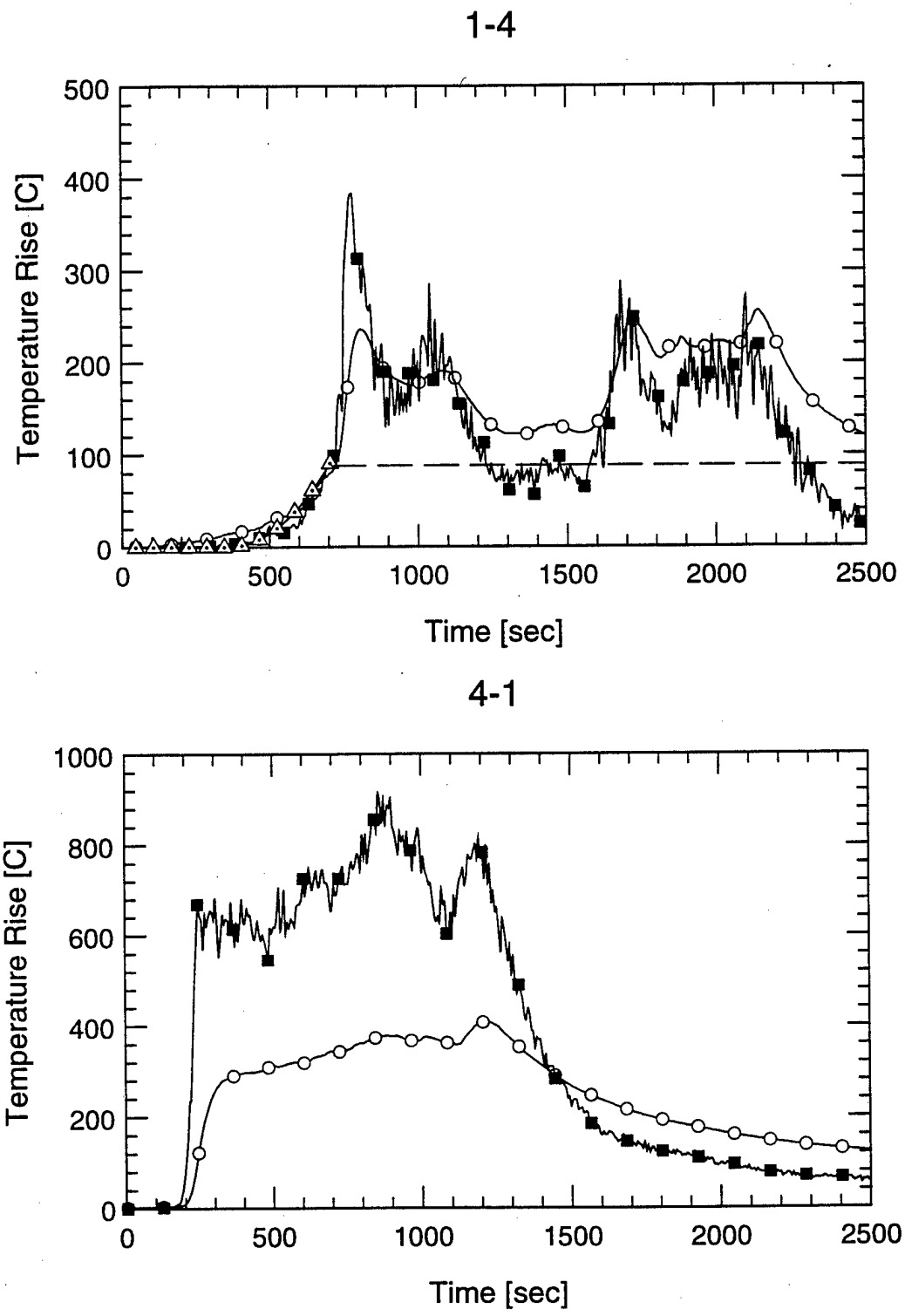

Figure 32. Comparison of measured and predicted compartment temperature rises for Test 1-4 and Test 4-1

Overall, the predictions which were generated using Model 16 show that the fire growth rate parameter, alpha, is appropriate. As seen in Figure 30, Model 16 underpredicts the actual temperature rise by less than 20 °C for Test 1-1 and overpredicts the actual temperature rise by approximately 50 °C in Test 1-2a. Furthermore, this model underpredicts the actual results from Test 2-1 by approximately 60 °C (Figure 31). In contrast, the actual temperature rise measured in Test 2-2 is predicted well by Model 16. As seen in Figure 32, Model 16 underpredicts Test 1-4 and Test 4-1 by 160 and 300 °C, respectively. This model performed the poorest for Tests 1-4 and 4-1. Both of these tests incorporated a localized fuel load distribution.

A similar representation of these data is also shown in Figure 33. This figure compares the temperature predictions using FGM 16 with those measured experimentally for each fuel load density. Again, Test 4-1 was not included in this figure since it was inappropriate to use FGM 16 to model the fire growth.

11.0 CONCLUSIONS

Flashover was not achieved during any of these tests. Using the test which had a normal Type 5A configuration as the baseline, it was determined that the (1) fuel load density, (2) fuel load material properties, and (3) fuel load package distribution will each impact the severity of the fire. When the fuel load density was increased from 5 kg/m^2 to 10 kg/m^2, the material losses were more than twice those resulting from the normal density. In addition, material losses were greater when the FR cushions were tested than when the non-FR cushions were tested. This result was consistent with cone calorimeter data where the heat flux necessary to ignite the FR material was lower than that necessary to ignite the non-FR material. Furthermore, higher material losses resulted when the fuel load was not evenly distributed throughout the compartment than when it was evenly distributed. This result suggests that it is important to maintain the maximum amount of space possible between seat rows and to avoid placing seats back-to-back. In all tests, higher material losses were indicative of larger heat release rates and compartment temperatures.

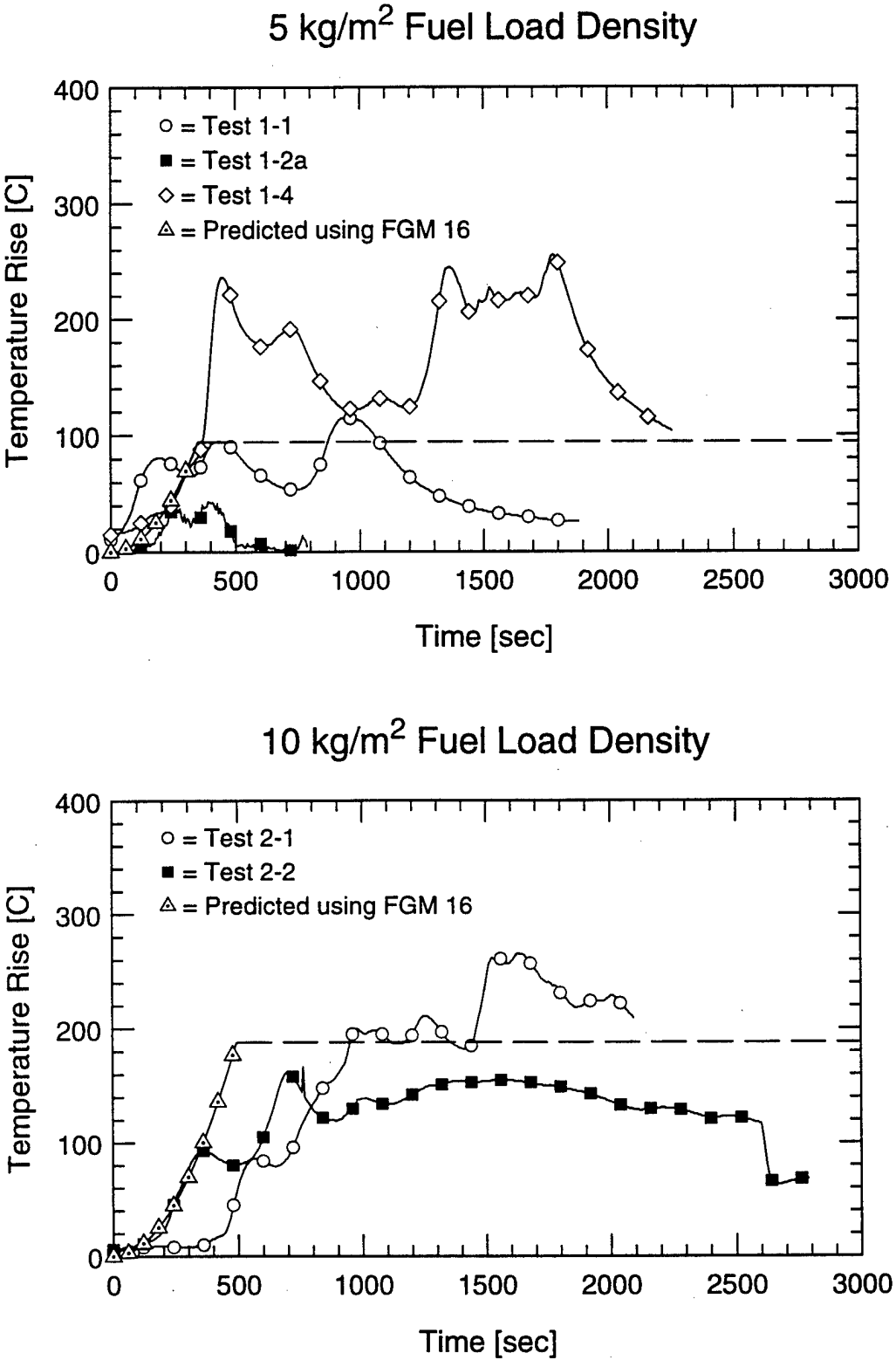

Figure 33. Comparison of measured and predicted temperature rises for 5 kg/m^2 and 10 kg/m^2 fuel load densities

Since these tests examined the case where ignition is low in the space and centrally located, small-scale tests were conducted to examine the case where ignition is adjacent to a bulkhead or near the ceiling. The results from these tests were compared with one- and two-dimensional heat transfer models. The predicted results were within 30 °C of the measured temperatures. In addition, the two-dimensional model estimated that a fire size of 180 kW would be necessary to heat the aluminum to its melting temperature. This model incorporated the use of a heat flux model which predicts the peak heat flux to a wall from an adjacent heat source.

Comparisons with SFSEM algorithms showed that Type 5A spaces may be modeled best using the very low density storage Fire Growth Model (FGM 16). The fire growth rate coefficient, alpha, associated with this model was found to be comparable to that measured during these experiments. The accuracy of the predictions is largely dependent on the fuel load distribution and the type of material in the space.

12.0 REFERENCES

1. PFM 1-94, Policy File Memorandum on Structural Insulation Requirements for Low Fire Load Spaces on Certain Vessels.

2. Sprague, C.M., and Dolph, B.L., "Theoretical Basis of the Ship Fire Safety Engineering Methodology," Report No. CG-D-30-96, September 1996.

3. McCaffrey, B.J., and Heskestad, G., "A Robust Bidirectional Low-Velocity Probe for Flame and Fire Application," Brief Communication, *Combustion and Flame*, **26**, 1976, pp. 125-127.

4. Dolph, B., and Weaver, E., "Test Plan for Low Fire Load Compartment Flashover Testing," Safety and Human Resources Division, United States Coast Guard Research and Development Center, January 8, 1997.

5. Janssens, M., and Parker, W.J., "Oxygen Consumption Calorimetry," *Heat Release Rate in Fires*, V. Babrauskas and S.J. Grayson, ed., Elsevier Applied Science, NY, 1992.

6. Tewarson, A., "Generation of Heat and Chemical Compounds in Fires," *The SFPE Handbook of Fire Protection Engineering*, Second Edition, P. J. DiNenno editor, 1995.

7. Winer, A., "Passive Fire Protection for Aluminum Structures," *Proceedings of 1975 International Symposium on Flammability and Fire Retardants*, May 22-23, 1975, pp. 202-213.

8. Kaufman, J.G., Kasser, R.C., "Fire Protection for Aluminum Alloy Structural Shapes, " *Civil Engineering*, **33** (3), March 1963, pp. 46-47.

9. Luzik, S.J., "Protection of Aluminum Overcast Constructions Against Fire," *Fire Technology*, **24** (3), August 1988, pp. 227-244.

10. Griffith, J.R., "Comparison Analysis and Fire Performance Evaluation of Class B Drop-Ceilings as Thermal Insulation for Aluminum Decks," Final Report for Southwest Research Institute Project No. 01-5362, Submitted to U.S. Coast Guard Academy, Contract No. DTCG39-93-C-E00561, June 1993.

11. Beene, D., "Fire Endurance of Aluminum and Steel Hatch Covers," Report Number CG-D-82-77, June 1977.

12. STAR*CD User's Manual, Version 3.0, Computational Dynamics, David Gossman, London, England, 1997.

13. Back, G., Beyler, C. L., DiNenno, P. J., and Tatem, P., (1994), "Wall Incident Heat Flux Distribution Resulting from an Adjacent Fire," Fire Safety Science - Proceedings of the

Fourth International Symposium, International Association of Fire Safety Science, 1994, pp. 214-252.

14. Peatross, M.J., and Beyler, C.L., "Thermal Environment Prediction in Steel-Bounded Preflashover Compartment Fires," *Fire Safety Science - Proceedings of the Fourth International Symposium*, International Association of Fire Safety Science, 1994, pp. 205 -215.

15. Peatross, M.J., Beyler, C.L., and Back, G.G., "Validation of Full Room Involvement Time Correlation Applicable to Steel ," United States Coast Guard Report No. CG-D-16-94, November, 1993.

Appendix A – Cone Calorimeter Experiments

Cone calorimeter experiments were conducted using both FR and non-FR cushion samples. The purpose of these tests was to examine the burning characteristics (i.e., ignition time, peak heat release rate, etc.) and determine the heat of combustion for each material type. All experiments were performed with an incident heat flux of 25 kW/m^2 with the exception of two experiments that were conducted at 15 kW/m^2.

Tests were conducted using the foam cushion only, the upholstery covering only, and the upholstered foam combination. The samples were 10.1 cm by 10.1 cm. The foam samples were 38 mm thick, the non-FR upholstery was approximately 1.0 mm thick, and the FR upholstery was 1.5 mm thick. For tests with upholstered foam, the upholstery was pinned down to the foam to prevent it from curling up.

The results of the experiments conducted with an incident heat flux of 25 kW/m^2 are summarized in Table A-1. The repeatability of the test results was calculated using the regression equations developed from the results of the ASTM inter-laboratory trials [1]. The peak heat release rates per unit area were 380, 328, and 406 kW/m^2 for the FR upholstered foam, upholstery, and foam, respectively. Heat release rate-time histories for the upholstered foam, upholstery, and foam are shown in Figures A-1 through A-3, respectively. The effective heat of combustion for the upholstered foam sample was 20,800 kJ/kg. A higher effective heat of combustion of 27,500 kJ/kg was measured for the FR upholstery while a lower value of 15,800 kJ/kg was measured for the FR foam. All ignition times were under 25 seconds with the foam being the shortest at 5 seconds and the upholstered foam being the longest at 21 seconds.

The heat release rate-time histories for the non-FR upholstered foam, upholstery, and foam are shown in Figures A-4 through A-6, respectively. The peak heat release rates per unit area for the non-FR upholstered foam, upholstery, and foam samples were 335, 309, and 335 kW/m^2, respectively. An effective heat of combustion of 22,700 kJ/kg was measured for the

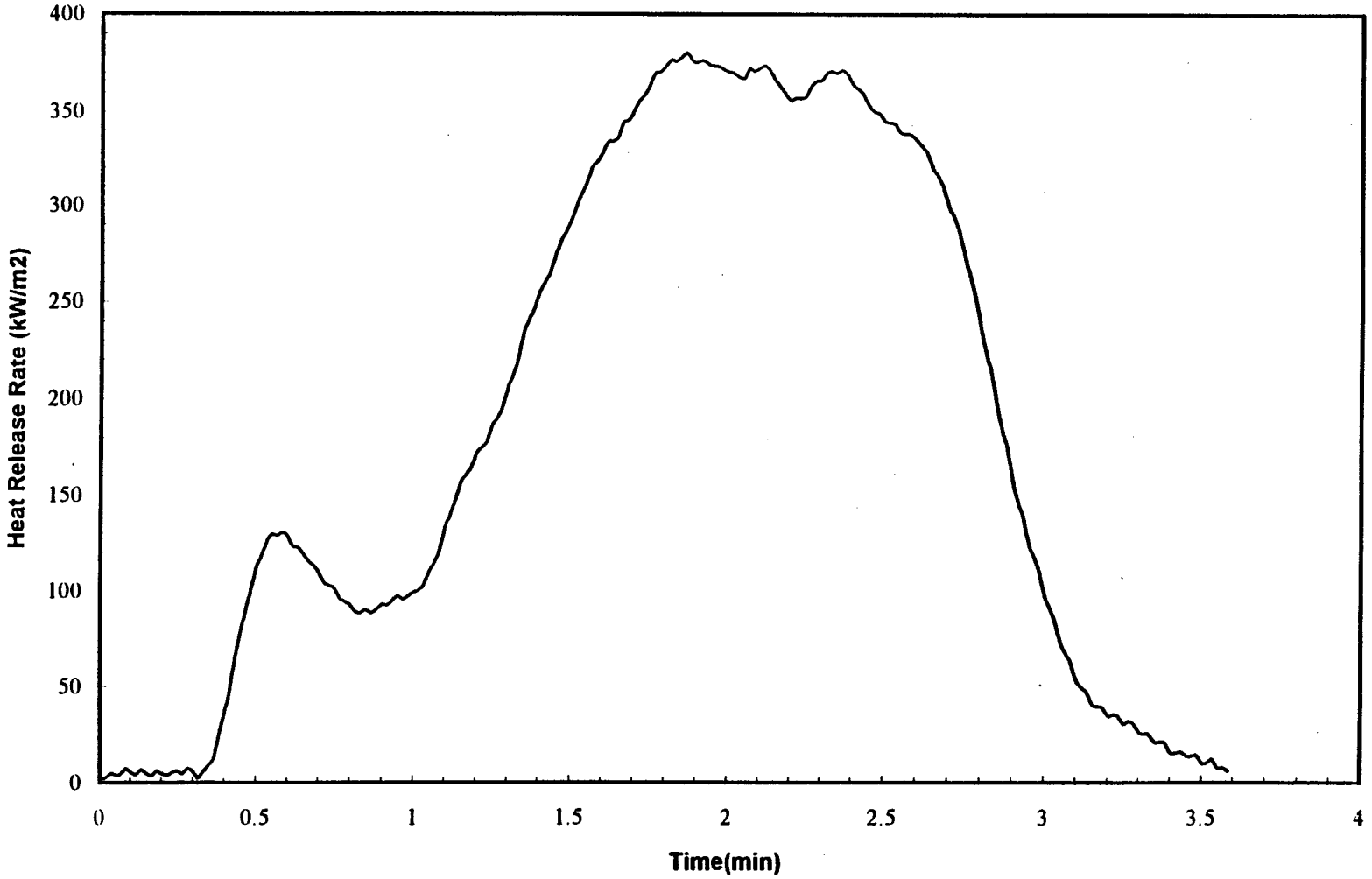

Figure A-1. Heat release rate per unit area for FR upholstered foam

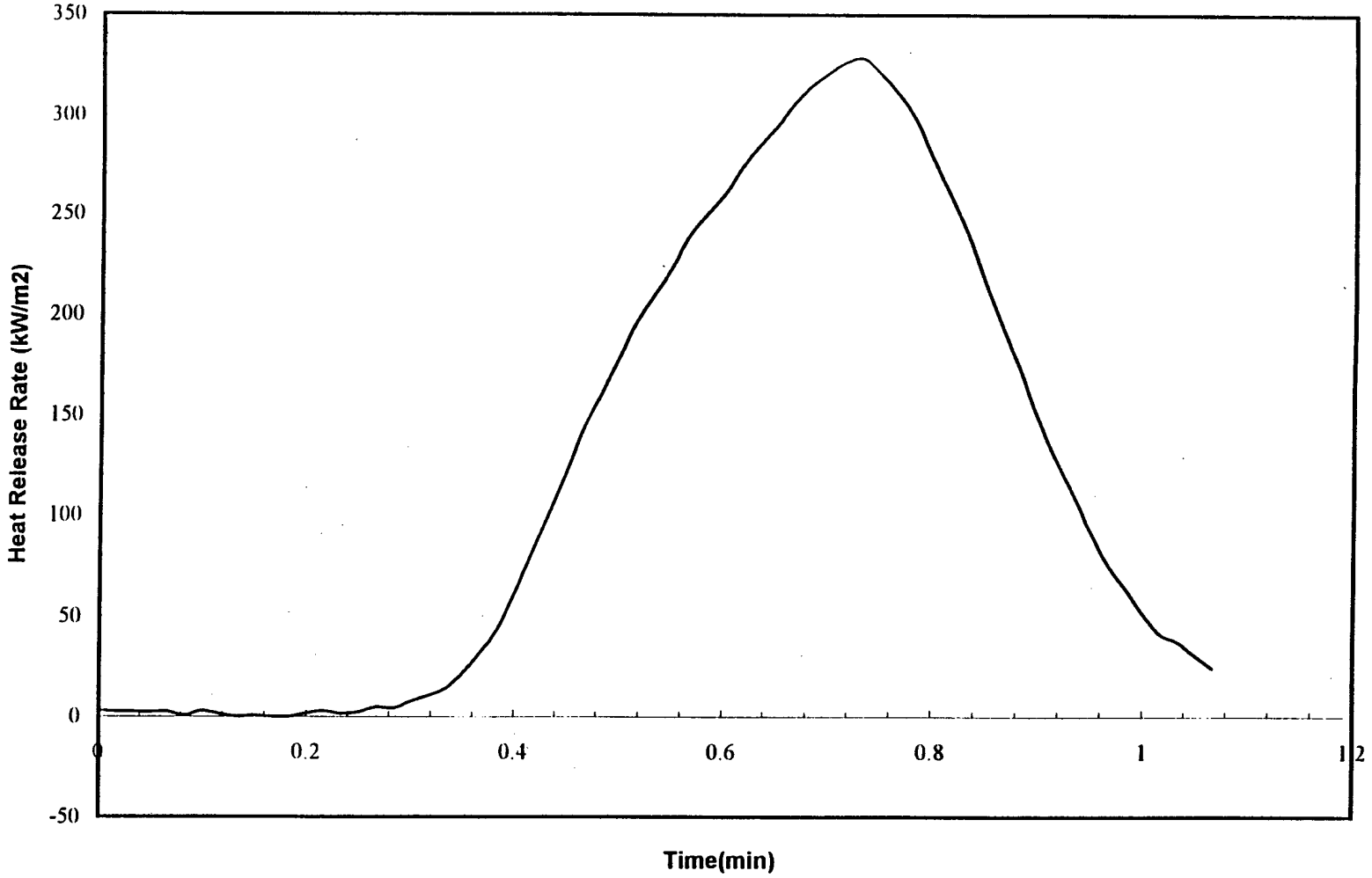

Figure A-2. Heat release rate per unit area – time history for FR upholstery

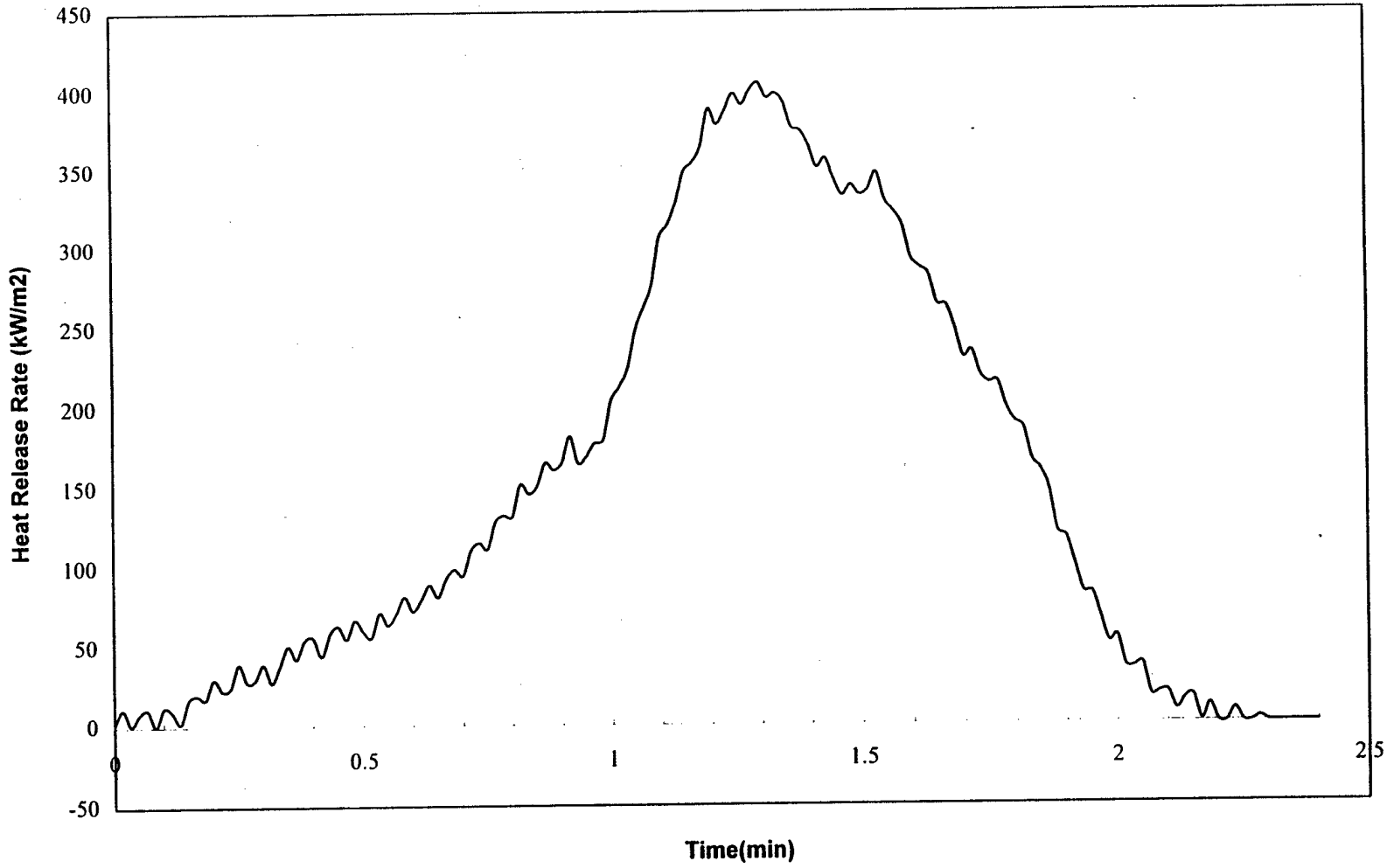

Figure A-3. Heat release rate per unit area – time history for FR foam

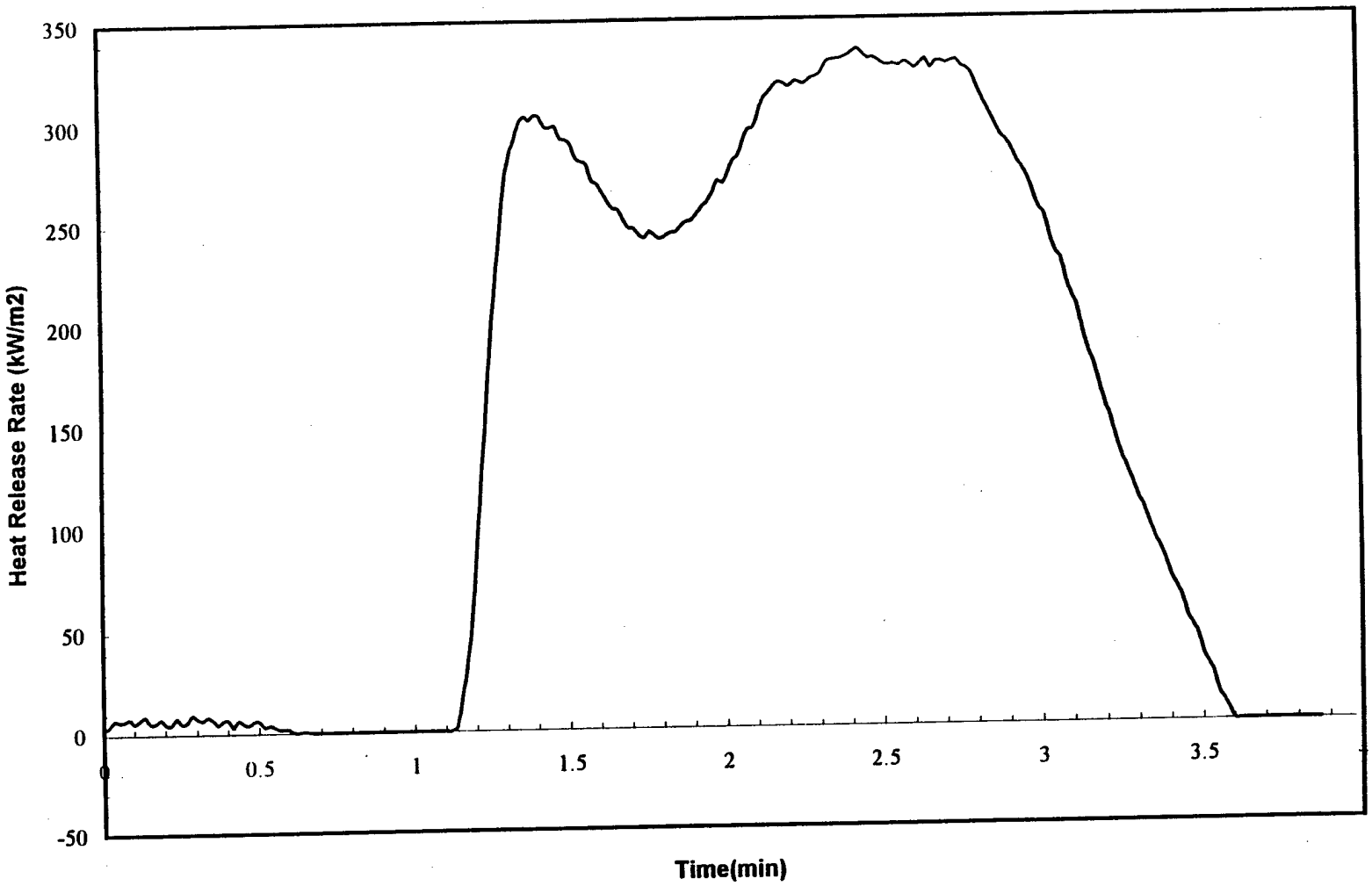

Figure A-4. Heat release rate per unit area – time history for non-FR upholstered foam

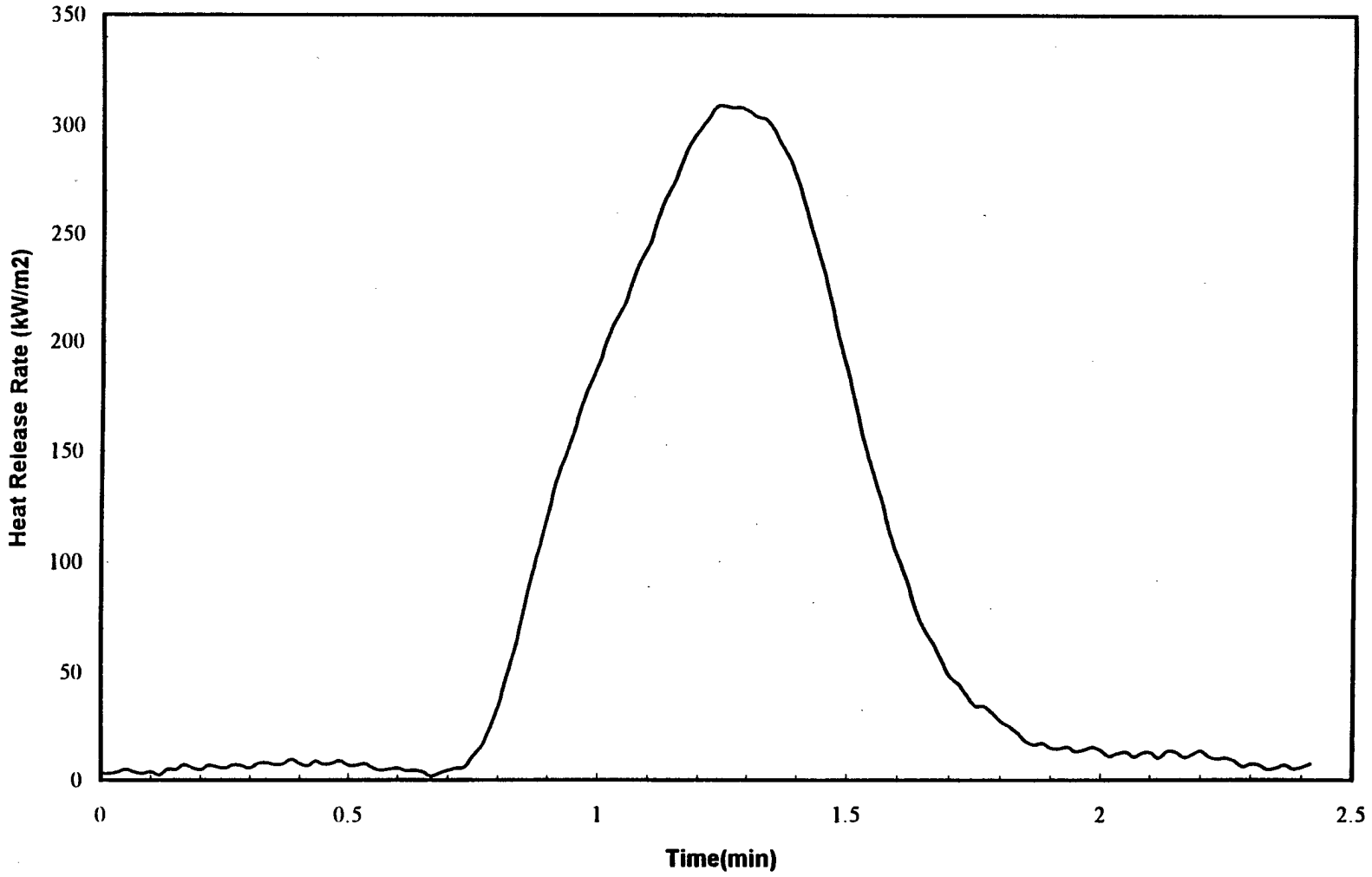

Figure A-5. Heat release rate per unit area – time history for non-FR upholstery

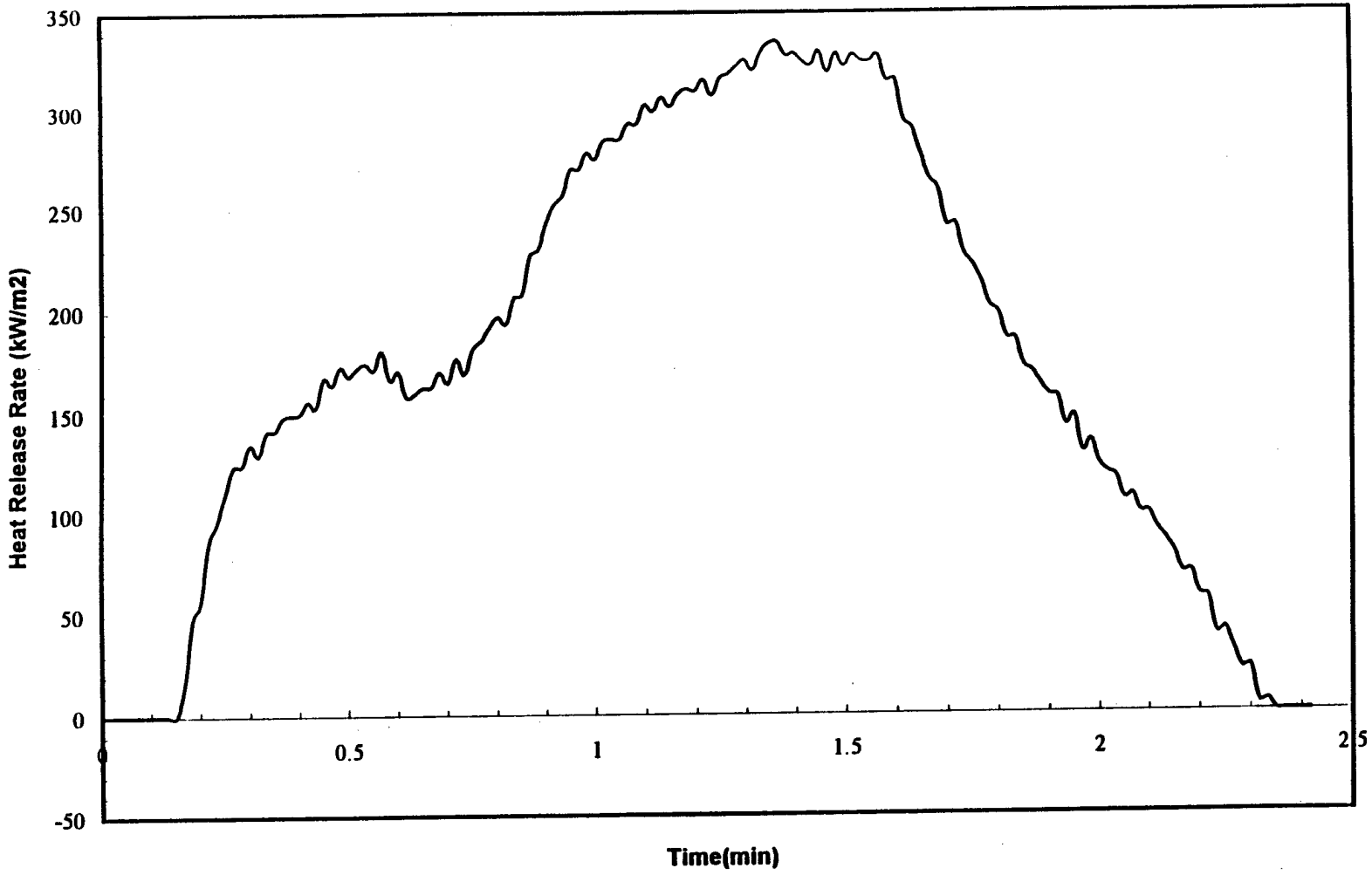

Figure A-6. Heat release rate per unit area – time history for non-FR foam

upholstered foam sample while a value of 27,600 kJ/kg was measured for the upholstery. The heat of combustion measured for the non-FR foam was comparable to that measured for the upholstered foam. Ignition times were much longer for the upholstered foam and the upholstery than for the foam. The foam ignited in 4 seconds, the upholstery ignited in 45 seconds, and the upholstered foam ignited in 68 seconds.

In comparing the non-FR upholstered foam samples with the FR upholstered foam samples, the non-FR sample took 47 seconds longer to ignite than the FR sample. Prior to the ignition of the non-FR sample, the upholstery melted over the foam forming a thermal resistance layer between the incident flux and the foam. The sample was heated for approximately 40 additional seconds before the sample surface ignited. When the FR cushion sample was heated, the upholstery also melted. However, instead of forming a layer over the foam, the upholstery broke apart and exposed the foam underneath. Ignition occurred approximately 5 seconds after the upholstery broke apart. Accounting for the test repeatability, the peak and average heat release rates and the effective heats of combustion from the non-FR upholstered foam sample were equal to those from the FR sample.

Following the same trend noted with the upholstered foam samples, the non-FR upholstery had an ignition time 26 seconds longer than that for the FR upholstery. However, both foam samples had a short ignition time of 4 to 5 seconds.

The separated burning of the upholstery and the foam is apparent in the heat release rate curves from the tests with upholstered foam. The heat release rates from tests with upholstered foam have a characteristic two peak shape (see Fig. A-1 and A-4). The first peak is attributed to the upholstery burning while the second peak is considered to be the foam burning. The second peak is typically higher and has a longer duration.

Table A-1. Results of the Cone Calorimeter Experiments (The Repeatability of the Results, Based on the ASTM Inter-laboratory Trials, Are Shown When Possible)

Cushion	Material	Time to Ignite, [sec]	Peak Heat Release Rate, [kW/m^2]	Time of Peak, [sec]	Average Heat Release Rate, [kW/m^2]*	Effective Heat of Combustion, [kJ/kg]
FR	Upholstery and Foam	21±6	380±63	91	203±30	20,800±1,420
	Upholstery	19±6	328±56	25	171±30	27,500±1,875
	Foam $\rho \approx 45$ kg/m^3	5±4	406±66	73	154±29	15,800±1,080
non-FR	Upholstery and Foam	68±12	335±57	78	216±31	22,700±1,550
	Upholstery	45±9	309±54	30	113±27	27,600±1,885
	Foam $\rho \approx 35$kg/m^3	4±3	335±57	78	184±30	22,100±1,510

* Average over the flaming duration of test. Repeatability was calculated using the 180 second heat release rate average equation from ASTM 1354.

Two tests were conducted using upholstered foam at an incident flux of 15 kW/m^2. One test was conducted using material from the non-FR cushion and the other was conducted using material from the FR cushion. The non-FR sample did not ignited after 8 minutes of exposure. However, the FR sample ignited after 178 seconds of exposure.

Based on these cone calorimeter test results, the non-FR cushion exhibited better resistance to fire than the FR cushion. The ignition times were notably longer for the non-FR cushion samples than for the FR cushion samples.

Reference

1. American Society for Testing and Materials, E 1354-94, "Standard Test Method for Heat and Visible Smoke Release Rates for Materials and Products Using an Oxygen Consumption Calorimeter," 1994.

(BLANK)

Appendix B – Heat Release Rate Calculations

Mass flow rates into and out of the compartment were calculated using bidirectional probes. There were 7 bi-directional probes located at heights of 2.0, 1.75, 1.5, 1.25, 1.9, 0.75, and 0.5 m above the deck. These locations have been numbered 1 through 7 with 1 corresponding to the highest probe (2.0 m above the deck) and 7 corresponding to the lowest probe (0.5 m above the deck). Bi-directional probe and thermocouple measurements were used to calculated flow velocities. A discharge coefficient of 0.68 was assumed. Table B-1 lists the height of the neutral plane and the bi-directional probe measurements by location number that were used to calculate the mass flow rate into and out of the compartment.

Table B-1. Neutral Plane and Bi-directional Probe Locations Used to Calculate Vent Flow Rates*

Test Name	Neutral Plane Location (m)	Probe Locations used in m_{in} calculation	Probe Locations used in m_{out} calculation
1-1	0.875	6, 7	3, 4
1-2a	0.875	6, 7	2, 3, 4, 5
1-4	0.875	6, 7	5
2-1	0.875	6, 7	5
2-2	0.875	6, 7	4, 5
4-1	0.625	7	2, 4, 5, 6

* Probes not listed were judged defective and were not used in the calculation.

The heat release rate was calculated twice using each mass flow rate measurement (into and out of the compartment). These values were integrated with respect to time to get a total energy release quantity based on the use of both mass flow rate measurements. These quantities are included in Table B-1. These values were compared to the total energy release values calculated based on the mass lost during the test. This involved multiplying the mass lost by the heat of combustion for both the cushions and the wood cribs. The heat of combustion for the

cushions was 21,000 kJ/kg obtained from cone calorimeter tests and the heat of combustion of the wood was assumed as 13,000 kJ/kg. The carpet was not included in this calculation because it did not contribute significantly to the total energy released.

Table B-2. Comparison of Total Energy Release Calculations

Test Name	Released Energy Based on Mass Lost (MJ)	Released Energy Using m_{in} (MJ)	Released Energy Using m_{out} (MJ)
1-1	110	120*	300
1-2a	30	20	20*
1-4	360	430*	590
2-1	520	510*	690
2-2	390	490*	680
4-1	2100	960	2200*

* Measurements which compared best with energy release based on mass lost.

The most accurate vent flow rate measurement was then determined by identifying which total energy release was closest to that based on mass loss. This measurement was then used in subsequent calculations for heat release rate and temperature predictions using the FRI Time correlation.

Appendix C – Graphical Results

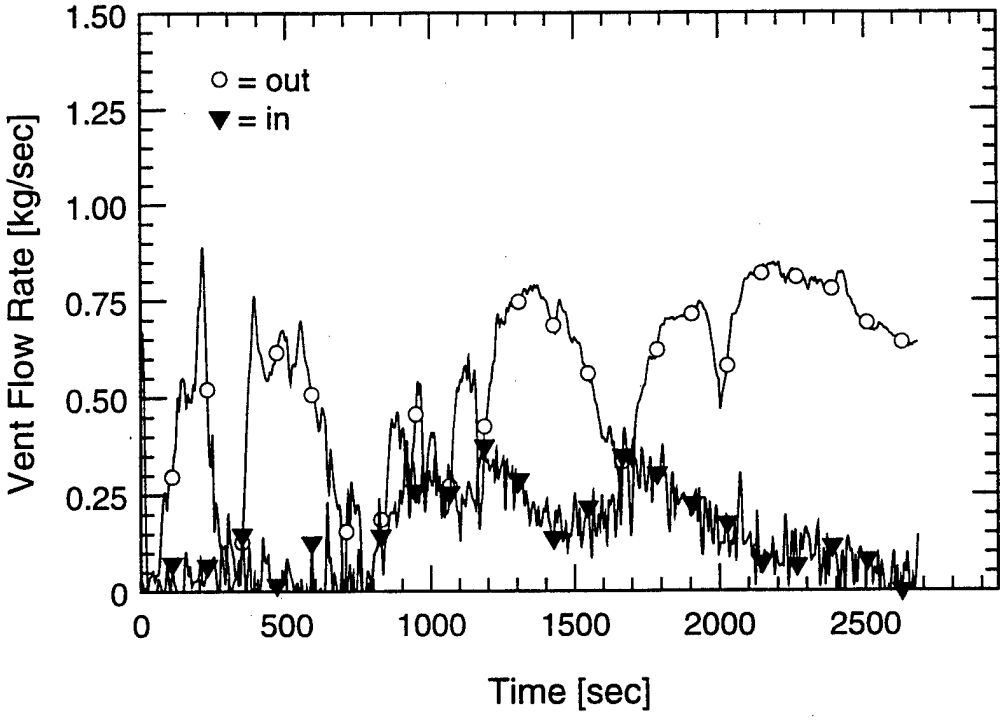

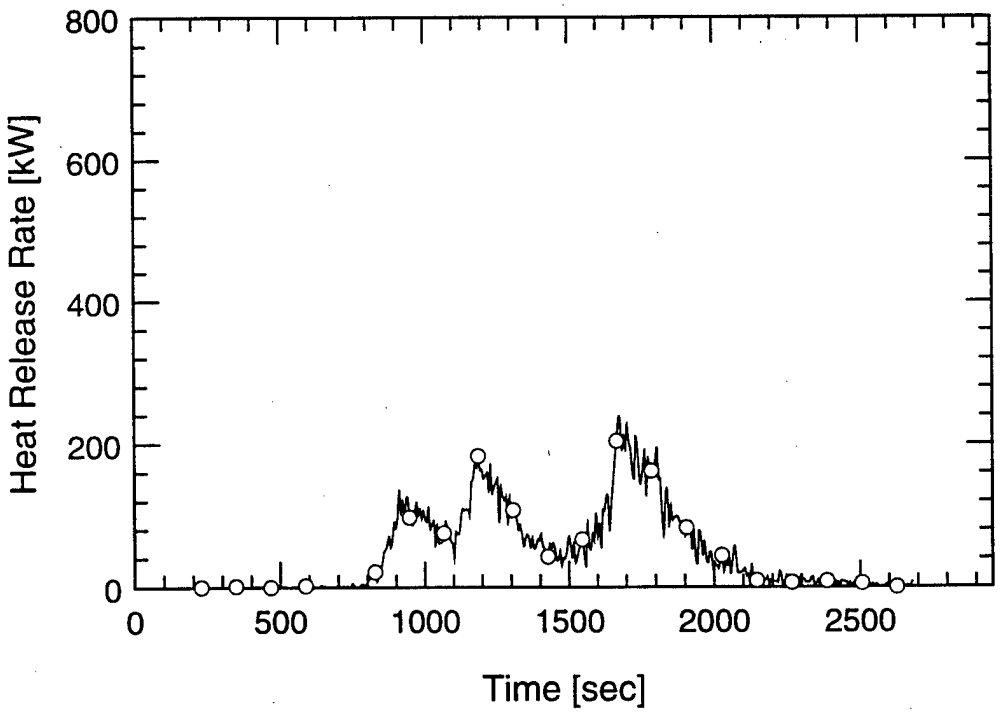

Vent Flow Rate and Heat Release Rate Measurements

Test 1-1

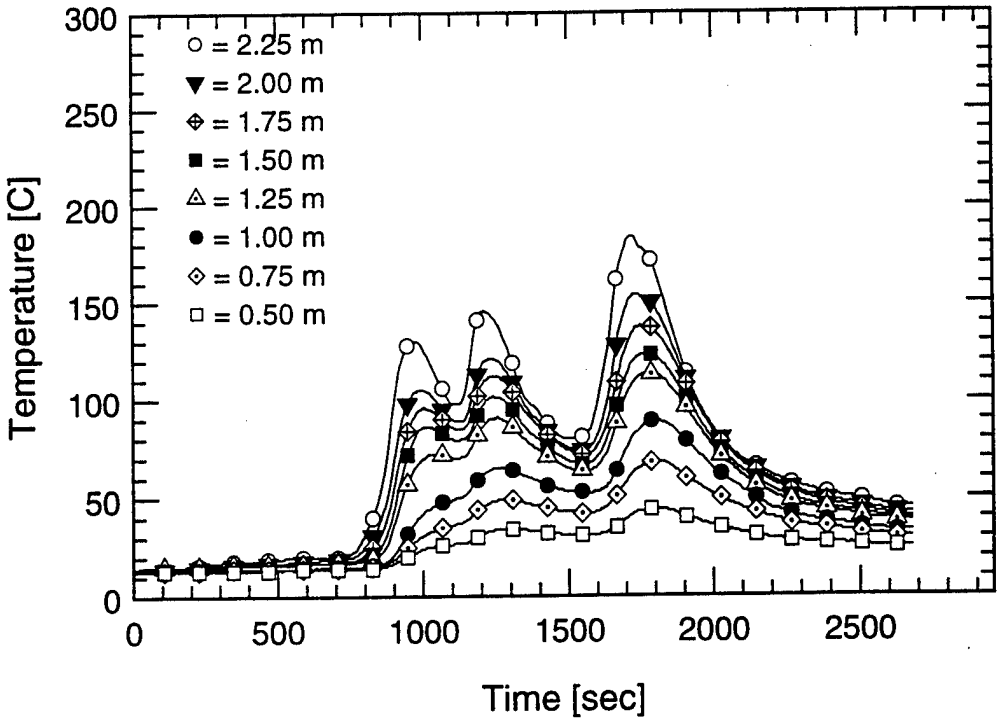

TC Tree #1

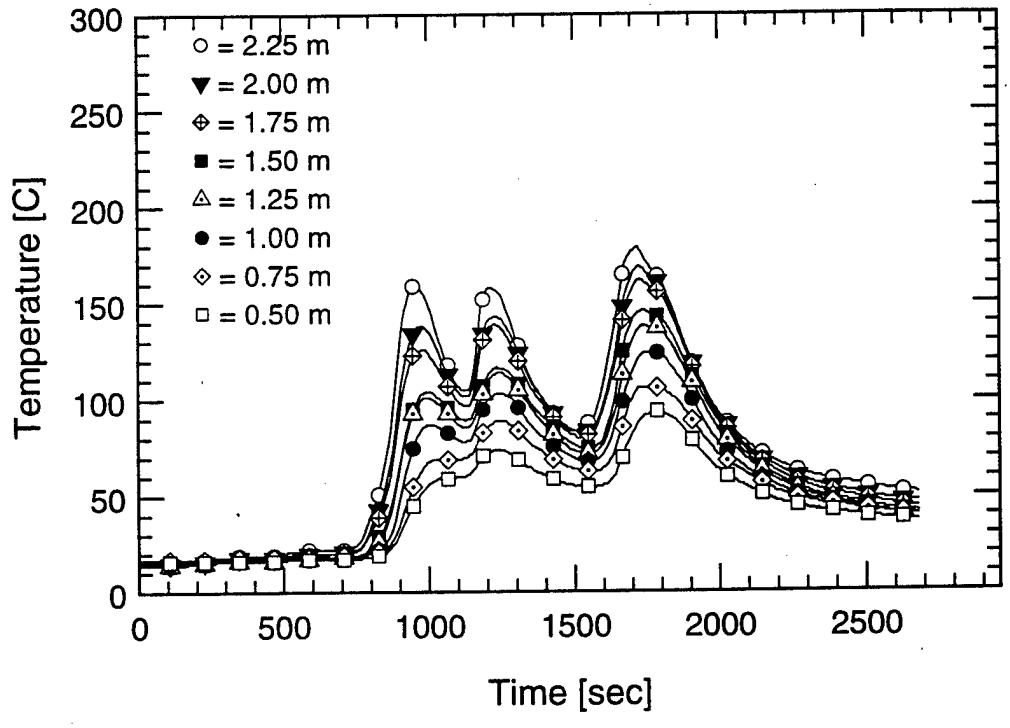

TC Tree #2

Temperature Measurements
Test 1-1

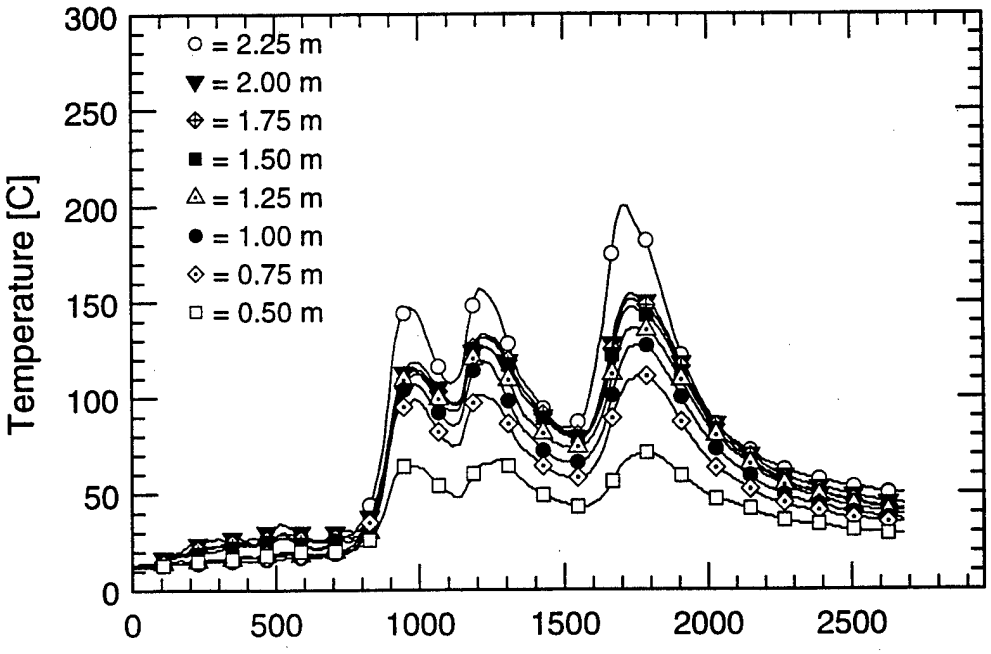

TC Tree #3

Temperature Measurements

Test 1-1

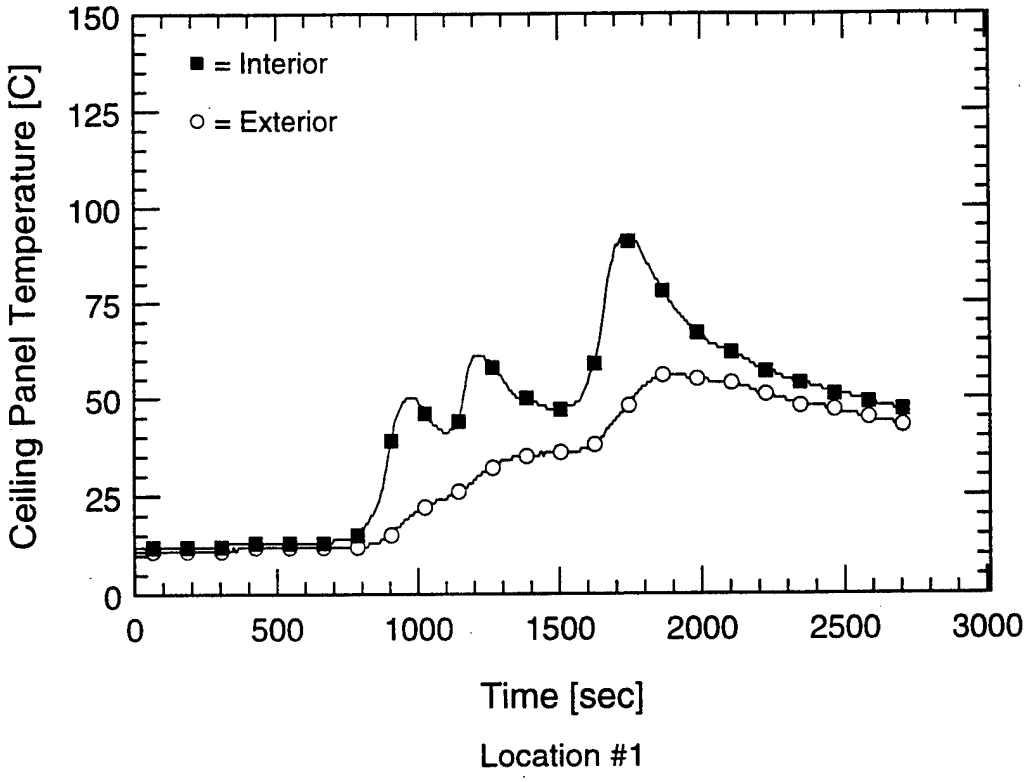

Location #1

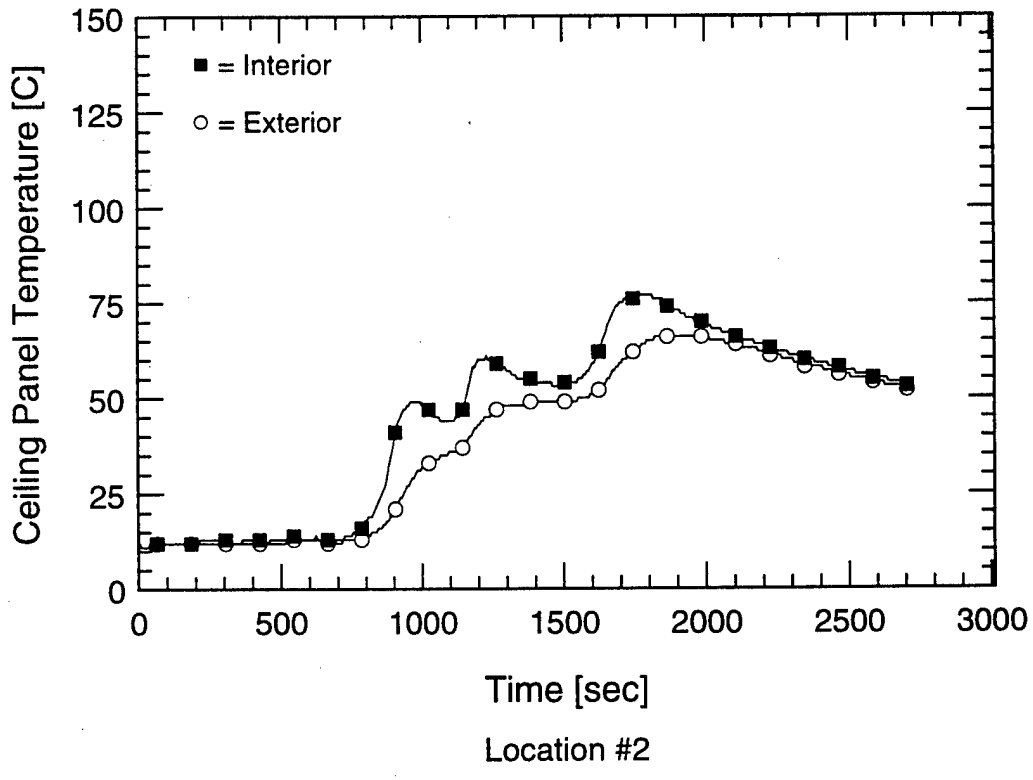

Location #2

Ceiling Panel Temperature Measurements
Test 1-1

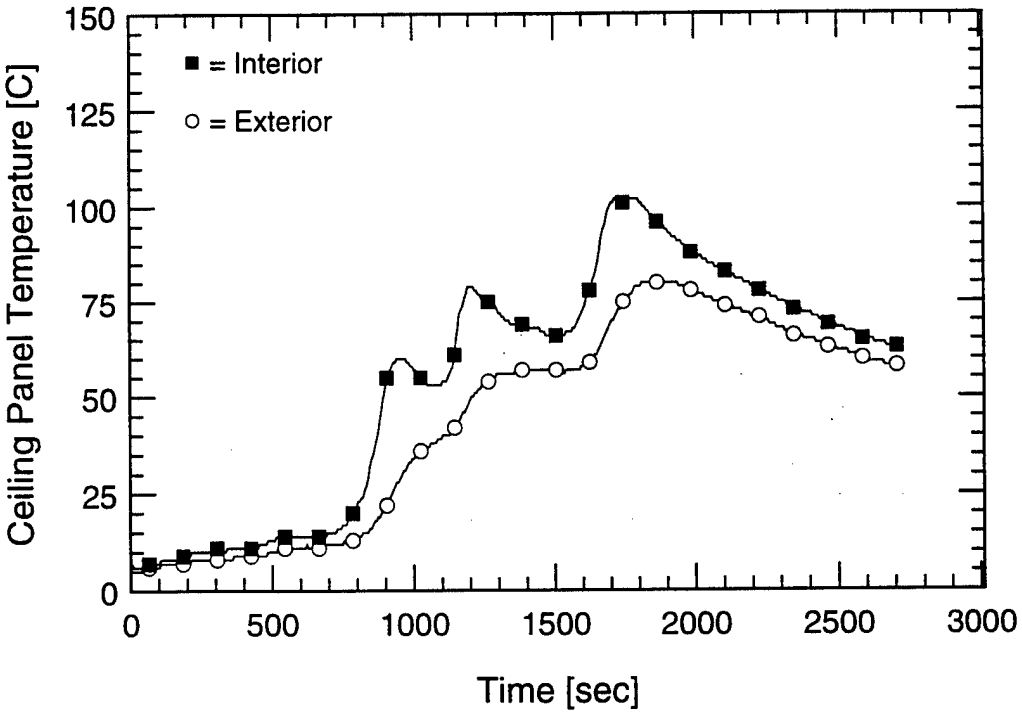

Location #3

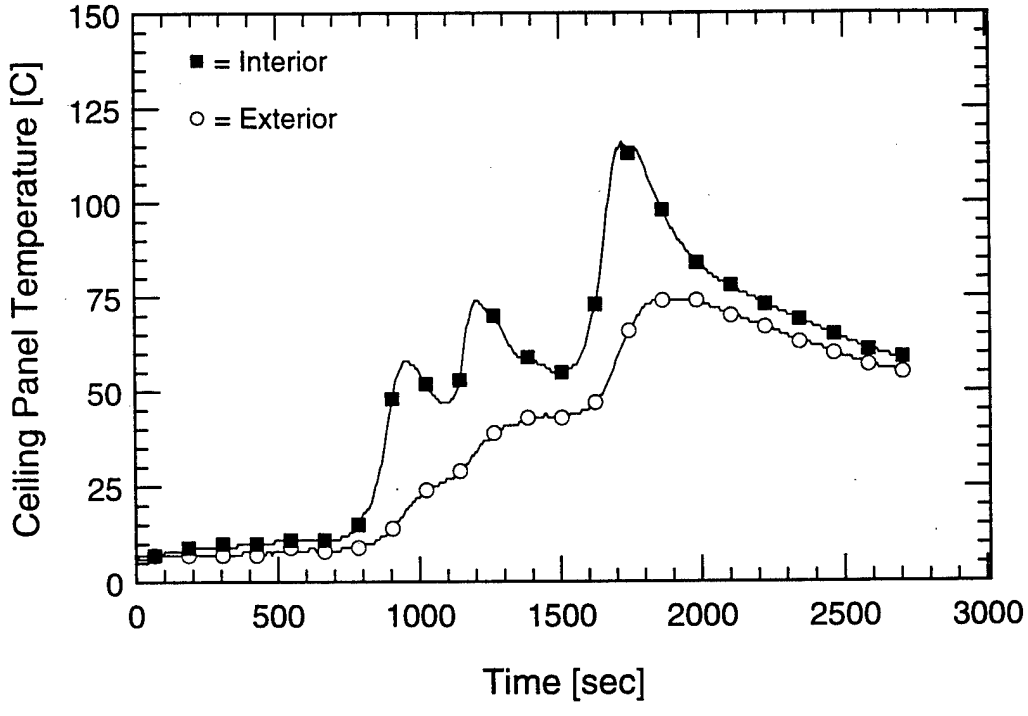

Location #4

Ceiling Panel Temperature Measurements
Test 1-1

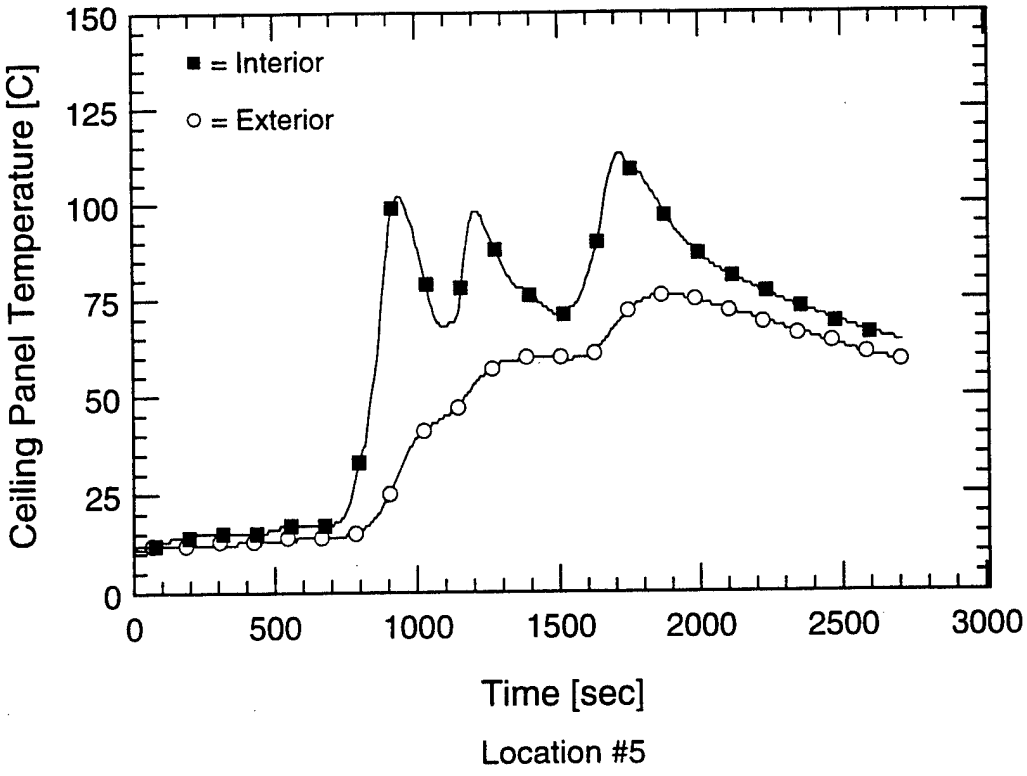

Ceiling Panel Temperature Measurements
Test 1-1

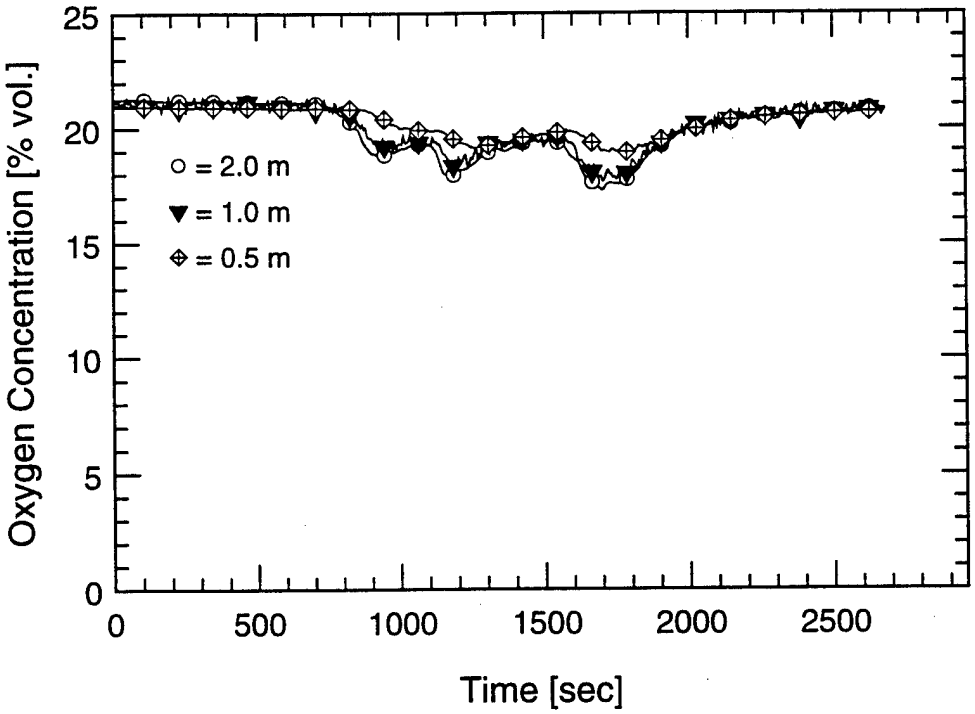

Gas Tree #1

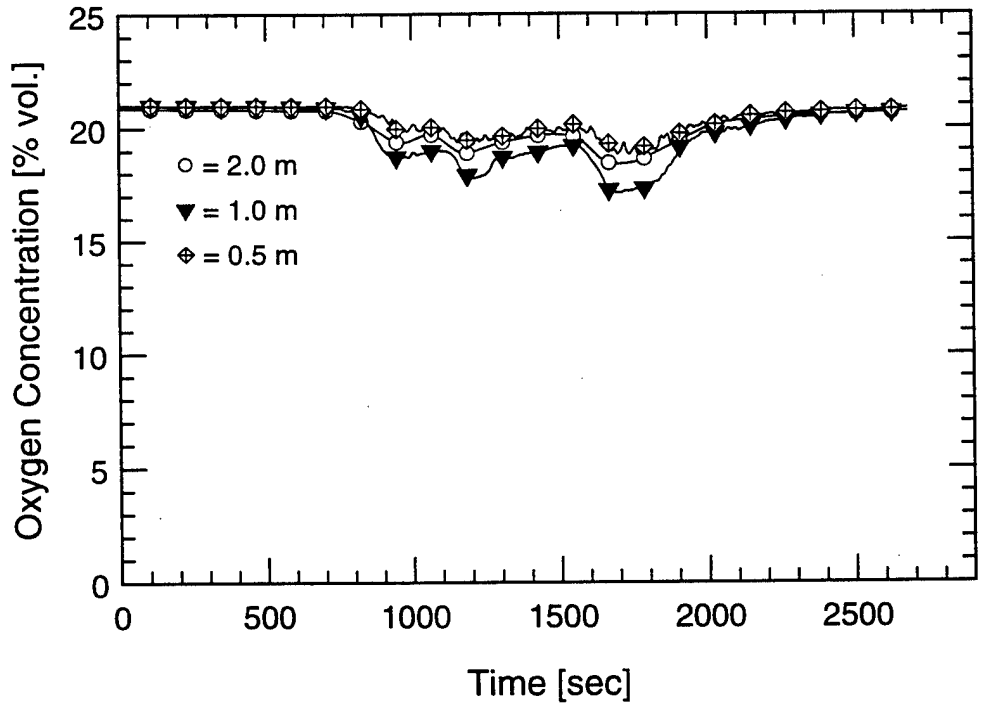

Gas Tree #2

Oxygen Concentration Measurements
Test 1-1

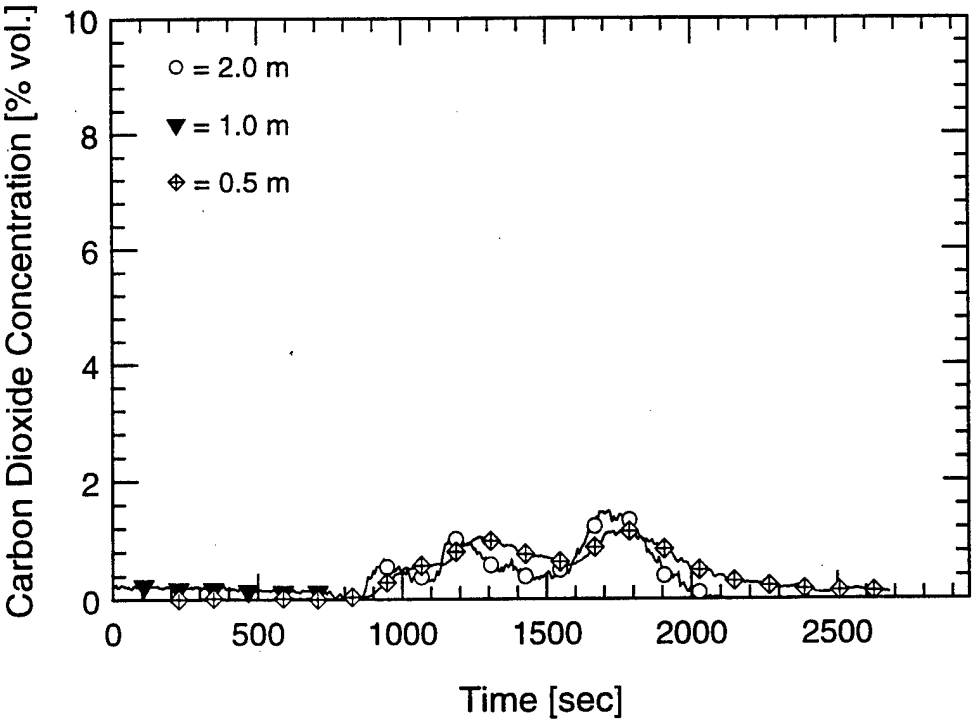

Gas Tree #1

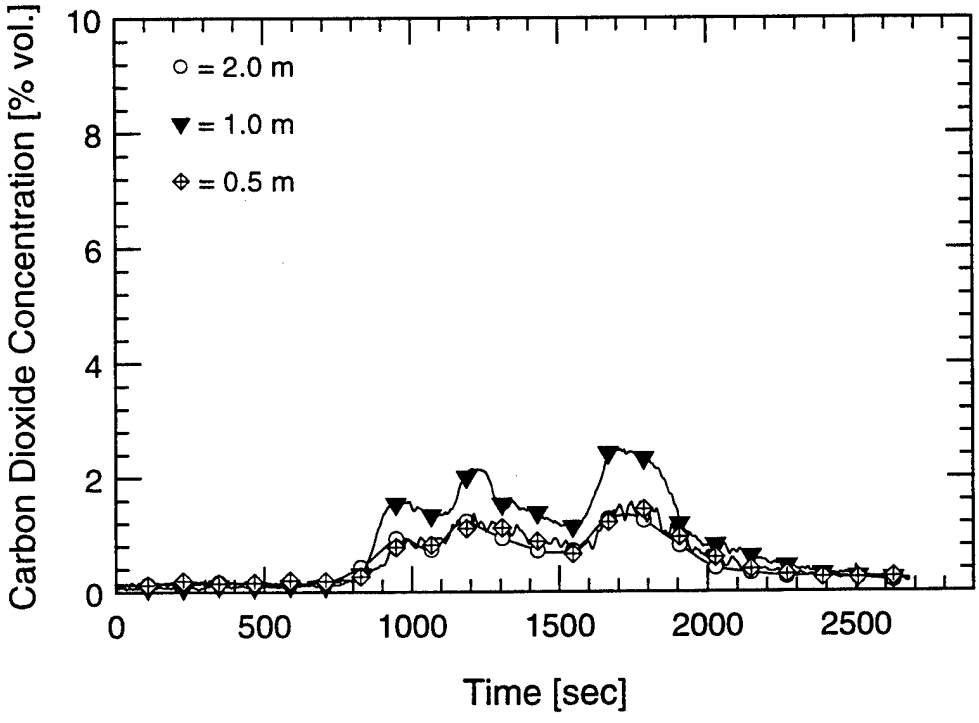

Gas Tree #2

Carbon Dioxide Concentration Measurements
Test 1-1

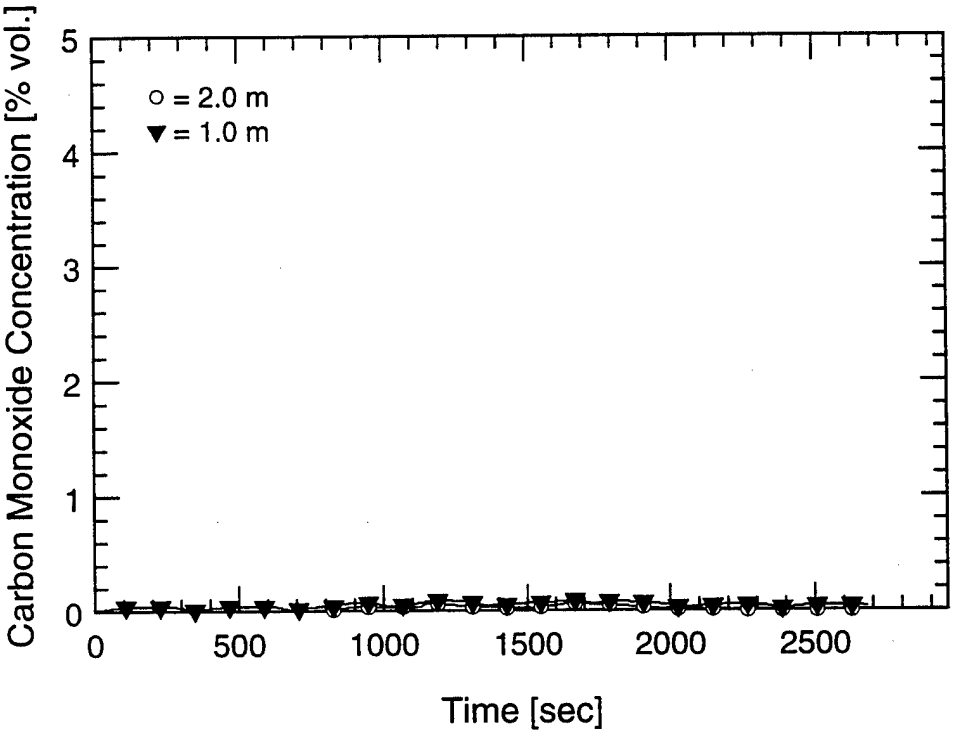

Gas Tree #1

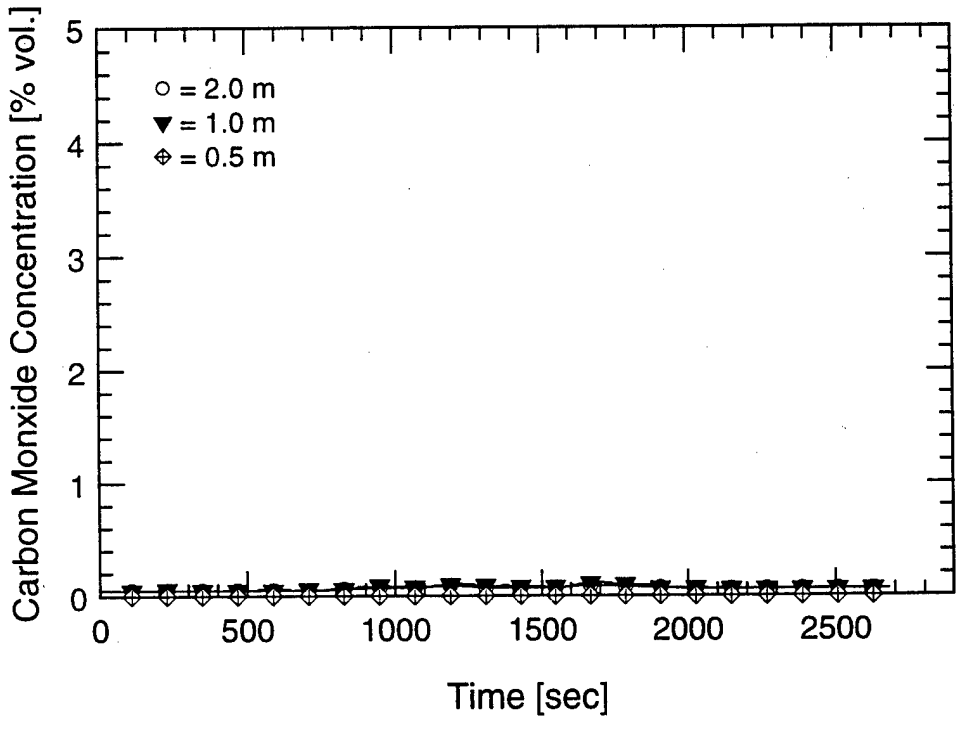

Gas Tree #2

Carbon Monoxide Concentration Measurements
Test 1-1

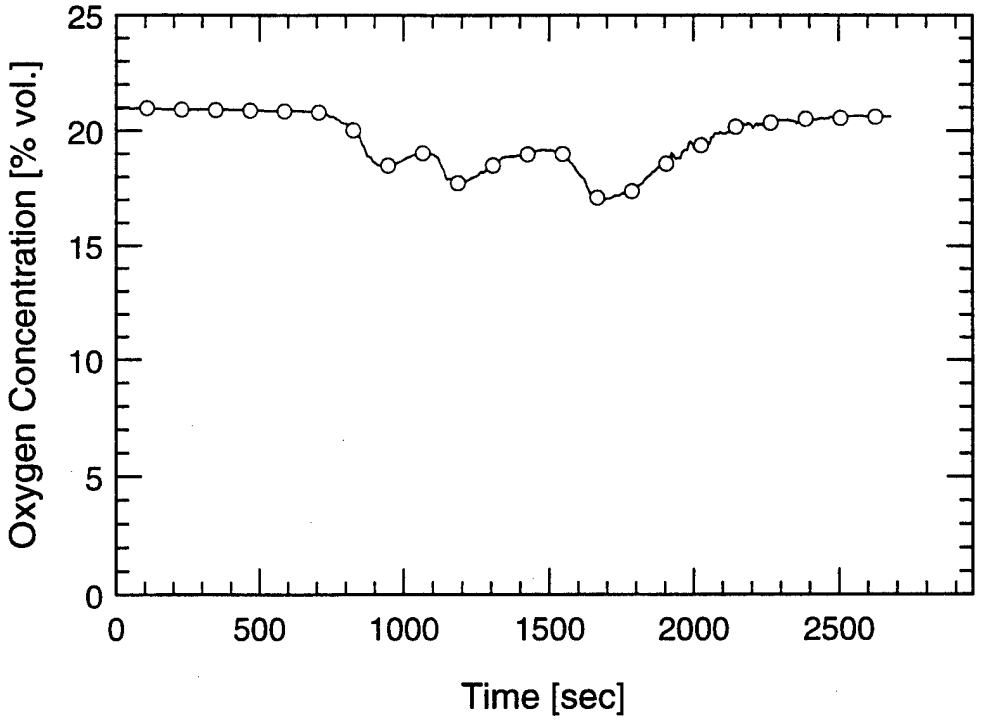

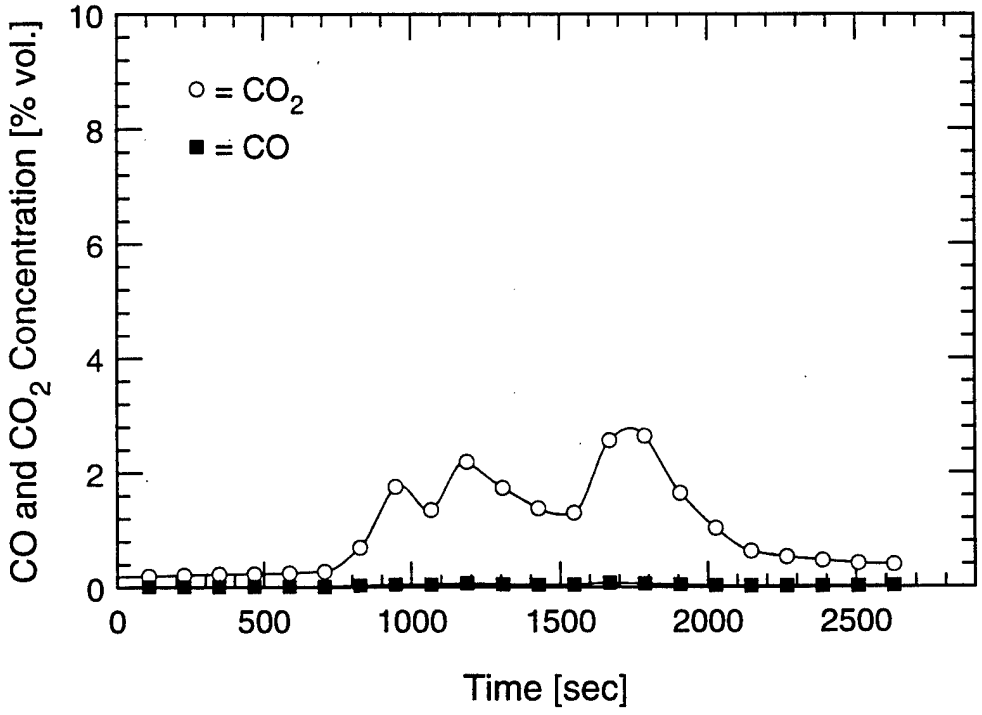

Gas Species Measurements in Doorway (GT3)
Test 1-1

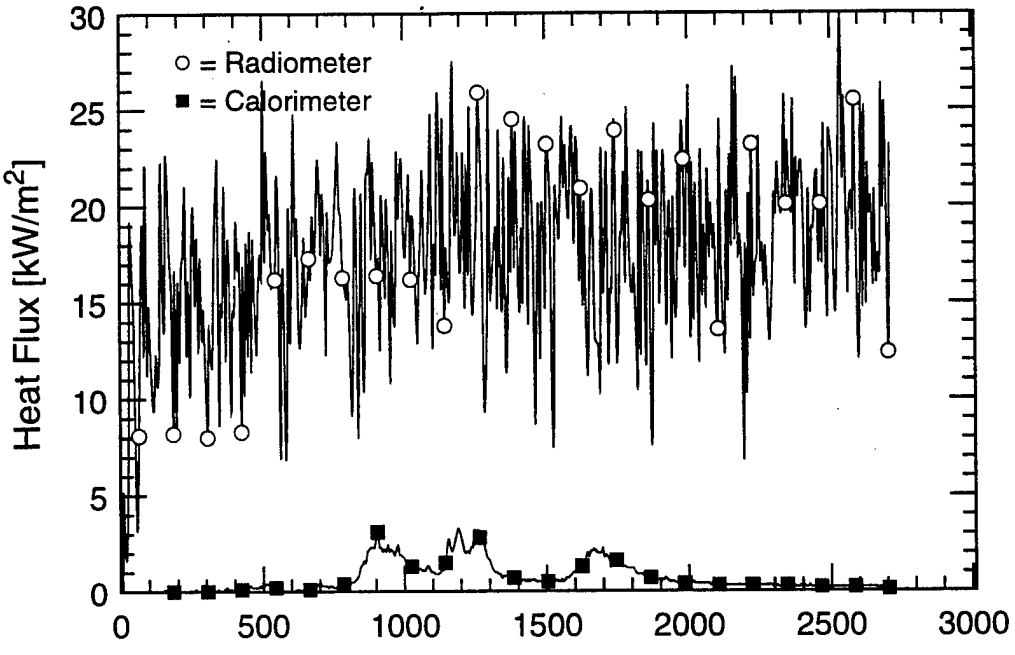

Location #1

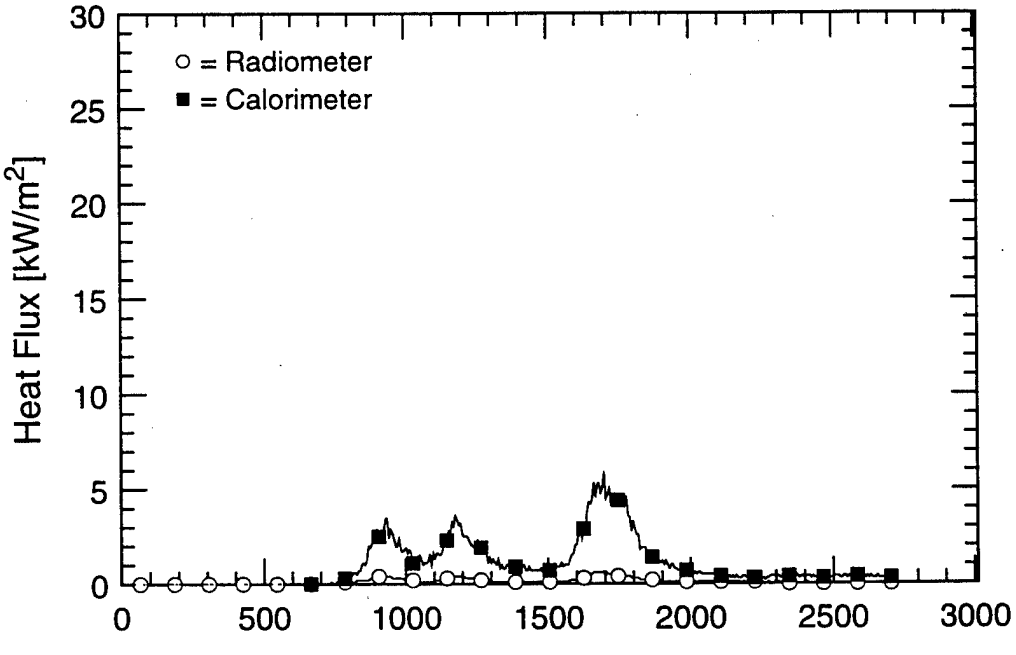

Location #2

Heat Flux Measurements
Test 1-1

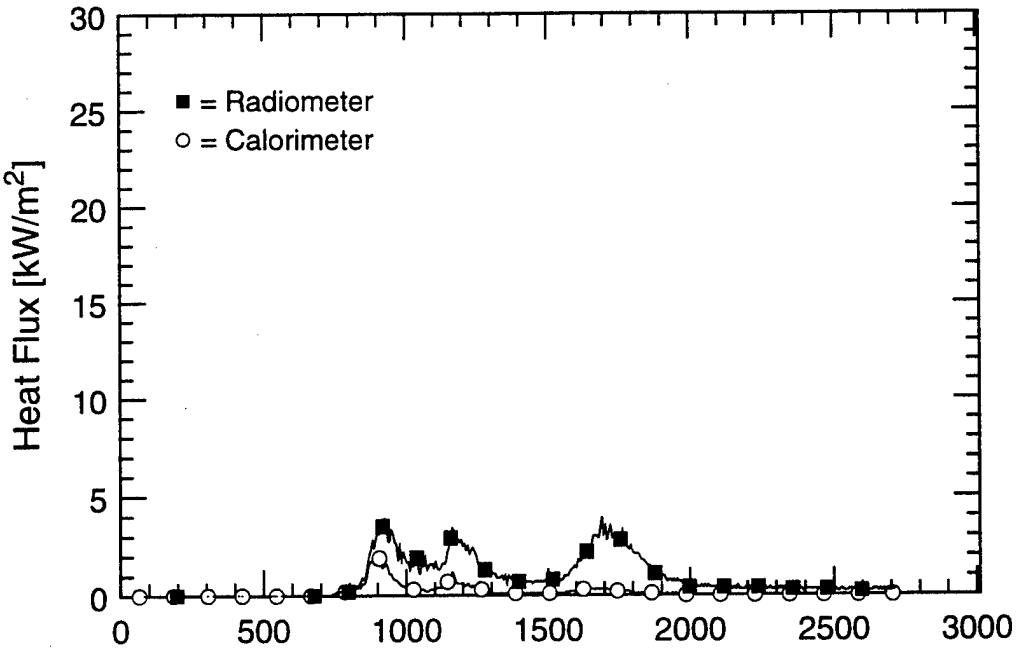

Location #3

Heat Flux Measurements

Test 1-1

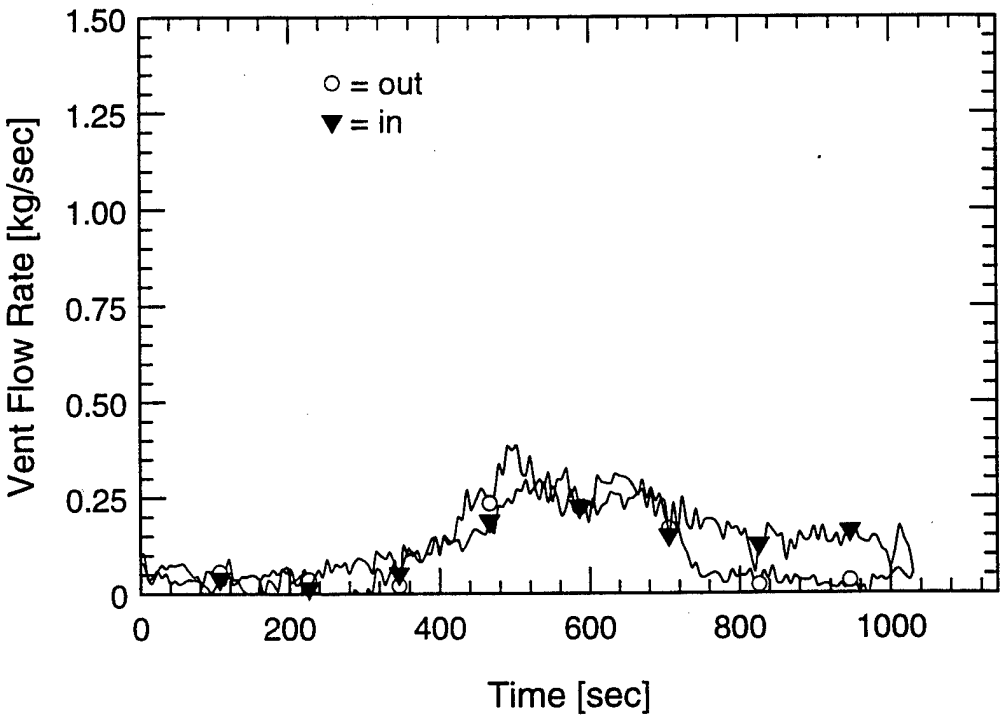

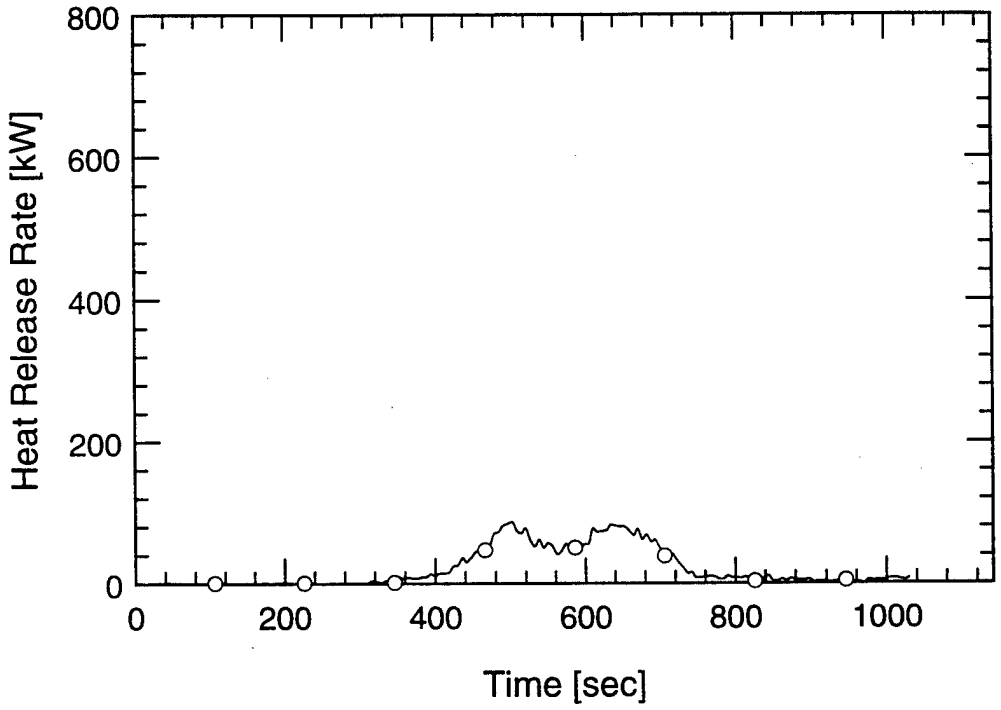

Vent Flow Rate and Heat Release Rate Measurements

Test 1-2A

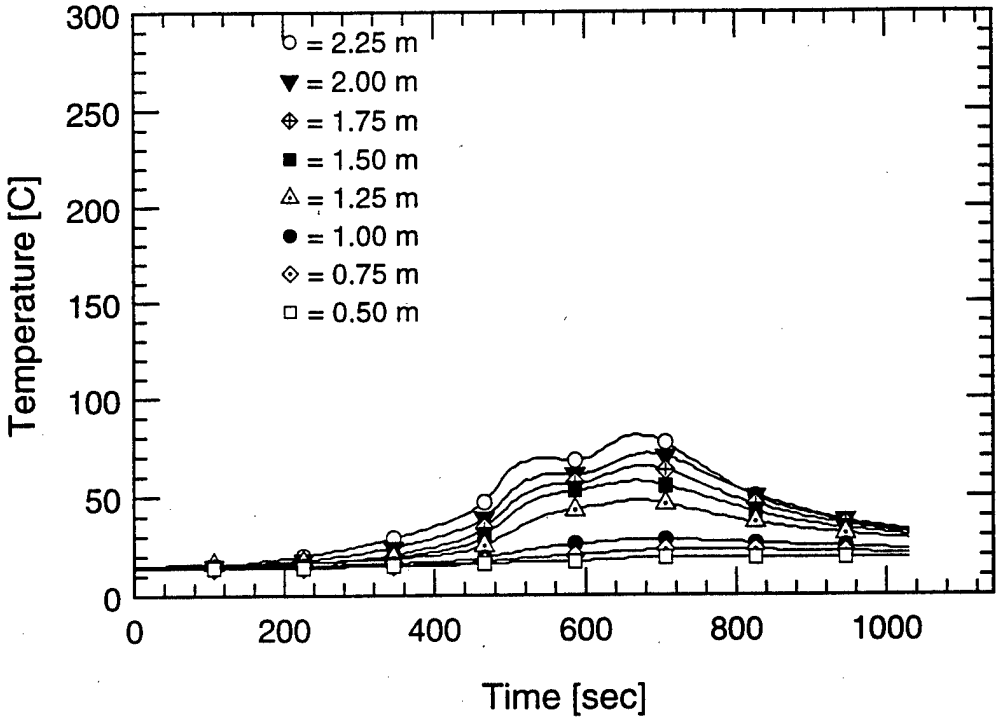

TC Tree #1

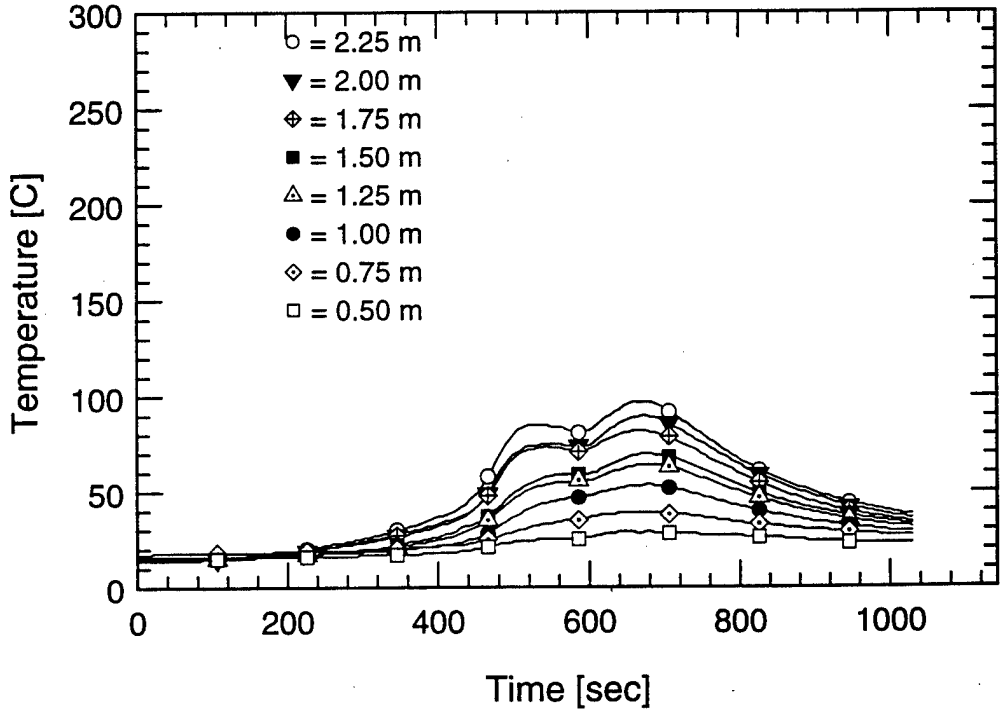

TC Tree #2

Temperature Measurements
Test 1-2A

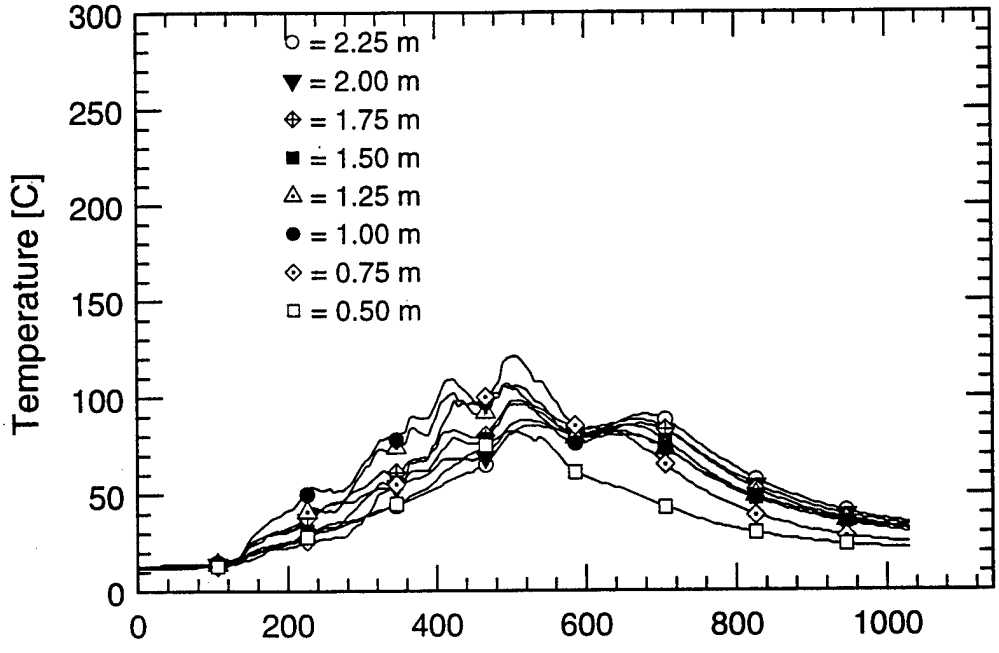

TC Tree #3

Temperature Measurements

Test 1-2A

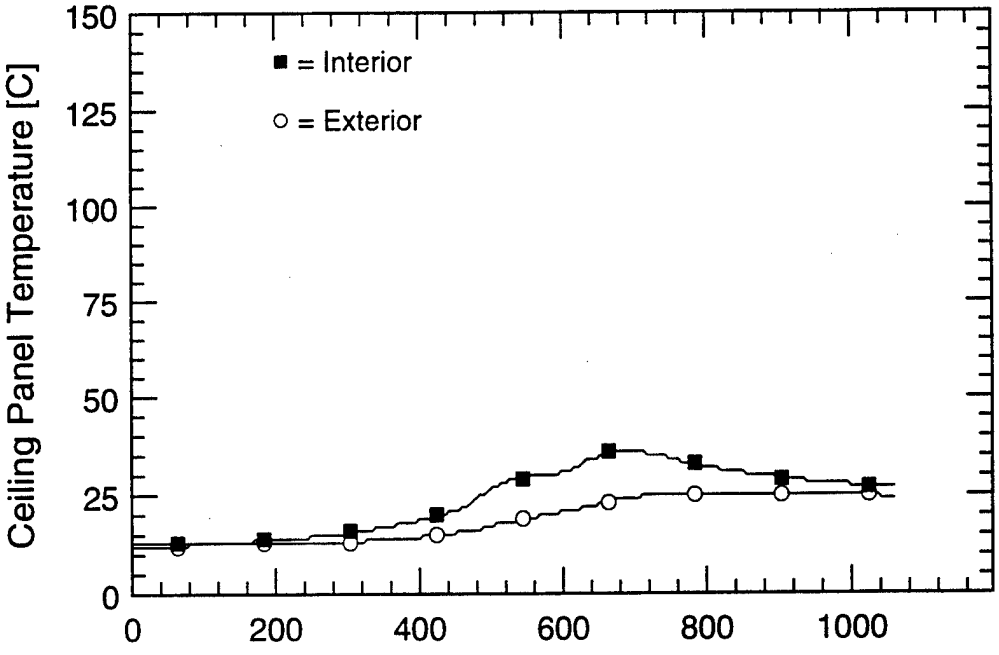

Location #1

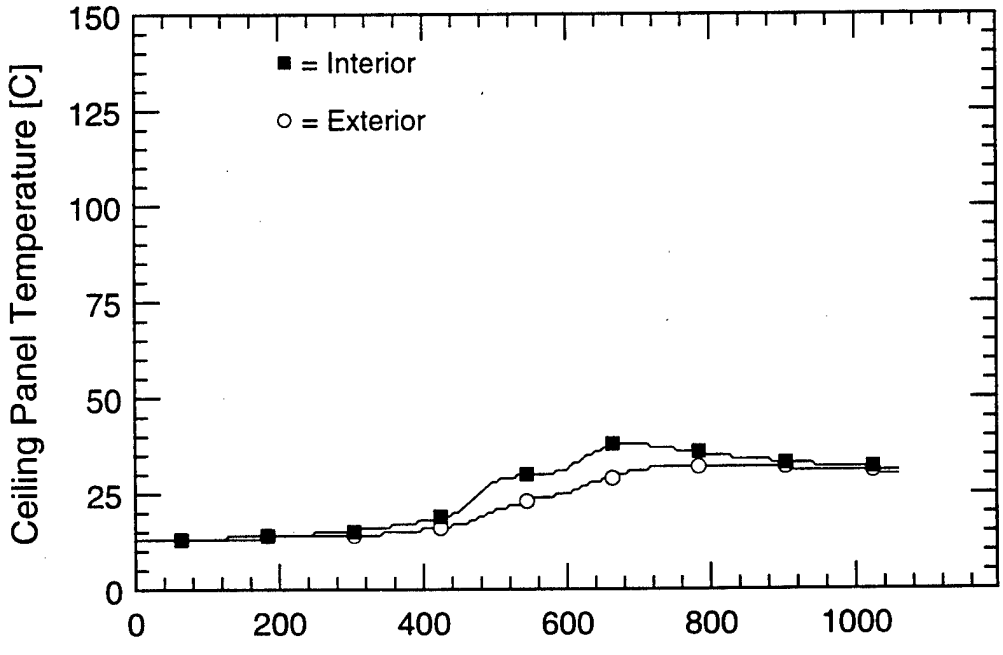

Location #2

Ceiling Panel Temperature Measurements
Test 1-2A

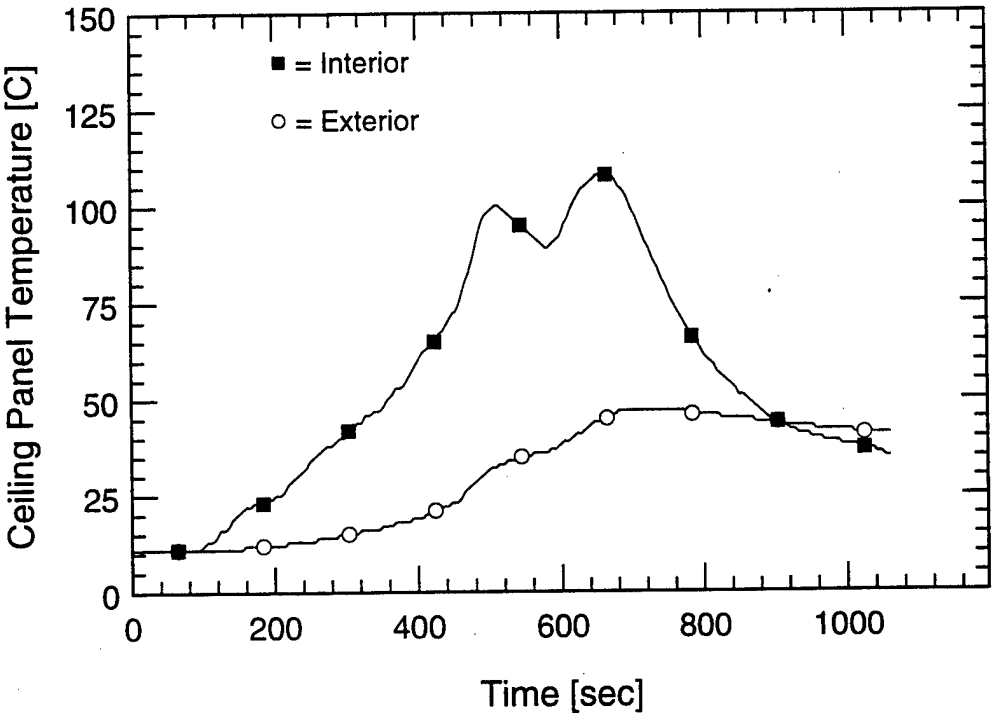

Location #3

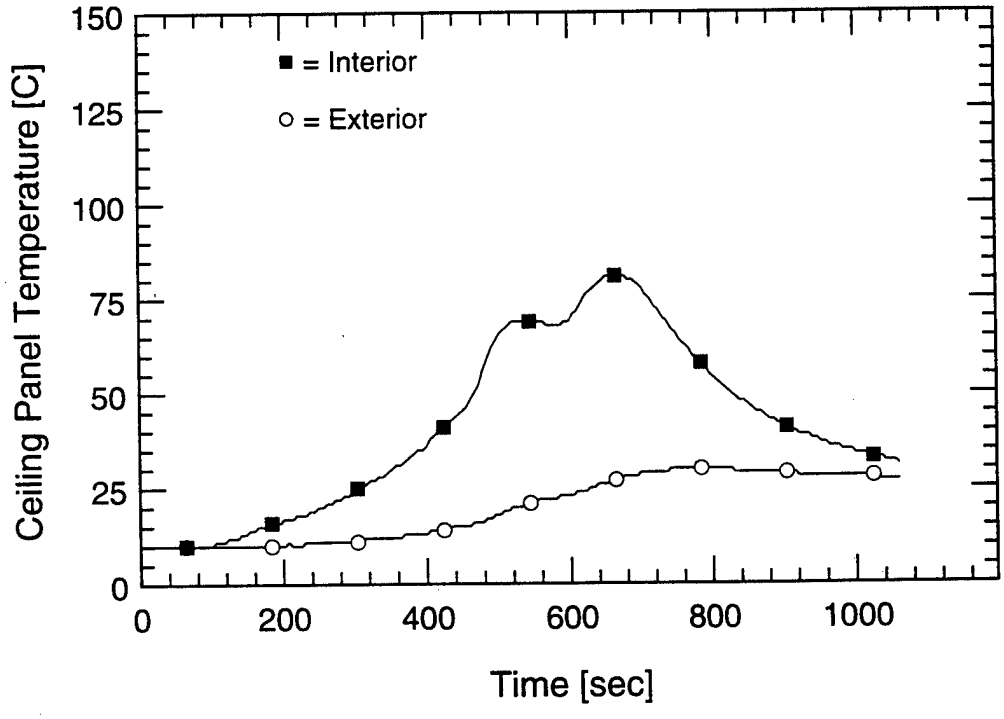

Location #4

Ceiling Panel Temperature Measurements
Test 1-2A

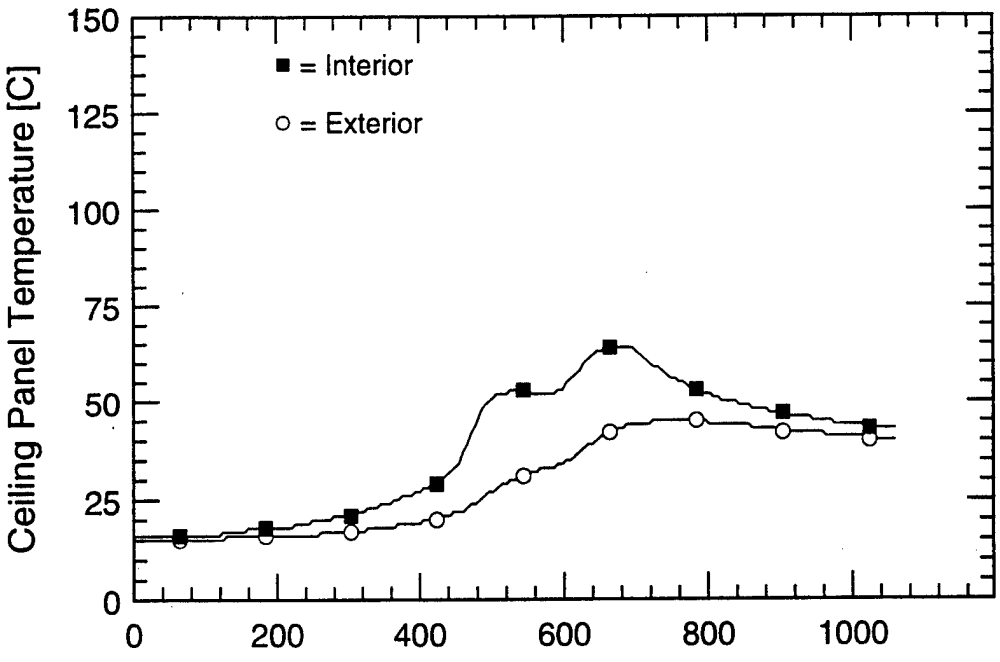

Location #5

Ceiling Panel Temperature Measurements
Test 1-2A

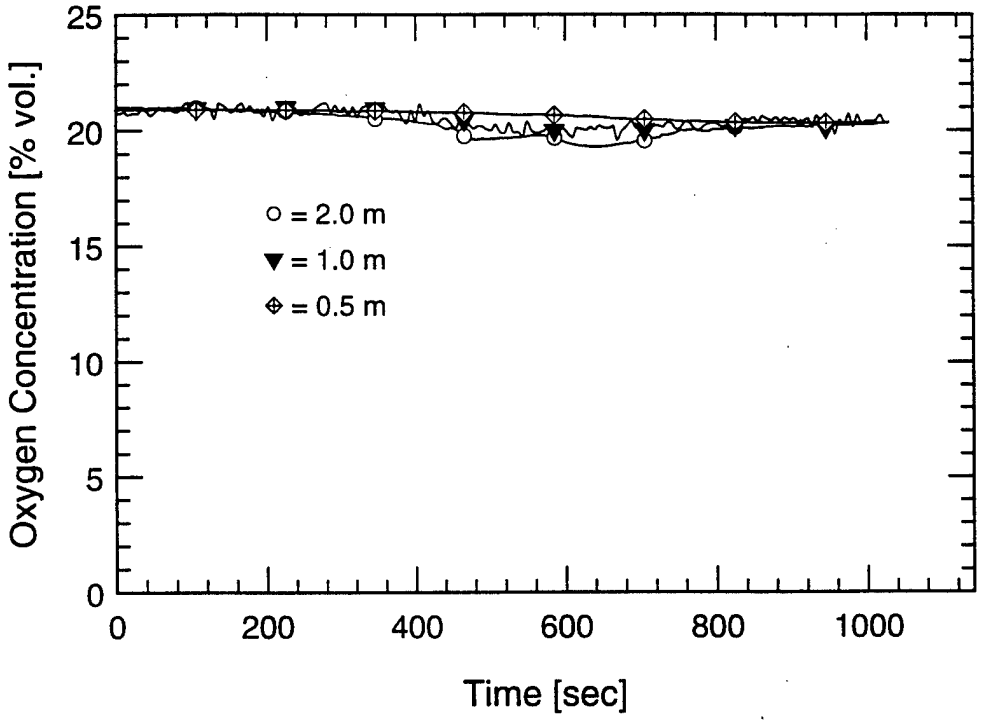

Gas Tree #1

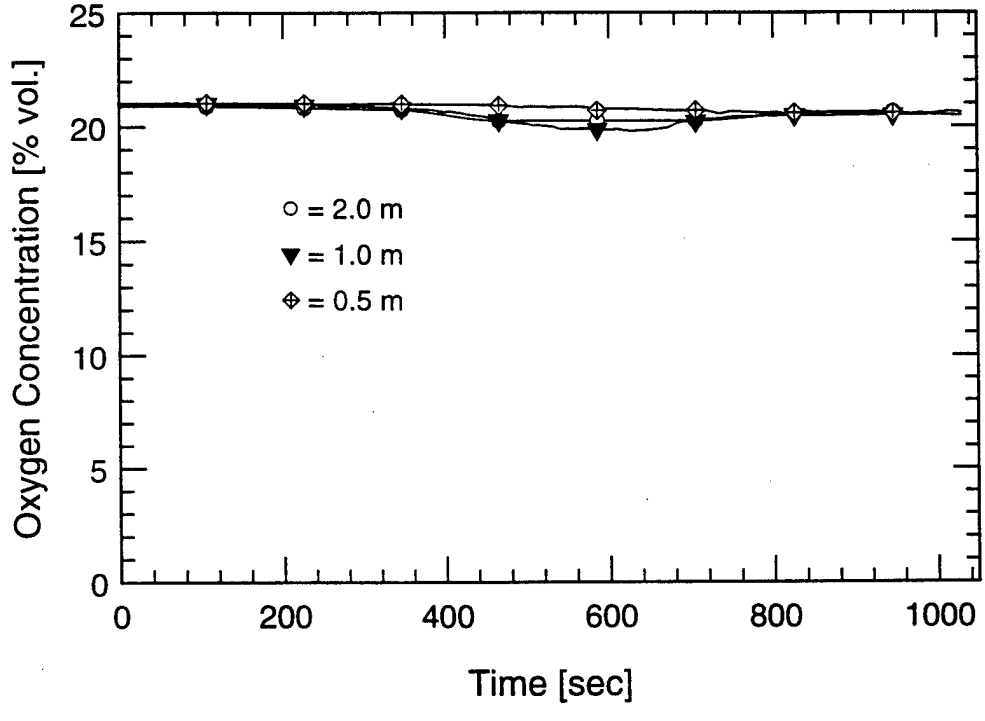

Gas Tree #2

Oxygen Concentration Measurements
Test 1-2A

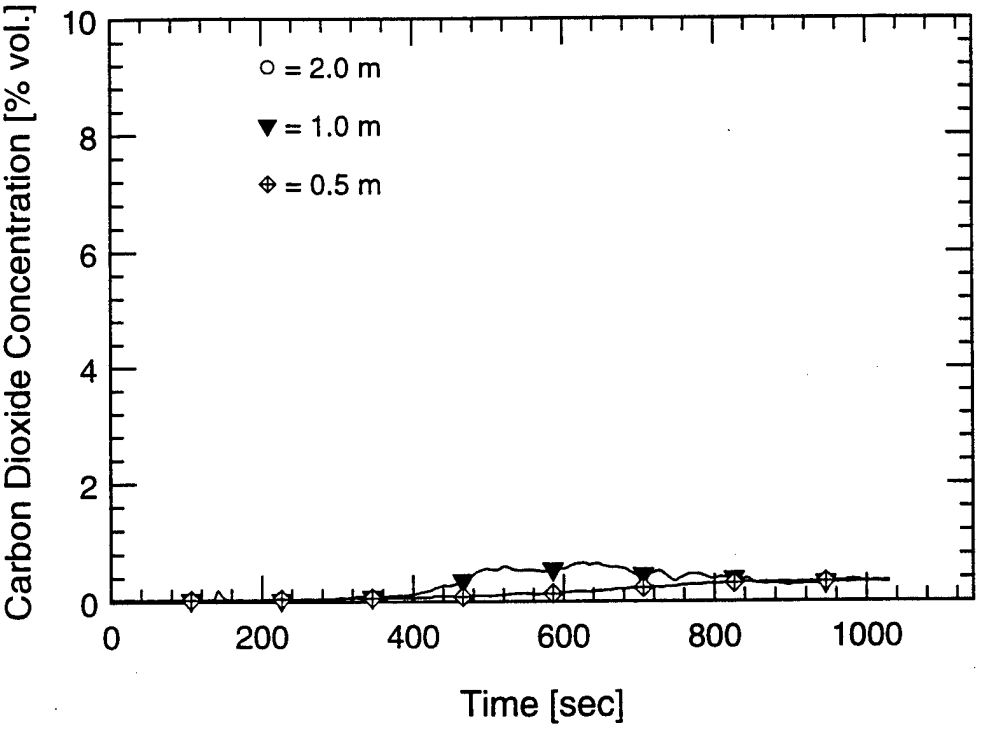

Gas Tree #1

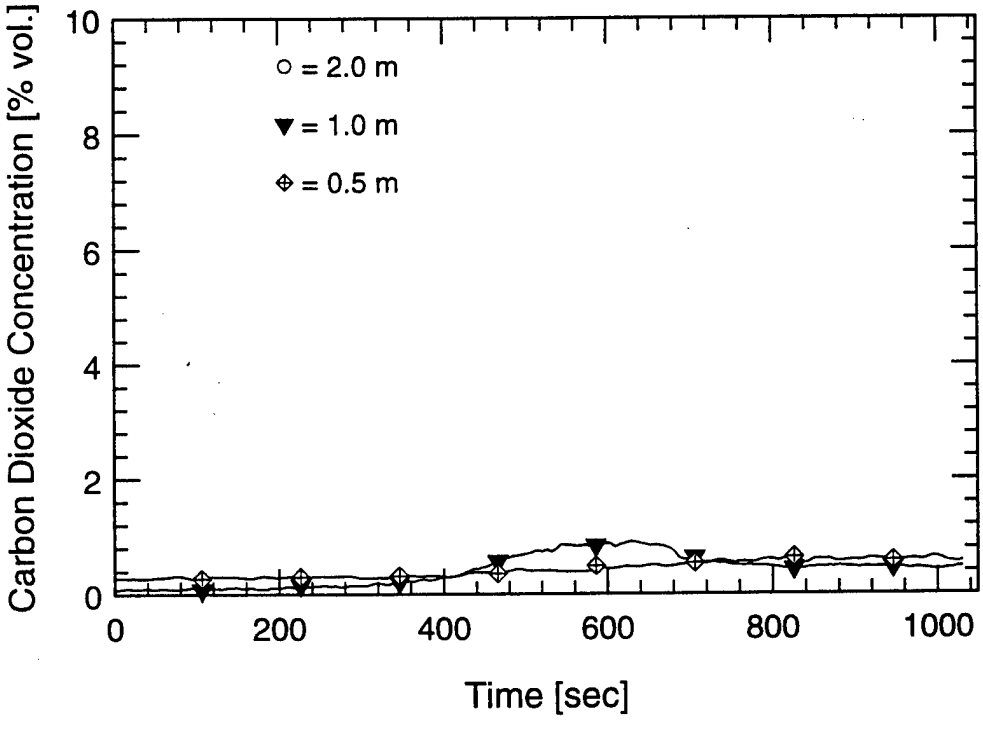

Gas Tree #2

Carbon Dioxide Concentration Measurements
Test 1-2A

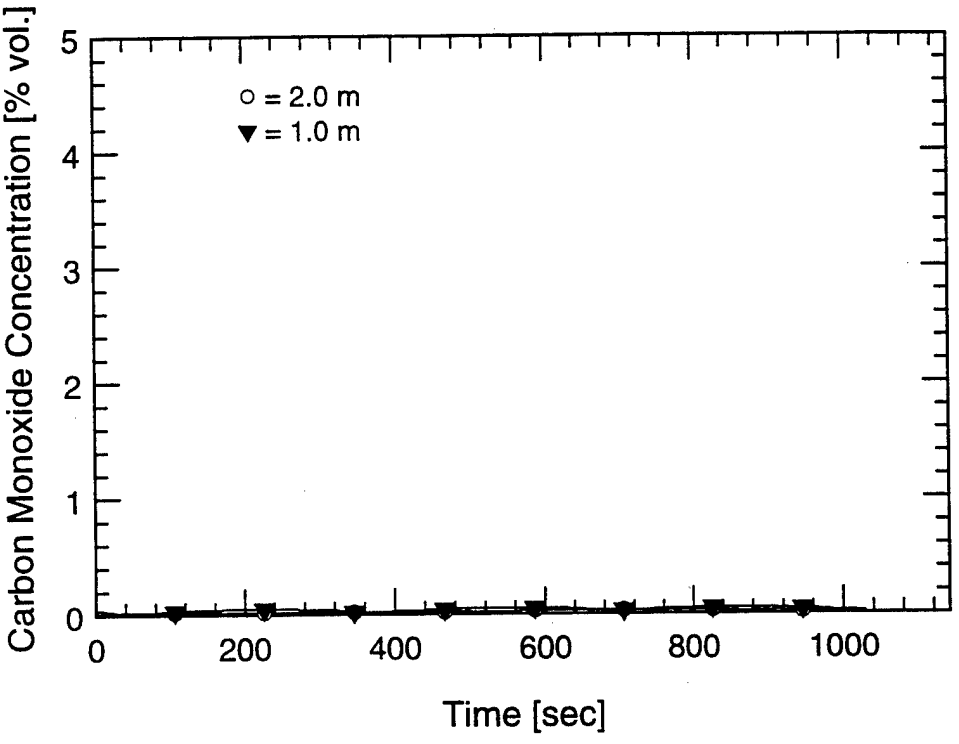

Gas Tree #1

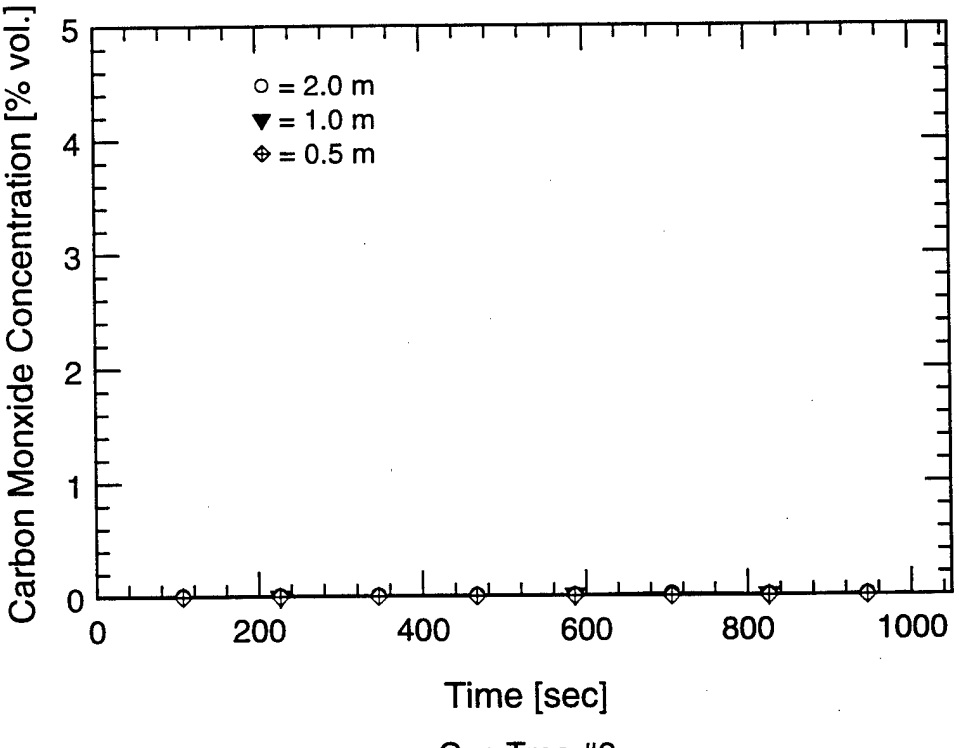

Gas Tree #2

Carbon Monoxide Concentration Measurements
Test 1-2A

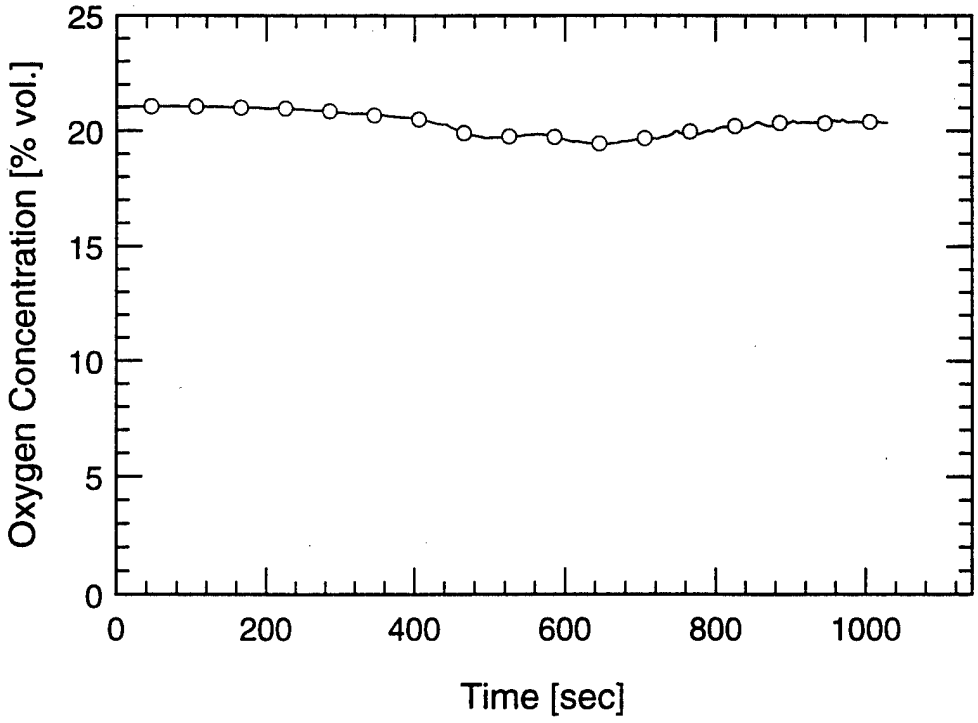

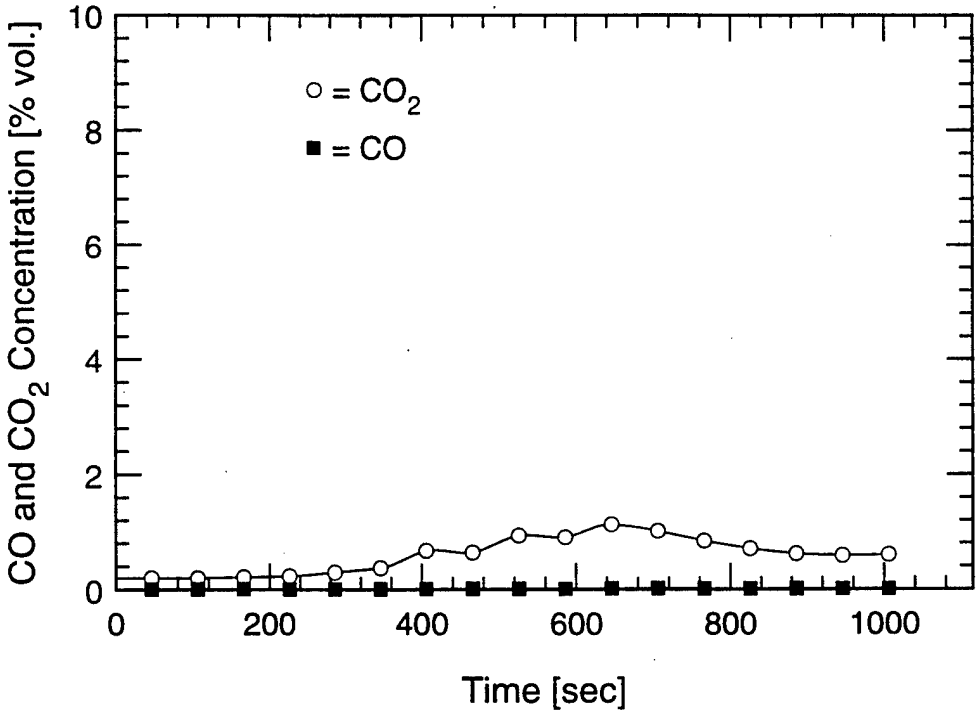

Gas Species Measurements in Doorway (GT3)

Test 1-2A

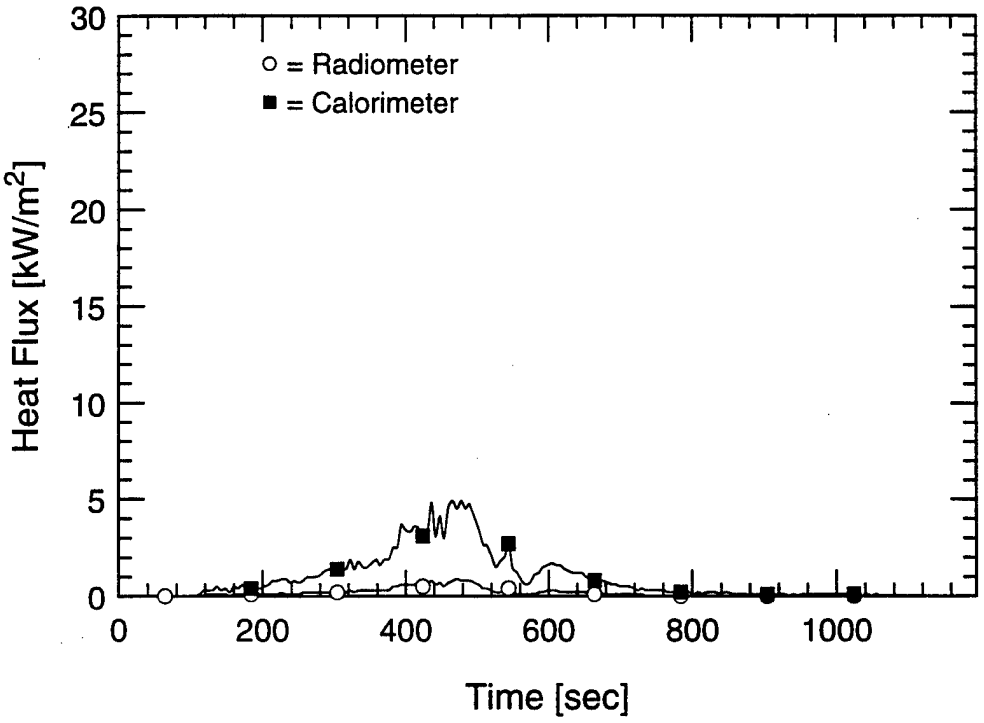

Location #1

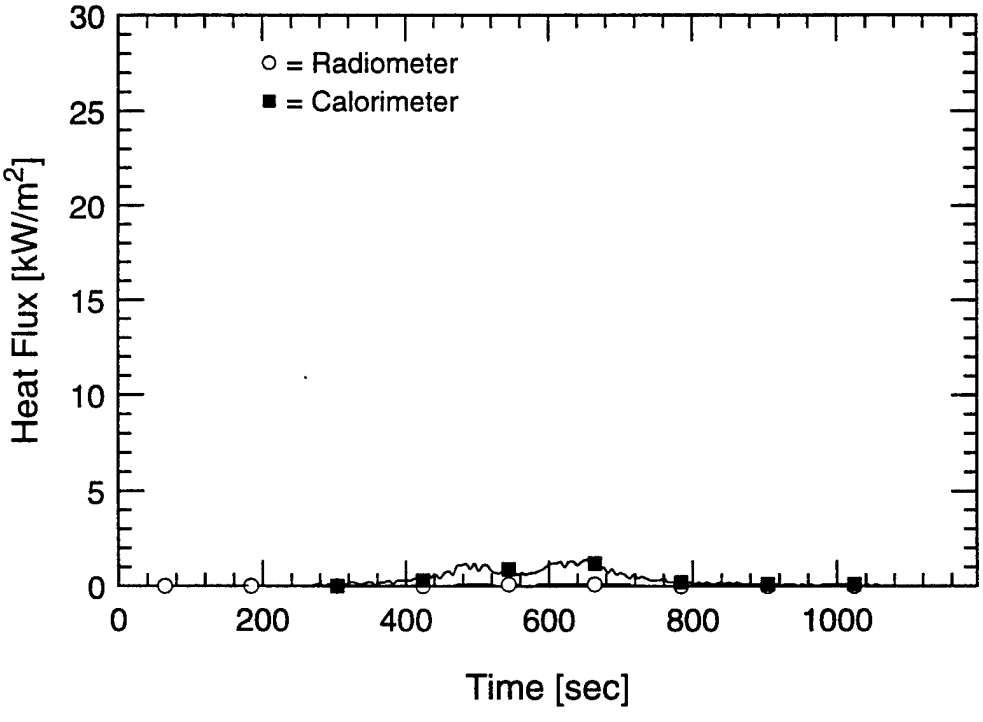

Location #2

Heat Flux Measurements
Test 1-2A

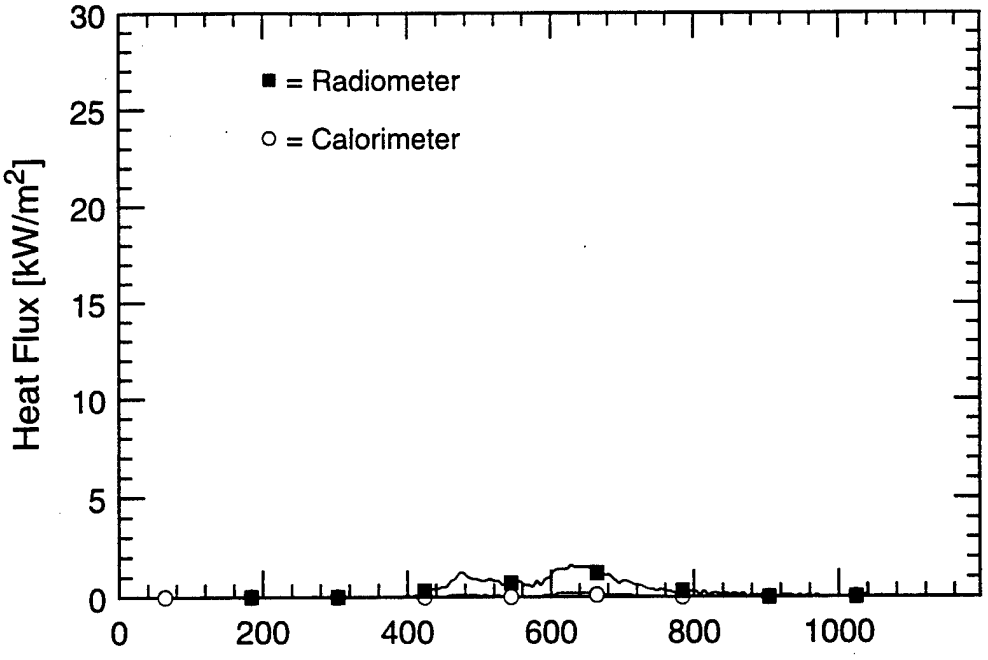

Location #3

Heat Flux Measurements

Test 1-2A

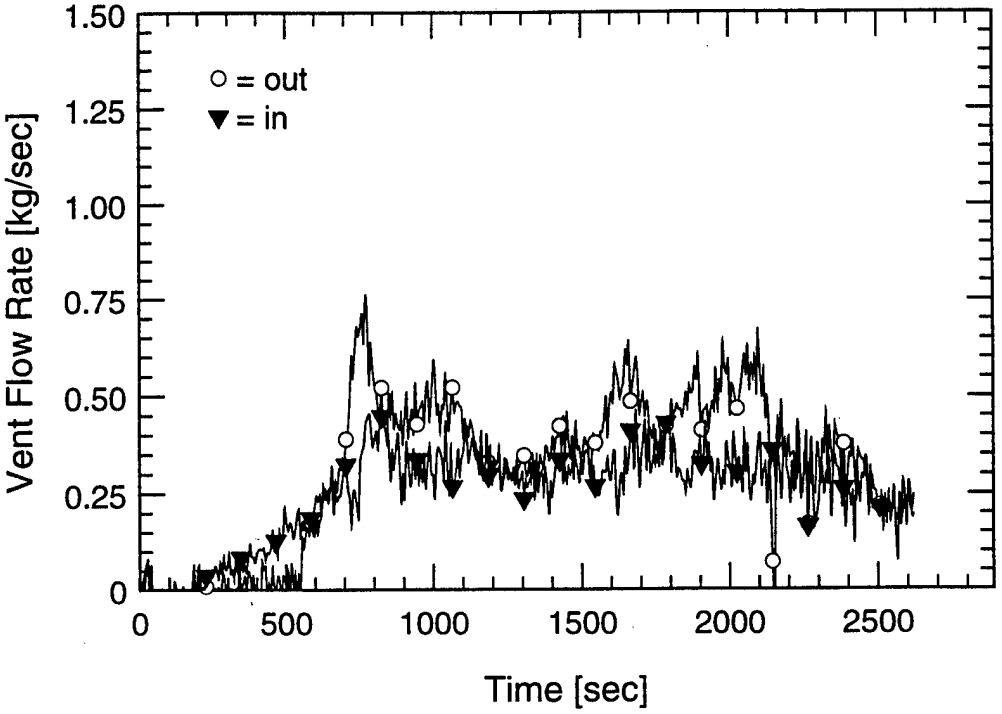

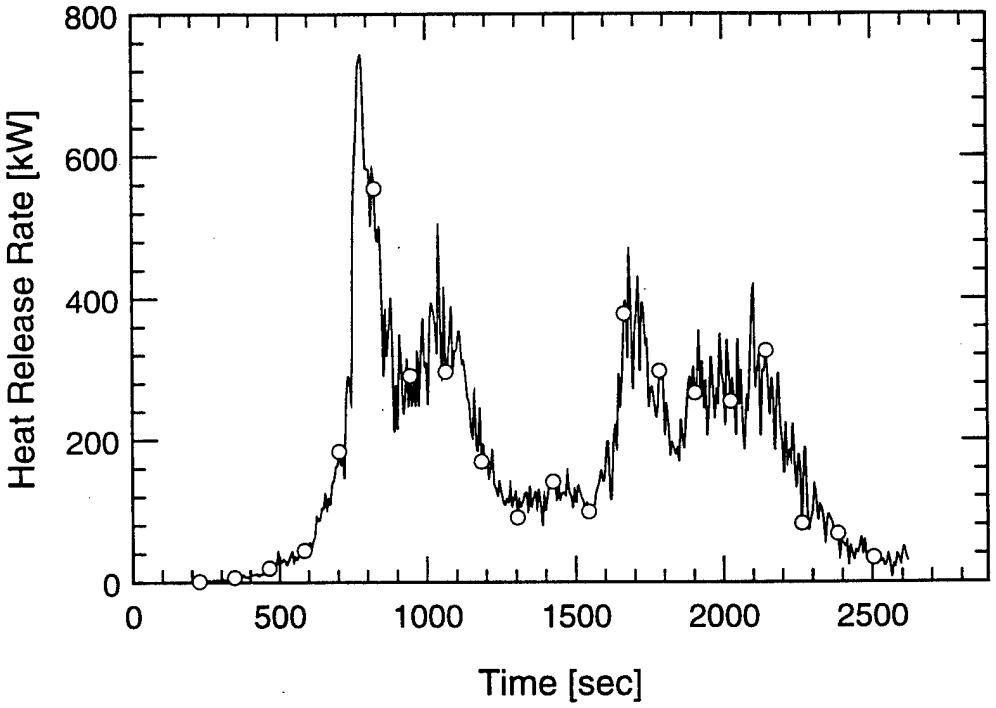

Vent Flow Rate and Heat Release Rate Measurements

Test 1-4

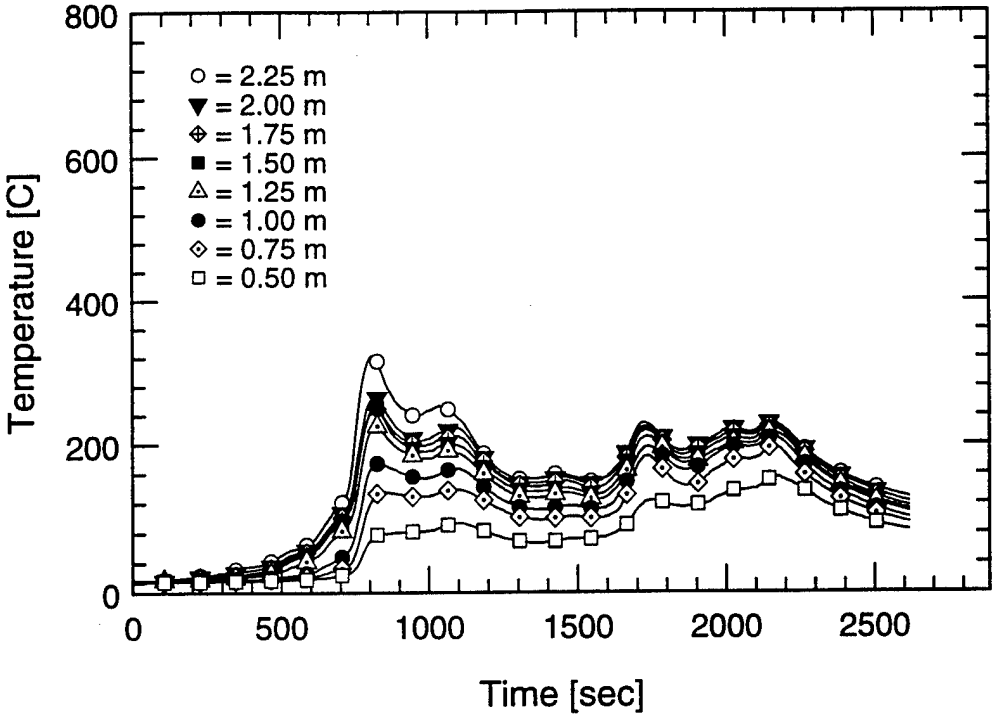

TC Tree #1

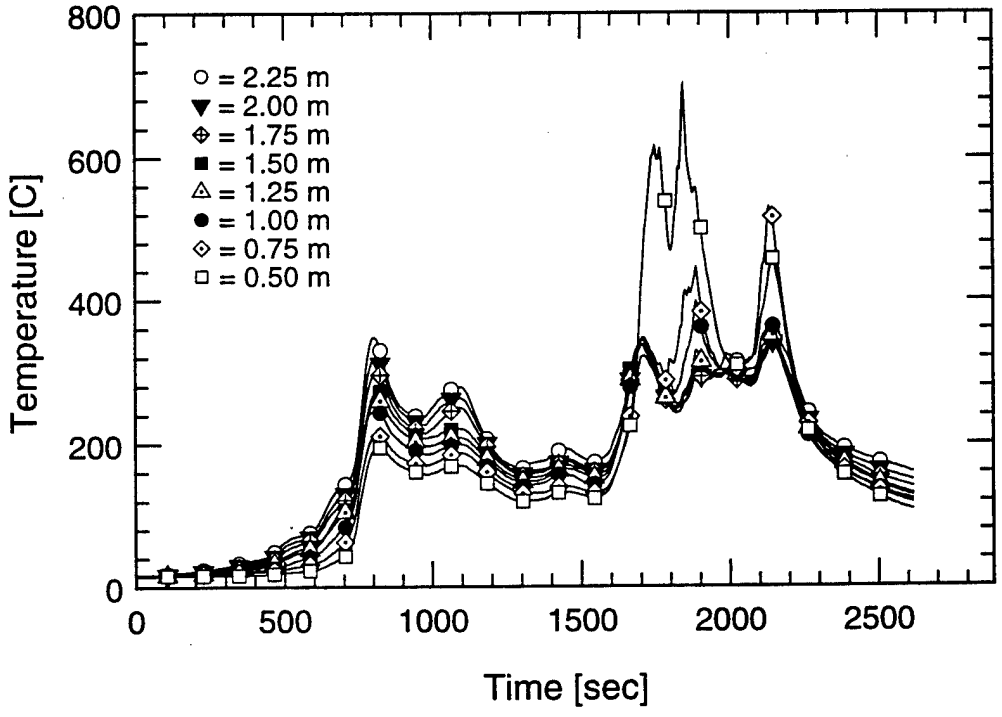

TC Tree #2

Temperature Measurements
Test 1-4

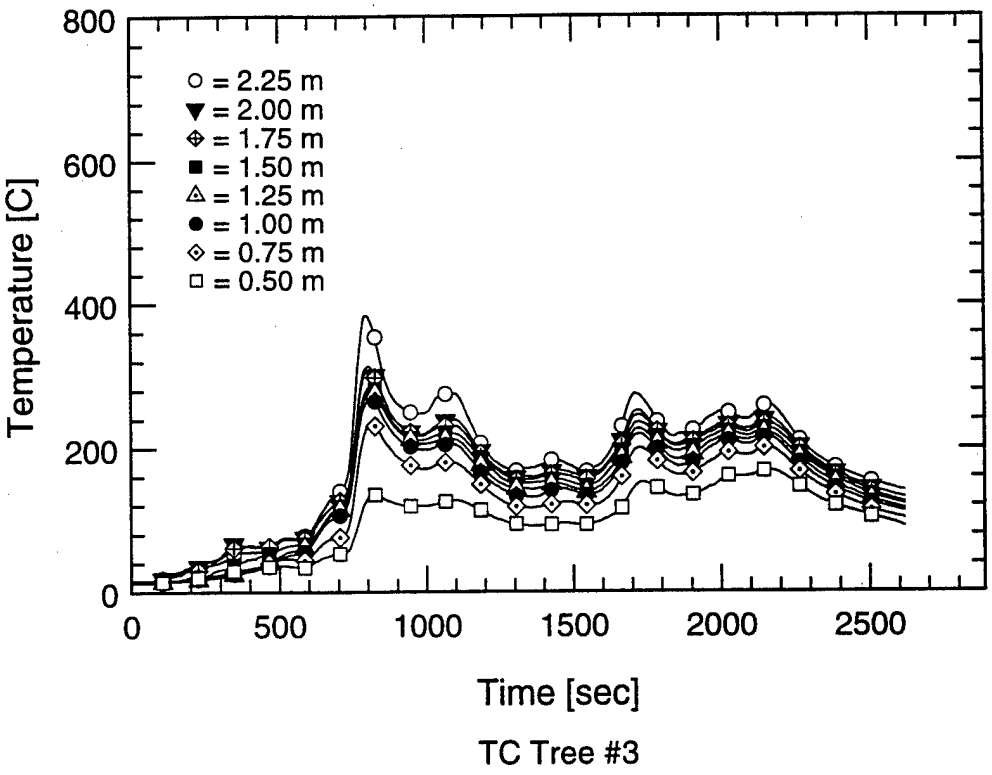

Temperature Measurements

Test 1-4

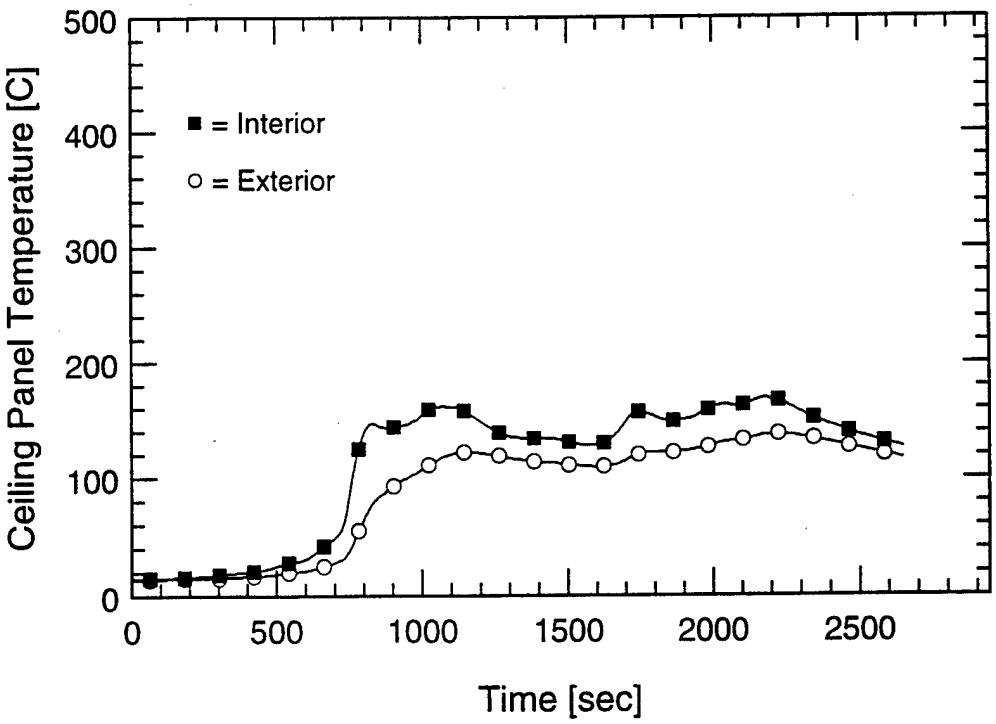

Location #1

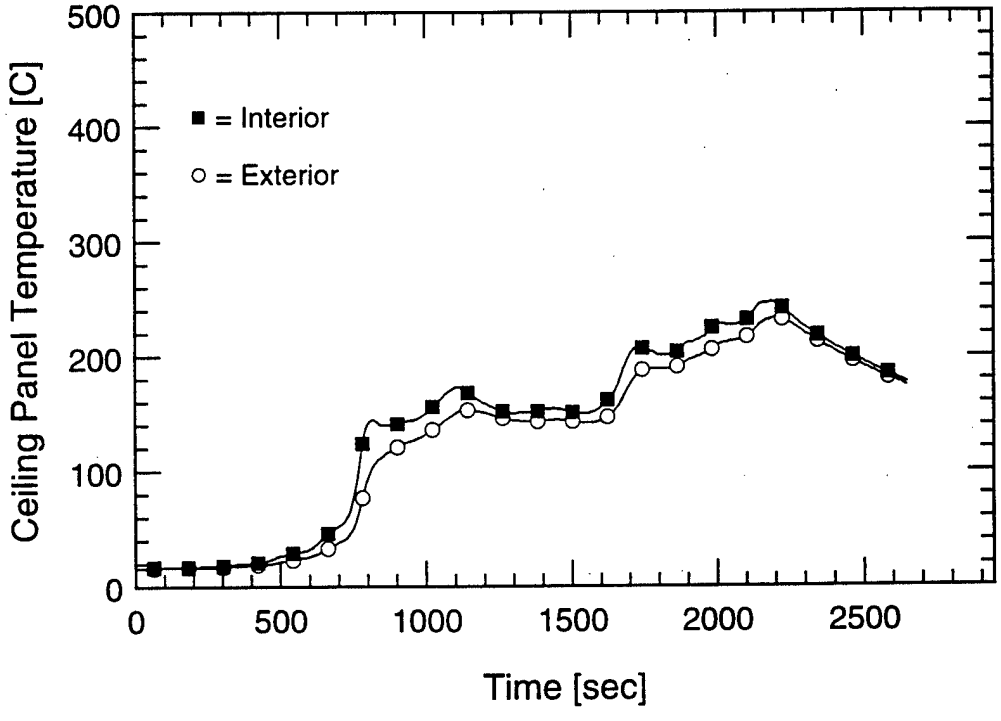

Location #2

Ceiling Panel Temperature Measurements
Test 1-4

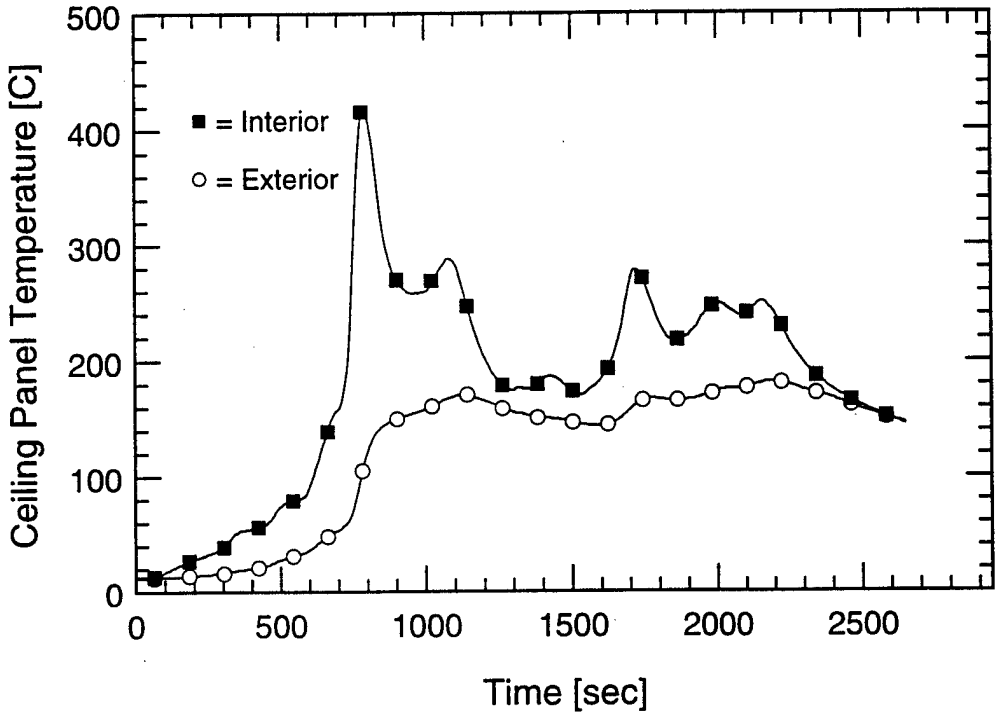

Location #3

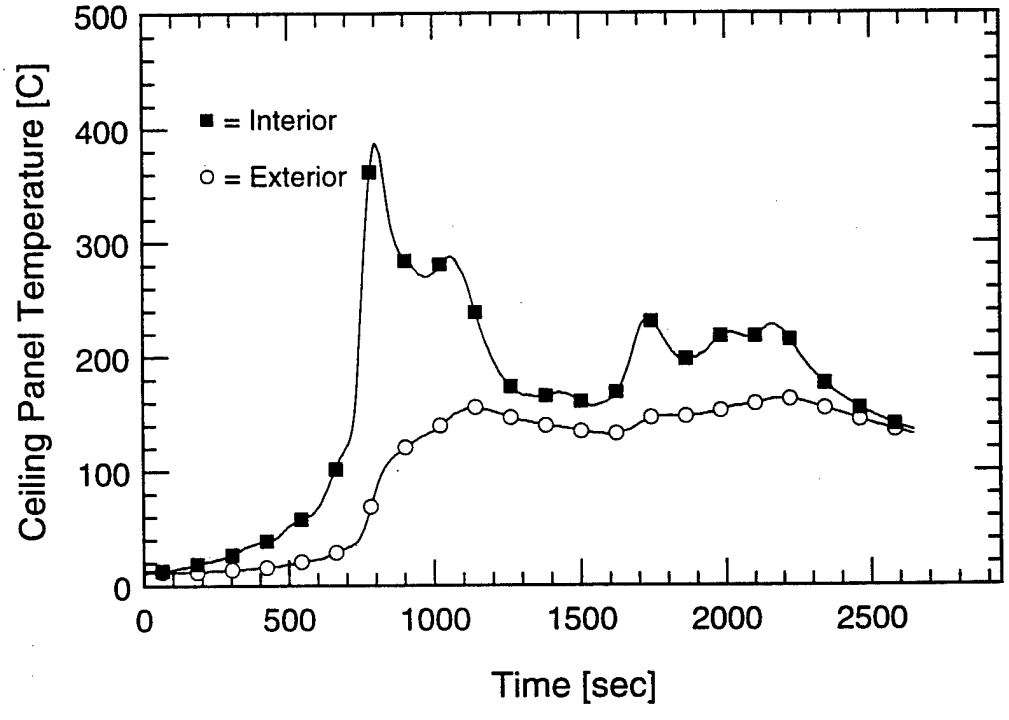

Location #4

Ceiling Panel Temperature Measurements
Test 1-4

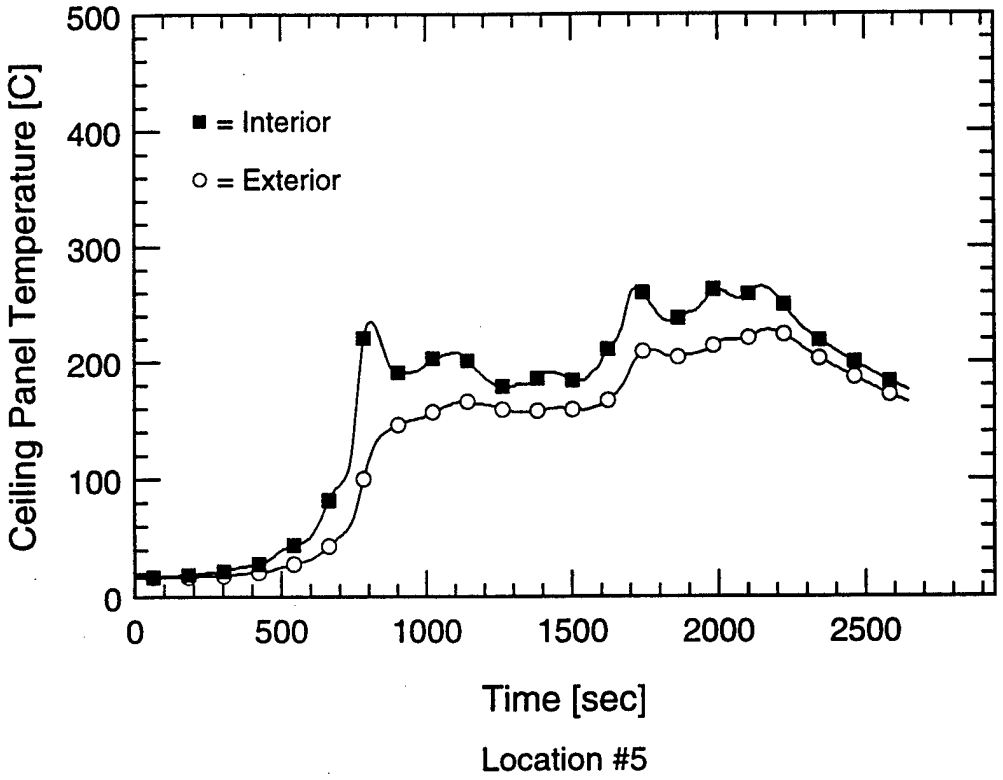

Ceiling Panel Temperature Measurements
Test 1-4

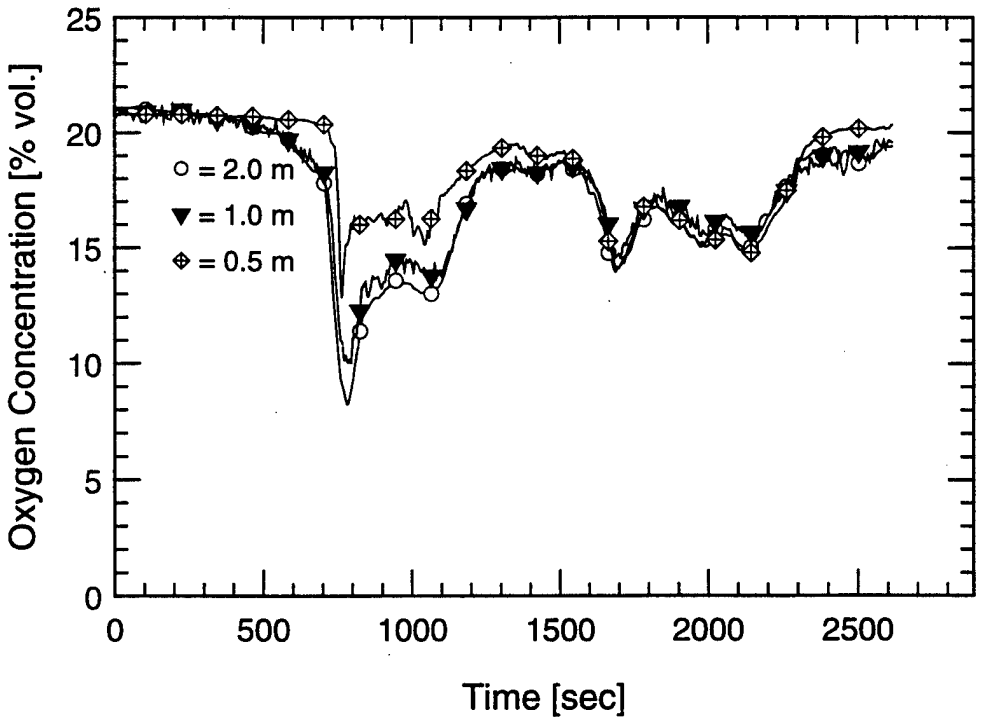

Gas Tree #1

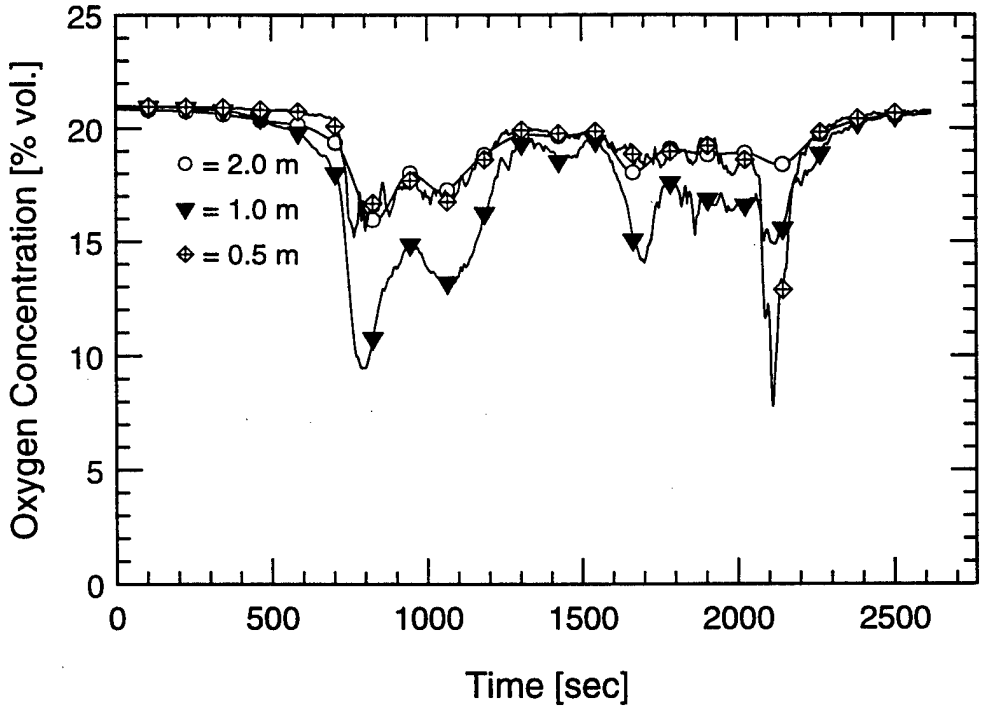

Gas Tree #2

Oxygen Concentration Measurements
Test 1-4

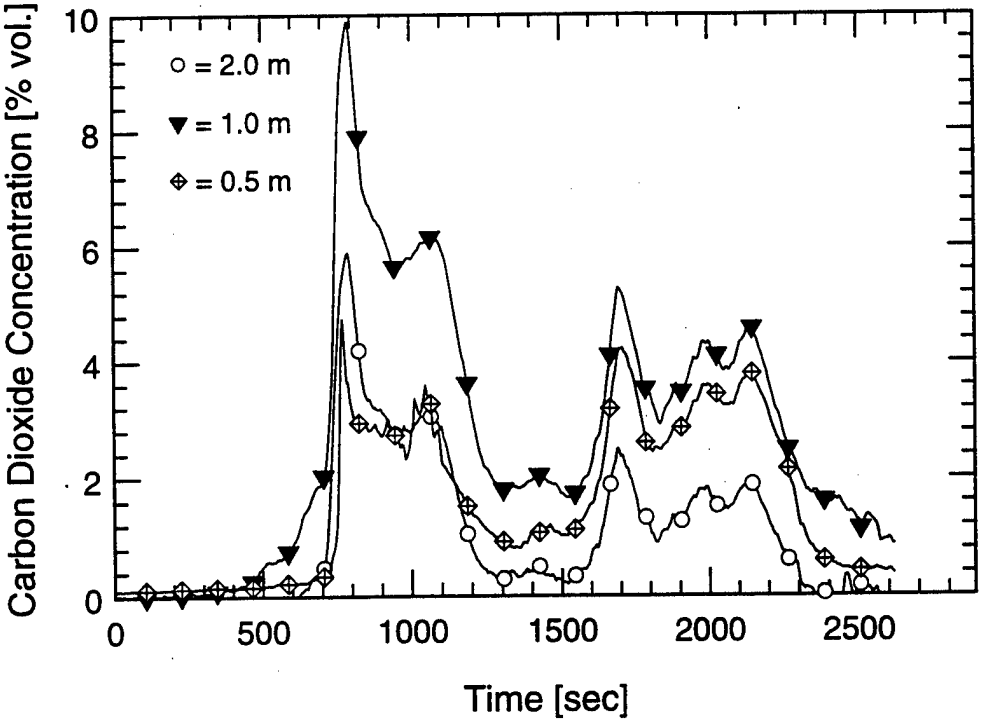

Gas Tree #1

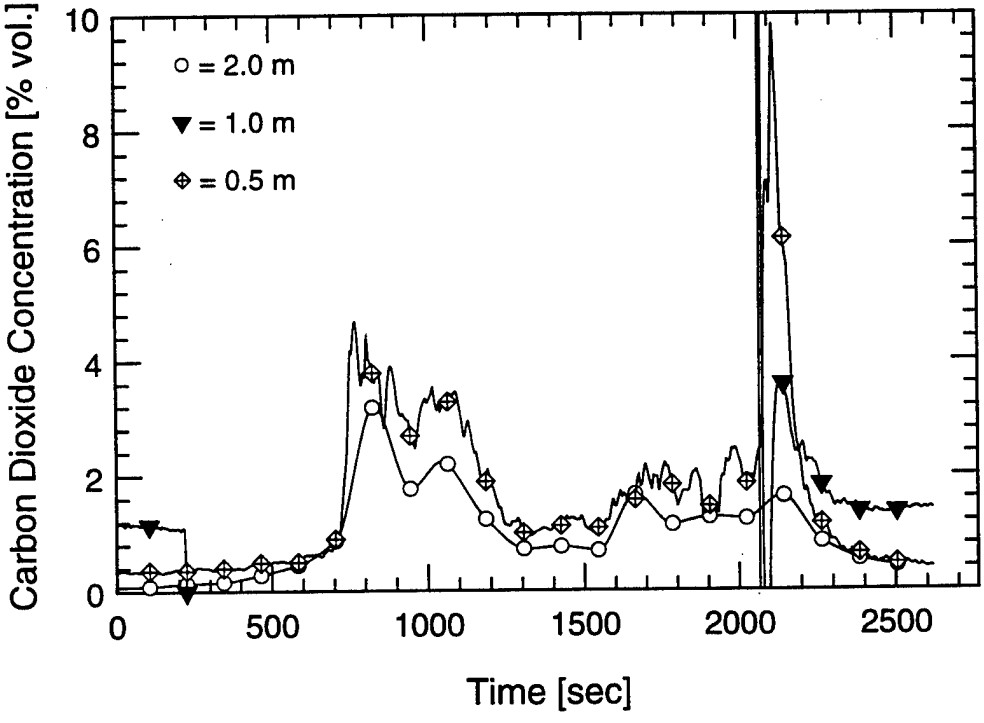

Gas Tree #2

Carbon Dioxide Concentration Measurements
Test 1-4

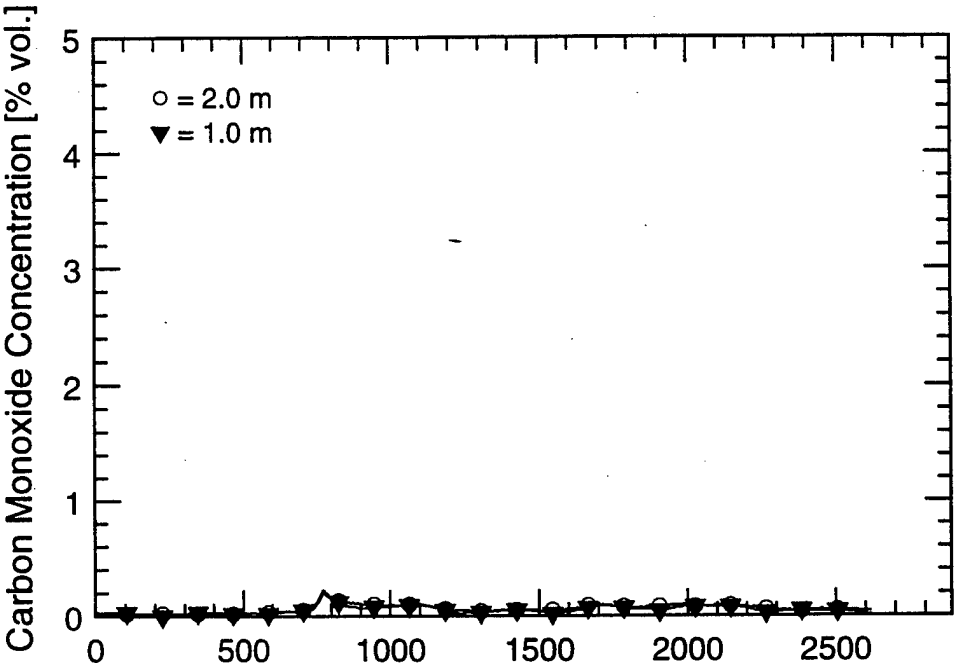

Gas Tree #1

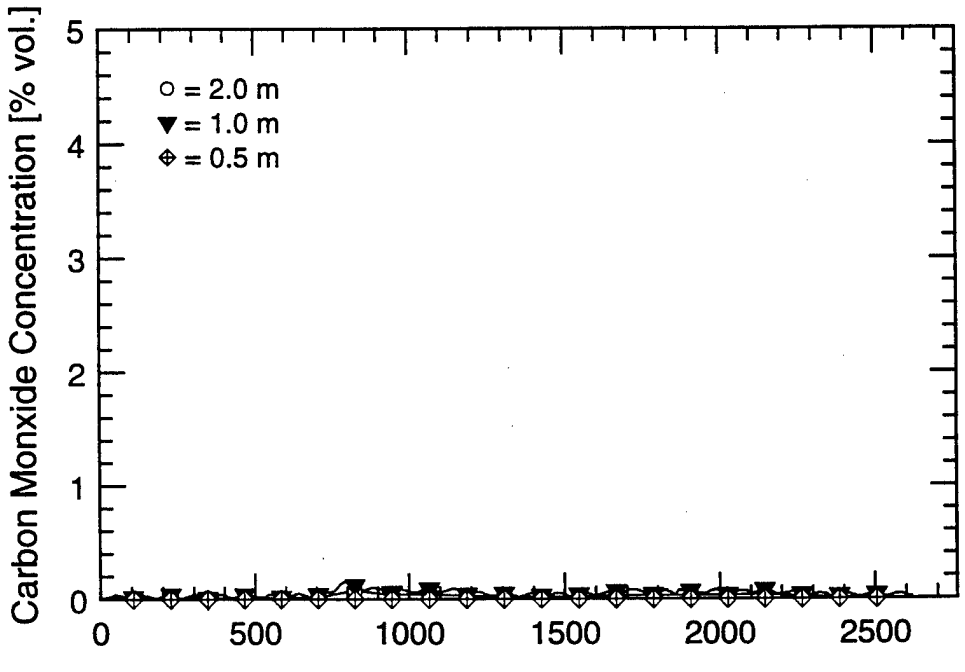

Gas Tree #2

Carbon Monoxide Concentration Measurements
Test 1-4

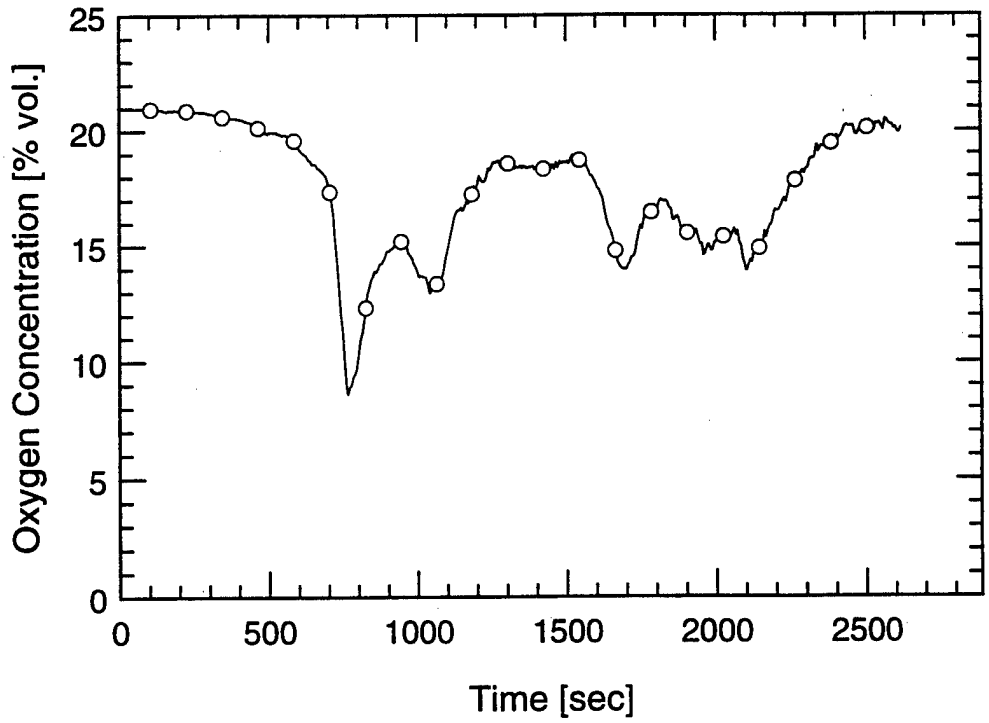

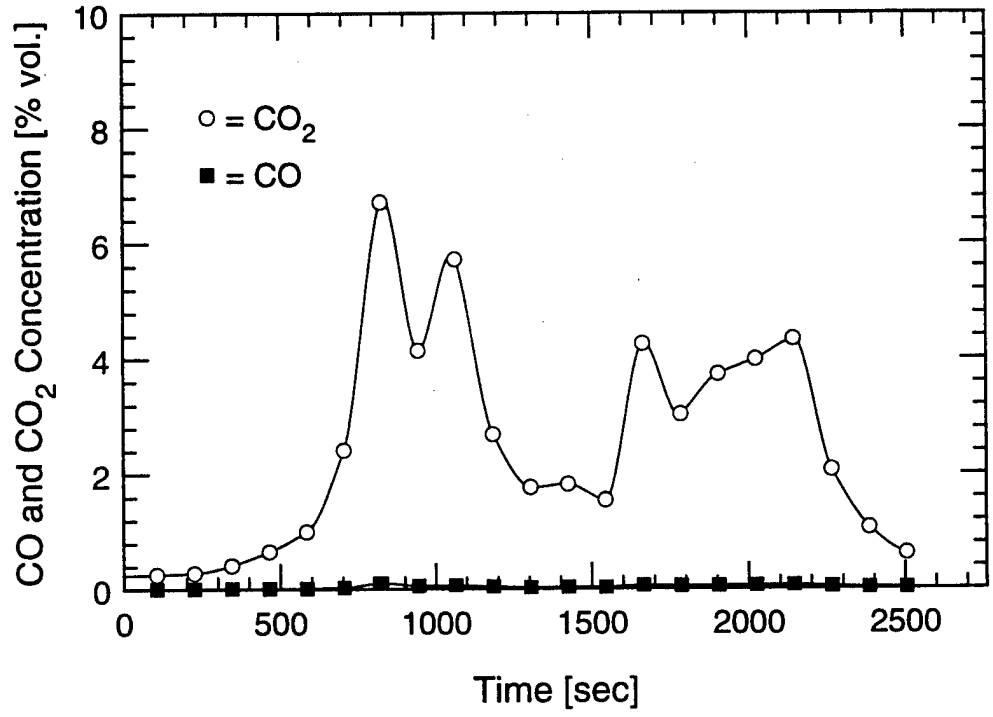

Gas Species Measurements in Doorway (GT3)

Test 1-4

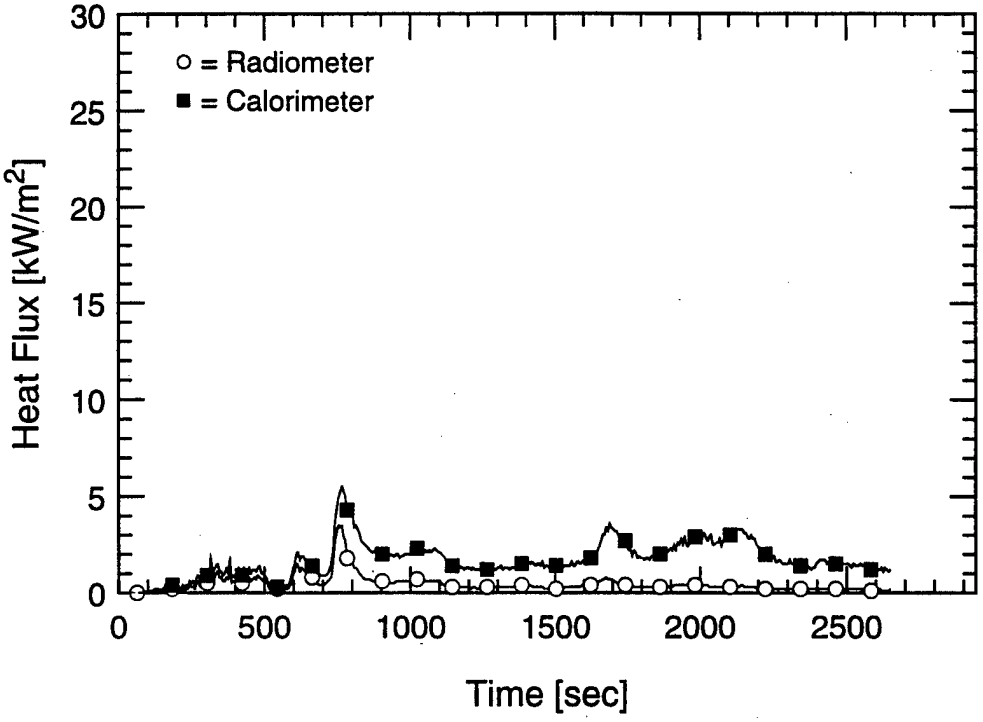

Location #1

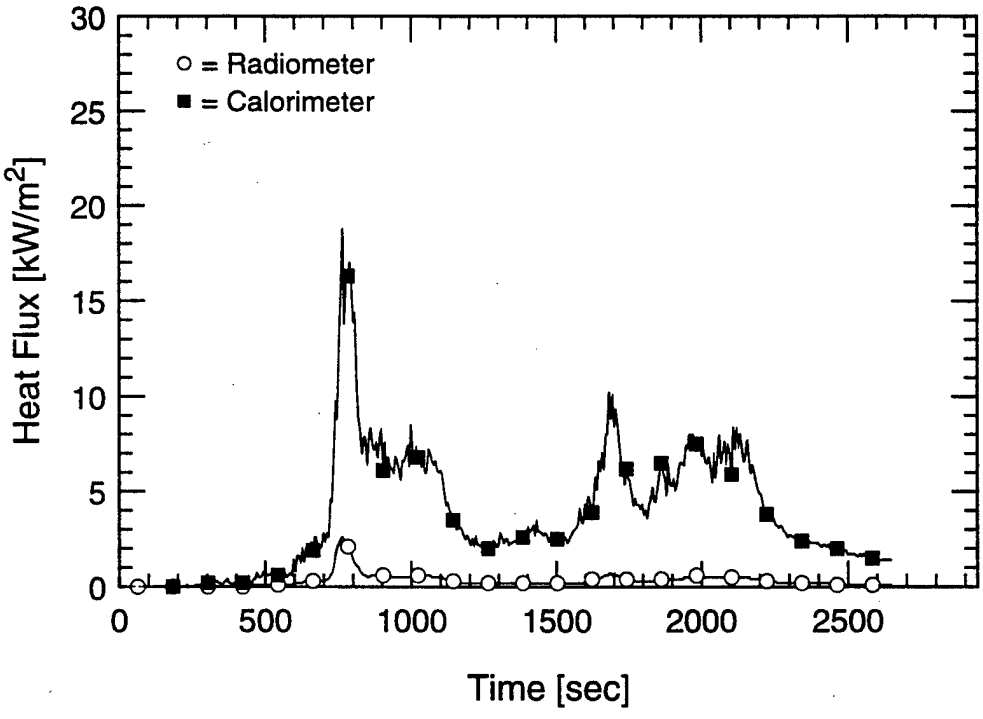

Location #2

Heat Flux Measurements
Test 1-4

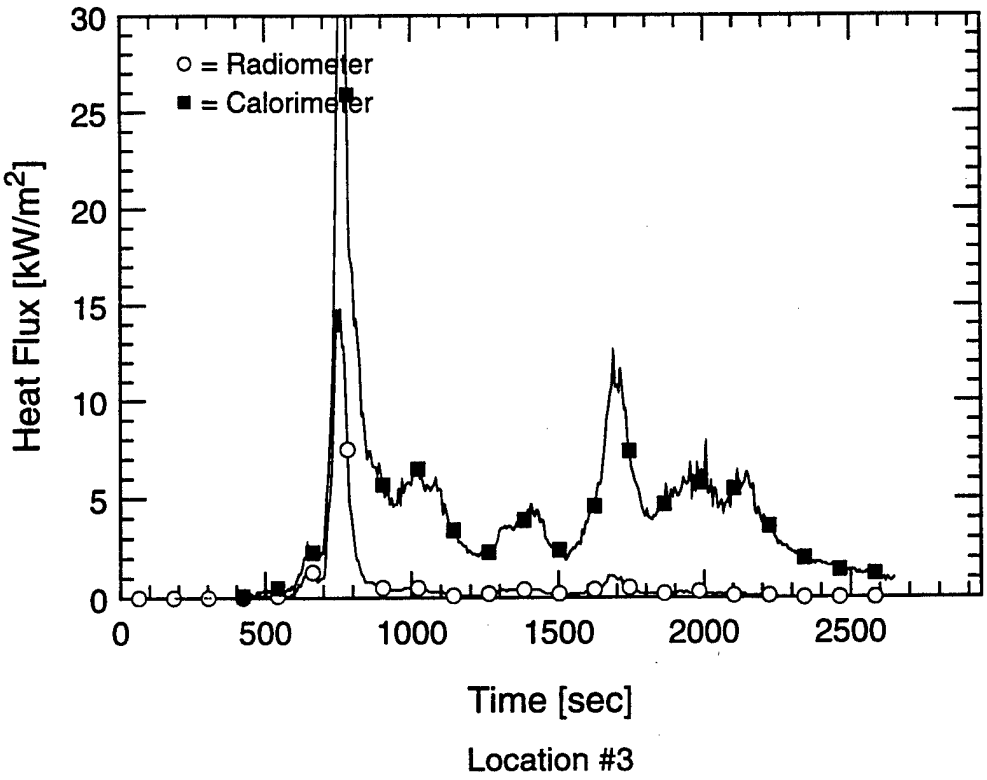

Heat Flux Measurements

Test 1-4

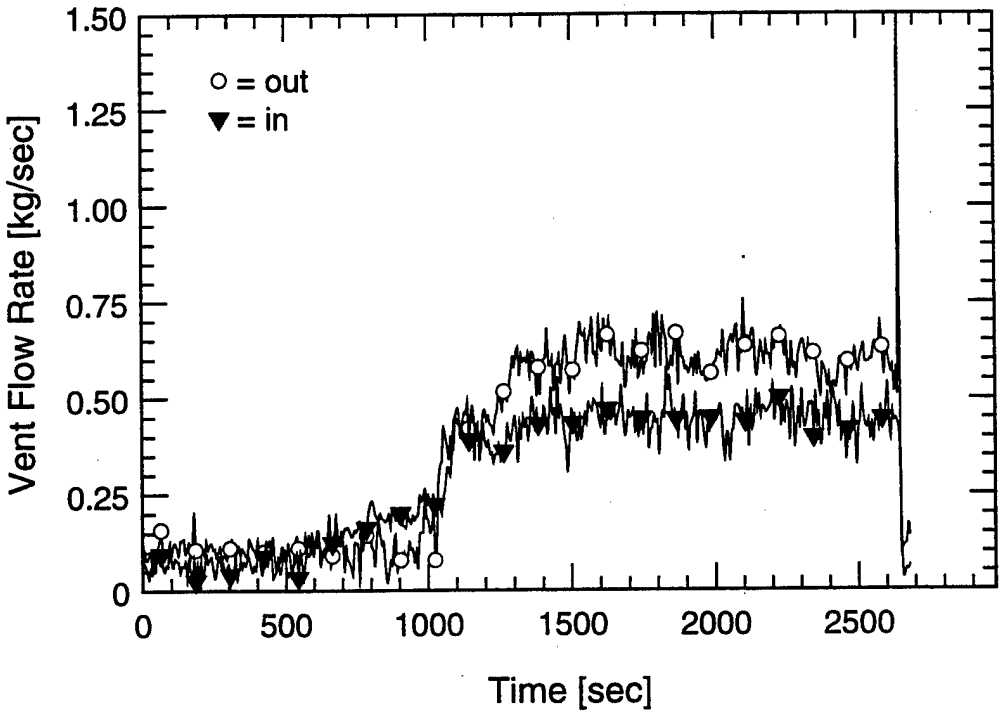

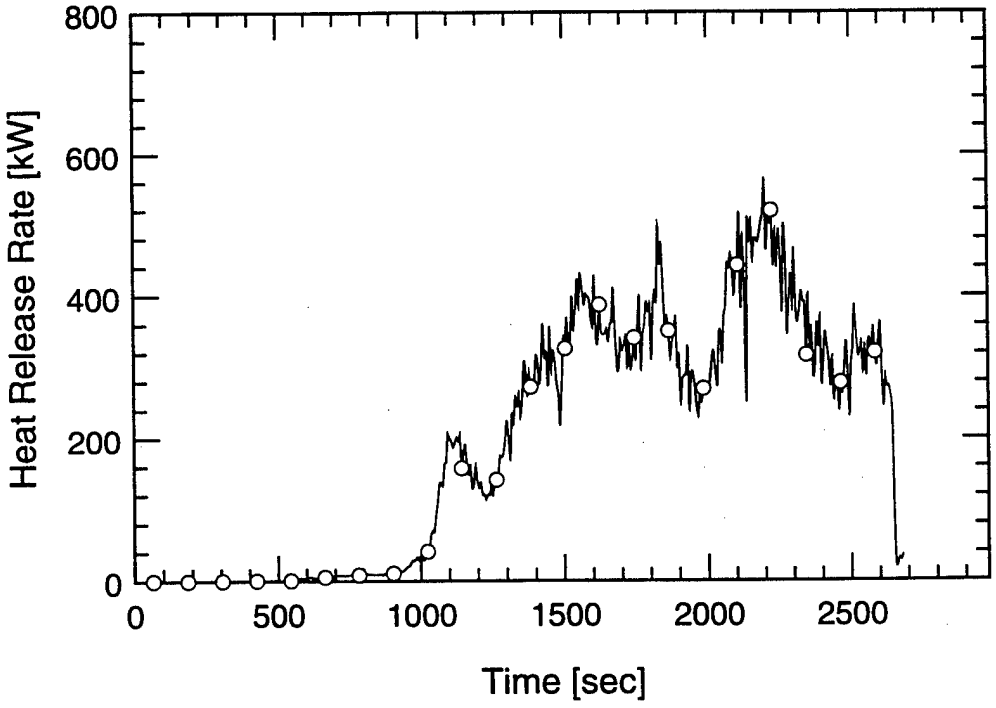

Vent Flow Rate and Heat Release Rate Measurements

Test 2-1

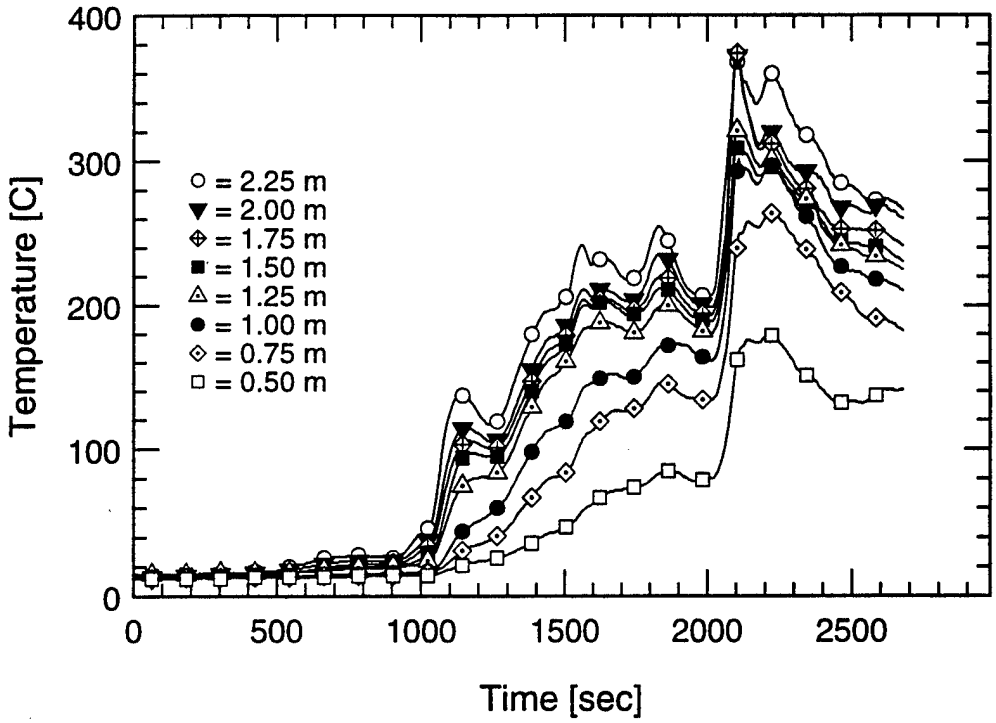

TC Tree #1

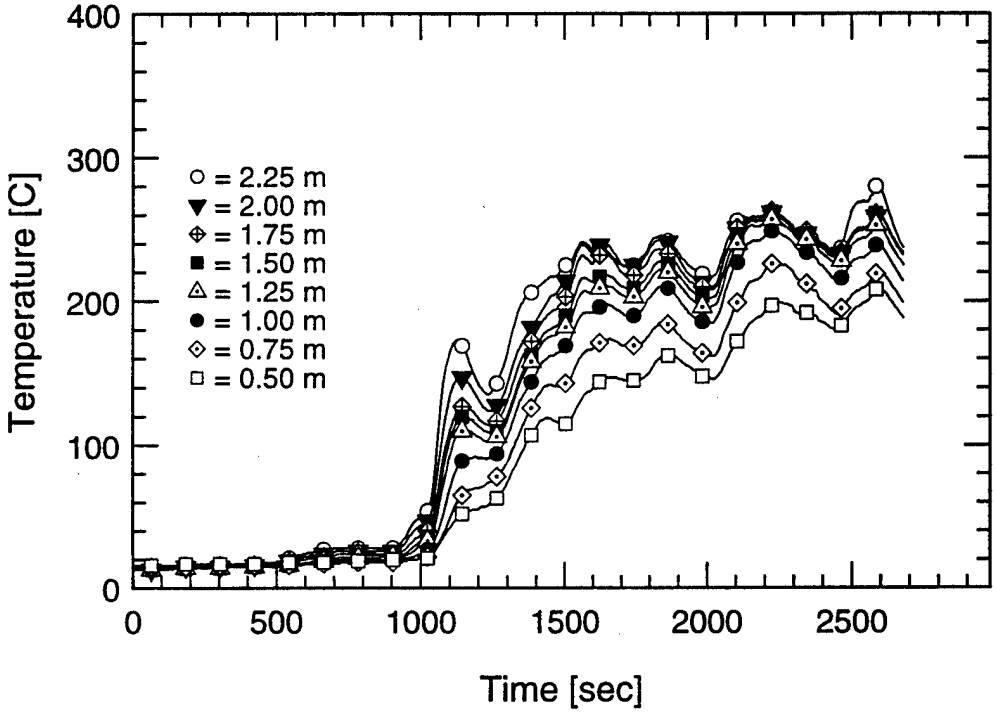

TC Tree #2

Temperature Measurements
Test 2-1

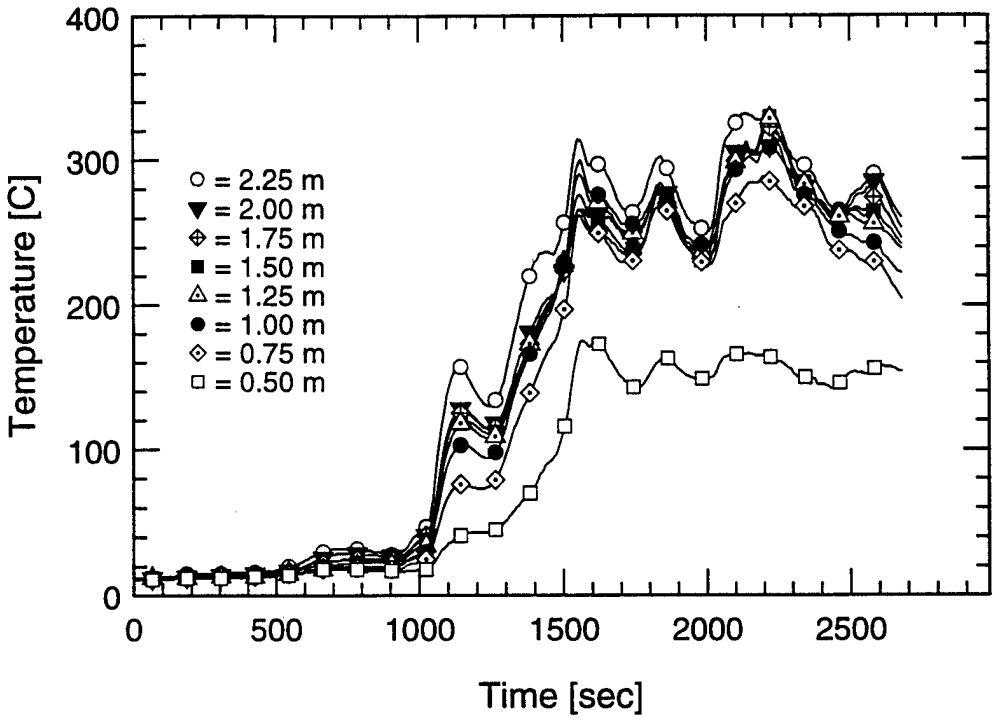

TC Tree #3

Temperature Measurements

Test 2-1

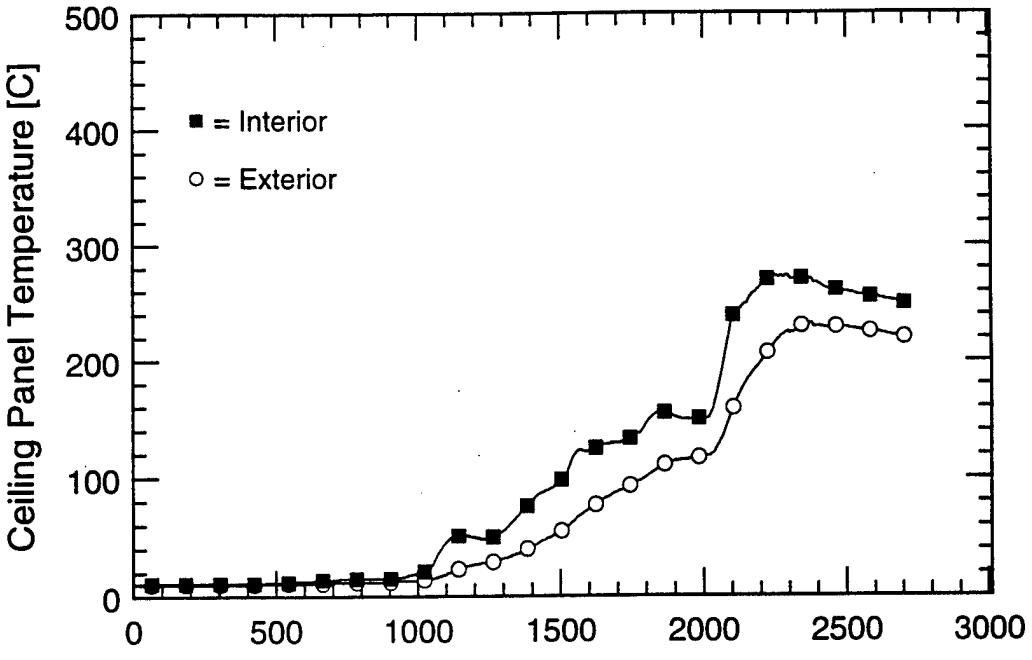

Location #1

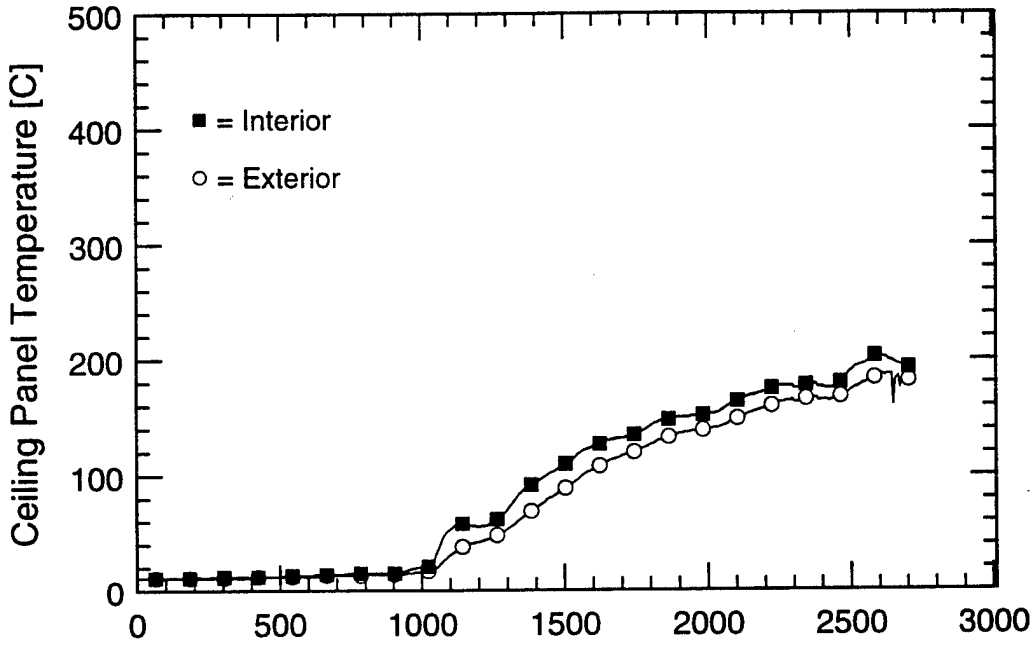

Location #2

Ceiling Panel Temperature Measurements
Test 2-1

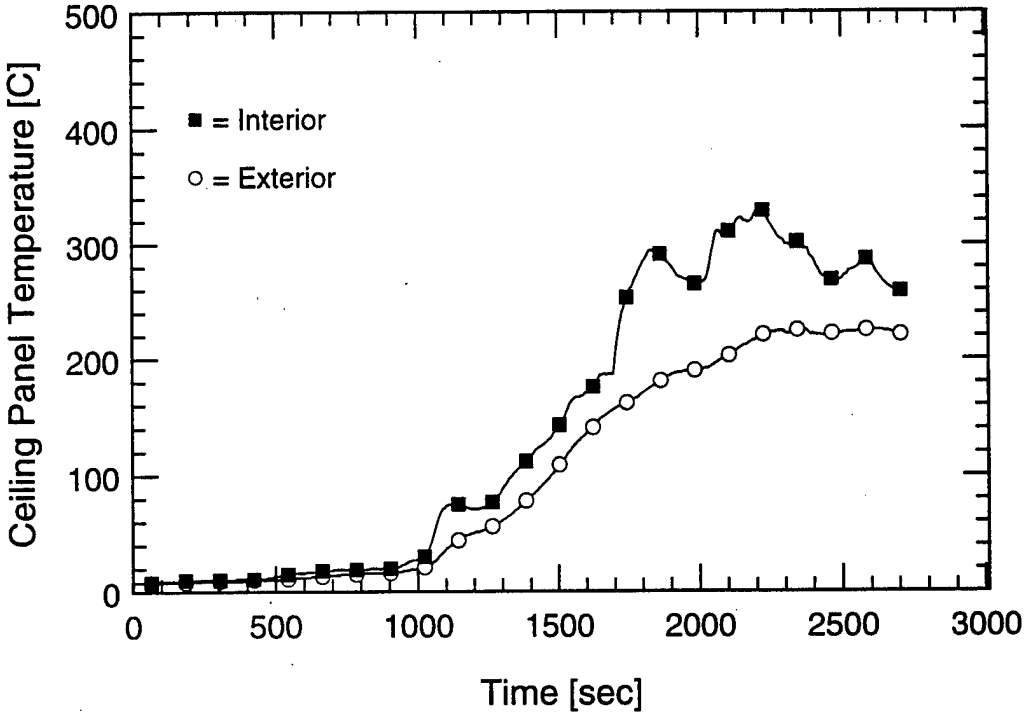

Location #3

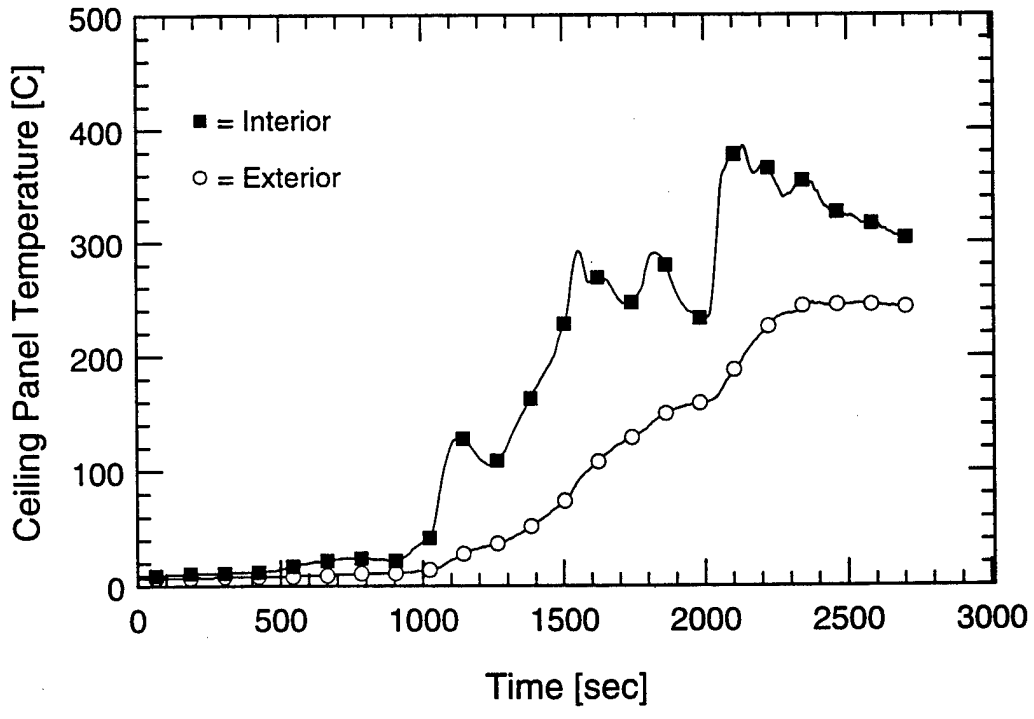

Location #4

Ceiling Panel Temperature Measurements
Test 2-1

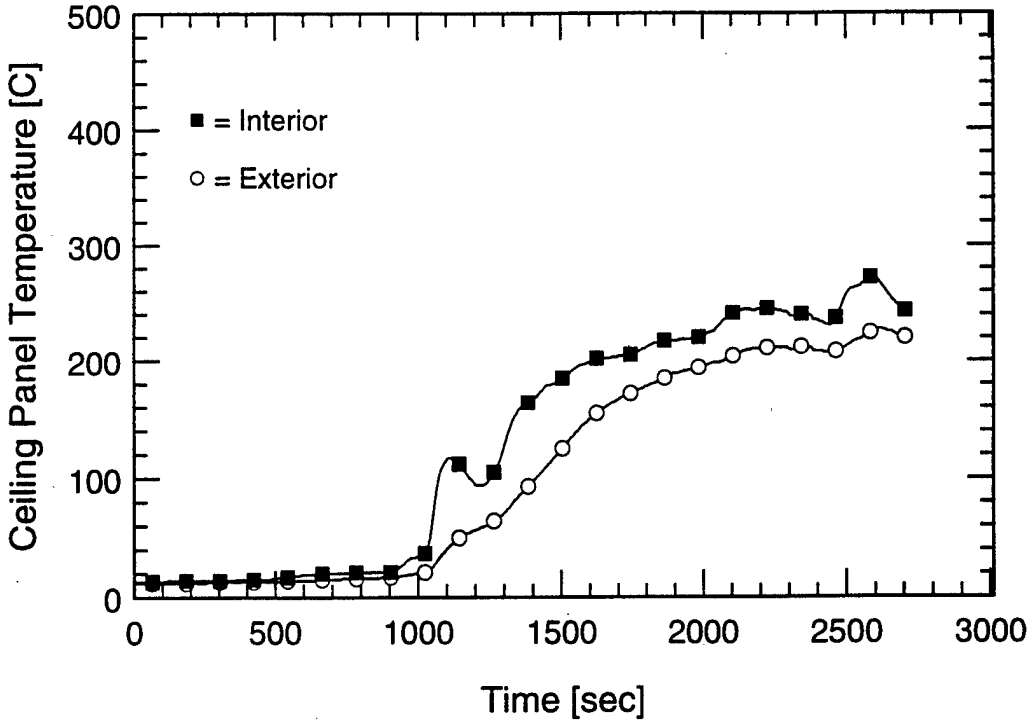

Location #5

Ceiling Panel Temperature Measurements
Test 2-1

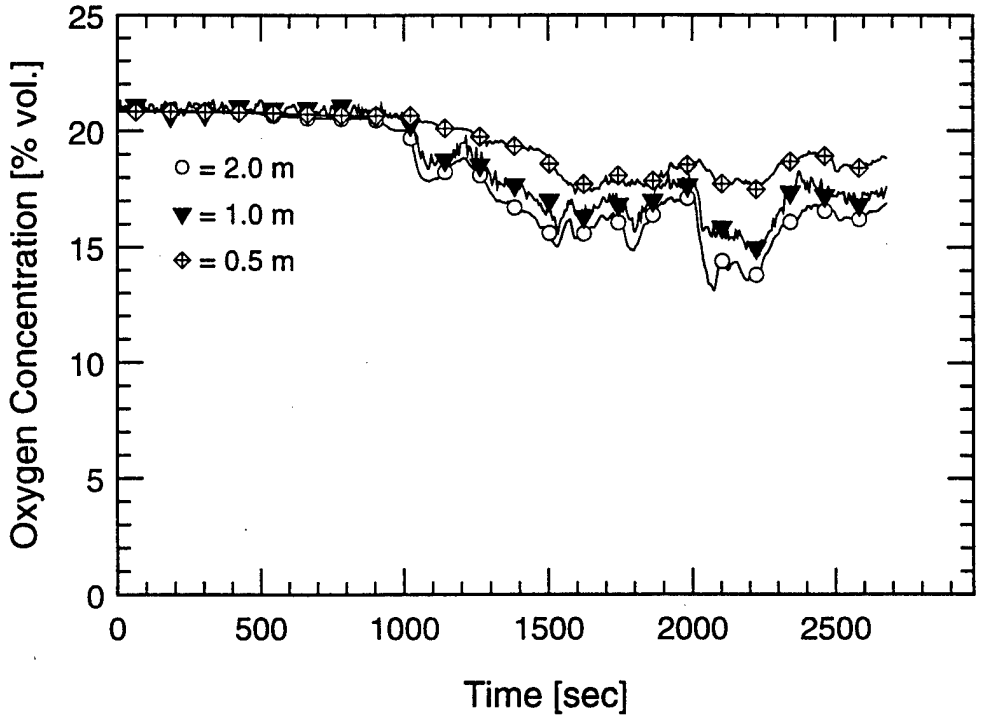

Gas Tree #1

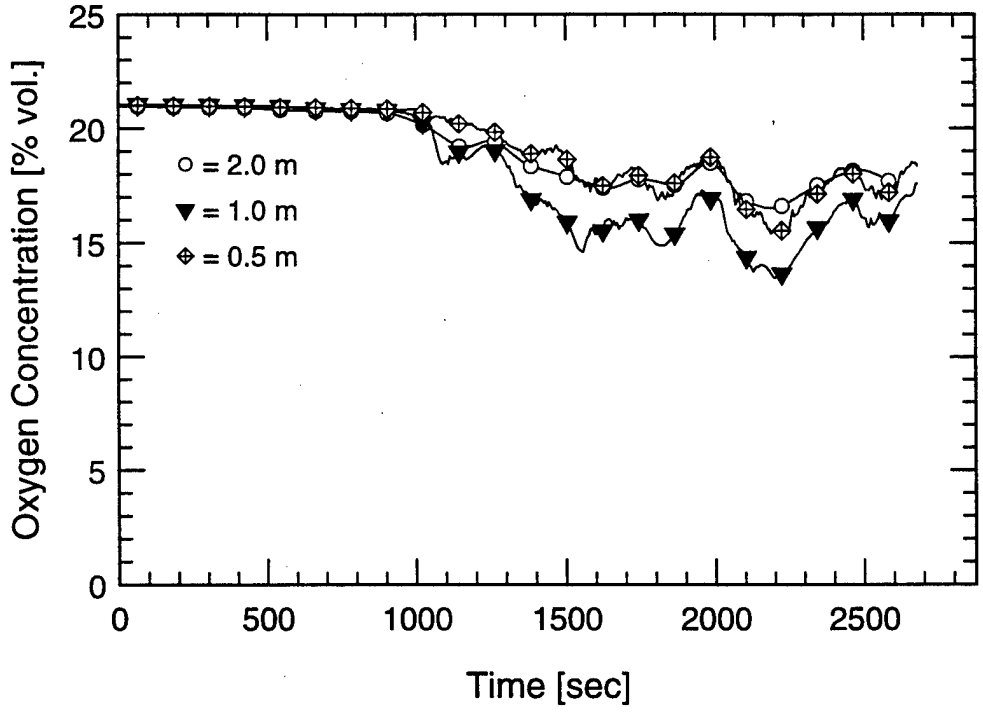

Gas Tree #2

Oxygen Concentration Measurements

Test 2-1

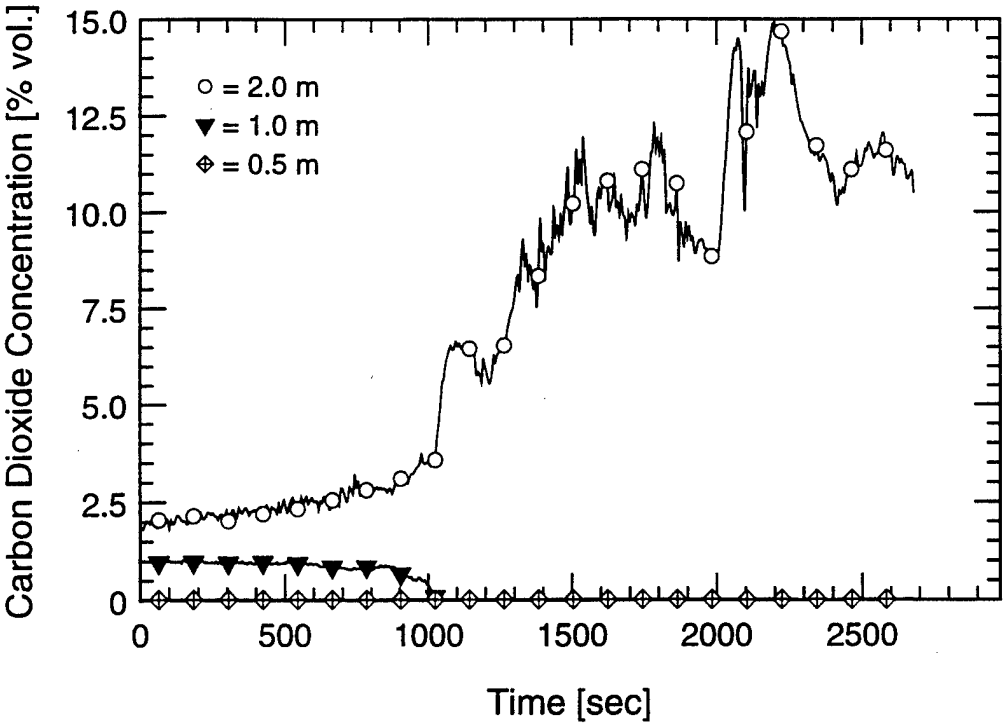

Gas Tree #1

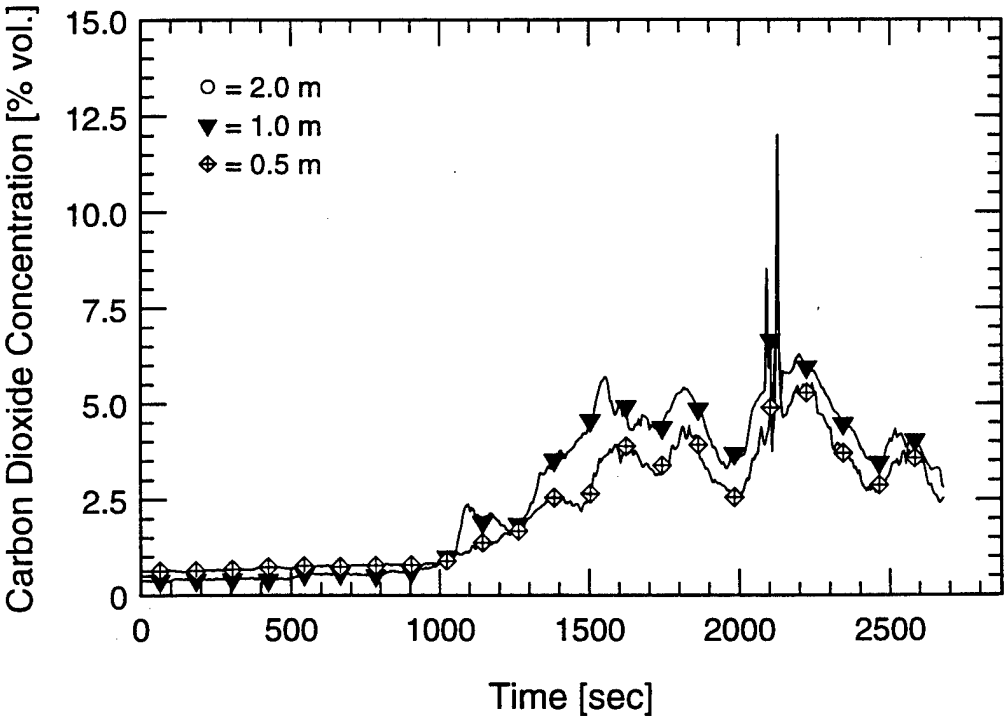

Gas Tree #2

Carbon Dioxide Concentration Measurements
Test 2-1

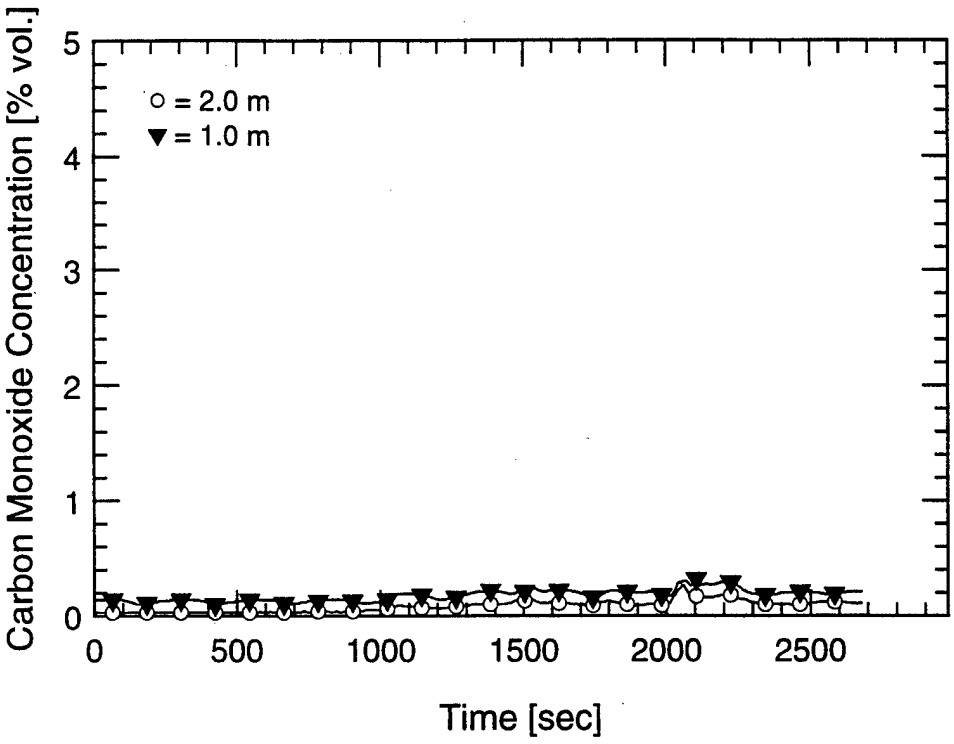

Gas Tree #1

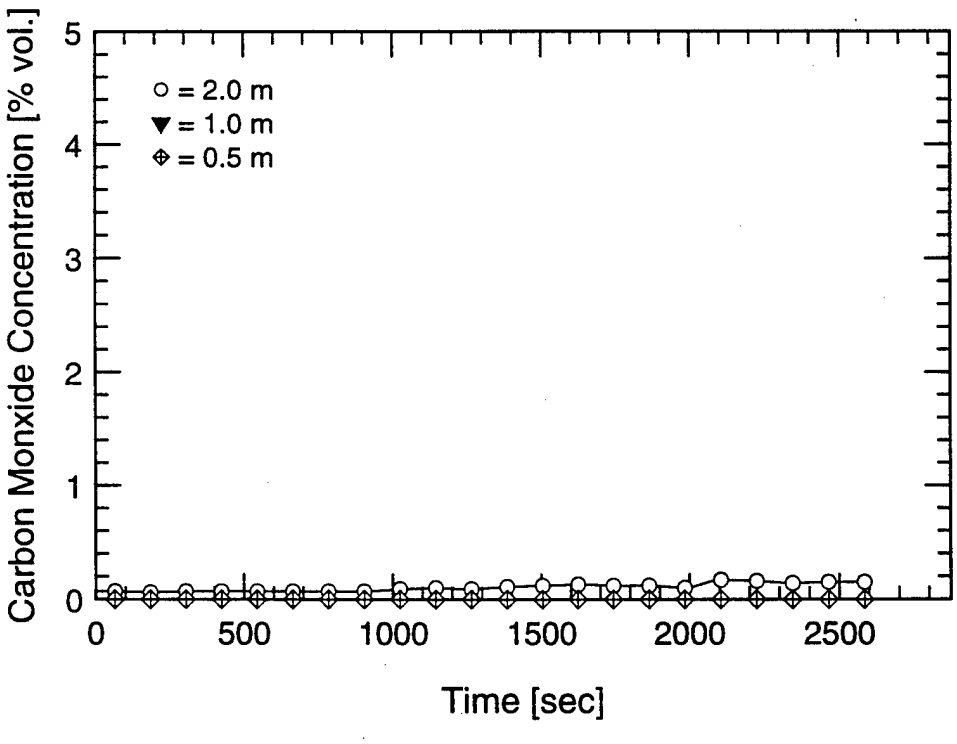

Gas Tree #2

Carbon Monoxide Concentration Measurements
Test 2-1

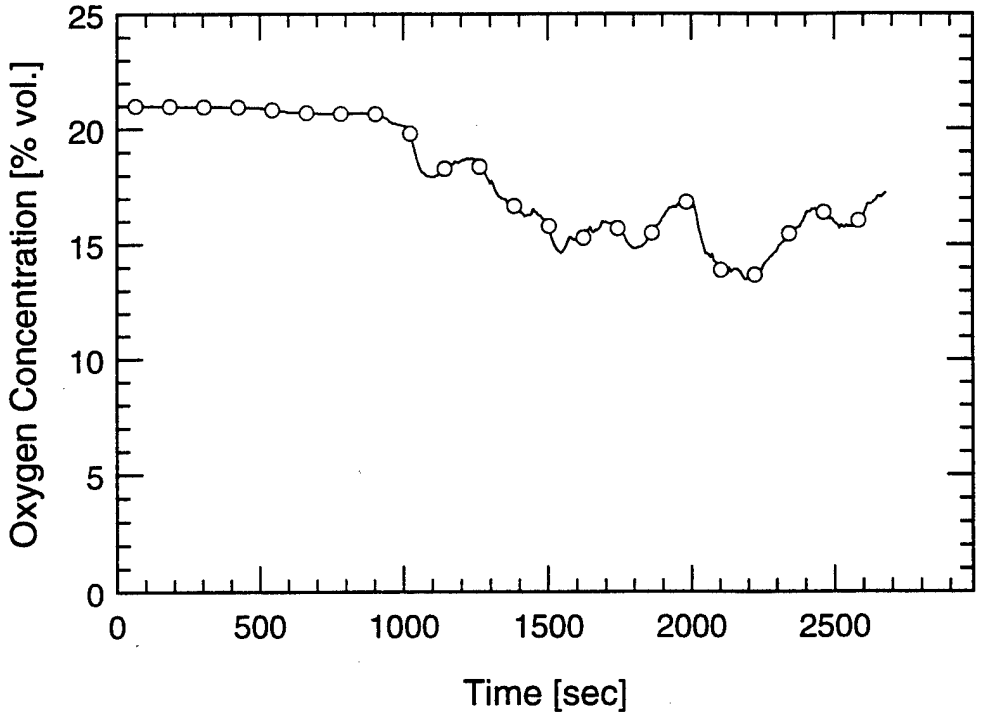

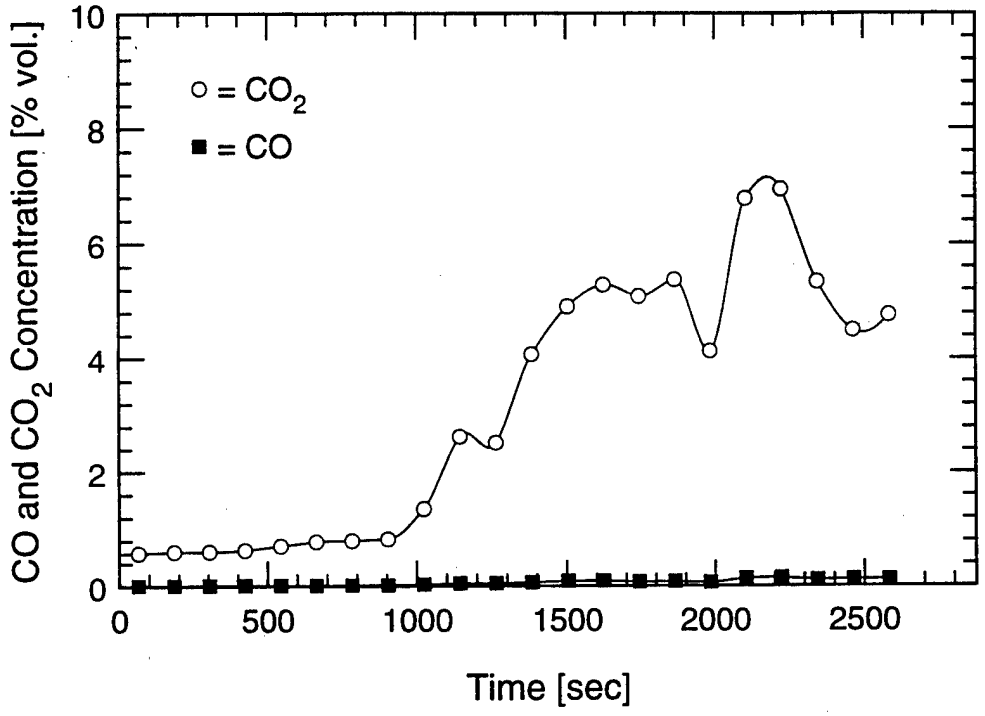

Gas Species Measurements in Doorway (GT3)
Test 2-1

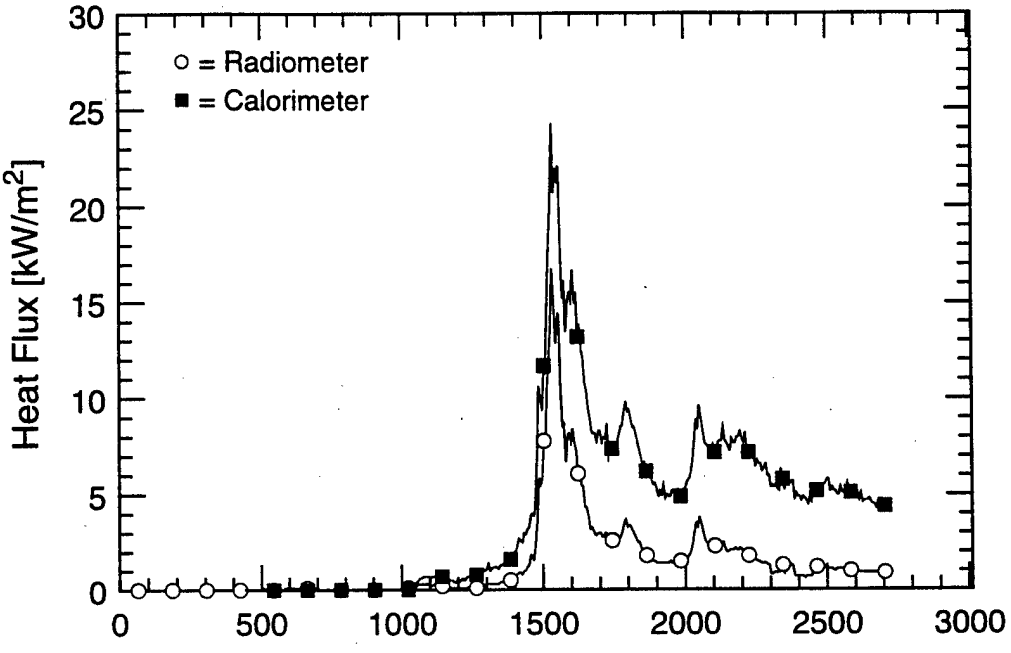

Location #1

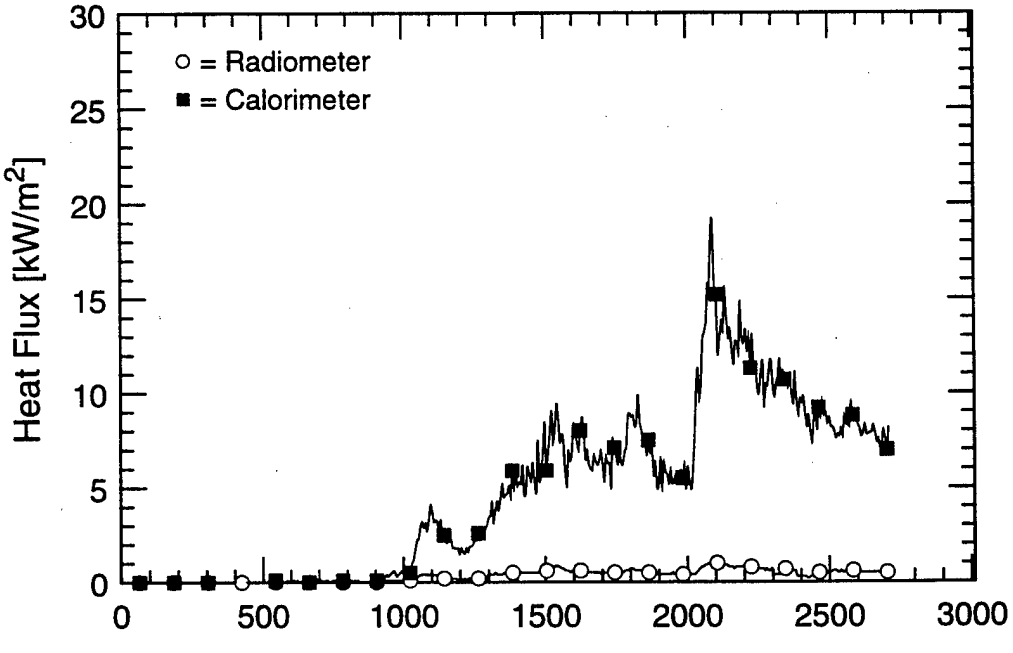

Location #2

Heat Flux Measurements
Test 2-1

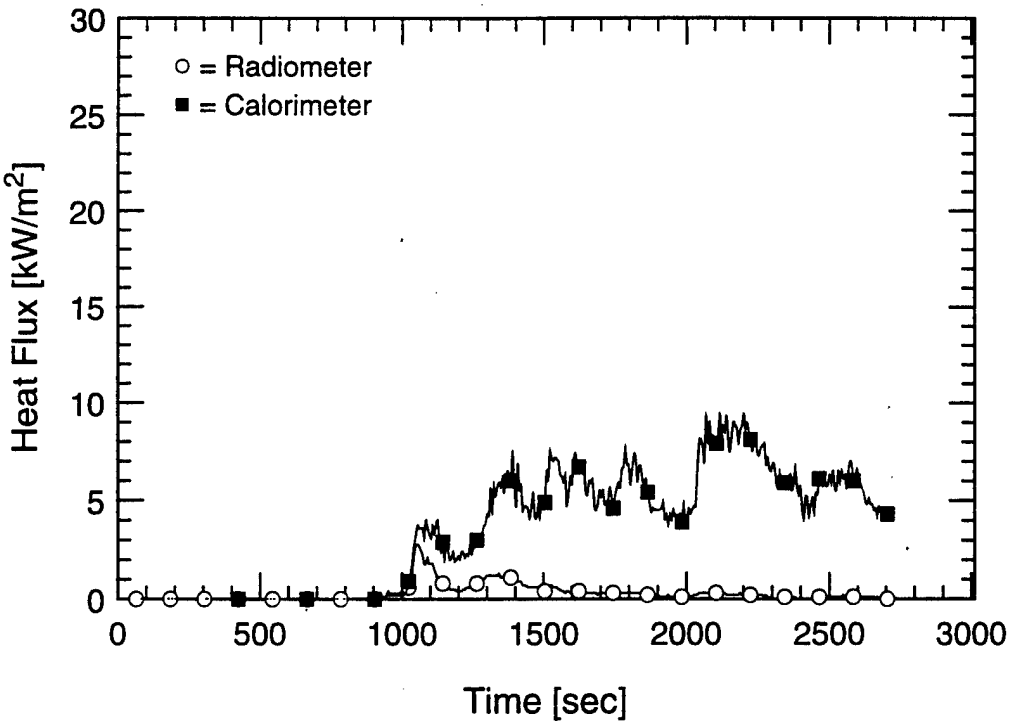

Location #3

Heat Flux Measurements

Test 2-1

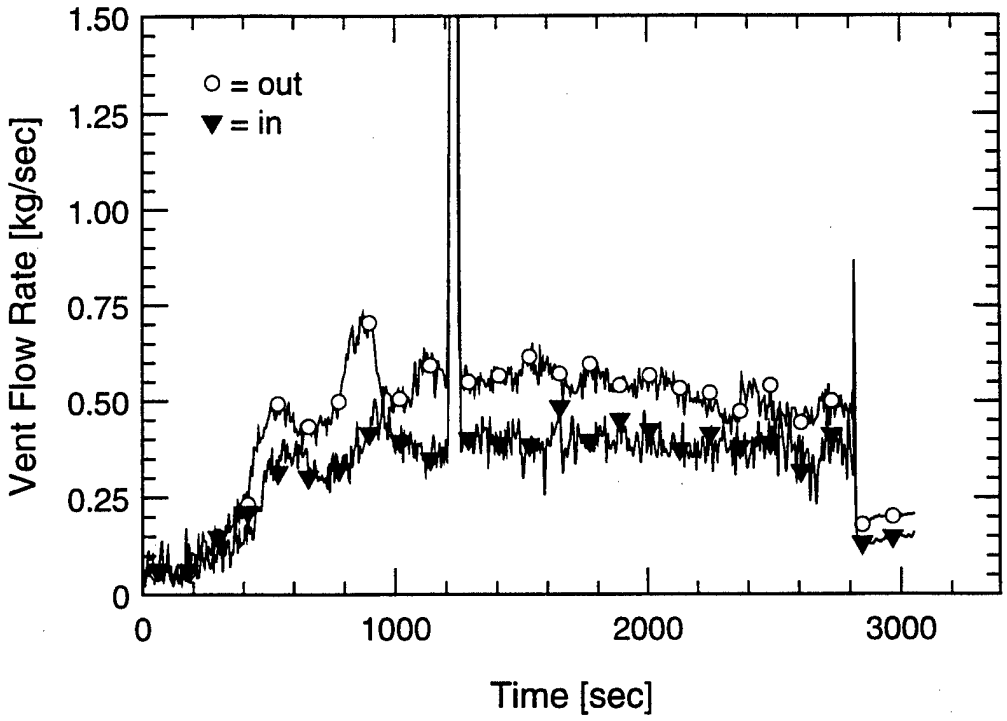

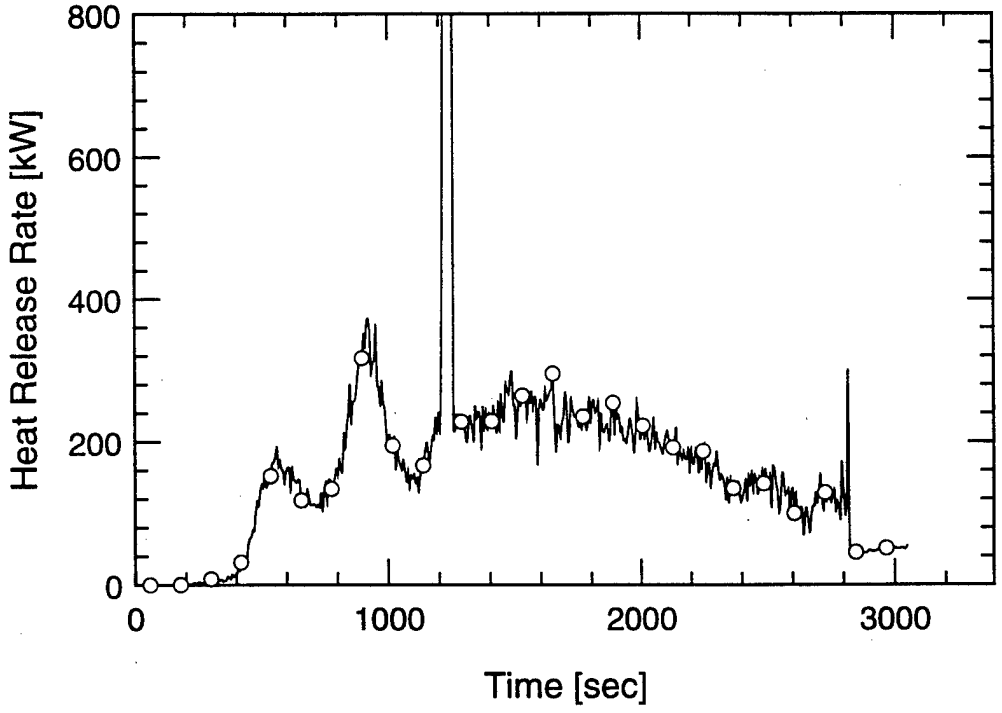

Vent Flow Rate and Heat Release Rate Measurements

Test 2-2

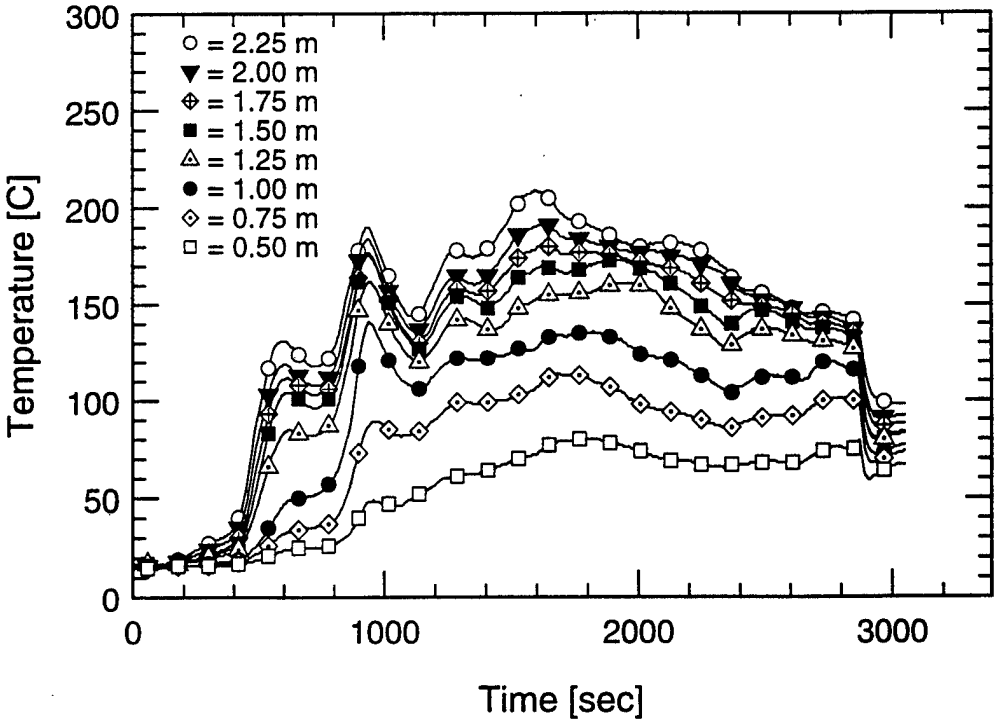

TC Tree #1

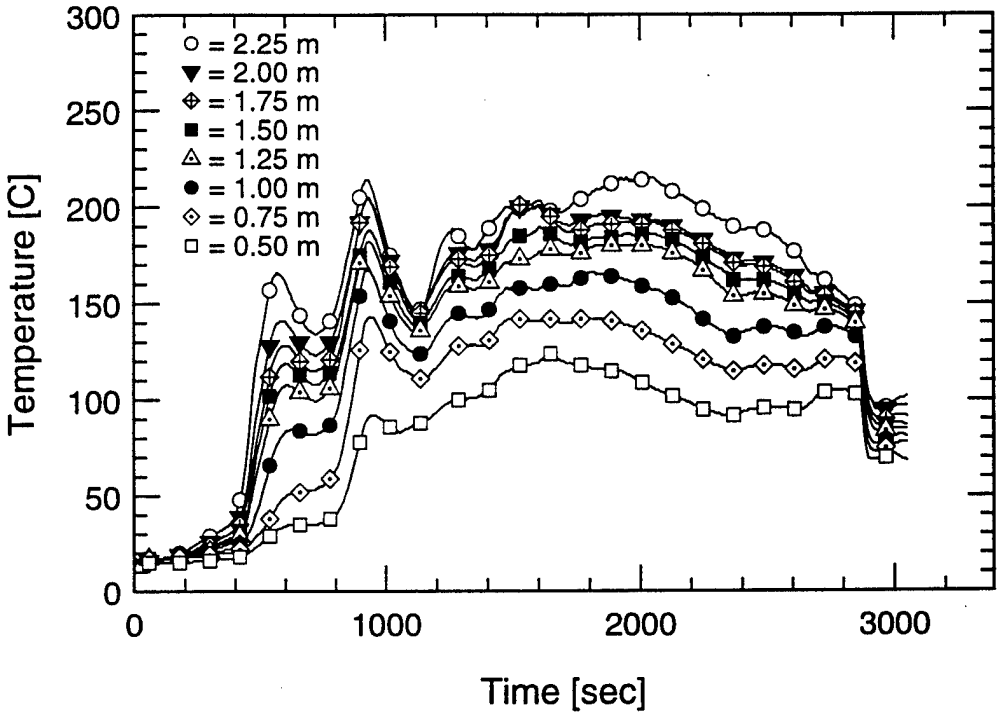

TC Tree #2

Temperature Measurements
Test 2-2

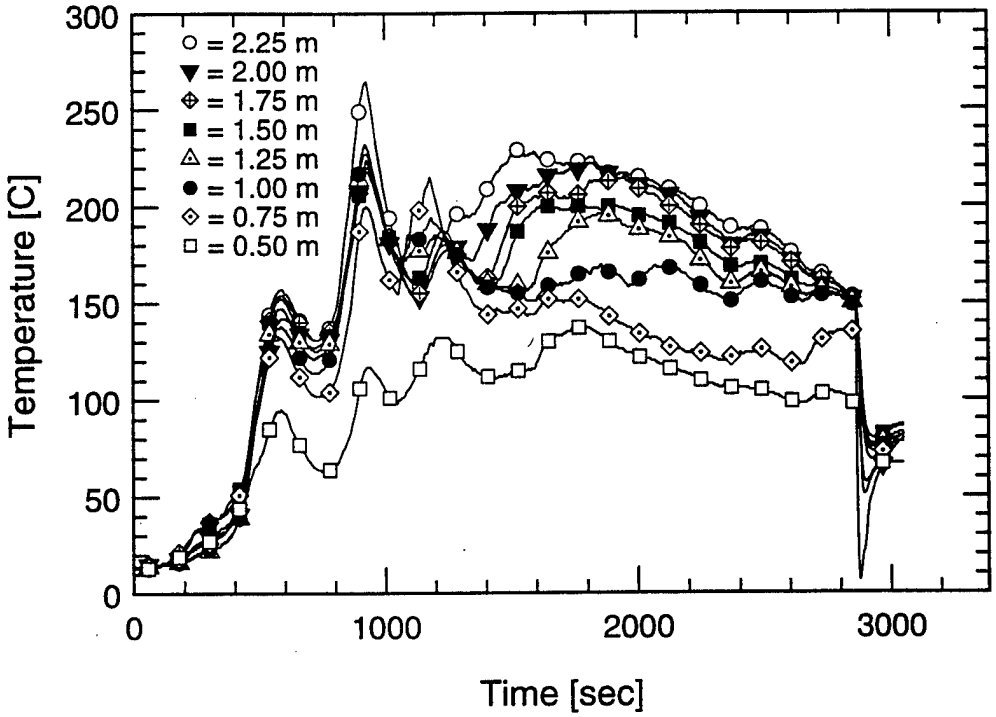

TC Tree #3

Temperature Measurements

Test 2-2

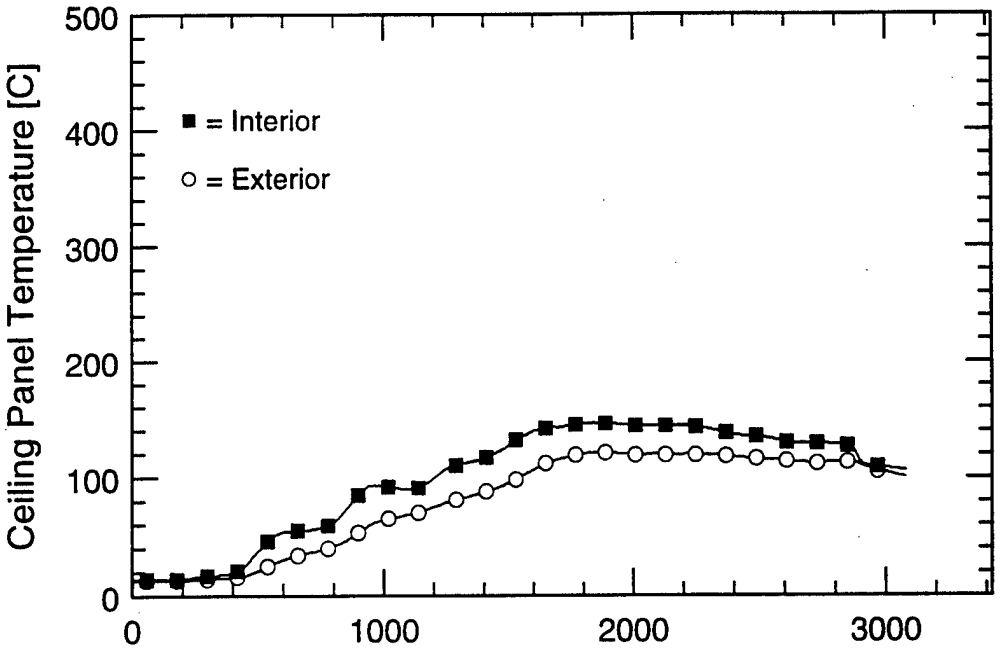

Location #1

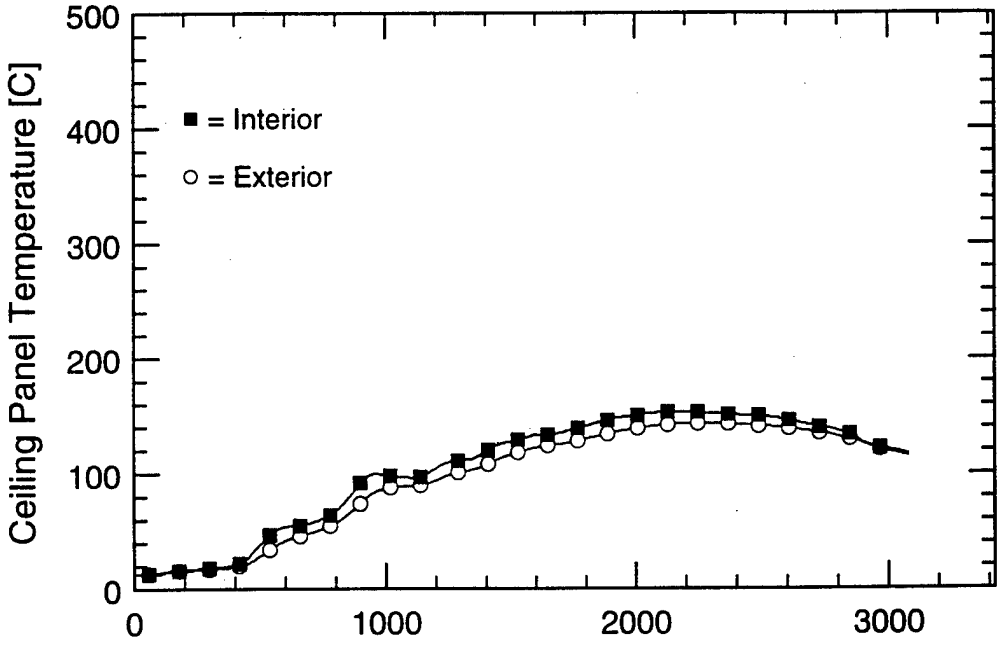

Location #2

Ceiling Panel Temperature Measurements
Test 2-2

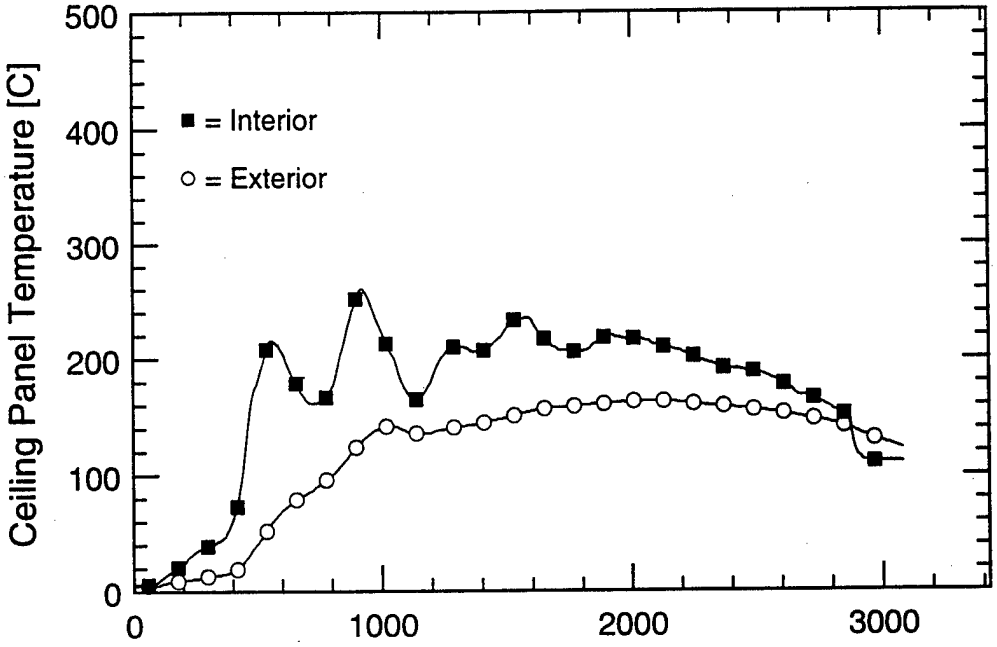

Location #3

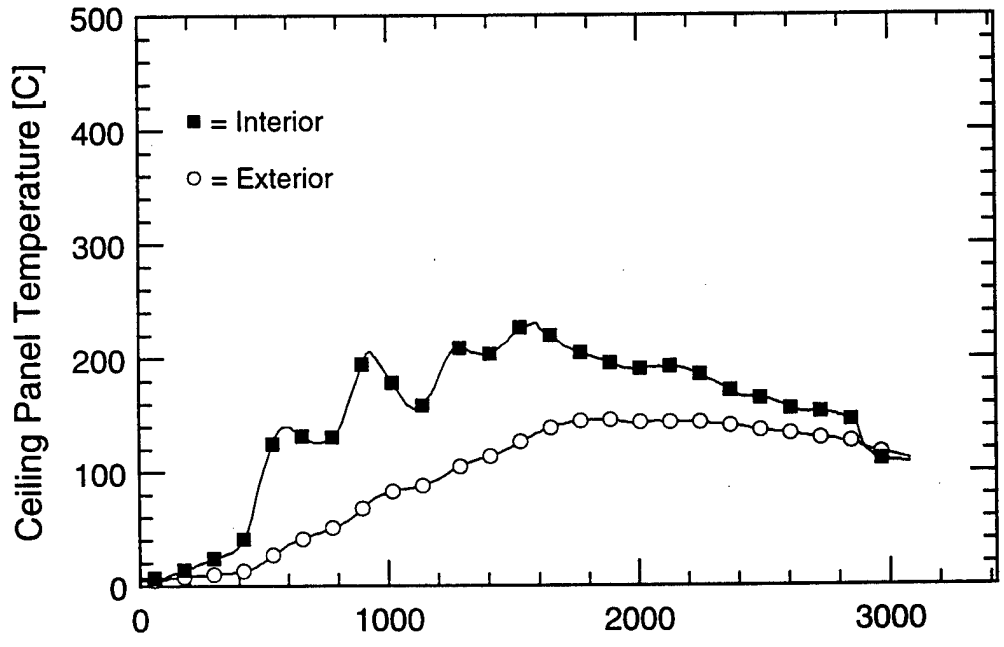

Location #4

Ceiling Panel Temperature Measurements
Test 2-2

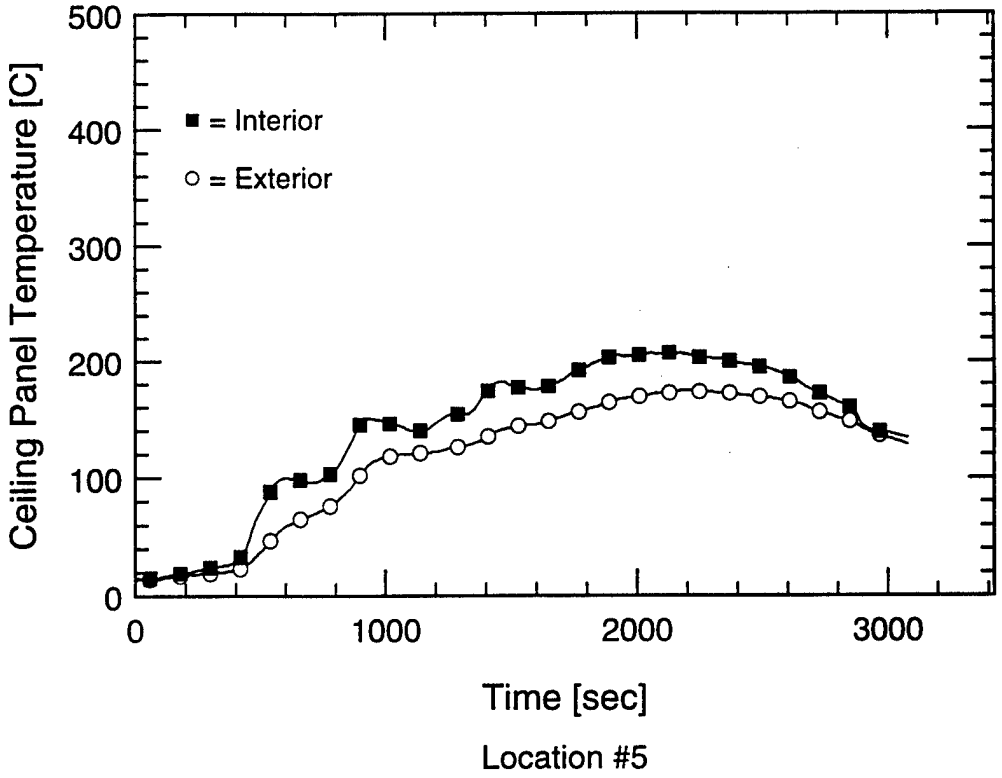

Ceiling Panel Temperature Measurements
Test 2-2

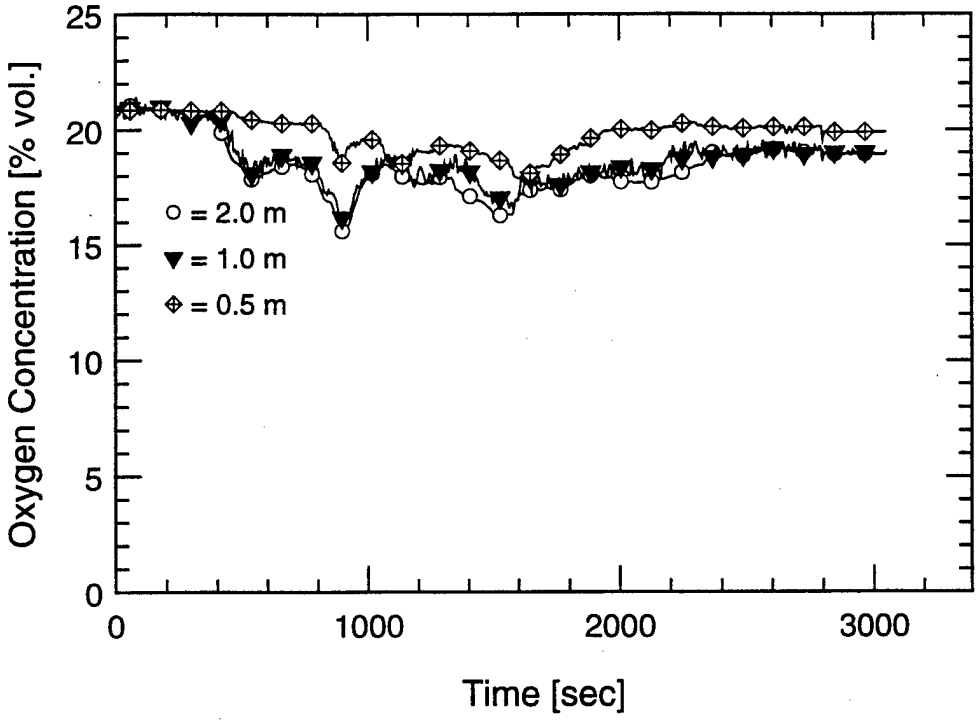

Gas Tree #1

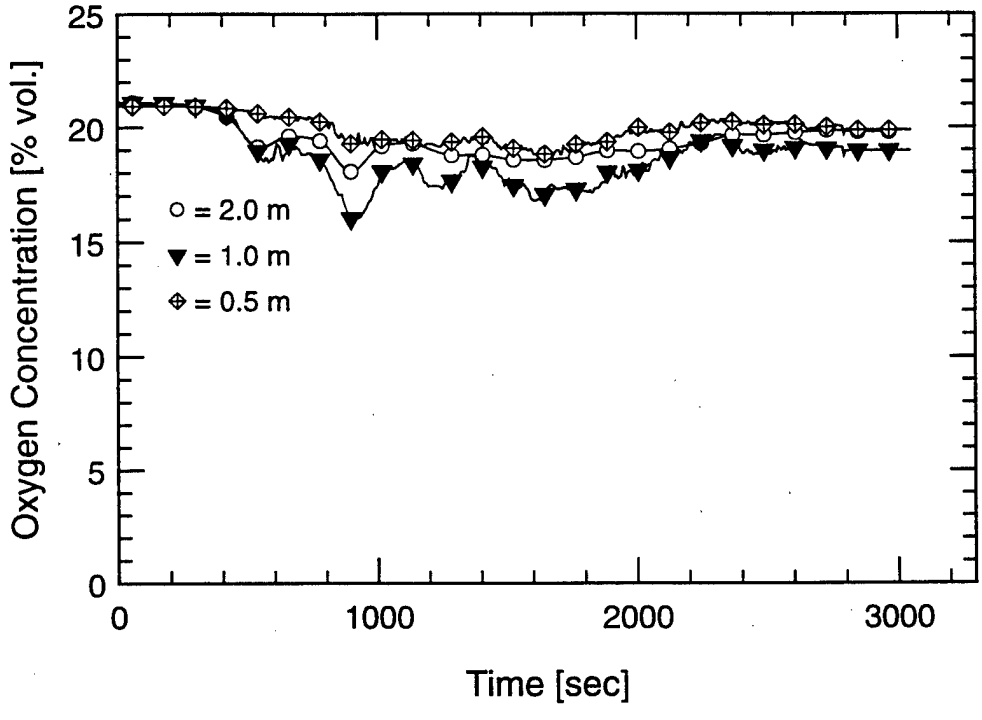

Gas Tree #2

Oxygen Concentration Measurements
Test 2-2

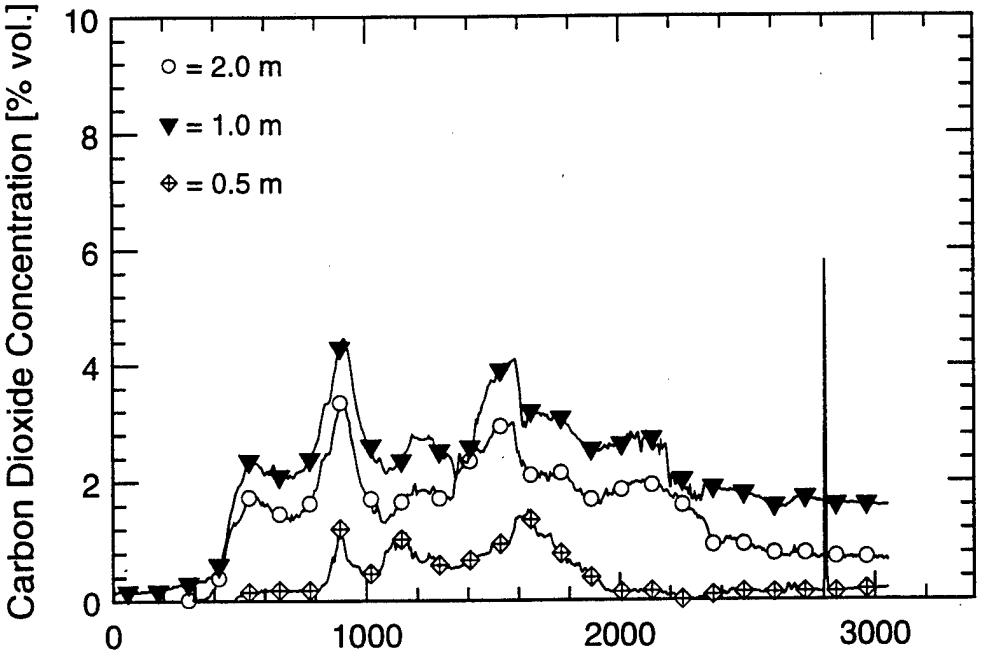

Gas Tree #1

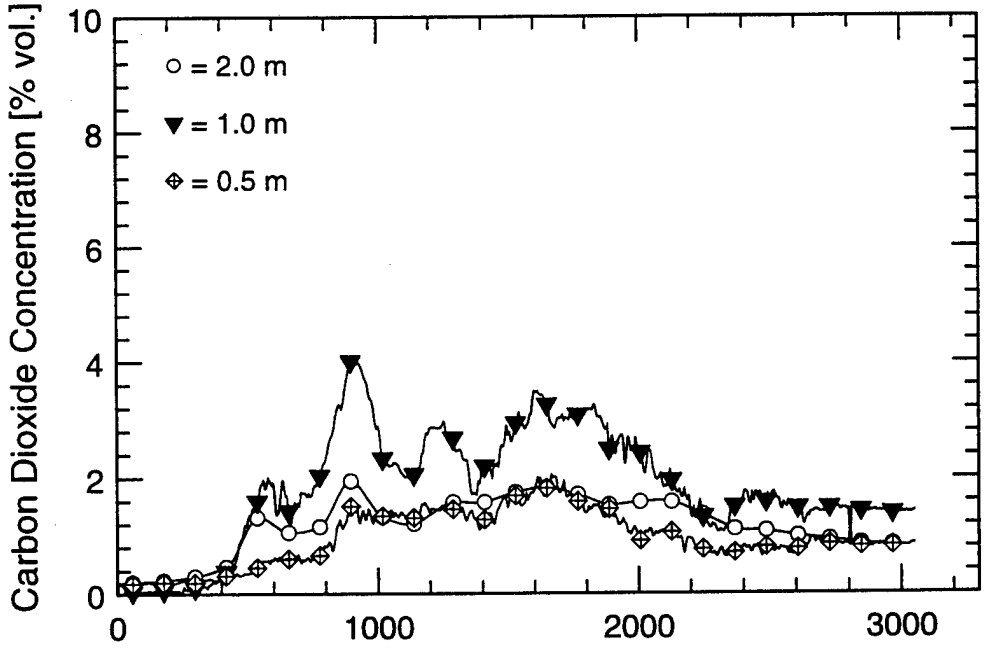

Gas Tree #2

Carbon Dioxide Measurements
Test 2-2

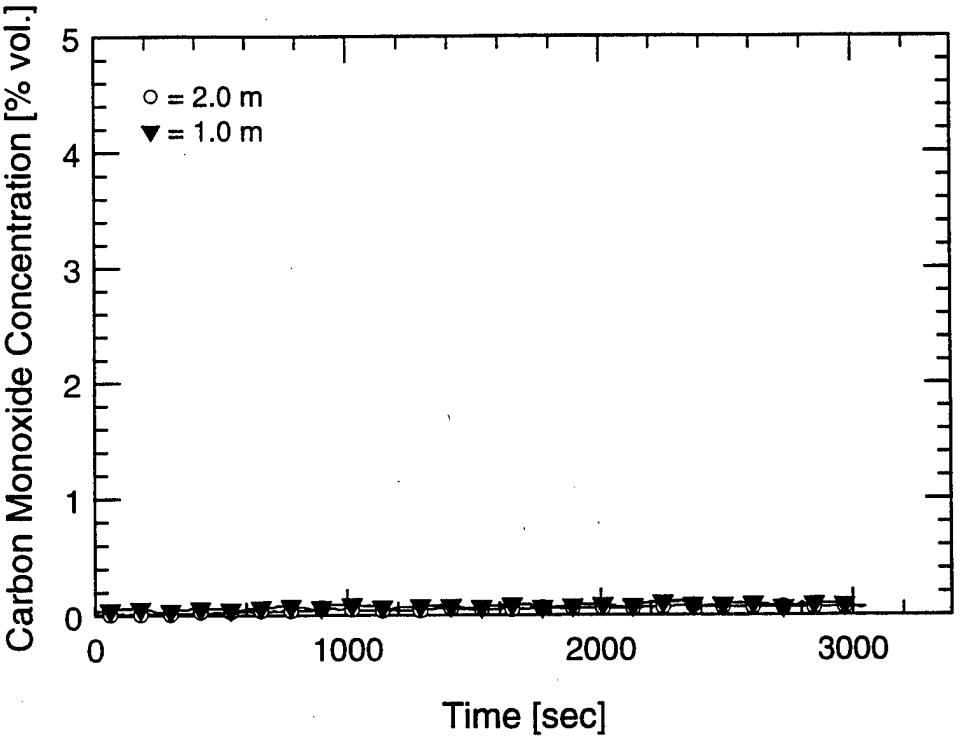

Gas Tree #1

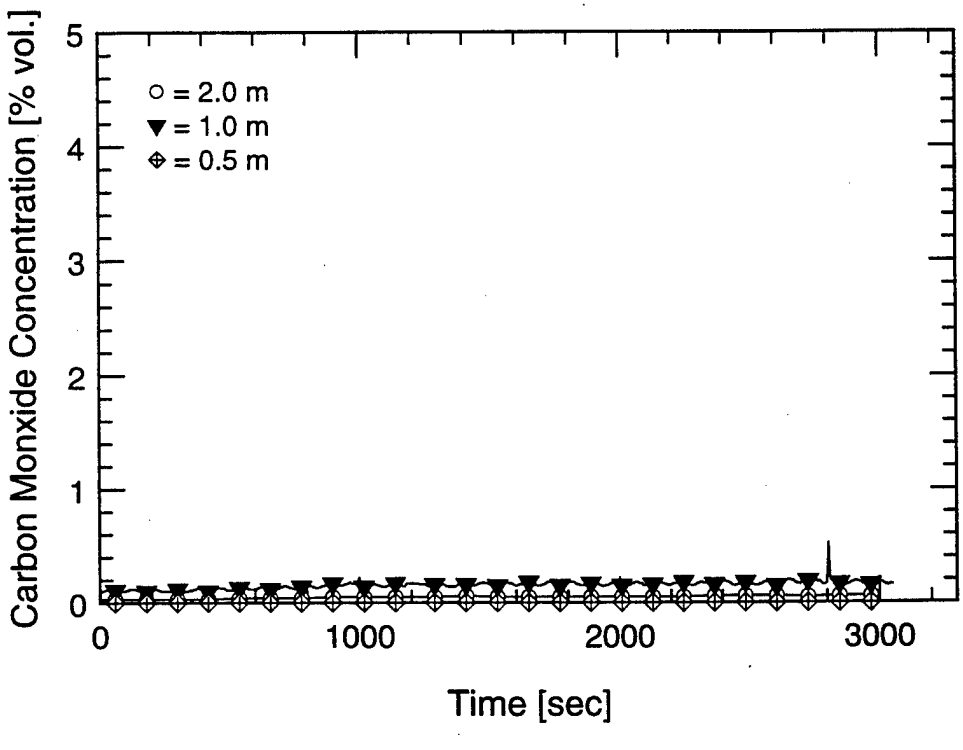

Gas Tree #2

Carbon Monoxide Concentration Measurements
Test 2-2

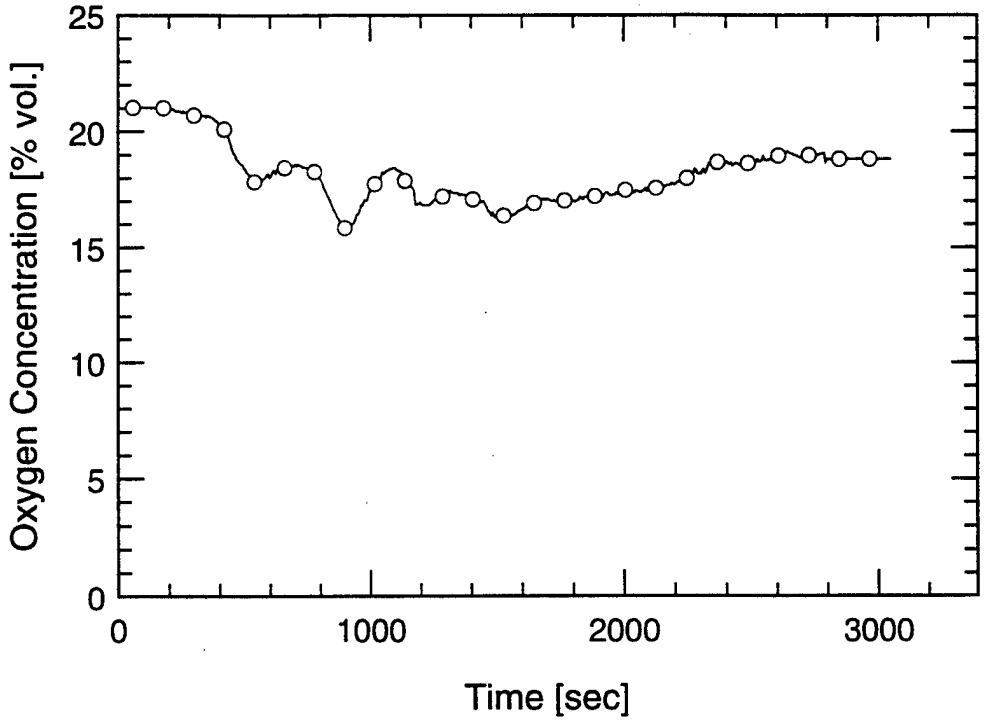

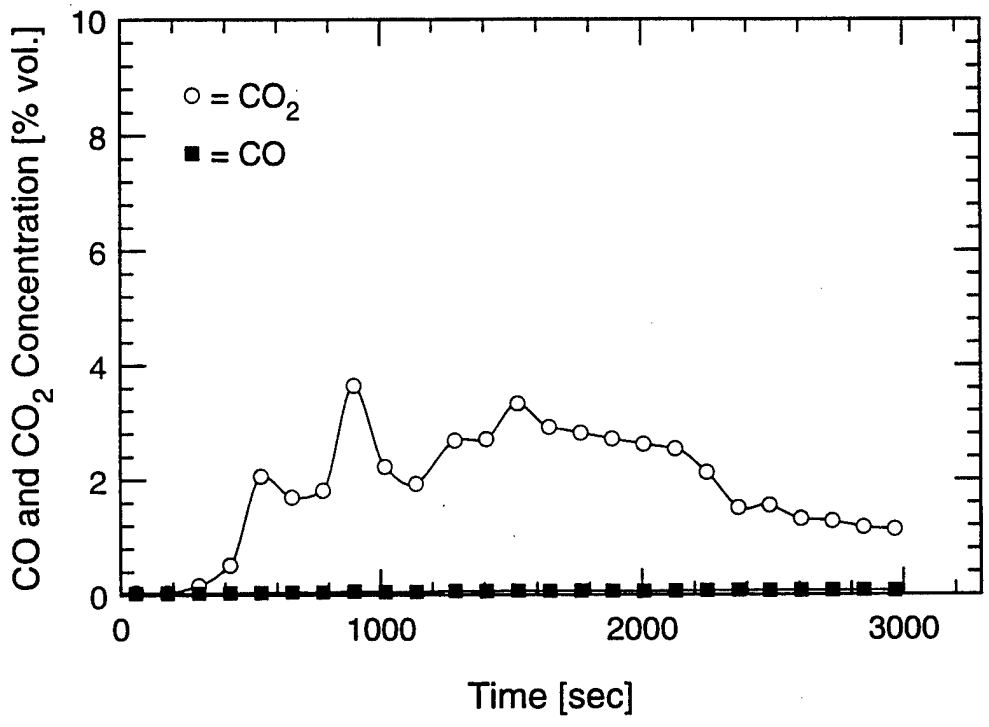

Gas Species Measurements in Doorway (GT3)
Test 2-2

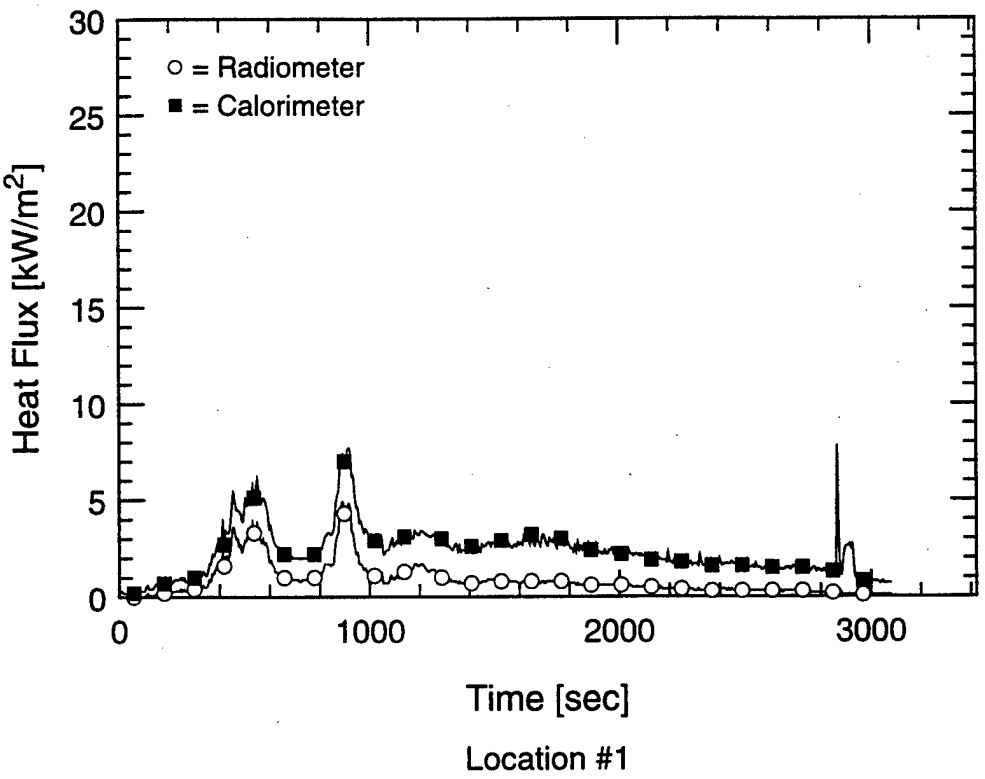

Location #1

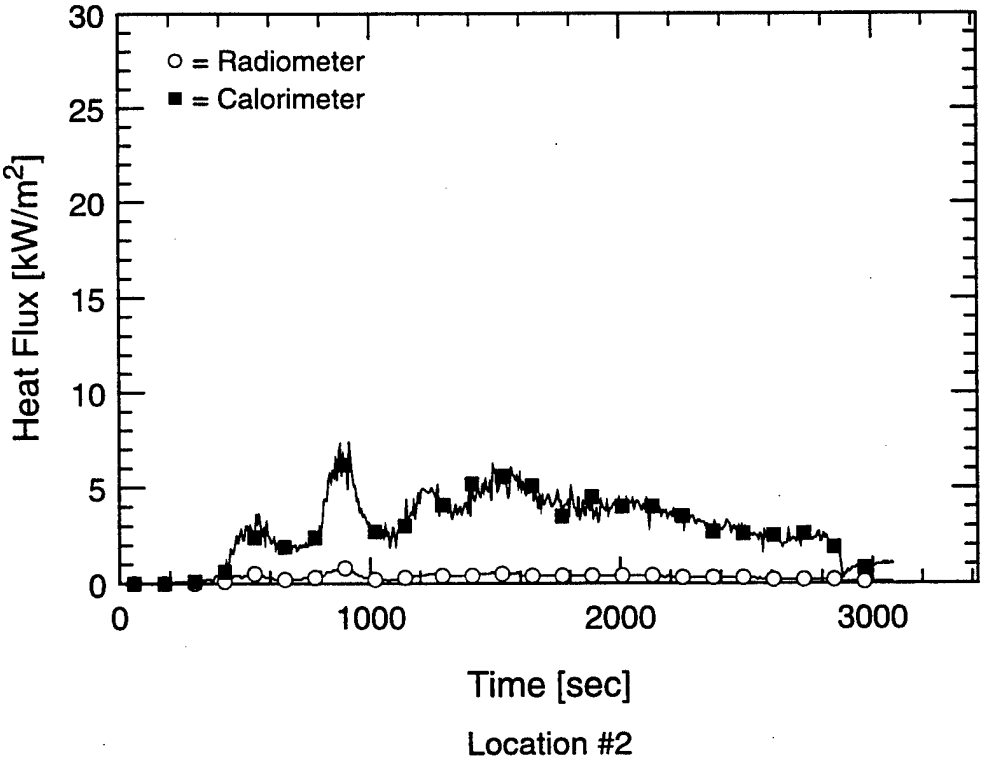

Location #2

Heat Flux Measurements
Test 2-2

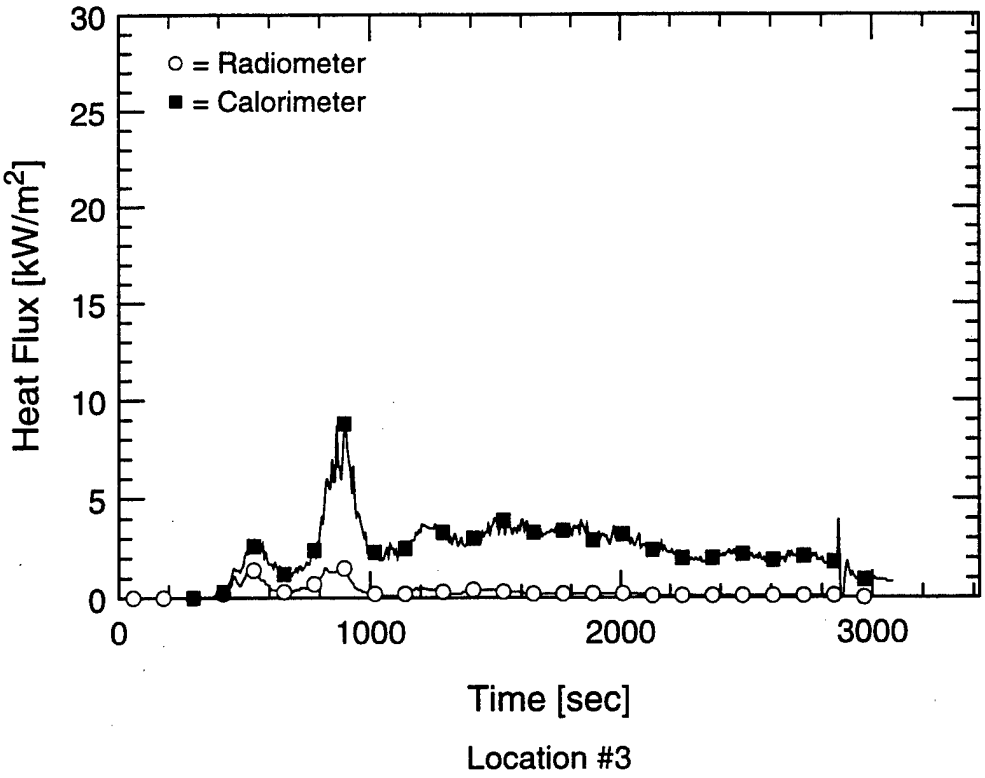

Heat Flux Measurements

Test 2-2

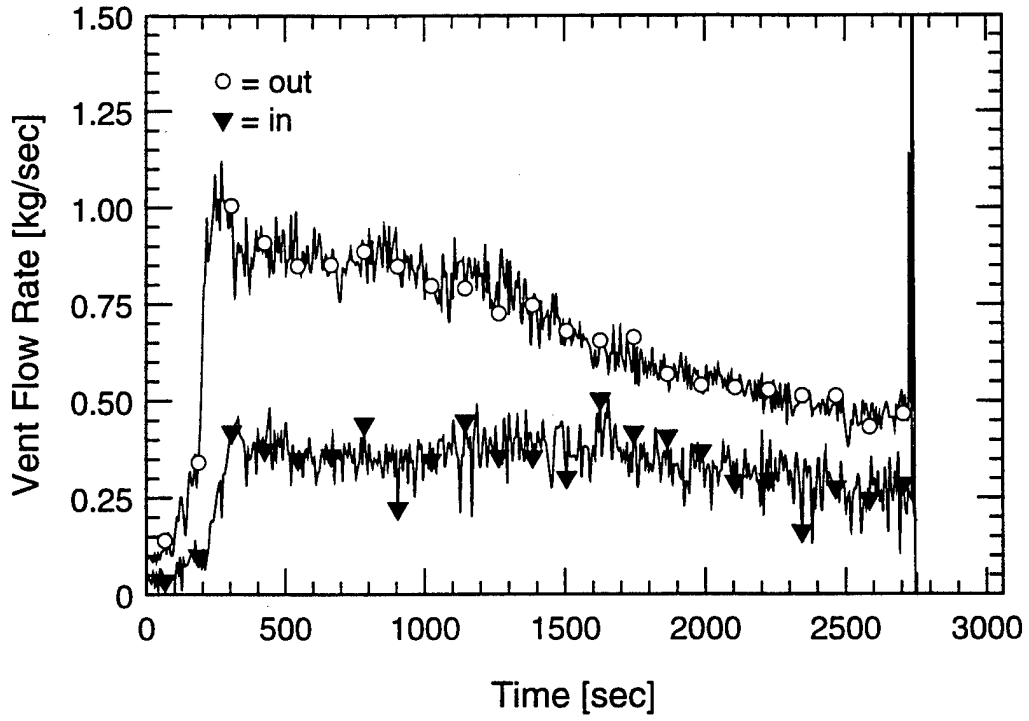

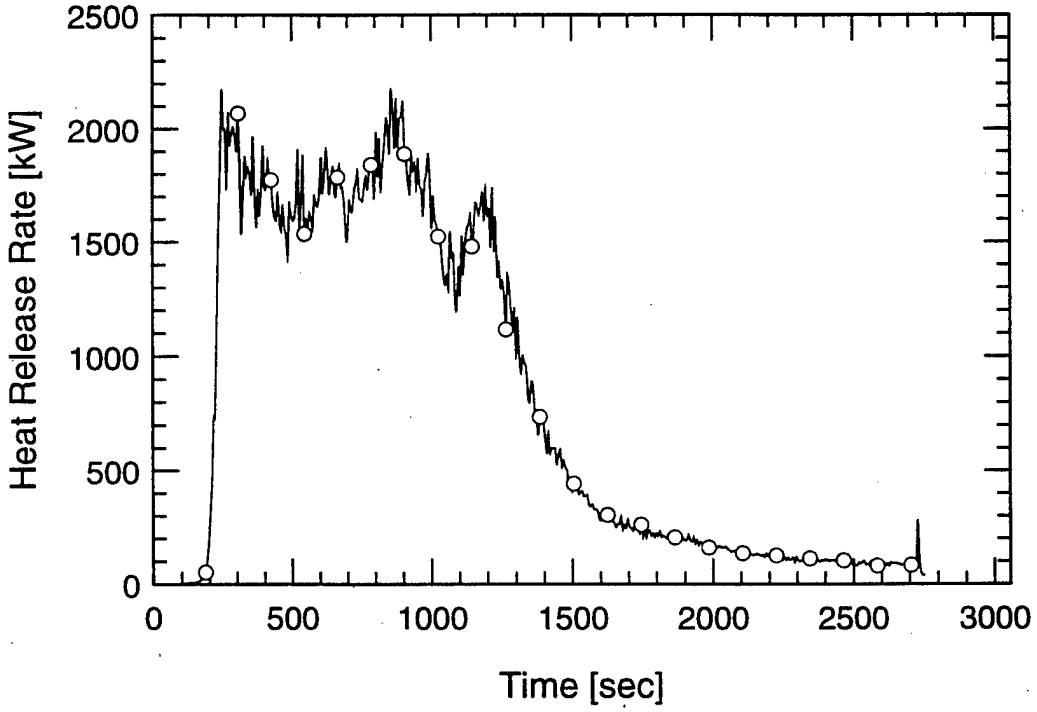

Vent Flow Rate and Heat Release Rate Measurements

Test 4-1

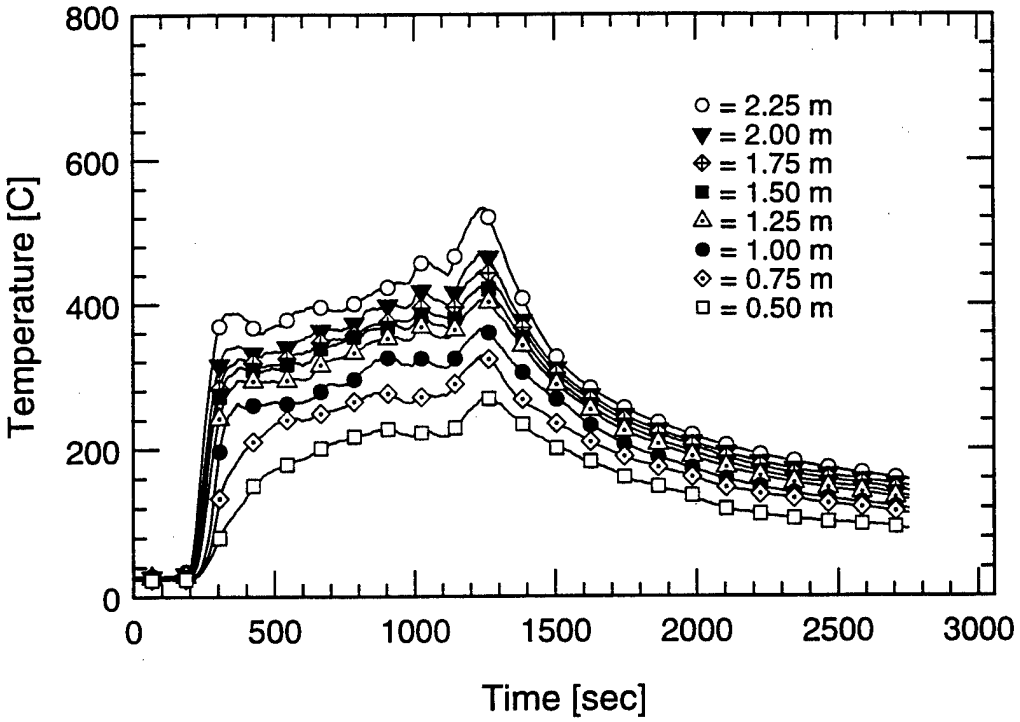

TC Tree #1

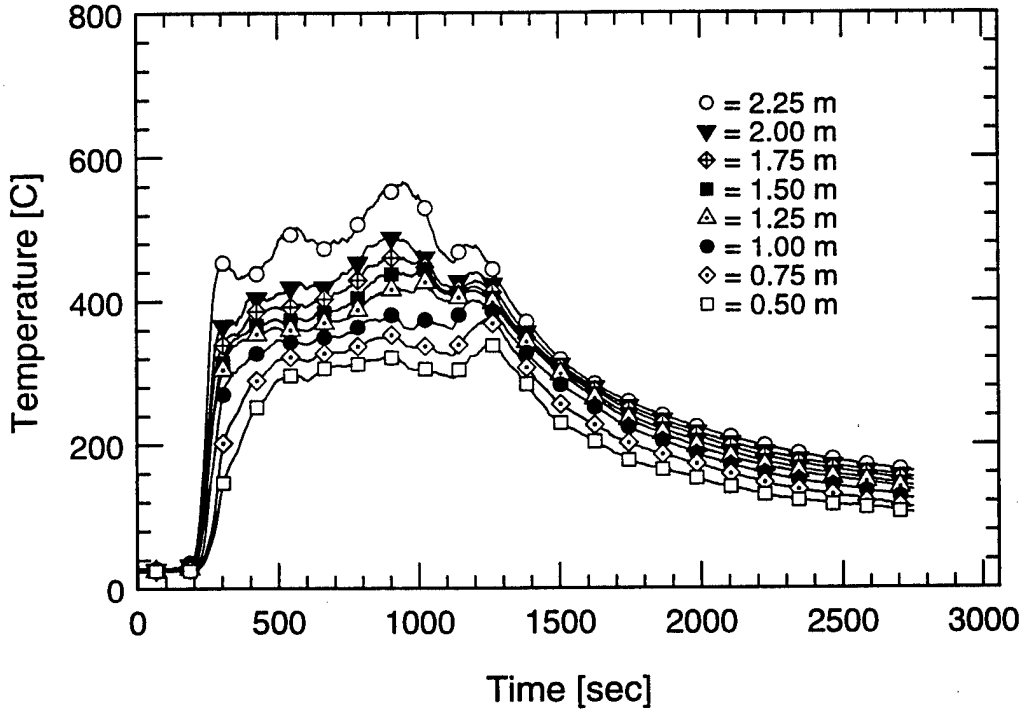

TC Tree #2

Temperature Measurements
Test 4-1

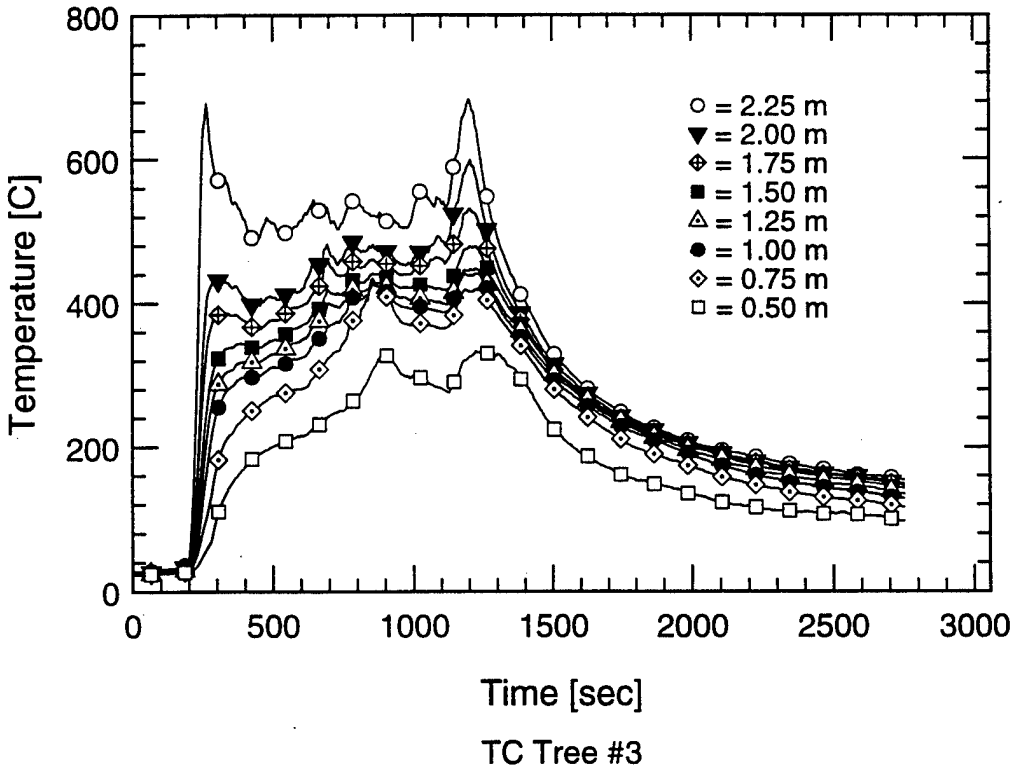

Temperature Measurements

Test 4-1

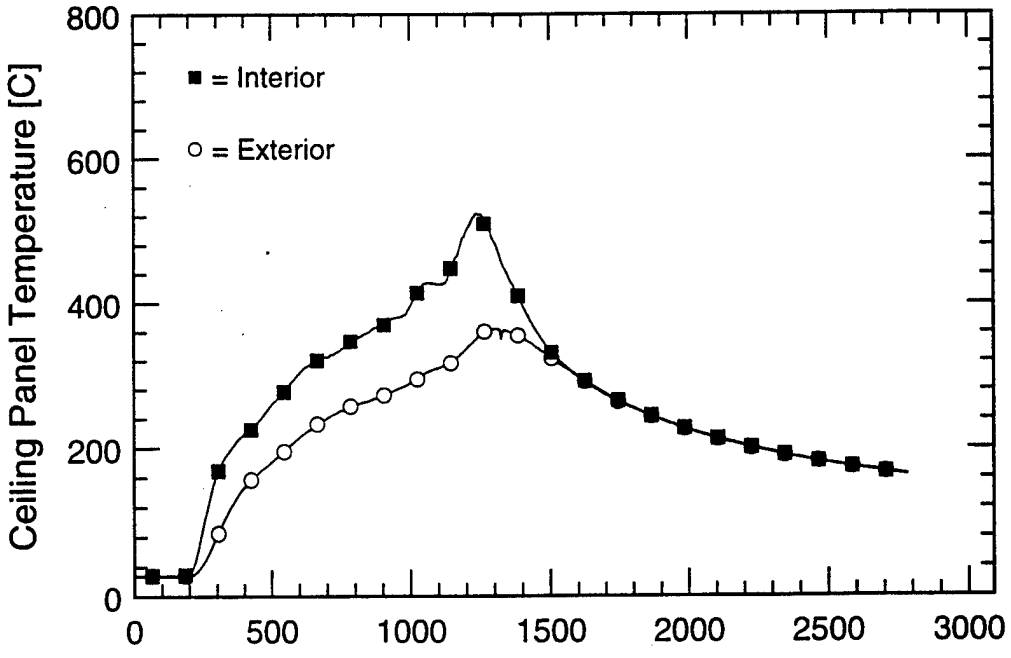

Location #1

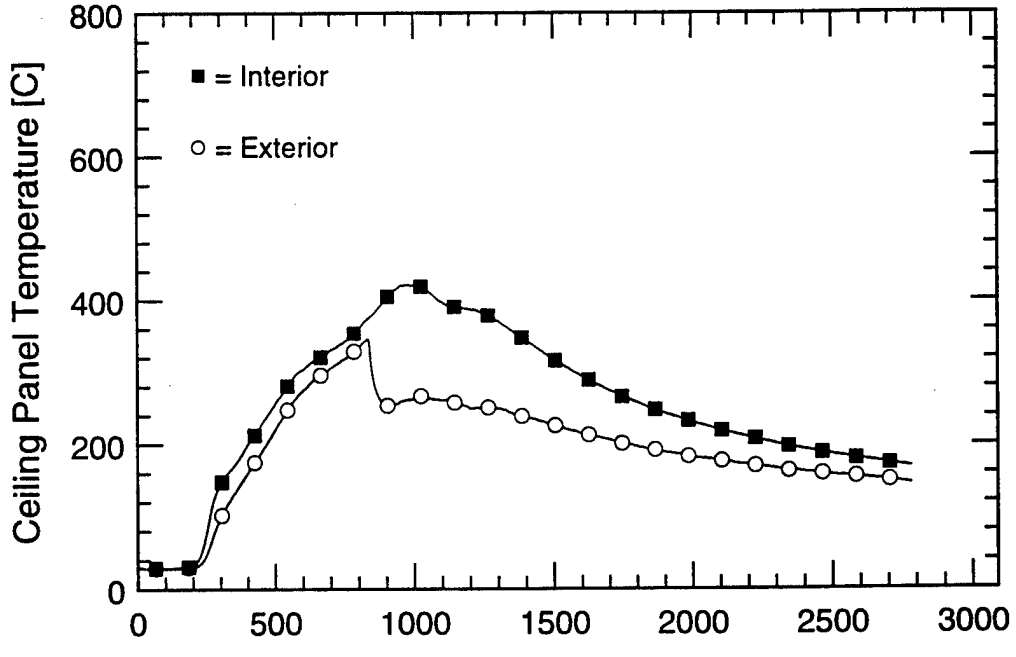

Location #2

Ceiling Panel Temperature Measurements
Test 4-1

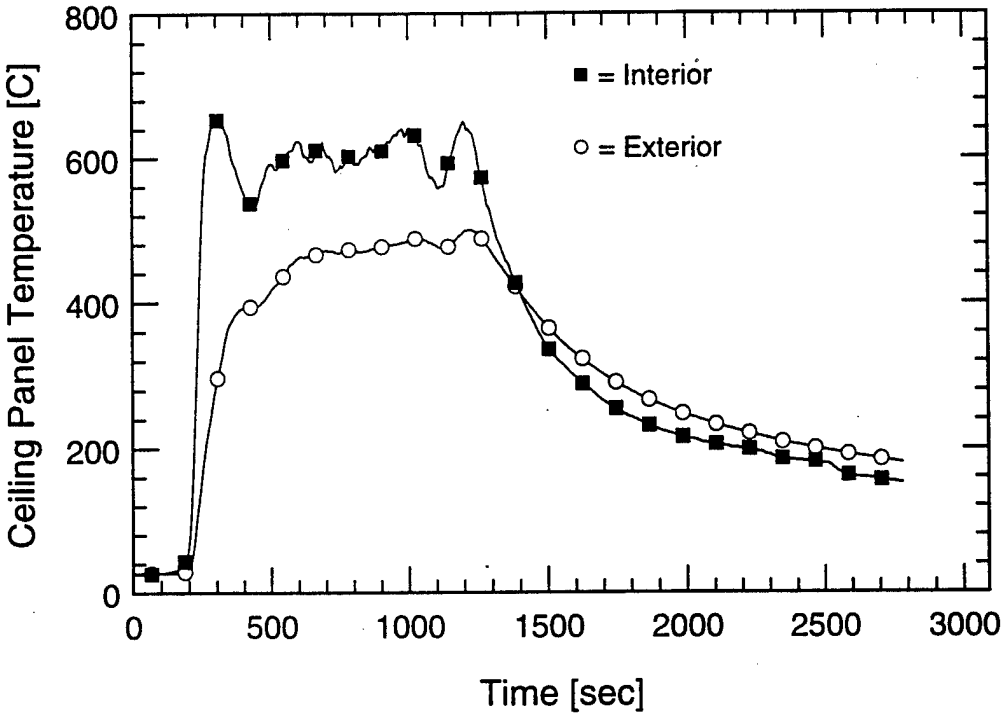

Location #3

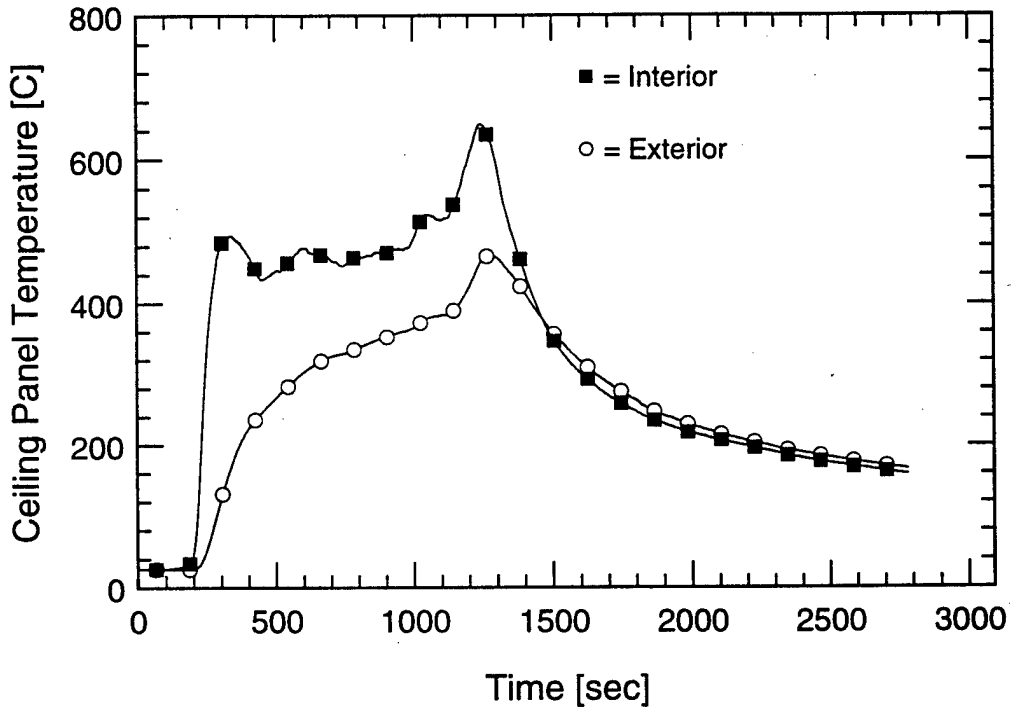

Location #4

Ceiling Panel Temperature Measurements
Test 4-1

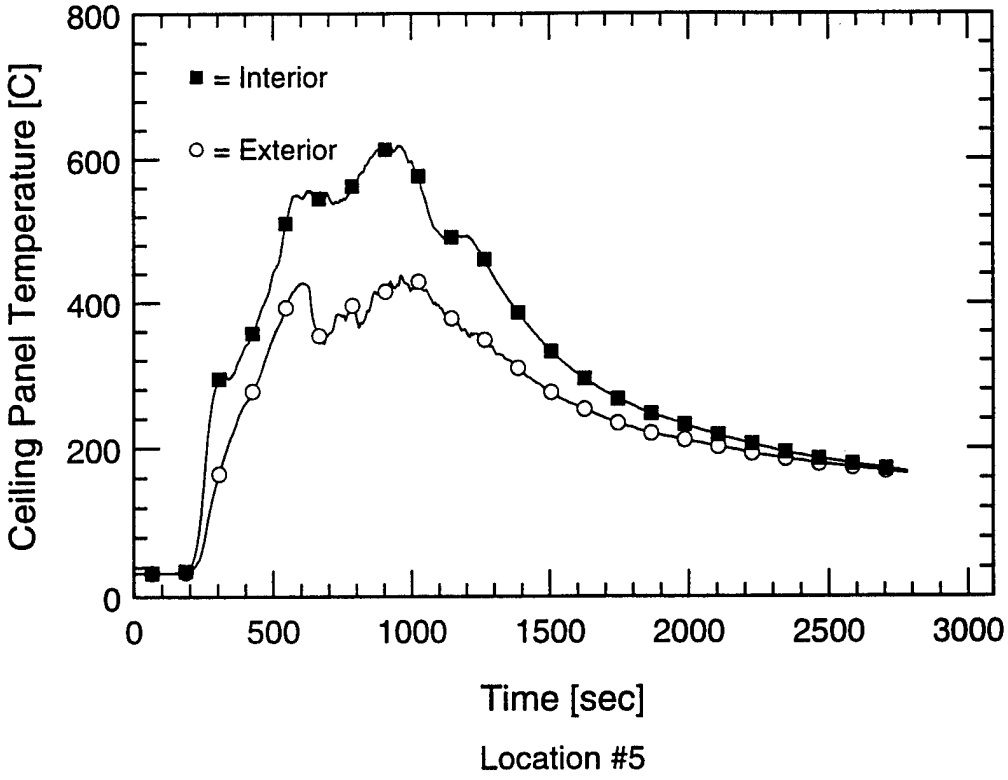

Ceiling Panel Temperature Measurements
Test 4-1

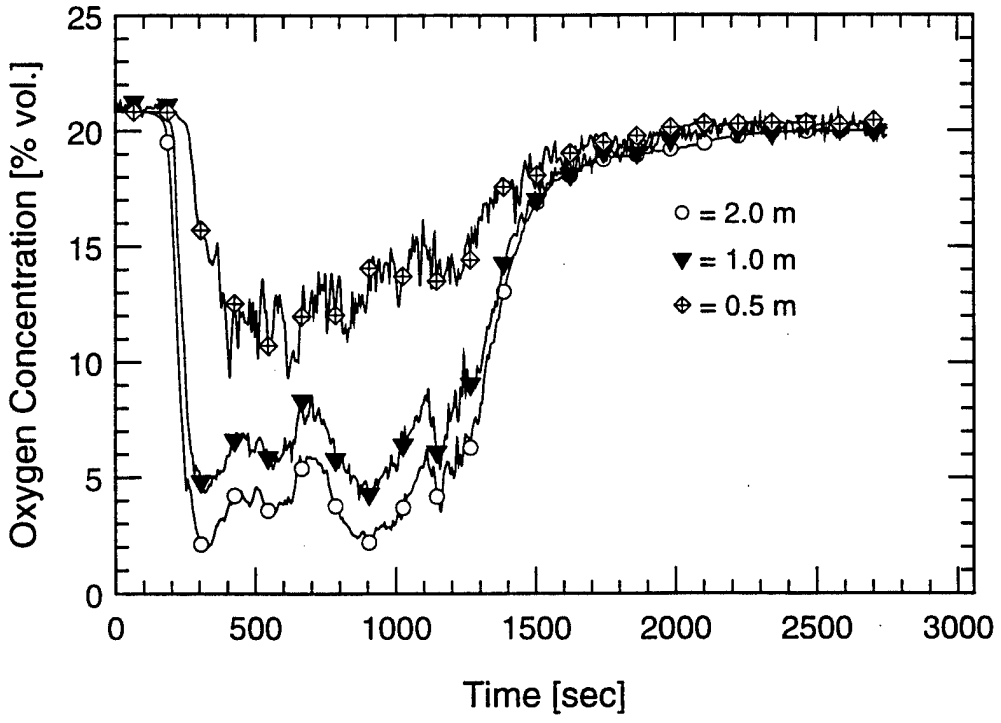

Gas Tree #1

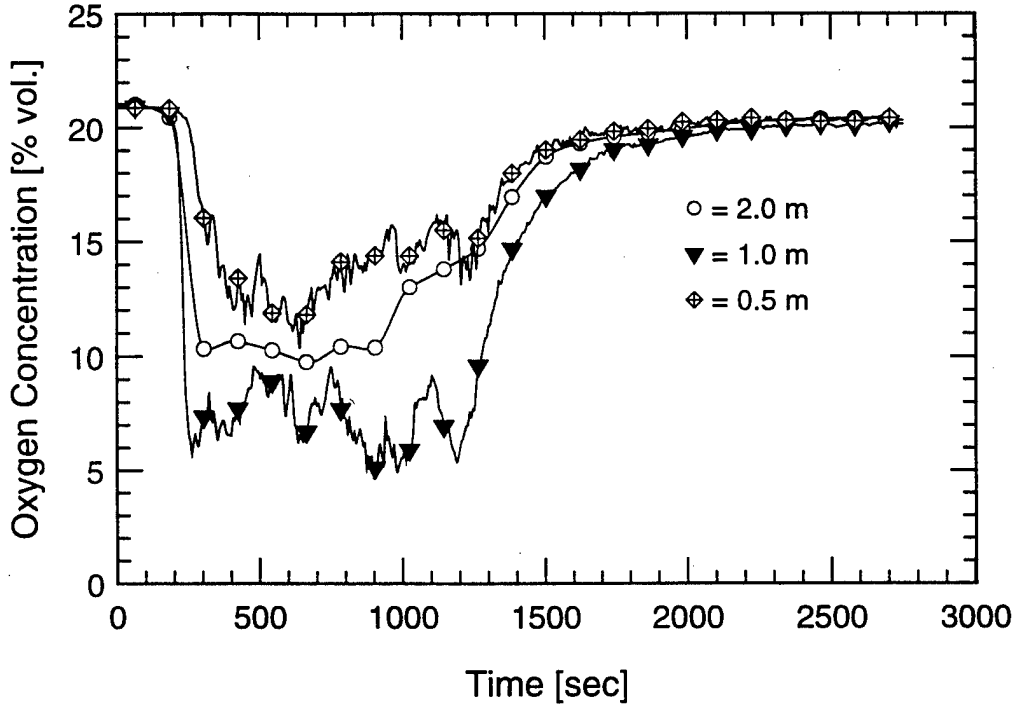

Gas Tree #2

Oxygen Concentration Measurements
Test 4-1

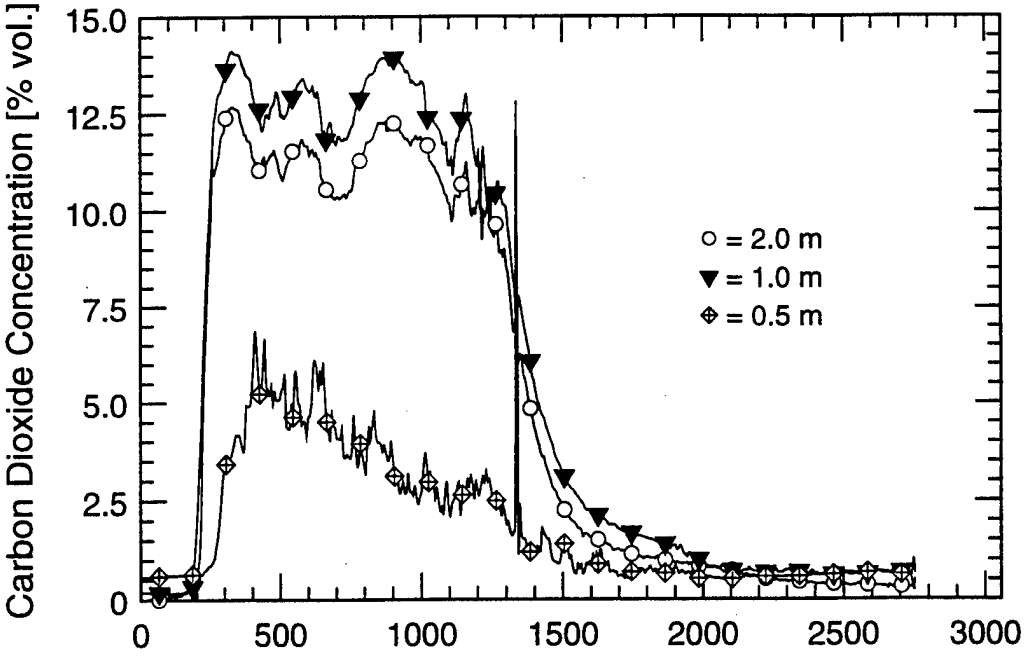

Gas Tree #1

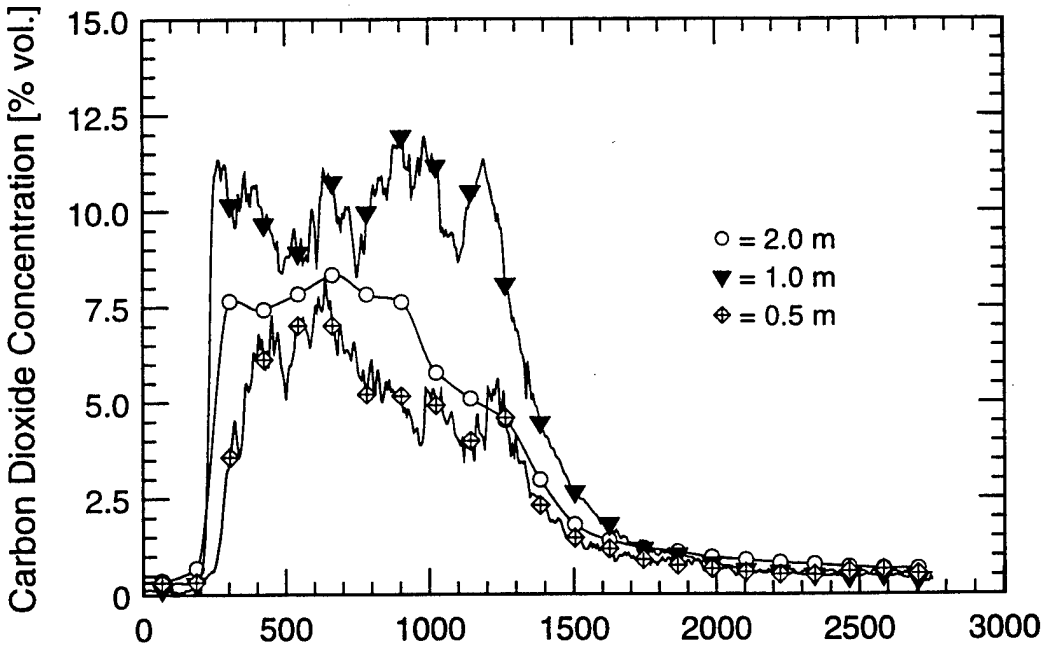

Gas Tree #2

Carbon Dioxide Concentration Measurements
Test 4-1

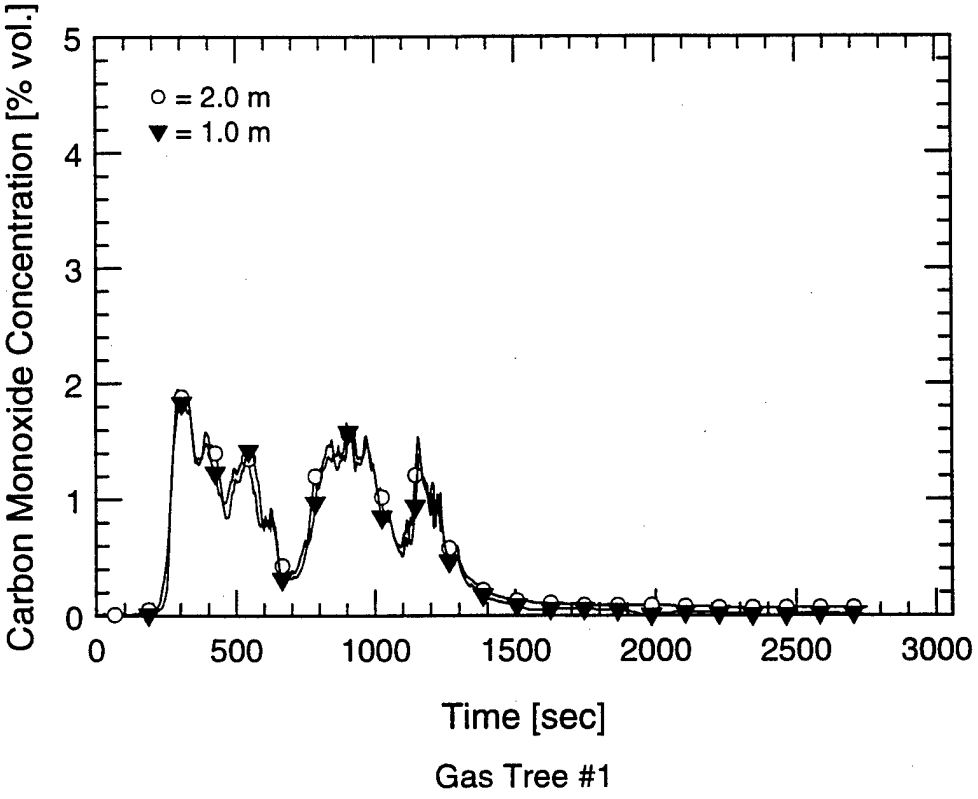

Gas Tree #1

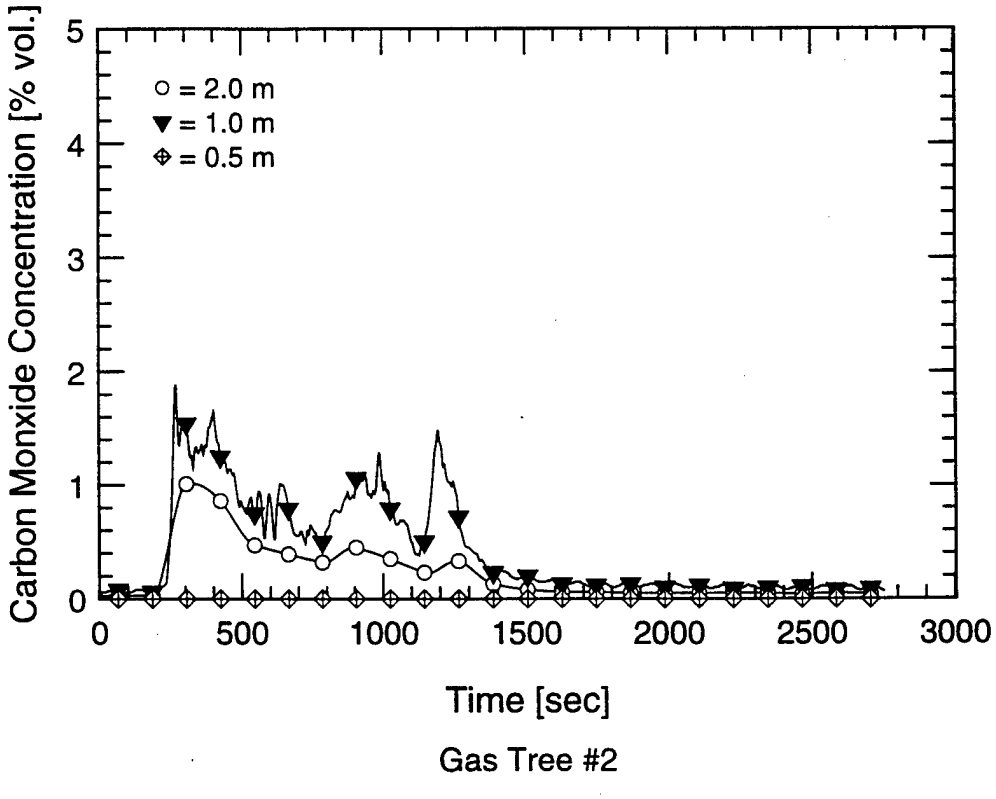

Gas Tree #2

Carbon Monoxide Concentration Measurements
Test 4-1

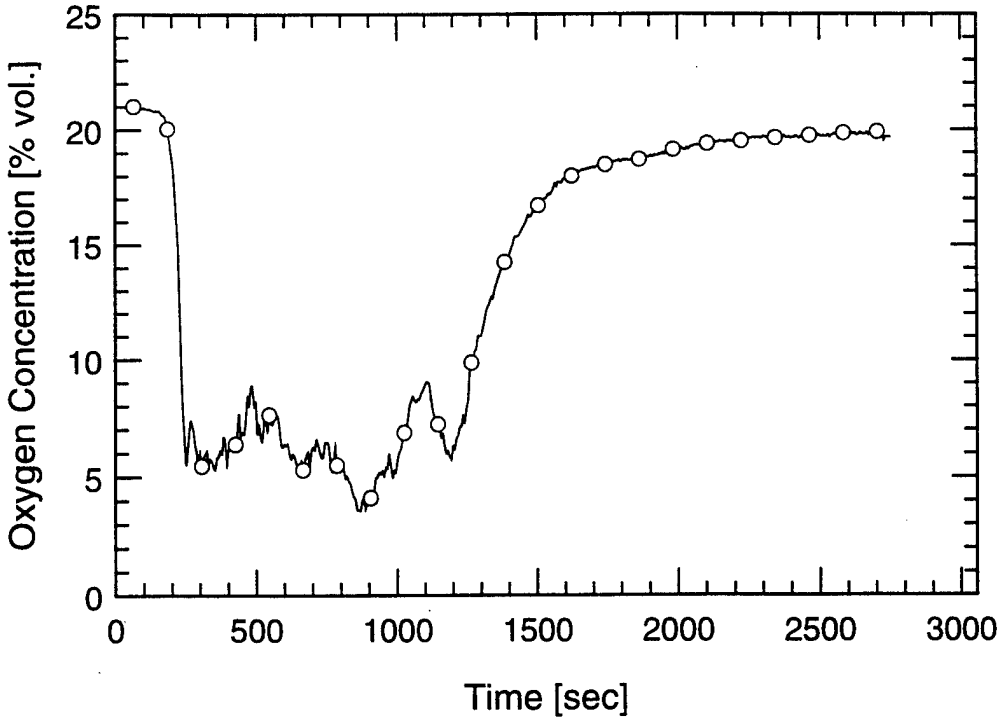

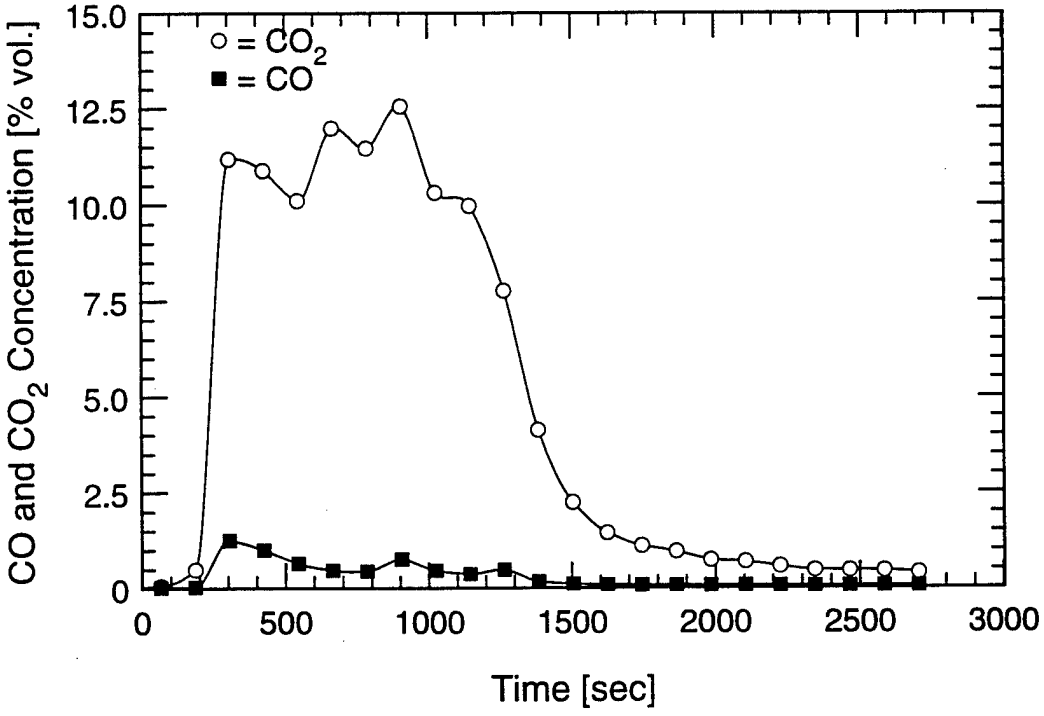

Gas Species Measurements in Doorway (GT3)
Test 4-1

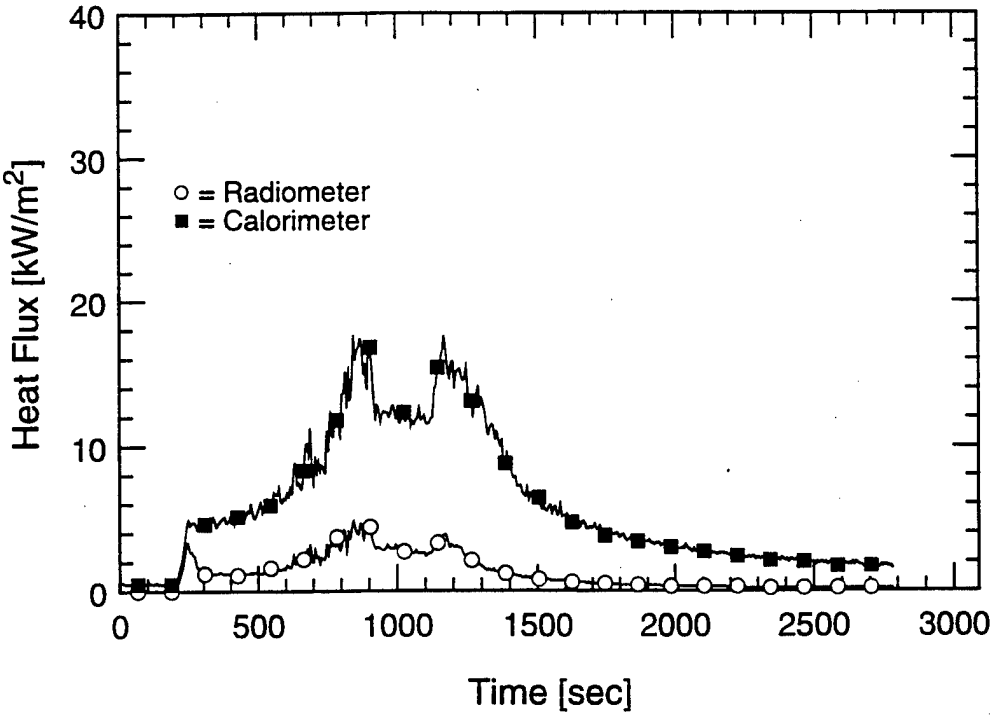

Location #1

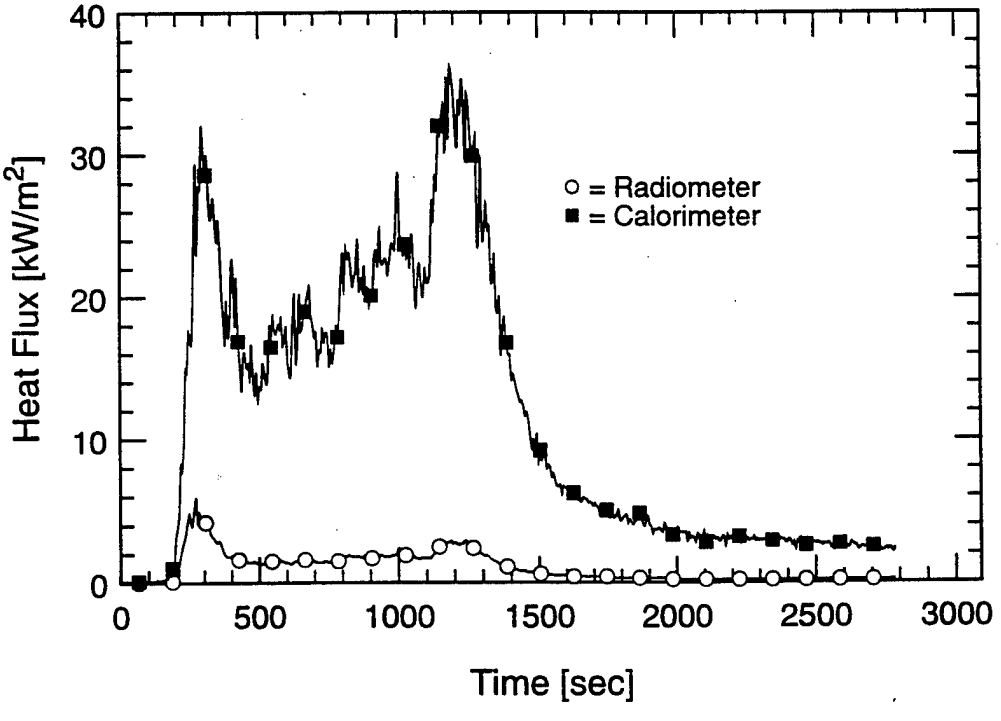

Location #2

Heat Flux Measurements
Test 4-1

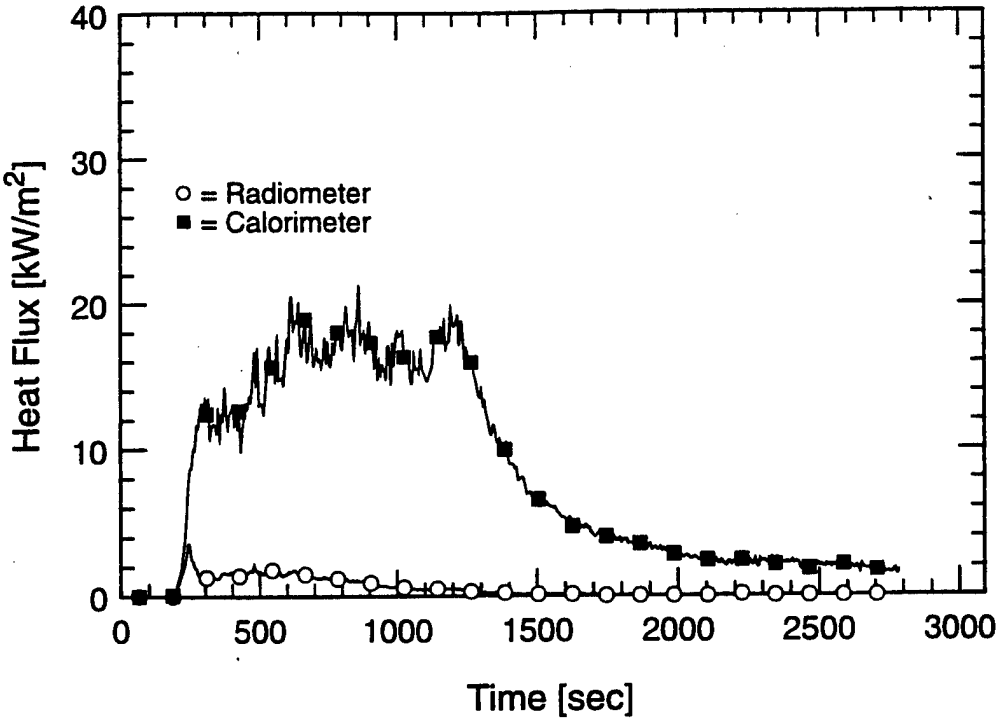

Heat Flux Measurements
Test 4-1